

# **The influence of allylic site abstraction reactions of olefin on cyclo-paraffin formation**

Von der Fakultät für Maschinenbau, Elektro- und Energiesysteme der Brandenburgischen Technischen Universität Cottbus–Senftenberg zur Erlangung des akademischen Grades eines

**Dr. –Ing.**

genehmigte Dissertation

vorgelegt von

**M.Sc.**

**Amruta Nawdiyal**

geboren am 29.01.1982 in Kolhapur, Indien

Vorsitzender: Prof. Dr.-Ing. Heiko Schmidt

Gutachter: Prof. Dr.-Ing. Fabian Mauß

Gutachter: Dr. Nils Hansen

Tag der mündlichen Prüfung: 05.12.2018

<https://doi.org/10.26127/BTUOpen-4852>

*Everything should be made as simple as possible but not simpler.*

*-Albert Einstein*

## **Acknowledgement**

I take immense pleasure to thank all the people who have been a part of this thesis and acted as support through the journey of my thesis writing.

First of all, I would like to thank Prof. Fabian Mauss for giving me the opportunity to do research with him and obtain the doctoral degree. Though he is a man of his own ideas and precision, he gave freedom for my own original thought and creativity, which I truly appreciate. I followed his words he said to me at our first meeting, which were “One has to master the art to work without stress”. This is just a gentle reminder which we should all give to us from time to time in today’s fast paced and over demanding world.

Secondly, I would like to thank Dr. Nils Hansen, for accepting my request to review my thesis. Our meeting was really interesting. He had new experiments and I had a new model. This gave us opportunity to work together and turned out to be a nice publication. I thank him for giving me this superb opportunity.

I would like to thank Christopher Alert who completed his Bachelor thesis under my supervision on the development of the cyclohexane model which has been used as part of my work. I would also like to thank my co-workers and friends Larisa Leon and Xiaoxiao Wang who have always been there in the brainstorming sessions throughout my doctoral period and for their endless moral support.

I would like to thank my parents, parents-in-laws for their faith and patience in me.

I would like to thank my husband Manish and my son Atharv for just being there for me and I dedicate my thesis to them.

Last but not the least; I thank God for giving me strength and patience.



# TABLE OF CONTENTS

<b>ACKNOWLEDGEMENT</b> .....	<b>4</b>
<b>TABLE OF CONTENTS</b> .....	<b>5</b>
<b>ABSTRACT</b> .....	<b>7</b>
<b>LIST OF RELEVANT RESEARCH WORK</b> .....	<b>8</b>
<b>THESIS OUTLINE</b> .....	<b>9</b>
<b>1. INTRODUCTION</b> .....	<b>10</b>
1.1. RESEARCH BACKGROUND .....	10
1.2. MOTIVATION .....	11
1.3. OBJECTIVES .....	14
<b>2. COMBUSTION FUNDAMENTALS</b> .....	<b>15</b>
2.1. FUELS IN COMBUSTION .....	15
2.2. THERMODYNAMICS.....	22
2.3. CHEMICAL KINETICS.....	28
2.3.1. <i>Rate law and direction of reaction</i> .....	28
2.3.2. <i>Temperature dependence of rate coefficients</i> .....	29
2.3.3. <i>Pressure dependence of rate coefficients</i> .....	31
2.4. REACTION MODELLING .....	33
2.4.1. <i>Reaction Mechanism</i> .....	33
2.4.2. <i>Pre-requisites of Reaction mechanisms</i> .....	34
2.4.3. <i>Analysis of Reaction mechanisms</i> .....	38
2.5. COMBUSTION REACTORS .....	41
2.5.1. <i>Shock tubes</i> .....	41
2.5.2. <i>Jet Stirred Reactor</i> .....	43
2.6. FLAMES .....	44
2.6.1. <i>Premixed flame</i> .....	46
2.6.2. <i>Non-Premixed flame</i> .....	48
<b>3. CYCLOHEXANE KINETIC MODEL</b> .....	<b>50</b>
3.1. STRUCTURE OF CYCLOHEXANE .....	50
3.2. RESEARCH BACKGROUND .....	50
3.3. CYCLOHEXANE KINETIC MODEL DEVELOPMENT .....	53
3.4. RESULTS AND ANALYSIS.....	57
3.4.1. <i>Shock Tube</i> .....	57
3.4.2. <i>Jet Stirred Reactor</i> .....	59
3.4.3. <i>Flame speed</i> .....	61
3.4.4. <i>Flow Analysis</i> .....	61
3.4.5. <i>Sensitivity Analysis</i> .....	63
3.5. CONCLUSION ON CYCLOHEXANE MODEL.....	65
<b>4. 1-HEXENE KINETIC MODEL</b> .....	<b>66</b>
4.1. STRUCTURE OF 1-HEXENE .....	66
4.2. RESEARCH BACKGROUND .....	67
4.3. 1-HEXENE KINETIC MODEL DEVELOPMENT .....	69
4.4. RESULTS AND ANALYSIS.....	76

4.4.1. <i>Shock tube</i> .....	76
4.4.2. <i>Flame structure</i> .....	78
4.4.3. <i>Flame speed</i> .....	84
4.4.4. <i>Flow Analysis</i> .....	84
4.4.5. <i>Sensitivity Analysis</i> .....	87
4.5. CONCLUSION ON 1-HEXENE MODEL .....	89
<b>5. METHYLCYCLOHEXANE KINETIC MODEL .....</b>	<b>90</b>
5.1. STRUCTURE OF METHYLCYCLOHEXANE .....	90
5.2. RESEARCH BACKGROUND .....	90
5.3. METHYLCYCLOHEXANE KINETIC MODEL DEVELOPMENT .....	93
5.4. RESULTS AND ANALYSIS.....	100
5.4.1. <i>Shock tube</i> .....	100
5.4.2. <i>Flame speed</i> .....	101
5.4.3. <i>Flame structure</i> .....	102
5.4.4. <i>Flow Analysis</i> .....	105
5.4.5. <i>Sensitivity Analysis</i> .....	107
5.5. CONCLUSION ON METHYLCYCLOHEXANE MODEL .....	109
<b>6. N-PROPYLCYCLOHEXANE KINETIC MODEL .....</b>	<b>110</b>
6.1. STRUCTURE OF N-PROPYLCYCLOHEXANE .....	110
6.2. RESEARCH BACKGROUND .....	110
6.3. N-PROPYL-CYCLOHEXANE KINETIC MODEL DEVELOPMENT .....	112
6.4. RESULTS AND ANALYSIS.....	118
6.4.1. <i>Shock tube</i> .....	118
6.4.2. <i>Flame speed</i> .....	119
6.4.3. <i>Flame structure</i> .....	120
6.4.4. <i>Flow Analysis</i> .....	123
6.4.5. <i>Sensitivity Analysis</i> .....	125
6.5. CONCLUSION ON N-PROPYLCYCLOHEXANE .....	127
<b>7. CONCLUSIONS AND FUTURE SCOPE .....</b>	<b>128</b>
7.1. SUMMARY OF CONCLUSIONS .....	128
7.2. FUTURE SCOPE .....	129
<b>REFERENCES .....</b>	<b>130</b>
<b>APPENDIX .....</b>	<b>138</b>
<b>I. SPECIE STRUCTURES.....</b>	<b>138</b>
<b>II. OTHER RESULTS .....</b>	<b>142</b>
<b>III. LOW TEMPERATURE OXIDATION OF 1-HEXENE .....</b>	<b>148</b>
<b>NOMENCLATURE .....</b>	<b>156</b>

## Abstract

This thesis is a combined work of understanding the high temperature oxidation chemistry of cycloalkanes viz. methylcyclohexane based on previously developed cyclohexane and extending it to generate the larger n-propylcyclohexane chemical kinetic mechanism. The detailed kinetic reaction mechanism model for the oxidation of 1-hexene previously developed has been added to account for the ring opening of cyclohexane forming 1-hexene. As an update to the publication, preference of allylic H-abstractions from 1-hexene has been taken into account and retro-ene reaction producing propene has been added. The complete model is composed of 329 species and 2065 reactions with 3796 reversible elementary reactions. Further, these models have been validated against different experiments such as shock tubes, jet stirred reactors and laminar flames to cover full range of temperatures, pressures and equivalence ratios making the models comprehensive and was found to be adequate to satisfactorily reproduce the experimental data. The allylic radicals ( $C_6H_{11}$ -D1R3) preferred abstractions from 1-hexene improves the  $C_6H_{11}$  profiles in the 1-hexene model. But it also influences the otherwise isomerization path of  $C_6H_{11}$ -D1R6 to  $CYC_6H_{11}$  (Cyclohexyl radical) which would further form cyclohexene ( $CYC_6H_{10}$ ). It is observed that  $CYC_6H_{10}$  profiles in 1-hexene flames and cyclohexane speciation are over-predicted. The major decomposition pathway of the cycloalkanes is through H-abstractions on the ring. The path which leads towards ring opening to form olefin is observed for cyclohexane and methylcyclohexane but is very low. The fulvene pathway influence on benzene profiles of 1-hexene is obvious but do not seem to affect the cycloalkanes. This infers there are other benzene formation pathways in cycloalkanes. Some possible pathways would be the dehydrogenation of dienes and dehydrogenation of cyclo-olefins.

## List of relevant research work

### *Publications in reviewed Journals and Proceedings*

1. A. Nawdiyal, N. Hansen, T. Zeuch, L. Seidel, F. Mauss, "Experimental and modelling study of speciation and benzene formation pathways in premixed 1-hexene flames", Volume 35, Issue 1, 2015, Pages 325–332. (DOI: 10.1016/j.proci.2014.06.047)

### *Publications in Conference Proceedings*

1. A. Nawdiyal, N. Hansen, T. Zeuch, L. Seidel, F. Mauss, "Experimental and Modeling study of speciation and benzene formation pathways in premixed 1-hexene flames", 35<sup>th</sup> International Symposium on Combustion, San Francisco, California, USA, 3 Aug - 8 Aug 2014 (Presentation).
2. A. Nawdiyal, X. Wang, L. Seidel, F. Mauss, T. Zeuch, "Kinetic model for surrogate diesel fuel comprising n-decane and  $\alpha$ -methyl-naphthalene", 24<sup>th</sup> International Colloquium on the Dynamics of Explosions and reactive systems (ICDERS), Taipei, Taiwan, 28 July - 2 Aug 2013.
3. A. Nawdiyal, X. Wang, L. Seidel, F. Mauss, T. Zeuch, "Kinetic model for surrogate diesel fuel comprising n-decane and  $\alpha$ -methyl-naphthalene", European Combustion Meeting, Lund, Sweden, 25 June - 28 June 2013.
4. A. Nawdiyal, X. Wang, M. Hilbig, T. Zeuch, G. Moréac, F. Mauss, "Computer Aided Detailed Mechanism Generation for Hydrocarbon Fuels", European Combustion Meeting, Cardiff, 28 June - 1 July 2011.

### *Poster presentations*

1. A. Nawdiyal, L. Leon, T. Zeuch, F. Mauss, "Development of a high temperature mechanism for Methyl-cyclohexane oxidation", 36<sup>th</sup> International Symposium on Combustion, Seoul, Korea, 31 July – 5 Aug 2016.
2. A. Nawdiyal, F. Mauss, "Development and validation of a detailed kinetic mechanism for 1-hexene oxidation", 3<sup>rd</sup> Annual meeting, CM0901-Detailed Chemical models for cleaner combustion, Sofia, Bulgaria, 5 Sept -7 Sept 2012.
3. A. Nawdiyal, F. Mauss, "Development and validation of a detailed kinetic mechanism of 1-hexene oxidation", 34<sup>th</sup> Symposium on Combustion, Warsaw, Poland, 29 July-3 Aug 2012.

## Thesis Outline

In Chapter 1 the motivation and objectives of the work are described along with the basic information about n-propyl-cyclohexane and the sub-fuels cyclohexane, methylcyclohexane and 1-hexene.

The Chapter 2 puts light on the basic concepts of combustion of fuels, reaction kinetics and the mathematical equations behind the solutions. Also, the various combustion reactors where the simulation is carried out are described in this chapter. The reactor modeling and instruments in modeling are also discussed here.

Chapters 3, 4, 5 and 6 discuss in detail the model development for the oxidation of cyclohexane, 1-hexene, methylcyclohexane and n-propylcyclohexane respectively. Each chapter starts with a literature review followed by the discussion of the reaction mechanism development and the reaction rates followed. Following this, the validation results for ignition delay, speciation, flame speeds and flow- and sensitivity analyses and conclusion are given in sub-chapters for all the fuels.

Lastly, in chapter 7 the summary of conclusions of all models discussed in chapters 3, 4, 5 and 6 and the future scope of this study is discussed.

The supplementary material in the form of specie structures and results not shown in the main text are presented in the Appendices I and II respectively.

# 1. INTRODUCTION

## 1.1. Research Background

The research in combustion helps to understand the fundamentals of physics of flames and high temperature molecular chemistry which helps in controlling emissions of various harmful pollutants. Reaction mechanisms are such tools which are a great benefit to understand the oxidative behavior of various fuels depending on their structure like alkanes, olefins, cycloalkanes and aromatics.

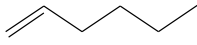
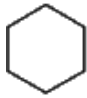
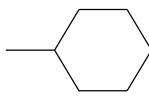
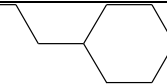
Today, combustion is a mature discipline with lot of research and development done and going on to improve the combustion characteristics of a certain fuel and to reduce emissions evolving from it. **Gasoline and diesel** are the common fuels we know which are used in the automotive industry in various combustors like spark ignition engines and homogeneous charge compression engines. **Kerosene** based fuels like Jet-A and JP-8 are important fuels used in the aviation industry. **Naphtha** a less processed and lighter fuel is now being researched for its capability of being used in the modern diesel engines to replace heavier fuels.

Naphtha is the first distillation product of crude oil and has boiling point between 30 °C and 200 °C. It is reformed through various processes like cracking and hydro-treatment etc. into heavier fraction of gasoline. This refining process leads to CO<sub>2</sub> emissions. But if naphtha in itself is used as a fuel, the reforming process is skipped which leads to reduction in CO<sub>2</sub> emissions. Also, since no reforming is required, the cost of manufacturing naphtha is considerably reduced. Thus, naphtha fuel can act as a source to reduce the demand gap between heavier and lighter fuels and is an attractive alternative to heavier fuels.

Real fuels are composed of several hundreds of hydrocarbons. It is close to impossible to model such fuels. One approach to achieve this is to create the so called surrogate fuel models. A surrogate considers components which are representative of the particular real fuel at the same time matching the important characteristics of that fuel. Many surrogate fuels have been proposed in last decade, which are studied numerically, and evaluated in engines and in reactor experiments.

One such surrogate fuel is the diesel gas surrogate which is *n*-decane and  $\alpha$ -methylnaphthalene formulated by IDEA program [2]. *n*-Decane alone and a mixture of *n*-decane, *n*-propylbenzene and *n*-propylcyclohexane are kerosene surrogates [3]. Gasoline surrogate fuels are *n*-heptane and *iso*-octane [4] with toluene added later by Andrae et al. [5] to represent the aromatic component of gasoline. In case of naphtha fuel, cycloalkanes will form the most important component apart from the *n*-alkanes as the naphtha surrogate fuel model.

This study focuses on high temperature oxidation of cycloalkanes which form important components of naphtha, gasoline, diesel and kerosene fuels and olefins which are major products of decomposition of alkanes. The major cycloalkanes found in liquid fuels are cyclohexane, methylcyclohexane and *n*-propylcyclohexane which are the fuels studied in this thesis. 1-Hexene was found as an important intermediate and is also discussed in detail.

	1-hexene	cyclohexane	MCH	<i>n</i> -PCH
<b>Chemical formula</b>	C <sub>6</sub> H <sub>12</sub> -D1	CYC <sub>6</sub> H <sub>12</sub>	CYC <sub>7</sub> H <sub>14</sub>	CYC <sub>9</sub> H <sub>18</sub>
<b>Chemical structure</b>				
<b>Density, g/cm<sup>3</sup></b>	0.673	0.7781	0.77	0.793
<b>Auto Ignition</b>	253 °C	245 °C	285 °C	247.8 °C
<b>Boiling Point</b>	63 °C	80.74 °C	101 °C	155 °C
<b>Melting point</b>	-139.8 °C	6.47 °C	-126.3 °C	-95 °C
<b>Vapor Pressure, mmHg</b>	140.26 (at 20 °C)	78 (at 20 °C)	37 (at 20 °C)	8.7(at 37.7 °C)
<b>RON (MON)</b>	76.5 (MON 63.4)	83 (MON 77.3)	74.8 (MON 71.1)	-
<b>Cetane number</b>	-	-	20	-

**Table I: Properties of four different fuels 1-hexene, cyclohexane, methylcyclohexane (MCH) and *n*-propylcyclohexane (*n*-PCH) assembled.**

## 1.2. Motivation

Liquid fuels are the primary source of energy in the transportation sector today and will remain so for many more years to come. Currently, around 95% of this energy is generated through petroleum based fuels. Two major road transport fuels are gasoline and diesel. While in the military and aviation sector mostly kerosene-based (Jet A, Jet A-1, JP-8) and naphtha-based (JP-4, Jet B) jet fuels are used.

According to the World Energy council [6], in the coming decades the demand would be more in the commercial sector rather than in the transportation sector. This means that, more investment needs to be done in refineries to produce heavier fuels like diesel and kerosene and less of gasoline. Another way is to focus on renewable alternatives to diesel like natural gas, gas to liquid and lighter fuels like naphtha. Naphtha can replace the heavier gasoline and diesel fuels owing to its less processing required. Since it is less processed, the cost of manufacturing is certainly reduced. In addition, since naphtha requires much less processing in the refinery as compared to diesel or gasoline, well to wheel CO<sub>2</sub> emissions are reduced. Studies have shown that if used in gasoline/diesel engine/s with some modifications it can reduce the fuel consumption considerably [7]. Thus, naphtha fuel can act as a source to reduce the demand gap between heavier and lighter fuels and is being quite researched as an attractive alternative to heavier fuels.

Along with alkanes and iso-alkanes, the cycloalkanes form a considerable portion of the composition of the liquid fuels which are used both in transportation and commercial sectors. Naphtha constitutes around 20-50% cycloalkanes depending upon the type of naphtha (where the distillation cut is made) and the source of crude oil. See Table II below.

HC Type	Proportion range						
	Gasoline <sup>1</sup>	Diesel <sup>1</sup>	Aviation Gasoline <sup>1</sup>	Jet fuels		Naphtha	
				Jet B (JP-4) <sup>2</sup>	Jet A, Jet A-1 <sup>2</sup>	Medium <sup>3</sup>	Heavy <sup>3</sup>
C range	C <sub>5</sub> -C <sub>12</sub>	C <sub>15</sub> -C <sub>18</sub>	C <sub>4</sub> -C <sub>10</sub>	C <sub>5</sub> -C <sub>15</sub>	C <sub>8</sub> -C <sub>16</sub>	C <sub>5</sub> -C <sub>6</sub>	C <sub>7</sub> -C <sub>9</sub>
<i>n</i> -Alkanes	4-8%	50-54%*	50-60%*	59%*	60%*	48.8%*	45.4%*
Alkenes	2-5%	1-2%	---	2%	2%	0%	0%
iso-alkanes	25-40%	TWA*	TWA*	TWA*	TWA*	TWA *	TWA *
<b>Cycloalkanes</b>	<b>3-7%</b>	<b>10-15%</b>	<b>20-30%</b>	<b>29%</b>	<b>20%</b>	<b>32%</b>	<b>40%</b>
Cyclo-alkenes	1-4%	---	---	--	---	---	---
Aromatics	20-50%	35%	<10%	10%	18%	18.8%	14.9%
TWA*-Together with alkanes							

**Table II: Hydrocarbon Composition of different fuels Source: Various sources, <sup>1</sup>[8] <sup>2</sup>[9] <sup>3</sup>[10]**

Heavy naphtha has around 40% cycloalkanes with around 15% aromatics and medium naphtha has 32% cycloalkanes with around 19% aromatics [10]. The kerosene based jet fuels like Jet A and JP-8 which are used in the military and aerospace applications constitute up to 20-30% cycloalkanes according one study in



1999 from Edwards and Maurice [9]. Gasoline and diesel are composed of 3-7% and 10-15% cycloalkanes respectively with very high aromatic content compared to jet and naphtha fuels [8].

Typical heavy naphthas				
Crude oil name ⇒ Location ⇒	Barrow Island Australia	Mutineer-Exeter Australia	CPC Blend Kazakhstan	Draugen North Sea
Initial boiling point, °C	149	140	149	150
Final boiling point, °C	204	190	204	180
Paraffins, liquid vol%	46	62	57	38
<b>Naphthenes, liquid vol%</b>	<b>42</b>	<b>32</b>	<b>27</b>	<b>45</b>
Aromatics, liquid vol%	12	6	16	17

**Table III: Typical heavy naphthas in different regions and their compositions [11]**

Naphtha is composed of different types of cycloalkanes ranging from the simplest ring cyclohexane and *n*-alkylated cycloalkanes like methylcyclohexane and *n*-propylcyclohexane. These cycloalkanes are also representatives of cyclo-species fraction in surrogate naphtha model fuels. Also, cycloalkanes are important since they have a high potential to form aromatics thus their chemistry becomes important to understand their ignition process and soot formation.

Along the cycloalkane decomposition path, olefins are also formed through their ring opening. 1-Hexene is the first product formed from cyclohexane combustion. It is also a major intermediate in larger alkanes like *n*-heptane and *n*-decane.

In spite of the importance of these cycloalkanes their chemistry is relatively little investigated. Among several cycloalkanes, only cyclohexane is studied extensively while alkylated cycloalkanes are relatively less studied. This thesis starts from development of chemical kinetic model for the oxidation of cyclohexane and goes up to alkylated cycloalkanes methylcyclohexane and finally to *n*-propylcyclohexane. 1-Hexene sub-mechanism is added to the final model which then describes olefin development from the different cycloalkanes.

### 1.3. Objectives

This thesis is a study on the development of the high temperature oxidation mechanism of cycloalkanes; namely cyclohexane, methylcyclohexane, and *n*-propylcyclohexane and both high and low temperature mechanism development of 1-hexene oxidation. The low temperature oxidation mechanism for cycloalkanes exists but is out of scope of this study.

The main objective of this work is to develop a high temperature model for the naphtha surrogate fuel *n*-propylcyclohexane. This is done with first modeling the smallest cyclohexane model and adding methylcyclohexane model to it and finally the *n*-propylcyclohexane model. The aim is to study the interconnection between the smaller and higher cycloalkanes which is the formation of olefin 1-hexene thereby the detailed model includes the sub-model for 1-hexene decomposition. Finally another important objective is to understand the aromatic formation particularly benzene through Fulvene or other pathways resulting in soot and particulates.

## **2. COMBUSTION FUNDAMENTALS**

Fire was believed to be one of the five basic elements of the universe. Thus, understanding fire and combustion was always seen to be very important. Combustion is an extremely widespread process which is a result of physical and chemical aspects. The first aspect is chemical which is the numerous chemical reactions occurring simultaneously which are called the elementary reactions. The second aspect is of heat transfer due to increase in the temperature during these exothermic reactions and the third aspect is of mass transfer which is due to the movement of the gases which make up a flame. The third aspect is related to the physics of the fluids.

Below are explained the different fuels in combustion along with their important properties. The thermodynamics involved in their combustion is further discussed. Further the rate law and other factors are explained in chemical kinetics. The method of reaction mechanism development is further covered. The reactors used for combustion modeling and finally chemistry of flames are described. These parts are assembled from various sources as described below individually.

### **2.1. Fuels in combustion**

Most part of this chapter has been assembled from the book of S. Turns [8].

Concerns over global warming, environmental degradation, and national energy independence have created a renewed interest in fuels. And this interest is not just limited to scientist and engineering communities. The alternative fuels e.g. biodiesel, ethanol, Frischer-Tropf liquids from coal or biomass, hydrogen etc. are being considered for transportation and other applications.

#### **Types of fuels**

1. Liquid fuels (e.g. gasoline, diesel)
2. Solid fuels (e.g. coal, wood)
3. Gaseous fuels (e.g. natural gas, hydrogen)

Natural gas, gasoline, and coal, perhaps the most widely used examples of these three forms, are each a complex mixture of reacting and inert compounds.

The knowledge of the fuel properties helps in selecting the right fuel for the right purpose and for the efficient use of the fuel.

**Fuel molecules in the fuel blends** The fuel blend is composed of several hydrocarbons. The Table IV shows detail of such hydrocarbon families.

Family name	Other designation	Molecular formula	Carbon-Carbon bonding	Primary molecular structure
<b>ALKANES</b>	Paraffins	$C_nH_{2n+2}$	Single bonds only	Straight or branched open chains
<b>ALKENES</b>	Olefins	$C_nH_{2n}$	One double bond, remainder single	Straight or branched open chains
<b>ALKYNES</b>	Acetylenes	$C_nH_{2n-2}$	One triple bond, remainder single	Straight or branched open chains
<b>CYCLANES</b>	Cycloalkanes Cyclo-paraffins, Naphthenes	$C_nH_{2n}$ or $(CH_2)_n$	Single bonds only	Closed rings
<b>AROMATIC</b>	Benzene family	$C_nH_{2n-6}$	Resonance hybrid bonds (Aromatic bonds)	Closed rings

**Table IV: Basic hydrocarbon families**

## Important properties of fuels

Apart from knowing the physical properties of a fuel like density, volatility, etc. it is important to know the chemical properties like heat value, ignition delay and laminar flame speeds. These properties are assembled from the book of S. Turns [8].

**1. Ignition Characteristics:** The ignition quality of a fuel is very important property for reciprocating engines. The ignition quality is related to the engine knock or auto-ignition i.e. the uncontrolled spontaneous ignition of the unburnt gas mixture ahead of the flame. It is measured in terms of octane number (ON) in spark-ignition engines and cetane number (CN) in diesel engines. While ON is measure of fuel's ability to resist knock, the CN is the ability of the fuel to auto-ignite.

**Octane number (octane rating):** Measuring ON is complex and is done by research octane number (RON) or motor octane number (MON) tests. It is also measured with antiknock index (AKI) which is an average of laboratory based **RON** and **MON** i.e. **AKI = (RON +MON)/2.**

**RON and MON tests:** Two reference fuels isooctane (*i*-C<sub>8</sub>H<sub>18</sub>) ON=100 and n-heptane (*n*-C<sub>7</sub>H<sub>14</sub>) ON=0 are used as standards to define the ON in SI engines. In these tests, a standardised variable-compression ratio, single-cylinder engine is equipped with knock sensor to measure knock intensity. In both procedures, the knock intensity of the fuel being rated is compared to that resulting from burning blend of two PRF fuels. The percentage of iso-octane in primary reference fuels that matches the fuel being tested defines the fuel's octane number.

Greater knock resistant fuels have ON>100. Regular gasoline has a typical AKI 87 (US). The octane number has no effect on the performance of an engine other than allowing the delivery of maximum power without knocking. For aviation gasoline (ON>100), mixture of tetraethyl lead with isooctane is used as the standard reference fuel. If an engine operates without knocking, use of higher-octane fuel will not result in more power or greater fuel economy.

**Cetane number (cetane rating):** The ignition characteristics of the fuel determine the start, and hence the timing of the combustion process. **Ignition delay (ID)** is the

time delay between the introduction of fuel and oxidizer in a vessel and the onset of ignition in form of a flame or any other indicator of ignition [12].

**CN test:** Two reference fuels *n*-cetane ( $C_{16}H_{34}$ ) CN=100 and heptamethyl nonane ( $C_{16}H_{34}$ ) CN=15 are used as standards to define the CN in CI engines. In these tests, a standardized variable-compression ratio, single-cylinder engine is equipped with sensors to measure ignition delay. ID of the fuel is rated with the results from operating reference fuels. The cetane number is determined by **CN = vol. % *n*-cetane + (0.15) vol. % heptamethyl nonane.**

Low cetane numbers result in long ignition delays and vice versa. A good diesel fuel is easy to auto-ignite thus shorter ignition delay is desired. A good gasoline fuel on the contrary is hard to auto-ignite. Typical cetane numbers are 30-65.

**2. Volatility:** It is the ability of the fuel to evaporate readily. Fuels with different volatilities are used in different combustion applications. Fuels with high volatility is required in SI engines to ensure uniform fuel-air mixture at the time of spark while diesel engines use less volatile fuels to prevent the formation of large quantities of combustible mixture during ignition delay. Engine cold starting characteristics and other drivability measures of automobiles is strongly dependent on the volatility. Vapor lock is a prevention formed in the flow within the fuel system due to the formation of fuel vapor and depends on fuel's vapor pressure. Volatility affects evaporative emissions of fuel and its safety and storage characteristics.

**Measures of fuel volatility:** Three different methods to measure volatility of fuel are;

1. Vapor pressure at a given temperature,
2. Equilibrium air distillation profiles
3. Liquid-vapor ratios at a given temperature

**3. Energy density:** Another important property of fuel is energy density. It is expressed on mass or volumetric basis. For a fixed fuel tank volume, the fuel energy density decides the range of the vehicle or aircraft. It is an important parameter in the specification of aircraft fuels.

Variations of energy densities between hydrocarbons are less as that compared to that between hydrocarbons and alcohols. Example: gasoline is 30% more dense (Volumetric energy density) than ethanol.

## Different types of fuels

**1. Conventional Gasoline:** Gasoline is a blend of several hydrocarbons and additives which is formulated for SI engines. Specifications for gasoline would be auto-ignition resistance, good cold start characteristics, homogeneous fuel-air mixture at the onset of combustion (volatility) not causing vapor lock or excessive emissions, storability, meet air quality regulations for pollutant emissions etc. Gasoline is a mixture of alkanes, alkenes and aromatics together around 200 or more individual hydrocarbons. Their compositions in general are shown in the Table II. These compositions can vary widely from region to region and is also dependent on the source of gasoline.

Other than conventional gasoline, reformulated gasoline (RFG) is formulated to improve air quality in selected regions in US. The Clean Air Act required gasoline producers to supply gasoline blends to reduce:

- Volatile organic compound (VOC) emissions
- Toxic air pollutant emissions (benzene, formaldehyde etc.). Restrict benzene to less than 1 vol.% due to carcinogenicity
- NO<sub>x</sub> emissions

To fulfill the original requirement of > 2 wt. % oxygen content in the fuel and renewable fuel component, previous choice of MTBE was replaced by ethanol. Emissions standards have been set for these parameters for each region according to the requirement.

Winter oxygenated fuel is another type used in winters to reduce CO emissions.

**2. Diesel:** Diesel is a blend of hydrocarbons sometimes with additives specifically for use in diesel engines. According to ASTM International standard there are 3 numerical grades of diesel:

- No.1-D: light middle distillate fuel

- No.2-D: a middle distillate fuel
- No.4-D: a heavy distillate fuel (or a blend of distillate and residual oil)

The mean molecular weight and viscosity increases with designation.

Further categorization of grades is S15, S500, and S5000 which means maximum sulphur content of 15, 500 and 5000 ppm respectively. Most on road diesel vehicles (buses, trucks) use No. 2-D S15 fuel. Maximum allowed sulphur content for No.4-D is 2 wt. %.

Diesel specifications are: good ignition and cold-start characteristics; sufficient lubricity, viscosity for proper functioning of fuel-injection system; low pressure operating conditions; stable, non-corrosive and clean, compatible with exhaust emissions control system; meet air quality regulations for emissions among others. Details can be found in S.Turns [8].

Diesel fuels are comprised mainly of blends of C<sub>9</sub>-C<sub>16</sub> hydrocarbons (No.1) and C<sub>11</sub>-C<sub>20</sub> hydrocarbons (No.2). General Diesel composition is given in Table II with more detailed analysis shown in Figure 1.

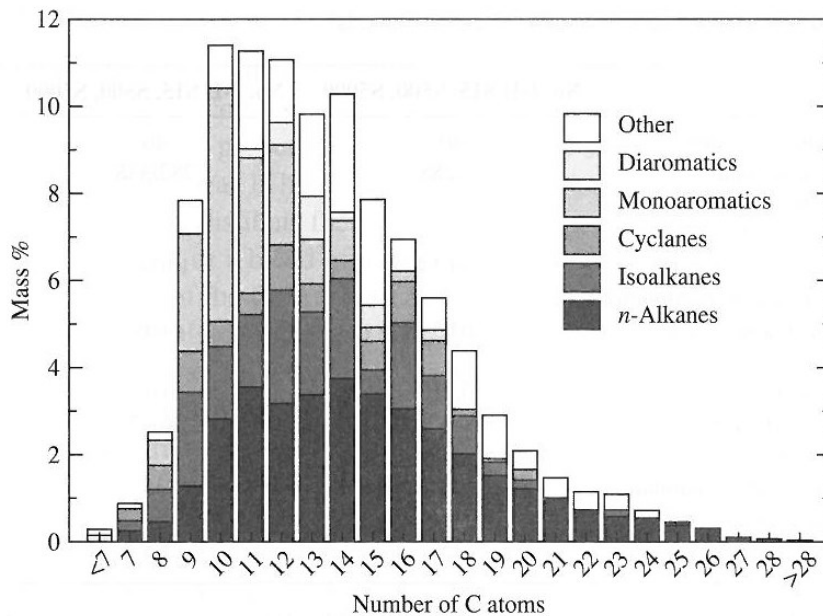


Figure 1: Detailed composition of commercial Diesel [8]



**3. Aviation fuels:** Aviation Gasoline is used in SI engines in general aviation while in jet engines kerosene-based fuels like Jet A, Jet A-1 and JP-8 are used.

**Aviation Gasoline:** Basic composition of aviation gasoline is shown in Table II. Specification of aviation Gasoline are: combustion characteristics and antiknock quality; fuel metering and aircraft range, as controlled by density and heat of combustion, carburetion and fuel vaporization, controlled by vapour pressure and distillation characteristics; corrosion; fluidity at low temperatures; and fuel cleanliness, handling and storage stability. The low aromatic content in aviation fuels as compared to automotive gasoline is required to have a high heating value and proper distillation characteristics and minimize the effects of the fuel on elastomers. Tetraethyl lead is added to aviation gasoline to meet ON or performance requirements. The decomposition products of tetraethyl lead scavenge radical species that lead to auto-ignition.

- **Aviation Turbine fuels:** Specifications for Jet A and Jet A-1 fuels consider a large number of characteristics: Energy content, combustion, volatility, fluidity, corrosion, thermal stability, contaminants and additives. To control maximum range of aircraft, heat of combustion plays an important role. In civil aviation, volumetric heating value (MJ/gallon) is important. Aromatics are precursors to soot formations thereby their content in the fuel is limited to 25 vol %. Freezing point is another important property which needs to be considered. Jet A-1 fuel has lower freezing point than Jet A.

**4. Heating oils:** Designated as No. 1 and No. 2 fuel oils like diesel. Composition and properties essentially same as the corresponding grade of diesel oil, differing in additive and sulphur contents. Heavier grades No.4, No.5, No.6 used in commercial and industrial applications. Specifications for these grades are provided by ASTM standard D396 control: Flash point, water and sediment, distillation characteristics, carbon residue, kinematic viscosity, ash, sulphur, corrosion, density and pour point.

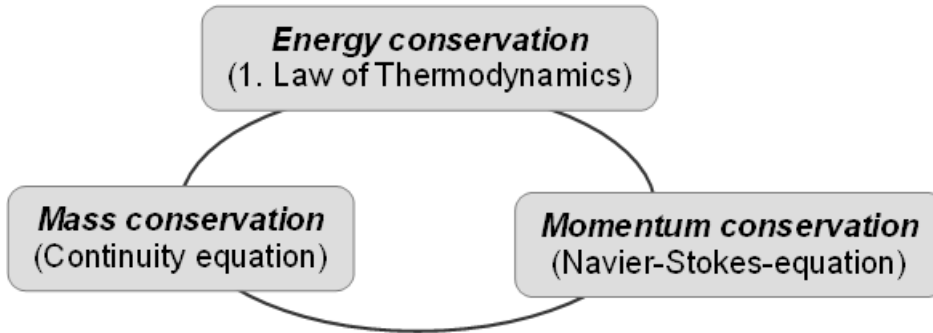
**5. Natural Gas:** It is found within or near oil fields. Its classification as associated gas means it's a product from an oil well and is non- associated gas if it's a product from a gas well. It is basically composed of methane, smaller other C<sub>2</sub>-C<sub>8</sub>

HC, N<sub>2</sub>, CO<sub>2</sub> and He with trace amounts of hydrogen sulphide, water, oxygen etc. It varies widely depending on the source. Processing removes solid matter, liquid HC, sulphur compounds, water, nitrogen, carbon dioxide, helium, and any undesirable compounds to meet specifications for distribution in pipeline systems. It is a relatively clean-burning fuel and ranks second to coal in the production of electricity in the US.

- 6. Coal:** Coal is a sedimentary rock formed principally from organic matter but it includes minerals of different types in different proportions. Proximate analysis of coal (mass %) divides into constituents as: moisture (10-30), volatiles (10-30), mineral matter (10-30) and char (balance). The mass percentage shows that the energy value of coal is limited due to the high content of moisture and mineral matter. This leaves the energy value of coal to volatiles and char. Ultimate analysis of coal (dry mineral free, mass %) which would be useful portion of coal is grouped into elemental composition as: C (65-95), H (2-6), O (2-25), S (<10), N (1-2). Low sulphur coals are desired since they can cause SO<sub>2</sub>, NO<sub>x</sub> and particulate matter emissions which needs to be regulated to meet the air quality standards. Apart from this coal combustion results in high CO<sub>2</sub> emissions as compared to that from fossil fuels and disposal of solid coal from power plants also faces environmental hazard.

## **2.2. Thermodynamics**

Thermodynamics is science which deals with energy, its transformation and change accompanied in the state of matter. It has two concepts attached to it, one which is energy and entropy whose principles are the first and second law of thermodynamics.



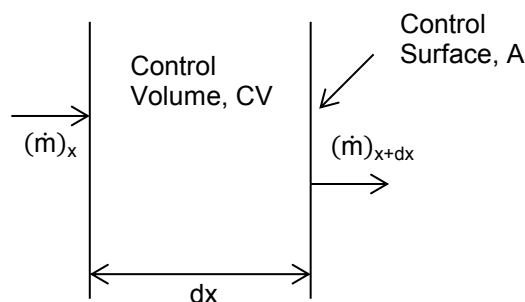
**Figure 2: Conservation equations and thermodynamics**

In thermodynamics, the principles of conservation includes,

- the **conservation of energy** which is given by the First law of thermodynamics which says that the energy can neither be created nor destroyed but can be transferred from one form to another
- the **conservation of mass** which is given by the continuity equation and,
- the **conservation of momentum** which is given by the Navier-Stokes equations.
- Heat transfer operations are often associated with masses or mass and momentum transfer processes.

The conservation equations derived below are taken from the book of S. R. Turns [8].

### Conservation of Mass



**Figure 3: Control Volume for 1-D analysis of mass conservation**

Consider a one dimensional (1-D) control volume as shown in Figure 3 of thickness  $dx$ . The rate of change of mass inside the control volume is the difference between the mass entering and leaving the control volume, which is given as below.

$$\dot{m} = (\dot{m})_x - (\dot{m})_{x+dx} \quad (2-1)$$

The above equation can be rewritten for  $m=\rho A dx$

$$\frac{\partial(\rho \cdot A \cdot dx)}{\partial t} = \frac{\partial(\rho \cdot A \cdot dx)_x}{\partial t} - \frac{\partial(\rho \cdot A \cdot dx)_{x+dx}}{\partial t} \quad (2-2)$$

Dividing through  $A \cdot dx$  and applying  $dx \rightarrow 0$ ,

$$\frac{\partial \rho}{\partial t} = - \frac{\partial(\rho \cdot u_x)}{\partial x} \rightarrow \text{this means} \rightarrow \boxed{\frac{\partial \rho}{\partial t} + \text{div}(\rho \cdot \vec{u}) = 0} \quad (2-3)$$

For steady flow, the left hand side = 0 gives

$$0 = \frac{\partial(\rho \cdot u_x)}{\partial x} \rightarrow \text{this means} \rightarrow \boxed{\rho \cdot u_x = \text{constant}} \quad (2-4)$$

## Conservation of Species

Similar to mass balance, the species conservation equation is formulated. For mass fraction  $Y_A$  for species A, the conservation equation is written as,

$$\frac{dm_A}{dt} = (\dot{m}_A'' \cdot A)_x - (\dot{m}_A'' \cdot A)_{x+dx} + \dot{m}_A''' \cdot V \quad (2-5)$$

Where,  $\dot{m}_A''$  is the mixture (bulk) mass flux of species A and  $\dot{m}_A'''$  = mass production rate of species A per unit volume.

For 1-D dimensional binary diffusion,  $\dot{m}_A''$  is expressed as the sum of bulk or total mixture mass flux ( $\dot{m}''$ ) and diffusion mass flux of species A ( $\dot{m}''_{A,diff}$ ) expressed through Fick's law as,

$$\dot{m}_A'' = (Y_A \cdot \dot{m}'') - (\dot{m}''_{A,diff}) = Y_A \cdot \dot{m}'' - \rho D_{AB} \frac{\partial Y_A}{\partial x} \quad (2-6)$$

Where,  $Y_A$  is the mass fraction of species A and  $D_{AB}$  is the binary diffusivity ( $m^2/s$ ).

Substituting in the above equation  $V = A \cdot dx$  and  $m_A = Y_A \cdot m = Y_A \cdot \rho \cdot V$  we get,

$$\frac{\partial(Y_A \cdot \rho \cdot A \cdot dx)}{\partial t} = \left[ A \left( Y_A \cdot \dot{m}'' - \rho D_{AB} \frac{\partial Y_A}{\partial x} \right) \right]_x - \left[ A \left( Y_A \cdot \dot{m}'' - \rho D_{AB} \frac{\partial Y_A}{\partial x} \right) \right]_{x+dx} + \dot{m}_A''' \cdot A \cdot dx \quad (2-7)$$

Dividing by A.dx and taking the limit as dx → 0, the above equation

$$\frac{\partial(Y_A \cdot \rho)}{\partial t} = -\frac{\partial}{\partial x} \left( Y_A \cdot \dot{m}'' - \rho D_{AB} \frac{\partial Y_A}{\partial x} \right) + \dot{m}_A''' \quad (2-8)$$

For steady flow,

$$\dot{m}_A''' - \frac{\partial}{\partial x} \left( Y_A \cdot \dot{m}'' - \rho D_{AB} \frac{\partial Y_A}{\partial x} \right) = 0 \rightarrow \text{This means} \rightarrow \boxed{\dot{m}_A''' - \text{div}(\dot{m}_A'') = 0} \quad (2-9)$$

The above equation can be rewritten as,

$$\underbrace{\frac{\partial}{\partial x} (Y_A \cdot \dot{m}'')}_{\text{Convection term}} - \underbrace{\frac{\partial}{\partial x} \left( \rho D_{AB} \frac{\partial Y_A}{\partial x} \right)}_{\text{Diffusion term}} = \underbrace{\dot{m}_A'''}_{\text{Net mass production}} \quad (2-10)$$

## Conservation of Energy

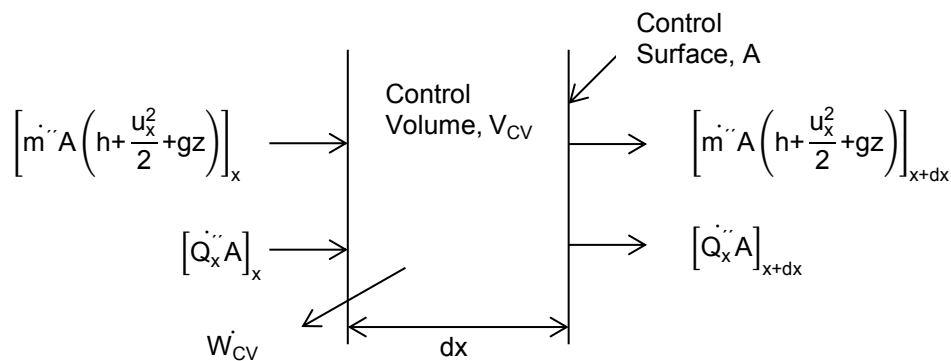


Figure 4: Control Volume for 1D, steady state analysis of energy equation [8]

In total, energy can be neither created nor destroyed. The temporal increase in the control volume stored energy is derived from the difference between energy inflow ( $\partial \dot{E}_{in}$ ) and outflow ( $\partial \dot{E}_{out}$ ) from the energy generated ( $\partial \dot{E}_g$ ) inside the body which is given below with the help of the general equation of energy balance as,

$$\partial \dot{E}_{\text{stored}} = \partial \dot{E}_{in} - \partial \dot{E}_{out} + \partial \dot{E}_g.$$

Figure 4 shows a control volume in one dimensional system; where in energy flows in and out of the plane layer of thickness dx.

According to the first law of thermodynamics,

$$\partial \dot{E}_{\text{stored}} = \left( \dot{Q}'' + \dot{m}''(e+pv) \right)_x \cdot A - \left( \dot{Q}'' + \dot{m}''(e+pv) \right)_{x+dx} \cdot A - W_{\text{CV}} \quad (2-11)$$

Where,  $e = u + \frac{1}{2}u_x^2 + gz$ , therefore  $(e+pv) = h + \frac{1}{2}u_x^2 + gz$  since  $h = u + pv$

$$\partial \dot{E}_{\text{stored}} = \left( \dot{Q}'' + \dot{m}'' \left( h + \frac{1}{2}u_x^2 + gz \right) \right)_x \cdot A - \left( \dot{Q}'' + \dot{m}'' \left( h + \frac{1}{2}u_x^2 + gz \right) \right)_{x+dx} \cdot A - W_{\text{CV}} \quad (2-12)$$

$$\partial \dot{E}_{\text{stored}} = (\dot{Q}_x'' - \dot{Q}_{x+dx}'')A - W_{\text{CV}} - \dot{m}'' A \left[ \left( h + \frac{u_x^2}{2} + gz \right)_{x+dx} - \left( h + \frac{u_x^2}{2} + gz \right)_x \right] \quad (2-13)$$

Assuming steady state ( $\partial \dot{E}_{\text{stored}} = 0$ ), no work done by the control volume and no change in potential energies of the inlet and outlet streams and dividing the above equation by A gives,

$$(\dot{Q}_x'' - \dot{Q}_{x+dx}'') = \dot{m}'' \left[ \left( h + \frac{u_x^2}{2} \right)_{x+dx} - \left( h + \frac{u_x^2}{2} \right)_x \right] \quad (2-14)$$

Dividing both sides by  $\partial x$  (where  $\partial x \rightarrow 0$ ) and with the definition of derivative

$$\frac{\partial \dot{Q}_x''}{\partial x} = \dot{m}'' \left( \frac{\partial h}{\partial x} + u_x \frac{\partial u_x}{\partial x} \right) \quad (2-15)$$

$\dot{Q}_x''$ ; heat flux comprises of heat flux through conduction as well as the enthalpy flux of species diffusing in and out of the control volume. Assuming no radiation, the heat flux in its vector form in general form is,

$$\dot{Q}_x'' = -\lambda \cdot \partial T + \sum \dot{m}_{i,\text{diff}}'' \cdot h_i \quad (2-16)$$

Where  $\dot{m}_{i,\text{diff}}''$  is the diffusion mass flux of species i and is given by  $\dot{m}_{i,\text{diff}}'' = \rho Y_i u_{i,\text{diff}} = \rho Y_i (u_{i,x} - u_x)$  where  $u_{i,x}$  and  $u_x$  are species velocity (total velocity) and bulk velocity resp.

For the 1-D plane layer the above equation can be rewritten as,

$$Q_x'' = -\lambda \frac{\partial T}{\partial x} + \sum \rho Y_i (u_{i,x} - u_x) h_i \Rightarrow Q_x'' = -\lambda \frac{\partial T}{\partial x} + \sum \rho Y_i u_{i,x} h_i + \sum \rho Y_i u_x h_i \quad (2-17)$$

$$Q_x'' = -\lambda \frac{\partial T}{\partial x} + \sum \dot{m}_i'' h_i + \sum \dot{m}'' u_x \quad (2-18)$$

Where,  $\dot{m}_i'' = \rho Y_i u_{i,x}$  and  $\dot{m}'' = \rho u_x$  and  $\sum Y_i h_i = h$

Substituting the value of  $Q_x''$  in the main equation we get,

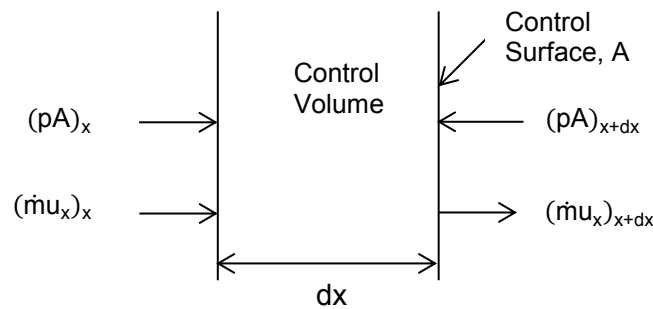
$$\frac{\partial}{\partial x} \left( -\lambda \frac{\partial T}{\partial x} \right) + \frac{\partial}{\partial x} \left( \sum \dot{m}_i'' h_i \right) + \dot{m}'' u_x \frac{\partial u_x}{\partial x} = 0 \quad (2-19)$$

Substituting  $\frac{\partial}{\partial x} (\sum \dot{m}_i'' h_i) = \sum \dot{m}_i'' \frac{\partial h_i}{\partial x} + \sum h_i \frac{\partial \dot{m}_i''}{\partial x}$  &  $\frac{\partial \dot{m}_i''}{\partial x} = \dot{m}_i'''$  in the above equation,

$$\frac{\partial}{\partial x} \left( -\lambda \frac{dT}{dx} \right) + \sum \dot{m}_i'' \frac{\partial h_i}{\partial x} + \dot{m}'' u_x \frac{\partial u_x}{\partial x} = - \sum \dot{m}_i''' h_i \quad (2-20)$$

This equation is the energy equation for multicomponent and binary systems.

### Conservation of Momentum



**Figure 5: Control Volume for 1-D analysis of momentum equation (neglecting all effects of viscosity) [8]**

For a steady state, momentum conservation is expressed as the sum of all forces acting on a control volume in a given direction equal to the net force acting on the control volume in the same direction. For a 1-D system it is given by,

$$(pA)_x - (pA)_{x+dx} = \dot{m} ([u_x]_{x+dx} - [u_x]_x) \quad (2-21)$$

Dividing the left- and right hand sides of the above equation with dx (taking limit  $\partial x \rightarrow 0$ ) and recognising that A and  $\dot{m}$  are constant, we get differential equation,

$$-\frac{\partial p}{\partial x} = \dot{m}'' \frac{\partial u_x}{\partial x} \quad (2-22)$$

Substituting mass flux as  $\dot{m}'' = \rho u_x$  in the above equation we get,

$$-\frac{\partial p}{\partial x} = \rho u_x \frac{\partial u_x}{\partial x} \quad (2-23)$$

## 2.3. Chemical Kinetics

The laws of thermodynamics deal with the “Equilibrium states” of a chemical reaction system. Chemical Kinetics is the study of rates at which the chemical reactions occurs in a chemical system on time scales comparable with the flow and other molecular transport processes. This part of the text has been taken from the book of J. Warnatz, U. Maas and R.W. Dibble [13].

From the standpoint of combustion, the interest in chemical kinetic phenomena is generally to know the conditions required for a reaction to be explosive (i.e. very rapid reaction). However, recently the research has been diverted to the non-explosive or steady reactions since the most complex pollutants are formed in steady zone and low temperature of these reactions [14].

### 2.3.1. Rate law and direction of reaction

For a chemical reaction,



Where, A, B and C are reactants and D, E and F are products. Thus, from the law of mass action (or chemical equilibrium), the rate of decomposition of A is proportional to the product of the concentrations of the reactants raised to their corresponding stoichiometric coefficient [14] which is given as;

$$\frac{d[A]}{dt} = -k \cdot [A]^a \cdot [B]^b \cdot [C]^c \quad (2-25)$$

Here a, b and c denote the reaction orders for the species A, B and C respectively and k is the rate coefficient of that reaction. Sum of a, b and c gives the overall reaction order.



The same equation above for simplification can be rewritten for constant B and C concentrations as;

$$\frac{d[A]}{dt} = -k_{\text{exp}} \cdot [A]^a \quad (2-26)$$

Where,  $k_{\text{exp}} = k \cdot [B]^b \cdot [C]^c$ .

The temporal change for the species A can be calculated by integrating the above equation. The different forms of equations for different orders of reactions are as follows;

$$1^{\text{st}} \text{ order (a=1): } \ln \frac{[A]_t}{[A]_0} = -k_{\text{exp}} \cdot (t-t_0) \quad (2-27)$$

$$2^{\text{nd}} \text{ order (a=2): } \frac{1}{[A]_t} - \frac{1}{[A]_0} = k_{\text{exp}} \cdot (t-t_0) \quad (2-28)$$

$$3^{\text{rd}} \text{ order (a=3): } \frac{1}{[A]_t^2} - \frac{1}{[A]_0^2} = 2k_{\text{exp}} \cdot (t-t_0) \quad (2-29)$$

For reverse reaction subscripted as (r), the rate law for producing A will be;

$$\frac{d[A]}{dt} = k^{(r)} \cdot [D]^d \cdot [E]^e \cdot [F]^f \quad (2-30)$$

At chemical equilibrium, both forward and backward reactions have the same rate on microscopic level. But if we consider macroscopic level, we do not observe any net reaction. Therefore, we can say that for a chemical equilibrium,

$$k^{(f)} \cdot [A]^a \cdot [B]^b \cdot [C]^c = k^{(r)} \cdot [D]^d \cdot [E]^e \cdot [F]^f \quad (2-31)$$

Or

$$\frac{k^{(f)}}{k^{(r)}} = \frac{[D]^d \cdot [E]^e \cdot [F]^f}{[A]^a \cdot [B]^b \cdot [C]^c}$$

Where  $\frac{k^{(f)}}{k^{(r)}} = K_c = \text{Equilibrium constant of the reaction}$

$$\text{Therefore, } \frac{k^{(f)}}{k^{(r)}} = K_c = \exp(-\Delta_R \overline{A}^0 / RT) \quad (2-32)$$

In kinetic calculations, using experimental forward rates, the backward rates are calculated from the equilibrium constant or vice versa.

### 2.3.2. Temperature dependence of rate coefficients

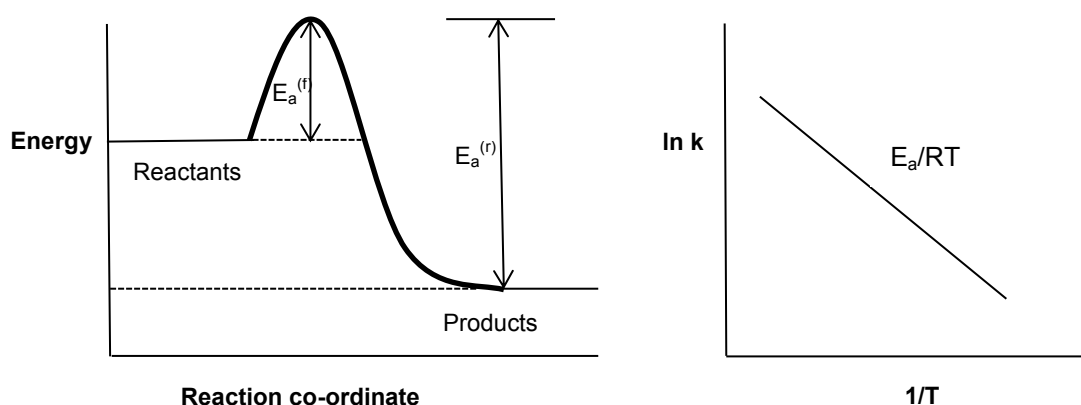
Svante Arrhenius in 1889 has developed a formula for the temperature dependence of rate coefficients which is called the Arrhenius law. According to Arrhenius, the rate

coefficients of a reaction increases exponentially (until it reaches a limit) with the increase in temperature. The rate constant  $k$  is given as;

$$k = A' \cdot \exp(-E_a/RT) \quad (2-33)$$

Where,  $A'$  = pre-exponential factor,  $E_a$ =activation energy,  $R$ =universal gas constant and  $T$ = absolute temperature. The temperature dependence of pre-exponential factor is given by,

$$k = A \cdot T^n \exp(-E_a/RT) \quad (2-34)$$



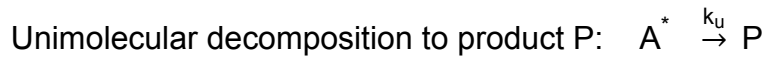
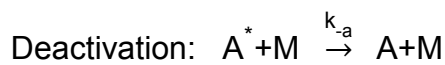
**Figure 6: Energy diagram (left) and Arrhenius plot (right)**

The temperature dependency of rate of chemical reaction can be expressed through Arrhenius plot as shown in Figure 6. It is usually expressed as  $\log k$  versus  $1/T$  and the activation energy is extracted from the slope which is given by  $E_a/RT$ .

In case of  $E_a=0$  or at high  $T$  values, the exponential term disappears and  $k$  is a function only of  $A'$  or  $(A \cdot T^n)$ . For unimolecular reactions, the value of  $A$  corresponds to the lifetime of the reactive molecule which is determined by bond vibration frequency (typically  $A' = 10^{14} - 10^{15} \text{ s}^{-1}$ ). While for bimolecular reactions  $A'$  corresponds to rate of collision and reaction probability (typically  $A' = 10^{13} - 10^{14} \text{ s}^{-1}$ ). In case of trimolecular reactions third body or collision partner (often denoted as  $M$ ) is involved, which is responsible to remove the energy of the reaction. In such reactions if there is no energy transfer, the product formed would dissociate back to its original constituents.

### 2.3.3. Pressure dependence of rate coefficients

**Lindemann model:** Lindemann in 1922 showed that the rate coefficients for dissociation and recombination of reactions are pressure dependent. According to the *Lindemann model*, unimolecular decomposition is only possible if it has been activated externally by some energy in order to break the bond. The activation leads to the excitation of the molecule which in turn might lead either to the deactivation of the reaction or decomposition into products. If A is a reactant specie and M is the non-reacting collision partner, then



The rate equations for this example are given as

$$\frac{d[P]}{dt} = k_u \cdot [A^*] \quad , \quad \frac{d[A^*]}{dt} = k \cdot [A] \cdot [M] - k_{-a} \cdot [A^*] \cdot [M] - k_u \cdot [A^*] \quad (2-36)$$

Assuming quasi-steady state for the intermediate  $A^*$  ( $\frac{d[A^*]}{dt} \approx 0$ ), its concentration is calculated as

$$[A^*] = \frac{k_a \cdot [A] \cdot [M]}{-k_{-a} \cdot [M] + k_u} \quad \text{and} \quad \frac{d[P]}{dt} = \frac{k_u k_a \cdot [A] [M]}{k_{-a} \cdot [M] + k_u} \quad (2-37)$$

At low pressures the concentration of collision partners is very small such that  $k_{-a} \cdot [M] \ll k_u$  we obtain an apparent second order rate law,

$$\frac{d[P]}{dt} = k_a \cdot [A] [M] = k_0 \cdot [A] [M] \quad (2-38)$$

Where  $k_0$  is the low pressure rate coefficient

At high pressures the concentration of collision partners is very large such that  $k_{-a} \cdot [M] \gg k_u$  we obtain an apparent first order rate law,

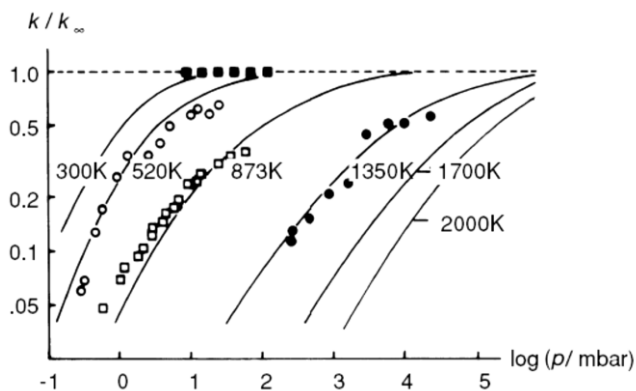
$$\frac{d[P]}{dt} = \frac{k_u k_a \cdot [A]}{k_{-a}} = k_\infty \cdot [A] \quad (2-39)$$

Where  $k_\infty$  is the high pressure rate coefficient

Therefore, when the pressure is increased, M increases and at high enough pressures the unimolecular decomposition dominates. While at low pressures, the

reaction rate highly depends on M. Thus, Lindemann model illustrates the pressure dependence of reaction rates but is limited only to one activated species.

For a large number of activated molecules different levels of activation (i.e. vibration or rotation) is required which is taken into account by *Theory of Unimolecular reactions*. This theory yields the so called **fall-off curves** which describe the pressure dependence of rate coefficients. The curves are obtained by plotting logarithm of rate coefficient versus the logarithm of pressure as shown in Figure 7.



**Figure 7: Fall-off curves for the unimolecular reaction  $C_2H_6=CH_3+CH_3$  ([13])**

For  $p \rightarrow \infty$ , the rate coefficient becomes independent of pressure

$$k = \frac{k_u k_a [M]}{k_{-a} [M] + k_u} \rightarrow k_\infty \quad (2-40)$$

For low pressures, the rate coefficient is proportional to  $[M]=p/RT$  which results in linear dependence.

The reaction rate  $k$  will decrease with temperature if the  $k_\infty$  has low activation energy.

**F-center treatment of Troe:** The pressure dependent reactions need appropriate treatment since much reaction kinetic experiments are done at atmospheric or low pressures while many processes in combustion operate at high pressures. Troe introduced four parameters to determine the rate coefficient at specified temperature and pressure (Table V below). The first line in the table gives the reaction along with the modified high pressure rate parameters, the second line the modified low pressure rate parameters, and the third line four parameters  $a$ ,  $T^{***}$ ,  $T^*$ ,  $T^{**}$ .

Reaction	A[cm,mol,s]	n	E <sub>a</sub> (kJ/mol)
OH + OH + M(1) = H <sub>2</sub> O <sub>2</sub> + M(1)	1.57E13	0.0	0.0
	LOW	5.98E19	-0.8 0.0
	TROE	0.50	0.0 0.0 0.0
	(a)	(T <sup>***</sup> )	(T <sup>*</sup> ) (T <sup>**</sup> )

**Table V: Example of Arrhenius parameters for pressure dependent reactions [13]**

The F-center value of the fall-off range is determined using the four parameters as,

$$F_{\text{cent}} = a \cdot \exp\left(\frac{T}{T^*}\right) + \exp\left(\frac{T}{T^{**}}\right) + (1-a) \cdot \exp\left(\frac{T}{T^{***}}\right) \quad (2-41)$$

This is in turn is used to determine F as,

$$\log F = \log F_{\text{cent}} \left\{ 1 + \left[ \frac{\log P_r + c}{n - d \cdot (\log P_r + c)} \right]^2 \right\}^{-1} \quad (2-42)$$

Where,  $c = -0.4 - 0.67 \log F_{\text{cent}}$ ,  $n = 0.75 - 1.27 \log F_{\text{cent}}$ ,  $d = 0.14$  and  $P_r = k_0 \cdot [M] / k_\infty$

Using the reaction rate is calculated from the equation,

$$k = k_\infty \left[ \frac{P_r}{1 + P_r} \right] \cdot F \quad (2-43)$$

## 2.4. Reaction Modelling

LOGEsoft [15] is a software specialized in analyzing and simulating complex chemistry processes in engineering applications and has been used as the modelling platform for this thesis work.

### 2.4.1. Reaction Mechanism

Reaction mechanism is a set of elementary reactions that are involved in the oxidation of a certain fuel at a certain temperature range from high to low.

Elementary reaction is the reaction which occurs exactly in the way which is described by the equation on the molecular level. Global reactions are a combination of several elementary reactions. A reaction mechanism is much complex and involves the elementary reactions taking place during combustion of a certain fuel in presence of an oxidizer. Since it describes the chemical kinetics it is also called kinetic mechanism. The reaction mechanism is a model developed with values of reaction rates obtained from experiments or from theory and is assumed to be

expressing the reality. This is checked by validating the mechanism against experimental data. It is a method to save time and money needed for experiments and also the burning of real fuels. The key to a good kinetic mechanism lies deep within chemical kinetics.

The kinetic model is composed of chemical reactions for the fuel along with the base mechanism. For the validation, we need thermodynamic data and transport data for the species involved. These are explained in detail in the following parts. The scheme of steps in model development and validation is expressed in Figure 8.

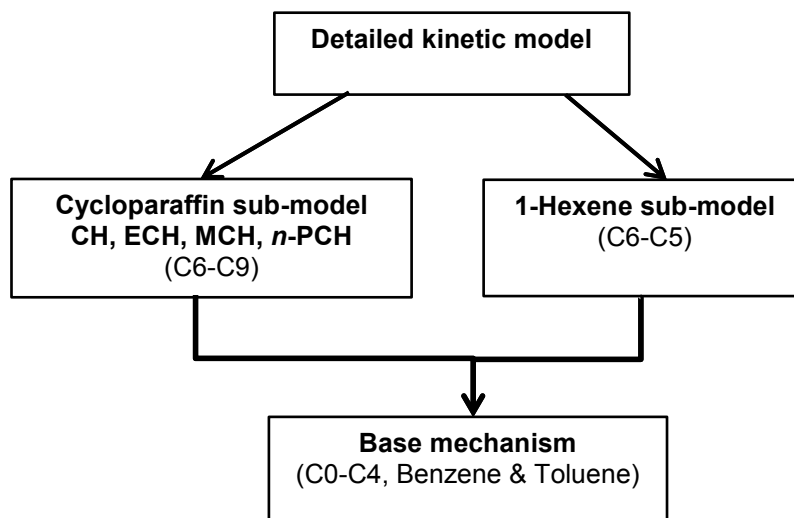


Figure 8: Scheme of Model development and validation, *n*-Propylcyclohexane (*n*-PCH), and smaller cycloalkanes (CH, ECH, MCH) and 1-Hexene (C<sub>6</sub>H<sub>12</sub>-D1)

#### 2.4.2. Pre-requisites of Reaction mechanisms

This part has been taken from the Book of Warnatz, Maas and Dibble [13].

**Thermodynamic data** are the chemical information of species for their heat capacity  $C_p$ , enthalpy and entropy stored as polynomials as a function of temperature. These are called the NASA polynomials.

The molar heat capacity  $\bar{C}_p^0$  is expressed as five-term polynomial of fourth order in temperature as,

$$\bar{C}_p^0/R = a_1 + a_2 \cdot T + a_3 \cdot T^2 + a_4 \cdot T^3 + a_5 \cdot T^4 \quad (2-44)$$

Along with these five constants  $a_1$  to  $a_5$ , two more constants are needed to take into account the enthalpy and entropy, viz.  $a_6$  and  $a_7$  respectively.

The enthalpy and entropy at any temperature T are calculated from the heat capacity as follows;

$$\bar{H}_T^0/R = a_6 + a_1 + \frac{a_2}{2} \cdot T^2 + \frac{a_3}{3} \cdot T^3 + \frac{a_4}{4} \cdot T^4 + \frac{a_5}{5} \cdot T^5 \quad (2-45)$$

$$\bar{S}_T^0/R = a_7 + a_1 \cdot \ln T + a_2 \cdot T + \frac{a_3}{2} \cdot T^2 + \frac{a_4}{3} \cdot T^3 + \frac{a_5}{4} \cdot T^4 \quad (2-46)$$

They are defined by setting temperature at 298K and demanding the standard enthalpy and standard entropy at 298K is equal to the enthalpy and entropy respectively at 298K.

The seven-term polynomial consists of 14 constants. The first set of 7 constants belong to the polynomial in the high range of temperature ( $T > 1000K$ ) and the second set of constants belong to the low temperature range ( $T < 1000K$ ) polynomial separated by break temperature usually at  $T = 1000K$  (See Table VI ).

These values have been calculated for an extensive number of species and managed in a database from Goos database [16]. Most of the values used in this thesis have been obtained from this source. For the missing species, the data is calculated using Benson's additivity method [17].

O	L 1/900	1	G	200.000	3500.000	1000.000	1
2.569428E+00	-8.597411E-05	4.194845E-08	-1.001777E-11	1.228336E-15			2
2.921757E+04	4.784338E+00	3.168267E+00	-3.279318E-03	6.643063E-06			3
-6.128066E-09	2.112659E-12	2.912225E+04	2.051933E+00				4

**Table VII: Example of thermodynamic data in form of NASA polynomials (Goos, Burcat, Ruscic [16]) Marked in grey are the first set of polynomials for high temperature.**

## Transport coefficients

The molecular transport processes are mass transfer, heat transfer and momentum transfer. Concentration gradients lead to mass transfer i.e. diffusion, temperature gradients lead to heat transfer i.e. heat conduction and velocity gradients leads to momentum transfer i.e. viscosity. Thus, these processes describe the transport of physical properties by the movement of gas molecules. The values of these properties are calculated from the Transport data file contents (described below).

To account for the intermolecular interaction which differs from the ideal potential of rigid elastic spheres, the Lennard-Jones potential model is used which is characterized by  $\epsilon$ = potential well depth or intermolecular interaction,  $\sigma$ = finite distance at which inter-particle potential is zero or molecular diameter which are then used to calculate the reduced collision integral  $\omega$ . The reduced collision integral is a unique function of the reduced temperature  $T^*$  which is defined by  $T^* = kT/\epsilon$ .

**Viscosity of gases:** Viscosity  $\eta$  is the measure of fluids resistance to flow and is a result of velocity gradient. Applying the kinetic theory of gases using the intermolecular potential model of rigid spheres, viscosity  $\eta$  is proportional to a product of particle density  $[n]$ , mean velocity  $\bar{u}$ , molecular mass  $m$  and mean free path  $l_{coll}$  which is,  $\eta \propto [n] \cdot \bar{u} \cdot m \cdot l_{coll}$  which leads to species viscosity of,

$$\eta_i = \frac{5}{16} \frac{\sqrt{\pi} \cdot m \cdot k \cdot T}{\pi \cdot \sigma_i^2 \omega_i(T)} = \frac{\lambda_{rigid\ sphere}}{\omega_i(T^*)} \quad (2-47)$$

For mixtures, the viscosity is given by,

$$\eta = \frac{1}{2} \left[ \sum_i \bar{x}_i \eta_i + \left( \sum_i \frac{\bar{x}_i}{\eta_i} \right)^{-1} \right] \quad (2-48)$$

**Thermal conductivity:** The temperature gradient causes heat transfer to occur which is defined by thermal conductivity  $\lambda$ . The kinetic theory of gases accounting for molecular interaction yields  $\lambda$  to be proportional to mean velocity  $\bar{u}$ , molecular heat capacity  $c_v$  and mean free path  $l_{coll}$  which is,  $\lambda \propto [n] \cdot \bar{u} \cdot c_v \cdot l_{coll}$  which leads to species conductivity of,

$$\lambda_i = \frac{25}{32} \frac{\sqrt{\pi} \cdot m \cdot k \cdot T}{\pi \cdot \sigma_i^2 \omega_i(T)} \cdot \frac{c_v}{m} = \frac{\lambda_{rigid\ sphere}}{\omega_i(T^*)} \quad (2-49)$$

Thermal conductivity of the mixture can be calculated from the thermal conductivities  $\lambda_i$  and mole fractions  $\bar{x}_i$  of the  $i$  species as,

$$\lambda = \frac{1}{2} \left[ \sum_i \bar{x}_i \lambda_i + \left( \sum_i \frac{\bar{x}_i}{\lambda_i} \right)^{-1} \right] \quad (2-50)$$



**Diffusion in gases:** Concentration gradient results in mass flux which is defined in terms of diffusion coefficient  $D$ . Applying the kinetic theory of gases and using the intermolecular potential model of rigid spheres, gives the diffusion coefficient to be proportional to the product of mean velocity  $\bar{u}$  and mean free path  $l_{coll}$  which is,  $D \propto \bar{u} \cdot l_{coll}$  which leads to species diffusion of,

$$D = \frac{3}{8} \frac{\sqrt{\pi \cdot m \cdot k \cdot T}}{\pi \cdot \sigma_i^2 \omega_i(T)} \cdot \frac{1}{\rho} = \frac{D_{\text{rigid sphere}}}{\omega_i(T)} \quad (2-51)$$

For a mixture of two compounds, binary diffusion coefficient  $D_{12}$  is obtained by replacing  $m$  with reduced mass  $(m_1 \cdot m_2 / m_1 + m_2)$  and mean molar parameters  $\sigma_i$  and  $\epsilon$  by  $\sigma_{12} = \sigma_1 + \sigma_2 / 2$  and  $\epsilon_{12} = \sqrt{\epsilon_1 + \epsilon_2}$

$$D_{12} = \frac{3}{8} \frac{\sqrt{\pi \cdot k \cdot T \cdot \frac{m_1 \cdot m_2}{m_1 + m_2}}}{\pi \cdot \sigma_{12}^2 \omega_i(T_{12}^*)} \cdot \frac{1}{\rho} \quad (2-52)$$

For mixtures, the diffusion coefficients are expressed as,

$$D_i = \frac{1 - x_i}{\sum_{j \neq i} \frac{x_j}{D_{ij}}} \quad (2-53)$$

**Molecular data file in LOGEsoft:** Example for transport data is shown in Table VII where column;

1. is the specie name,
2. is the structure indicator (0=atom, 1=linear and 2= non-linear molecule respectively).
3. is Lennard-Jonnes potential well depth,  $\epsilon/K$  (where  $K$ =Boltzmann constant)
4. is Lennard-Jonnes potential collision diameter,  $\sigma$
5. is the bond-dipole moment,  $\mu$
6. is the polarizability,  $\alpha$
7. is the rotational collision number,  $Z_{rot}$  (298 K)

C	0	71.4	3.3	0.0	0.0	0.0
H	0	145.0	2.05	0.0	0.0	0.0
O	0	80.0	2.75	0.0	0.0	0.0

**Table VII :** Table showing examples of Transport data in LOGEsoft [15]

### 2.4.3. Analysis of Reaction mechanisms

A reaction mechanism can be very huge and consume lot of resources. Many reactions can be neglected maintaining the result. Question is how to choose which reactions to neglect. The answer is given through some important instruments of analysis viz. **flow analysis** which determines the important reaction pathways and **sensitivity analysis** which identifies the rate limiting reactions. The description has been adopted from the manual of LOGEsoft [15].

#### Flow analysis

Reaction flow analysis (or simply flow analysis) gives the important pathways of the fuel decomposition and the related species. It is calculated in LOGEsoft by the transfer rate of elements between species. LOGEsoft predicts the important species involved through determination of the flows of atoms between the different reacting molecules. An integral flow analysis is the one considering the overall consumption or formation of species. The reaction flow of atom *a* between species *i* and species *j* is given by [15],

$$f_{i,j}^a = \sum_{k=1}^{N_r} \omega_k (n_i^a v_{i,k} - n_j^a v_{j,k}) \quad (2-54)$$

Where,  $\omega_k$  is the reaction rate of the set of  $N_r$  irreversible reactions,  $n_i^a$  and  $n_j^a$  are the numbers of atom *a* in molecules *i* and *j* resp. while  $v_{i,k}$  and  $v_{j,k}$  are the stoichiometric coefficients of molecules *i* and *j* respectively in reaction *k*.

LOGEsoft gives the possibility to look at the formation and consumption of species separately which makes it able to capture the reversible reactions pairs with high forward and backward rates which would otherwise not affect the net flow.

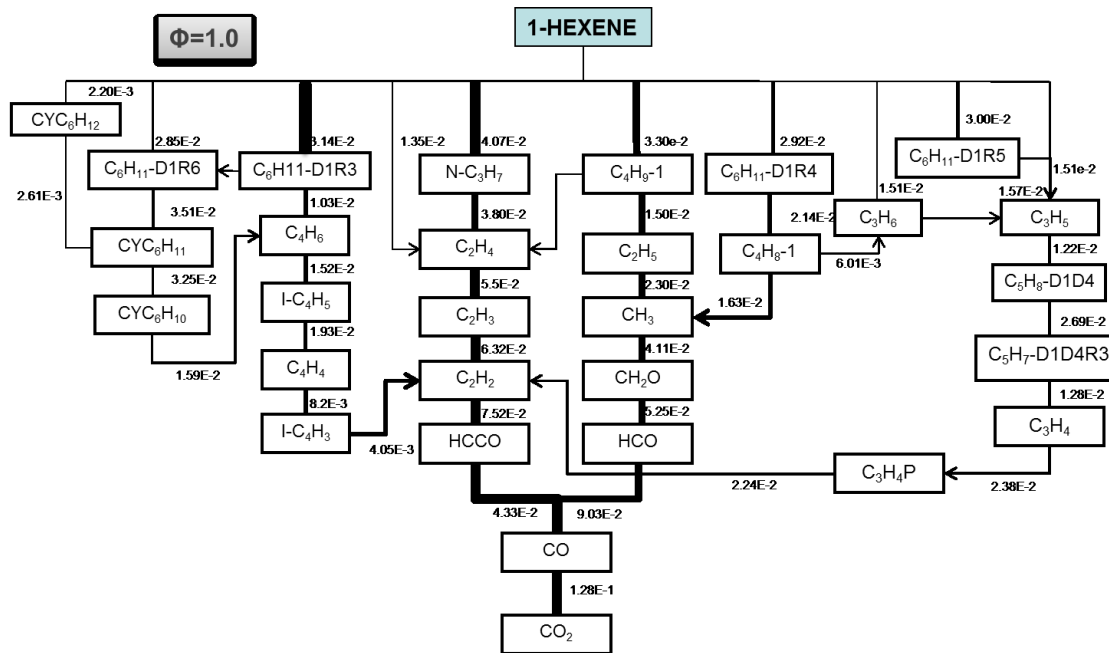
$$\text{Formation of species: } f_{i,j}^a = \sum_{k_f=1}^{N_r} (\omega_{k_f} \cdot v'_{j,k_f} \cdot v''_{i,k_f}) \frac{n_i^a}{\Delta n_{k_f}^a} \quad (2-55)$$

$$\text{Consumption of species: } c_{i,j}^a = \sum_{k_b=1}^{N_r} (\omega_{k_b} \cdot v'_{j,k_b} \cdot v''_{i,k_b}) \frac{n_j^a}{\Delta n_{k_b}^a} \quad (2-56)$$

Where,  $f$  denotes formation and  $c$  denotes consumption,  $\Delta n_{k_f}^a = \sum_{i=1}^{N_s} \nu'_{i,k_f} n_i^a$ , the total number of atoms  $a$  is normalised to the total number of atoms transported in the reaction.

The net integral flow is calculated by taking integral over time as,

$$F_{i,j}^a = \int_{t=t_0}^{t_1} f_{i,j}^a dt - \int_{t=t_0}^{t_1} c_{i,j}^a dt \quad (2-57)$$



**Figure 9: Flow analysis for a premixed laminar flame for 1-hexene/air mixture  $\phi=1.0$ ,  $p=15$  Torr at 353 K [18]**

Figure 9 gives one example of integral flow analysis of 1-hexene in a jet stirred reactor at 750 K for stoichiometric mixture. The number on the branch indicates the integrated carbon flow in  $\text{mol}/\text{cm}^3$ . This graph shows the flow of C-atoms for the reaction mechanism of 1-hexene. It can be seen that the consumption of 1-hexene is taking through several paths but the most important is the one forming the  $\text{N-C}_3\text{H}_7$  radical. It is also important to look at the other important species in the flow and in general if it makes logical sense. Sometimes, irrational rates bring up the species in the flow analysis but it is also important to note such species. Also, the flow analysis will change according to the conditions one chooses, like stoichiometry and temperature or pressure ranges.

## Sensitivity Analysis

The conservation equations for mass, species, energy are presented in Section 2.2 can be generally formulated as  $F(c, y_i, h) = 0$ . Ideal reactors at constant “p” work at constant “h”. Further the chemical rate coefficients are important parameters of the system, hence the system of equations can be reformed as  $F(c_1 \dots c_s, k_1 \dots, k_r)$ .

Sensitivity as the name suggests is the sensitivity of the reaction rates on the concentration of the species. Changes in such reaction rates of such reactions changes the outcome and thus are called rate determining steps. For R reactions among S species, the absolute and relative sensitivities are given as

$$E_{i,r} = \frac{\partial c_i}{\partial k_r} \quad \text{and} \quad E_{i,r}^{\text{rel}} = \frac{k_r}{c_i} \frac{\partial c_i}{\partial k_r} = \frac{\partial \ln c_i}{\partial \ln k_r} \quad (2-58)$$

Where,  $c_i$  is the species concentrations for i variables,  $k_r$  is the parameter under consideration.

The sensitivity analysis is done automatically using LOGEsoft. The numeric behind it are given by differentiating the rate law given as

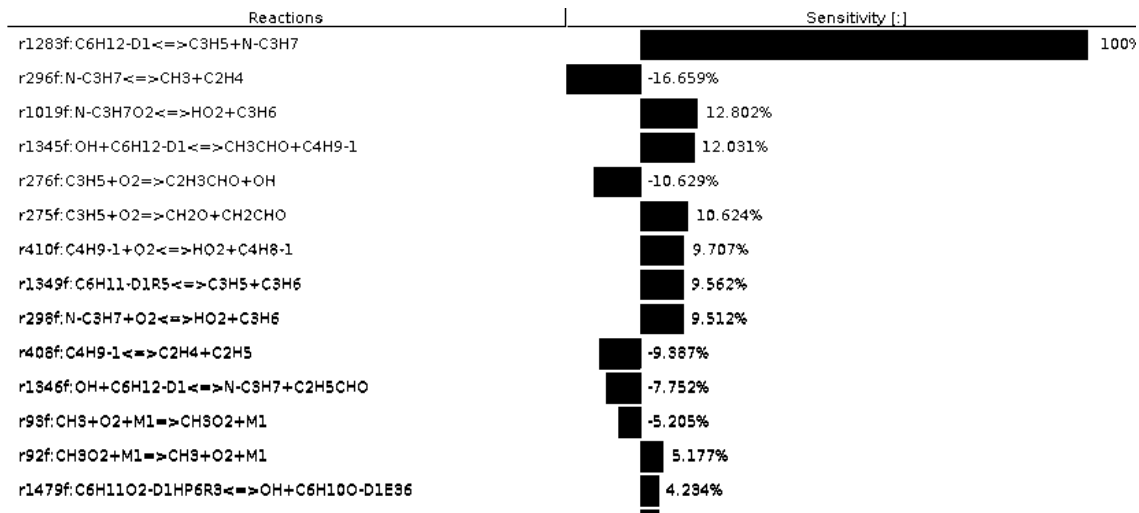
$$\frac{\partial}{\partial k_r} \left( \frac{\partial c_i}{\partial t} \right) = \frac{\partial}{\partial k_r} F_i(c_1, \dots, c_s; k_1, \dots, k_R) \quad (2-59)$$

Rearranging and using partial derivative keeping  $c_i$  and  $c_{i \neq n}$  as constant except  $c_n$ ,

$$\frac{\partial}{\partial t} \left( \frac{\partial c_i}{\partial k_r} \right) = \left( \frac{\partial F_i}{\partial k_r} \right)_{c_i, k_l \neq R} + \sum_{n=1}^S \left\{ \left( \frac{\partial F_i}{\partial c_n} \right)_{c_i \neq n, k_l} \left( \frac{\partial c_n}{\partial k_r} \right)_{k_l \neq j} \right\} \quad (2-60)$$

$$\frac{\partial}{\partial t} E_{i,r} = \left( \frac{\partial F_i}{\partial k_r} \right)_{c_i, k_l \neq R} + \sum_{n=1}^S \left\{ \left( \frac{\partial F_i}{\partial c_n} \right)_{c_i \neq n, k_l} E_{n,r} \right\} \quad (2-61)$$

This system of linear differential equations is solved automatically in LOGEsoft to find the sensitivity. Examples from the software output are shown in Figure 10. The pathway from flow analysis which gives N-C<sub>3</sub>H<sub>7</sub> as the important species comes up in the sensitivity analysis. But here it becomes clear the reaction responsible for this. This is the rate limiting step and is important that the reaction rates are accurate. Other important reactions are also seen in the Figure 10 and the rates for these can be checked for accuracy to get the best result.



**Figure 10: Sensitivity coefficients for shock tube ignition delay for 1-hexene/air mixture  $\phi=1$ ,  $p=10$  bar at 750K**

## 2.5. Combustion Reactors

Fundamental combustion properties of a combustible fuel mixture are ignition characteristics, laminar flame speed etc. Knowledge about ignition characteristics will help to design the engine devoid of auto-ignition which is harmful to it and also to optimize mixing time so that the emissions are controlled. The combustion properties are studied in experimental reactors which are able to reproduce the thermodynamic conditions of real combustors like internal combustion engines, turbines etc. where combustion takes place. Below are few common reactors used for experimental studies.

### 2.5.1. Shock tubes

The description of the principle of a shock tube is taken from the book of B. Leclerc, Simmie and Blurock [19]. A shock tube is a device which is used for measuring the ignition delay times of hydrocarbons through development of a shock wave. The tube consists of two regions; high pressure region and low pressure region separated by a diaphragm which is ruptured in order to form a shock wave which propagates in the low pressure region where the species of interest are contained. The shock wave heats up the test gas and increases its pressure and maintains it until the expansion fan wave cools the sample rapidly (quenching) maintaining the composition. The sampling is conducted during this time using mass spectrometer or gas chromatography depending upon when the sampling is done.

Every experiment collects information on speciation with respect to pressure and temperature. A scheme of a shock tube is shown in Figure 11 below. The temperature behind the incident shock wave is low and so is the retention time as compared to that behind the reflected shock wave. The pressure remains constant for some time after the arrival of reflected shock wave and due to arrival of the expansion fan it rapidly decreases.

Suitable quantitative monitors of the ignition event could be

- the maximum in light output, or other spectroscopic data, or
- the maximum rate of temperature or pressure change in a closed system.

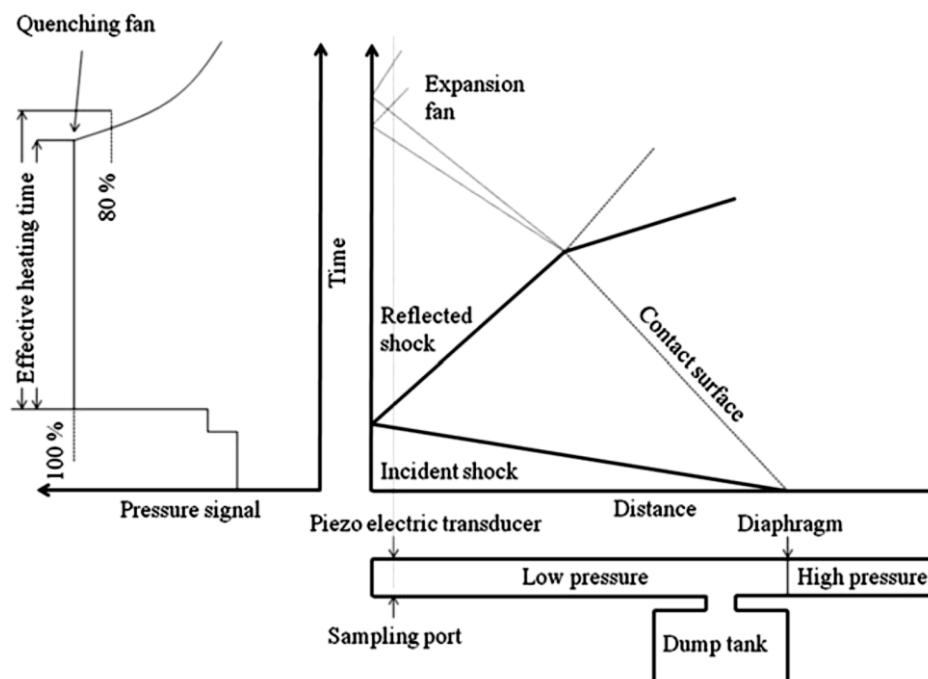


Figure 11: Scheme of a shock tube [19]

### Analysis and governing equations

Conservation laws applied here are considering shock tube as a constant volume reactor which is a closed system where volume is constant and pressure is allowed to change.

Mass conservation is given by equation (2-4) and for a closed system is,

$$\frac{\partial m}{\partial t} = 0 \quad (2-62)$$

Species conservation is simplified to,

$$\frac{\partial Y_i}{\partial t} = \frac{\dot{m}_i'''}{\dot{m}'''} = \frac{\dot{m}_i''' W_i}{\rho} \quad (2-63)$$

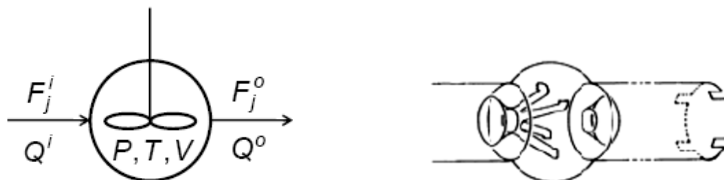
The energy conservation is in terms of internal energy since volume is constant

$$\rho c_v \frac{\partial T}{\partial t} = \sigma \varepsilon \frac{A}{V} (T^4 - T_w^4) - \sum_i^{N_s} \dot{m}_i''' U_i \text{ or} \quad (2-64)$$

$$\rho c_v \frac{\partial T}{\partial t} = \frac{\partial}{\partial x} \left( -\lambda \frac{\partial T}{\partial x} \right) - \sum \dot{m}_i''' U_i$$

### 2.5.2. Jet Stirred Reactor

A perfectly stirred reactor is an ideal reactor in which mixing is perfectly achieved inside a control volume. The jet stirred reactor (JSR) is a type of perfectly stirred reactor. The oxidation and pyrolysis of hydrocarbons and oxygenated fuels is studied in such reactors. JSR coupled with a gas chromatograph helps to record the reactant conversion into products as a function of different parameters like reaction temperature, pressure and composition of the inlet gas along with the residence time. When operated at a steady state and constant residence time, temperature and pressure, the JSR can be easily modelled by simple mass balance. Figure 12 shows a typical scheme of a JSR.



**Figure 12: Schematic of a jet stirred reaction a) simplified scheme b) Real view of a jet stirred reactor [2]**

It is composed of a sphere often made up of fused silica or Pyrex glass in which the reaction takes place. The fresh gas enters through the inlet and goes through the four nozzles in form of turbulent jets to ensure perfect mixing. The residence time;  $\tau$  is defined as the ratio of volume of the reactor to flow rate of volume of the gas and is given by  $\tau = \rho V / \dot{m}$ .

### Mass conservation equation for species i in an integral control volume

$$\frac{\partial m_i}{\partial t} = \dot{m}_{i,in} - \dot{m}_{i,out} + \dot{m}_i''' \cdot V \quad (2-65)$$

$\dot{m}_i''' \cdot V$  is the generation term which can be positive or negative depending whether species are formed or destroyed during the reaction.

### Species conservation

$$\frac{\partial Y_i}{\partial t} = \frac{Y_{i,in} - Y_i}{t} + \frac{\dot{m}_i''' \cdot W_i}{\rho} \quad (2-66)$$

**Energy conservation equation for a steady-state and steady-flow jet stirred reactor is,**

$$\dot{Q} = \dot{m}(h_{out} - h_{in}) \quad (2-67)$$

In terms of individual species, the above equation is rewritten as,

$$\dot{Q} = \dot{m} \left( \sum_{i=1}^N Y_{i,out} h_i(T) - \sum_{i=1}^N Y_{i,in} h_i(T_{in}) \right) \quad (2-68)$$

## 2.6. Flames

A flame is described as a self-sustaining propagation of a localized reaction zone that moves with respect to the gas supporting it at subsonic velocities [8]. Flames can be either stationary flame on a burner and propagating from the burner tube or they can be freely propagating flames into initial gas mixture. Stationary flames are of two types; **premixed** where fuel and oxidizer (typically air) are mixed prior to combustion and **non-premixed** (or diffusion) where mixing of fuel and oxidizer occurs at combustion interface. Each of these flames is sub-divided into laminar and turbulent flames. Here, focus is on laminar flames.

Laminar premixed flames, along with diffusion flames have application in many industrial devices and also commercial and residential processes like ovens, heating appliances, Bunsen burners etc. Laminar premixed flames are important and form a basis to understand turbulent flames. Both laminar and turbulent flames are ruled by



the same physical processes with the turbulent flame theories being framed based on laminar flame structure.

### Principal flame characteristics

1. **Flame speed;  $S_L$  (or burning velocity or flame velocity):** It is the velocity of a plane flame front in the direction normal to itself. In Figure 13 for a conical flame of a Bunsen burner, the flame speed is given by  $S_L = u_{fl} \cdot \sin\alpha$ . The burning velocity of a flame depends on the flame temperature, on local gas properties like viscosity, thermal conductivity and diffusion coefficient and also on pressure, temperature, air-fuel ratio and heat of reaction. It is independent of the flame geometry, size of the burner and flow rate. It can be measured using two general methods. One is the stationary method and the other propagation method.
2. **Flame temperature (Adiabatic flame temperature);  $T_b$ :** It is the temperature of the burnt gases leaving the reaction zone and the most important characteristic of the flame. The flame temperature for premixed flames can be calculated with the thermodynamic properties of the original well-defined mixture. In a diffusion flame, it needs to be experimentally obtained and cannot be calculated since the reactant compositions are not well defined. For most common fuels at stoichiometric ratio, the flame temperature is approximately 2000 K while at flammability limits it is 1400-1500 K.
3. **Preheat and Reaction zones:** The **preheat zone** is the region where there is a small amount of heat released. In the **reaction zone** is where bulk of chemical energy is released. Further the reaction zone is divided into thin fast chemistry region and wider slow chemistry region. In the thin fast chemistry region, fuel decomposition into intermediates occurs. Bi-molecular reactions also take place in this region. Since this region is thin approximately 1 mm at 1 atm, gradients in temperature and speciation occur which help the flame to be self-sustaining by diffusing heat and radicals to the preheat zone. In hydrocarbon flames, this region appears to be blue in excess of air owing to the excited CH radicals and blue-green for excess of fuel as a result of excited  $C_2$ . Soot is formed in very rich flames. In the slow chemistry region, the third body reactions are dominant making the region as long as several millimeters.

### 2.6.1. Premixed flame

Premixed flames can be **freely propagating flame** and **burner stabilized flame**. A flame is called freely propagating when it is initiated in a tube which contains the mixture to be combusted. The co-ordinate system is fixed to the propagating combustion wave with the unburned mixture approaching with the flame speed;  $S_L$ . For a freely propagating flame, the velocity of burned gas is greater than that of the unburned gas which is given by;  $\rho_u S_L A = \rho_b u_b A$ , where, the subscripts u and b stand for unburned and burned gases respectively. A burner stabilized flame is that which originates from a burner which is comprised of various small pipes through which the premixed gas flows.

#### Governing equations

For a premixed laminar flame with  $\dot{m}$  mass flowrate of fuel and oxidizer in x-direction with unburned mixture at  $x \rightarrow -\infty$  and burned mixture at  $x \rightarrow \infty$ , the conservation equations can be written for mass, species and energy for the differential control volume of  $dx$  thickness as follows.

#### Conservation of total mass

For a premixed laminar flame, the total mass flux is conserved and is a product of density and linear velocity of the gas at any position in the flame.

$$\dot{m}'' = \rho \cdot u_x = \text{constant} \quad \text{or} \quad \frac{\partial(\rho \cdot u_x)}{\partial x} = 0 \quad (2-69)$$

Where  $\partial x$  is distance from the burner on which the flame properties like gas composition and temperature depend.

#### Conservation of species

$$\frac{\partial \dot{m}''}{\partial x} = \dot{m}''_i \quad (2-70)$$

Applying Fick's law the above equation can be rewritten as,

$$\underbrace{\frac{\partial}{\partial x} (Y_i \cdot \dot{m}'')}_{\text{Convection term}} - \underbrace{\frac{\partial}{\partial x} \left( \rho D_{AB} \frac{\partial Y_i}{\partial x} \right)}_{\text{Diffusion term}} = \underbrace{\dot{m}''_i}_{\text{Net mass production}} \quad (2-71)$$

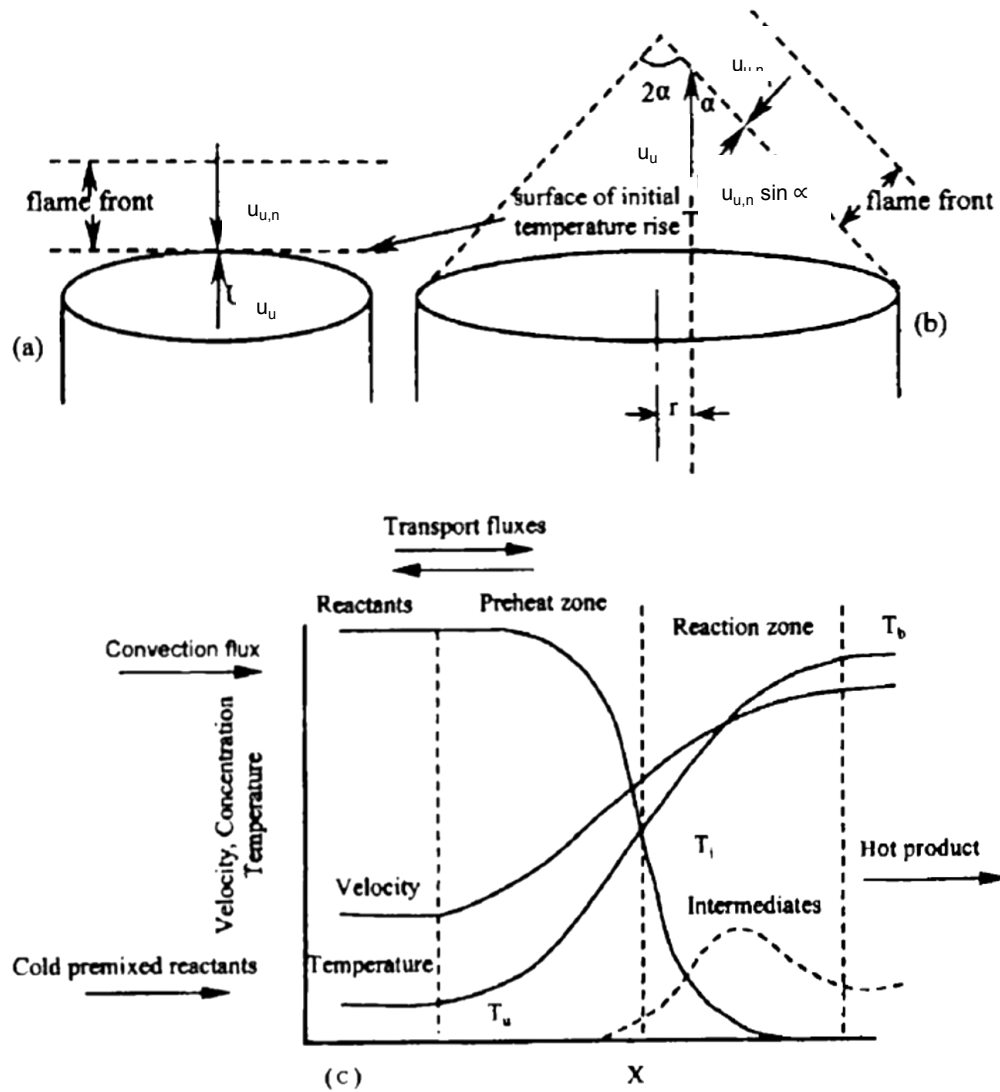


Figure 13: Velocity of burned gas vs unburned gas for a) Flat flame and b) Bunsen (conical) Flame and c) Temperature, concentration and velocity profiles through an idealized 1-D stationary premixed laminar flame [20].

### Conservation of Energy

The general energy conservation equation (2-20) is,

$$\sum \dot{m}_i \left[ c_p \frac{\partial T}{\partial x} + \frac{\partial}{\partial x} \left( -\lambda \frac{\partial T}{\partial x} \right) \right] + \dot{m} u_x \frac{\partial u_x}{\partial x} = - \sum h_i \dot{m}_i \quad (2-72)$$

For steady, laminar flames, the species diffusion velocity  $u_{i,diff}$  is included in the above equation,

$$\sum \dot{m}_i \left[ c_p \frac{\partial T}{\partial x} + \frac{\partial}{\partial x} \left( -\lambda \frac{\partial T}{\partial x} \right) \right] + \sum_{i=1}^N \rho Y_i u_{i,diff} c_{p,i} \frac{\partial T}{\partial x} = - \sum_{i=1}^N h_i \dot{m}_i \quad (2-73)$$

## 2.6.2. Non-Premixed flame

A non-premixed flame is where the fuel and oxidizer do not mix. Such a setup is shown in Figure 14 below which shows a counter-flow flame with the opposing jets of fuel and oxidizer. A counter-flow flame enables to understand the detailed structure of a non-premixed flame.

**Counter-flow flames:** Owing to the opposing jets of fuel and oxidizer, a stagnation plane is created  $u_x=0$  between fuel and oxidizer nozzles. The temperature and mass fractions of the species depends only on the y-coordinate normal to the flame.

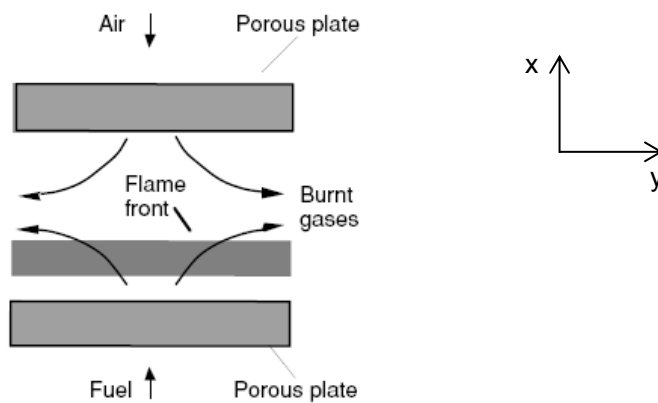


Figure 14: Scheme of Counter-flow non-premixed flame in an opposed-jet burner [13]

The conservation equations for non-premixed flames are similar to that of premixed flames.

### Conservation of total mass

$$\frac{\partial(\rho \cdot u_y)}{\partial y} + (l+1)\rho G = 0 \quad (2-74)$$

Where  $G = \frac{\partial u_x}{\partial x}$  is the tangential velocity gradient and  $l=1$  for rotationally symmetrical configuration and 0 for planar configuration.

### Conservation of species

$$\frac{d(Y_i \dot{m}_i)}{dy} - \rho \cdot u_y \frac{\partial Y_i}{\partial y} = \dot{m}_i \quad (2-75)$$

### Conservation of Energy

$$\dot{m}'' c_p \frac{\partial T}{\partial y} + \frac{\partial}{\partial y} \left( -\lambda \frac{\partial T}{\partial x} \right) + \sum_{i=1}^N \rho Y_i u_{i,diff} c_{p,i} \frac{\partial T}{\partial y} = - \sum_{i=1}^N h_i \dot{m}''_i \quad (2-76)$$

Where  $c_p = \sum Y_i c_{p,i}$  for  $N$  species

### Conservation of momentum

$$\rho u_x \frac{\partial G}{\partial y} = -\rho G^2 - H + \frac{\partial}{\partial y} \left( \mu \frac{\partial G}{\partial y} \right) \quad (2-77)$$

**Where,**  $H = \frac{1}{x} \frac{\partial p}{\partial x}$  and is calculated from strain rate  $a_\infty$  as  $H = \rho_\infty \alpha_\infty^2$

### 3. CYCLOHEXANE KINETIC MODEL

In this chapter, the development of cyclohexane high temperature chemical kinetic model has been discussed in detail. The various chemical interactions between the species during oxidation and their rate coefficients are discussed and tabulated. The mechanism for the base species is the core C0-C4 chemistry which is the *base mechanism*. This work was extended to include 1-hexene chemistry (discussed in Chapter 4) which together has been previously published [18].

Below, the detailed class to class description of the oxidation of cyclohexane has been done analogous to the alkane oxidation grouped into nine high temperature reaction classes.

#### 3.1. Structure of Cyclohexane

The chemical structure of cyclohexane is as shown in Figure 15. Some important properties of cyclohexane are compiled in Table VIII.

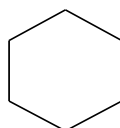


Figure 15: Structure of Cyclohexane

	<b>Cyclohexane</b>
<b>Chemical formula</b>	CYC <sub>6</sub> H <sub>12</sub>
<b>Density</b>	0.7781 g/mL
<b>Auto Ignition</b>	245°C
<b>Boiling Point</b>	80.74°C
<b>Melting point</b>	6.47 °C
<b>Vapor Pressure (mmHg)</b>	78 (at 20°C)
<b>RON</b>	83(MON 77.3)
<b>Cetane number</b>	-

Table VIII: Some properties of Cyclohexane

#### 3.2. Research background

The literature is rich in models and experiments of oxidation and combustion of cyclohexane. In recent years, more theoretical modelling studies [21] have been published whereas before the focus was on experimental studies [22-26] which partly

included models [23, 27, 28], too. There have been investigations on ignition delay times [22-26], mole fractions [29] and flame speeds [24, 30-32] with different techniques of measurement. Since all mechanisms are based on former mechanisms the literature review is indispensable.

### **Experimental studies**

In 1978, Tsang [21] was the first who studied the decomposition of cyclohexane. He used a single-pulse shock tube and found ethylene and 1,3-butadiene as products of its decomposition. He concluded that isomerization to 1-hexene was the initial reaction and derived the rate constant for it (see Table IX). He also stated that 1-hexene could not arise from cyclohexyl radicals. Brown et al. [33] in 1986 focused on investigating the kinetic data through low pressure experiments in the range of 900–1223 K. His results were in agreement with Tsang's results. He derived rate parameters from the C-C bond fission in open-chain alkanes. Gulati and Walker [34] in 1989 studied the addition of cyclohexane to H<sub>2</sub>-O<sub>2</sub> mixture at 480 °C. They found cyclohexene, epoxy-cyclohexene and cyclohexaneoxide as major initial products. Benzene and were found as secondary products. They constructed a similar oxidation mechanism for alkanes and cyclohexane. In 1998, Voisin [29] and co-workers published the first experimental and kinetic modelling study for a jet stirred reactor (JSR) in a temperature range of 750 to 1100 K at 10 atm. Mole fractions were measured and sensitivity and reaction path analyses were performed. As 1-hexene was not detected, the major pathway leads over H-abstraction from cyclohexane to cyclohexyl radical which either breaks via  $\beta$ -scission to form 1-hexenyl radical and then ethylene or successive dehydrogenations to benzene or cyclopentene. He gained a reasonable agreement for all experimental conditions. This study was cited several times because there are few experiments for JSR. Bakali et al. [35] in 2000 conducted the same experiment for 10 atm but also for 1 and 2 atm. At 1 atm, 1-hexene was observed but not at 10 atm. The results showed accordance between experimental results and computed mole fractions. The model was validated against flame speed as well. Steil et al. [22] in 2005 carried out an experimental study on the pyrolysis of cyclohexane with two different shock tube techniques. One experiment investigated the initial step and the other one the dominant reaction routes. He used the rate expression from Voisin et. al [29] for base

modelling. It was deduced that the isomerization is slower whereas the H-abstraction is faster. The branching ratio of both channels is about 1:1. Further, shock tube experiments have been published [23-25] and revealed that ignition delay times decrease with increasing pressure and increasing equivalence ratio for lean to stoichiometric mixtures and that negative temperature coefficient (NTC) behaviour was not observed. Different modelling studies [23, 27, 28] were compared with the ignition delay time. Furthermore there have been investigations on cyclohexane flames [24, 30-32]. To complete the experimental techniques, plug flow reactor [36] and rapid compression machines studies [37, 38] are available, too.

### **Modelling studies**

On the basis of pyrolysis and oxidation of linear and branched alkanes Granata et al. [39] evaluated kinetic parameters. So a semi-detailed mechanism for low and high temperature was developed. This was a first step towards a more methodical way of mechanism generation. Buda et al. [28] reinvestigated that mechanism and took into account all possible elementary steps for every isomer of peroxy and hydroperoxy radicals. Thus, especially the low temperature region was extended. Cavallotti et al. [40] investigated the kinetics on pyrolysis and oxidation of cyclohexane through detailed kinetic modelling. One part of the coefficients was taken from the literature and another part was estimated through "ab initio" calculation. Both Cavallotti and Granata refer to coefficients from Ranzi [41] and validated their results against several experiments. With the work by Silke et al. [27], who refers to the reaction classes from Curran [42], yet another mechanism for high and low temperature is available. Their model reproduces the reactivity of cyclohexane oxidation well, particularly for rapid compression machine. Zhang et al. [43] refined his Utah Surrogate Mechanism from methylcyclohexane to reproduce the stoichiometric premixed cyclohexane flame measured by Law et al. [44]. With generic rates the prediction of benzene and butadiene, two major fuel decomposition products, was satisfying. The latest study was carried out by Gong et al. [45]. He integrated the mechanisms by Sirjean et al. [46], Zhang et al. [43] and Granata et al. [39] but used transition-state theory to obtain rate constants.



### 3.3. Cyclohexane kinetic model development

Generating a mechanism is a complex subject particularly if species become larger. Therefore mechanisms are generally built in a stepwise fashion meaning to extend an existing mechanism. As a matter of fact, cyclohexane decomposes into 1-hexene and into 1-hexenyl radical. Thereby the mechanism of 1-hexene is added (discussed in Chapter 4) in the mechanism of cyclohexane. What are left are the reactions of decascading H-abstraction to form benzene and the ring opening. In total the mechanism consists of 281 species and 3092 reversible elementary reactions. As a super ordinate structure the reaction classes 1-9 following the approach of Curran et al. [4] were used. Due to the fact that the rules are for straight chains and cyclohexane is a ring, data from the literature were preferred. For this reason, apart from Ahmed et al. [47] for straight chain rates, most of the coefficients adopted are from Zhang et al. [43] and Tsang [21] amongst others.

#### Class 1: Unimolecular fuel decomposition

As a matter of course, these reactions are important in high and low temperature mechanism because it is the initiation step and affects all other classes. Three different pathways are possible. Some authors [21, 26, 48] consider the ring opening reaction to form 1-hexene and a direct decomposition to ethylene while the other authors [22] state decomposition via H-abstraction as the main pathway. Here, Steil et al. [22] coefficients are used for latter two reactions while for the former one Tsang coefficients [21] are used (See Table IX).

Reactions	A ( $\frac{\text{cm}^3}{\text{mol}\cdot\text{s}}$ )	n	E <sub>a</sub> ( $\frac{\text{cal}}{\text{mol}}$ )	Ref.
<b>1. Ring Opening</b>				
a. $\text{CYC}_6\text{H}_{12} \Rightarrow 3\text{C}_2\text{H}_4$	1.600E+16	0.00	90000.0	[22]
b. $\text{CYC}_6\text{H}_{12} \Rightarrow \text{C}_6\text{H}_{12}\text{-D1}$	5.010E+16	0.00	88224.8	[21]
<b>2. H-abstraction</b>				
$\text{CYC}_6\text{H}_{12} = \text{CYC}_6\text{H}_{11} + \text{H}$	9.950E+17	0.00	94992.7	[22]

Table IX: Kinetic data for Class 1: unimolecular fuel decomposition of cyclohexane

All of them are included in the mechanism and characterized by high activation energy and thus they are important at higher temperature. The H abstraction serves in reverse direction as H-atom sink.

## Class 2: H-atom abstractions from the fuel

This class has a key role in consuming the fuel. Thirteen different radicals (OH, O, CH<sub>3</sub>, H, HO<sub>2</sub>, C<sub>2</sub>H<sub>3</sub>, C<sub>3</sub>H<sub>5</sub>, C<sub>2</sub>H<sub>5</sub>, HCO, CH<sub>3</sub>O, CH<sub>3</sub>O<sub>2</sub>, O<sub>2</sub>CHO, C<sub>2</sub>H<sub>5</sub>O<sub>2</sub>) are considered. Reactions with H radical are of primary importance in the high temperature region and OH in the intermediate temperature region and HO<sub>2</sub> in the low temperature regime. Consequently, they were modified to improve the results. For the most radicals coefficients of Ahmed et al. [47] are followed while Voisin [29] and Zhang [43] coefficients are used.

Reactions	A ( $\frac{\text{cm}^3}{\text{mol}\cdot\text{s}}$ )	n	E <sub>a</sub> ( $\frac{\text{cal}}{\text{mol}}$ )	Ref.
CYC <sub>6</sub> H <sub>12</sub> + OH = CYC <sub>6</sub> H <sub>11</sub> + H <sub>2</sub> O	1.100E+09	1.61	-34.890	[43]*
CYC <sub>6</sub> H <sub>12</sub> + H = CYC <sub>6</sub> H <sub>11</sub> + H <sub>2</sub> O	0.450E+07	2.00	5002.00	[47]*
CYC <sub>6</sub> H <sub>12</sub> + HO <sub>2</sub> = CYC <sub>6</sub> H <sub>11</sub> +H <sub>2</sub> O <sub>2</sub>	1.000E+13	0.00	17057.0	[29]*
CYC <sub>6</sub> H <sub>12</sub> +O= CYC <sub>6</sub> H <sub>11</sub> +OH	1.180E+05	2.50	2201.00	[47]
CYC <sub>6</sub> H <sub>12</sub> +CH <sub>3</sub> =CYC <sub>6</sub> H <sub>11</sub> +CH <sub>4</sub>	2.000E+11	0.00	9506.00	[47]
CYC <sub>6</sub> H <sub>12</sub> +C <sub>2</sub> H <sub>3</sub> =C <sub>2</sub> H <sub>4</sub> +CYC <sub>6</sub> H <sub>11</sub>	2.000E+11	0.00	16810.0	[47]
CYC <sub>6</sub> H <sub>12</sub> +C <sub>3</sub> H <sub>5</sub> =CYC <sub>6</sub> H <sub>11</sub> +C <sub>3</sub> H <sub>6</sub>	1.350E+12	0.00	9540.00	[29]
CYC <sub>6</sub> H <sub>12</sub> +C <sub>2</sub> H <sub>5</sub> =CYC <sub>6</sub> H <sub>11</sub> +C <sub>2</sub> H <sub>6</sub>	2.500E+10	0.00	10410.0	[47]
CYC <sub>6</sub> H <sub>12</sub> +HCO=CYC <sub>6</sub> H <sub>11</sub> +CH <sub>2</sub> O	1.350E+12	0.00	9540.00	[29]
CYC <sub>6</sub> H <sub>12</sub> +CH <sub>3</sub> O=CYC <sub>6</sub> H <sub>11</sub> +CH <sub>3</sub> OH	4.320E+11	0.00	4473.00	[29]
CYC <sub>6</sub> H <sub>12</sub> +CH <sub>3</sub> O <sub>2</sub> =CYC <sub>6</sub> H <sub>11</sub> + CH <sub>3</sub> O <sub>2</sub> H	2.020E+12	0.00	17710.0	[47]
CYC <sub>6</sub> H <sub>12</sub> +O <sub>2</sub> CHO=CYC <sub>6</sub> H <sub>11</sub> +HO <sub>2</sub> CHO	2.020E+12	0.00	17710.0	[47]
CYC <sub>6</sub> H <sub>12</sub> +C <sub>2</sub> H <sub>5</sub> O <sub>2</sub> =CYC <sub>6</sub> H <sub>11</sub> +C <sub>2</sub> H <sub>5</sub> O <sub>2</sub> H	2.020E+12	0.00	17710.0	[47]

\*=updated

Table X: Kinetic data Class 2: H-abstraction from the fuel cyclohexane

In the work of Alert 2013 [49], different permutations were tested and this combination provided the best results. Therefore the abstraction with OH was increased by factor 4 whereas the A factor was decreased for the other two reactions by 0.2 and a factor 3, respectively.

## Class 3: Alkyl radical decomposition

Cyclohexyl radicals can be consumed via unimolecular decomposition which is the major pathway of decomposition and via H abstraction which contributes to the formation of cyclohexene; CYC<sub>6</sub>H<sub>10</sub> [43].

Reactions	A ( $\frac{\text{cm}^3}{\text{mol}\cdot\text{s}}$ )	n	E <sub>a</sub> ( $\frac{\text{cal}}{\text{mol}}$ )	Ref.
CYC <sub>6</sub> H <sub>11</sub> = CYC <sub>6</sub> H <sub>10</sub> + H	1.000E+14	0.00	38000.0	[43]
CYC <sub>6</sub> H <sub>11</sub> + O = CYC <sub>6</sub> H <sub>10</sub> + OH	1.810E+14	0.00	0.0	[43]
CYC <sub>6</sub> H <sub>11</sub> + OH = CYC <sub>6</sub> H <sub>10</sub> + H <sub>2</sub> O	4.840E+13	0.00	0.0	[43]
CYC <sub>6</sub> H <sub>11</sub> + H = CYC <sub>6</sub> H <sub>10</sub> + H <sub>2</sub>	3.600E+12	0.00	0.0	[43]

Table XI: Kinetic data for some important reactions in Class 3: decomposition of cyclohexyl radicals

#### Class 4: Alkyl radical + O<sub>2</sub> to produce olefin + H<sub>2</sub>O<sub>2</sub>

This class of reaction is relevant only to species up to four carbon atoms thus for cyclohexane, this class of reactions is irrelevant and thus excluded.

#### Class 5: Alkyl radical isomerization

Radical isomerization does not take place because all C-atoms are secondary type. Instead the ring opening is dominant reaction here. Although a C-C bond is broken the molecular formula remains the same. That is why it is called ring opening isomerization. The generic rate originates from the study by Orme et al.[50].

Reactions	A ( $\frac{\text{cm}^3}{\text{mol}\cdot\text{s}}$ )	n	E <sub>a</sub> ( $\frac{\text{cal}}{\text{mol}}$ )	Ref.
C <sub>6</sub> H <sub>11</sub> -D1R6 = CYC <sub>6</sub> H <sub>11</sub>	1.000E+08	0.90	5900.0	[50]

Table XII: Kinetic data for Class 5: Isomerisation reactions of cyclohexyl radical

#### Class 6: Abstraction reactions from olefin

Reactions	A ( $\frac{\text{cm}^3}{\text{mol}\cdot\text{s}}$ )	n	E <sub>a</sub> ( $\frac{\text{cal}}{\text{mol}}$ )	Ref.
CYC <sub>6</sub> H <sub>10</sub> + OH = CYC <sub>6</sub> H <sub>9</sub> + H <sub>2</sub> O	2.350E+07	1.61	-35.850	[47]
CYC <sub>6</sub> H <sub>10</sub> + H = CYC <sub>6</sub> H <sub>9</sub> + H <sub>2</sub> O	3.450E+07	2.00	5000.00	[47]*
CYC <sub>6</sub> H <sub>12</sub> + HO <sub>2</sub> = CYC <sub>6</sub> H <sub>9</sub> +H <sub>2</sub> O <sub>2</sub>	6.440E+12	0.00	17000.0	[47]*
CYC <sub>6</sub> H <sub>10</sub> +O=CYC <sub>6</sub> H <sub>9</sub> +OH	1.180E+05	2.50	2200.0	[47]
CYC <sub>6</sub> H <sub>10</sub> +CH <sub>3</sub> =CYC <sub>6</sub> H <sub>9</sub> +CH <sub>4</sub>	2.000E+11	0.00	9500.0	[47]
CYC <sub>6</sub> H <sub>10</sub> +HO <sub>2</sub> =CYC <sub>6</sub> H <sub>9</sub> +H <sub>2</sub> O <sub>2</sub>	6.440E+12	0.00	17000.0	[47]
CYC <sub>6</sub> H <sub>10</sub> +CH <sub>3</sub> O=CYC <sub>6</sub> H <sub>9</sub> +CH <sub>3</sub> OH	1.000E+13	0.00	47600.0	[47]
CYC <sub>6</sub> H <sub>10</sub> +O <sub>2</sub> =CYC <sub>6</sub> H <sub>9</sub> +HO <sub>2</sub>	1.000E+13	0.00	47600.0	[47]
CYC <sub>6</sub> H <sub>8</sub> +O=CYC <sub>6</sub> H <sub>7</sub> +OH	1.180E+05	2.50	2200.0	[47]
CYC <sub>6</sub> H <sub>8</sub> +OH=CYC <sub>6</sub> H <sub>7</sub> +H <sub>2</sub> O	2.350E+07	1.61	-35.850	[47]
CYC <sub>6</sub> H <sub>8</sub> +H=CYC <sub>6</sub> H <sub>7</sub> +H <sub>2</sub>	3.450E+07	2.00	5000.0	[47]*
CYC <sub>6</sub> H <sub>8</sub> +CH <sub>3</sub> =CYC <sub>6</sub> H <sub>7</sub> +CH <sub>4</sub>	2.000E+11	0.00	9500.0	[47]
CYC <sub>6</sub> H <sub>8</sub> +HO <sub>2</sub> =CYC <sub>6</sub> H <sub>7</sub> +H <sub>2</sub> O <sub>2</sub>	6.440E+12	0.00	17000.0	[47]*
CYC <sub>6</sub> H <sub>8</sub> +CH <sub>3</sub> O=CYC <sub>6</sub> H <sub>7</sub> +CH <sub>3</sub> OH	1.000E+13	0.00	47600.0	[47]
CYC <sub>6</sub> H <sub>8</sub> +O <sub>2</sub> =CYC <sub>6</sub> H <sub>7</sub> +HO <sub>2</sub>	1.000E+13	0.00	47600.0	[47]

\*=updated

Table XIII: Kinetic data for Class 6: Abstraction reactions from olefin CYC<sub>6</sub>H<sub>10</sub> and CYC<sub>6</sub>H<sub>8</sub>

The radicals H, O, OH, CH<sub>3</sub> and HO<sub>2</sub> are considered here to abstract H-atom from the olefins CYC<sub>6</sub>H<sub>10</sub> and CYC<sub>6</sub>H<sub>8</sub>. In analogy to Class 2 here also reactions with H, OH and HO<sub>2</sub> radicals were modified to improve the results. For the coefficients of Ahmed et al. [47] only secondary C-atoms rates are used. Vinylic abstractions are not considered but rather addition of radical to olefin takes place as shown in Class 7 below.

### Class 7: Addition of radical species to olefin

In this class, addition takes place on the double bond and it breaks to form products. The rate constants followed here are from Nawdiyal et al. [18] with zero activation for H and OH additions.

Reactions	A ( $\frac{\text{cm}^3}{\text{mol}\cdot\text{s}}$ )	n	E <sub>a</sub> ( $\frac{\text{cal}}{\text{mol}}$ )	Ref.
CyC <sub>6</sub> H <sub>10</sub> + OH = C <sub>3</sub> H <sub>6</sub> CHO-1 + C <sub>2</sub> H <sub>4</sub>	2.00E+13	0.00	0.00	[18]
CyC <sub>6</sub> H <sub>10</sub> + H = C <sub>4</sub> H <sub>7</sub> p-1 + C <sub>2</sub> H <sub>4</sub>	5.00E+12	0.00	0.00	[18]

Table XIV: Kinetic data for Class 7: Addition of radical species to cyclohexene

### Class 8: Alkenyl radical decomposition

In contrast to n-alkanes, radical attack by H, OH and CH<sub>3</sub> were added to this class as well as the decomposition reactions. For both radicals, CYC<sub>6</sub>H<sub>9</sub> and CYC<sub>6</sub>H<sub>7</sub>, same rate coefficients have been applied. Decomposition of CYC<sub>6</sub>H<sub>9</sub> through H-abstraction is described using Gong coefficients [45]. Decascading reactions to benzene (A1) were taken from Zhang et al. [43] and Wang et al. [36]. For C-C bond fission 1-hexene rates are used [18].

Reactions	A ( $\frac{\text{cm}^3}{\text{mol}\cdot\text{s}}$ )	n	E <sub>a</sub> ( $\frac{\text{cal}}{\text{mol}}$ )	Ref.
CYC <sub>6</sub> H <sub>9</sub> =H+CYC <sub>6</sub> H <sub>8</sub>	3.140E+11	0.92	46765.4	[45]
CYC <sub>6</sub> H <sub>9</sub> +H =CYC <sub>6</sub> H <sub>8</sub> +H <sub>2</sub>	1.800E+12	0.00	0.0	[43]
CYC <sub>6</sub> H <sub>9</sub> +OH =CYC <sub>6</sub> H <sub>8</sub> +H <sub>2</sub> O	2.420E+13	0.00	0.0	[43]
CYC <sub>6</sub> H <sub>9</sub> +CH <sub>3</sub> =CYC <sub>6</sub> H <sub>8</sub> +CH <sub>4</sub>	1.100E+13	0.00	0.0	[36]
CYC <sub>6</sub> H <sub>9</sub> =N-C <sub>4</sub> H <sub>5</sub> +C <sub>2</sub> H <sub>4</sub>	1.000E+13	0.00	35000.0	[18]
CYC <sub>6</sub> H <sub>7</sub> +H=A1+H <sub>2</sub>	1.800E+12	0.00	0.0	[43]
CYC <sub>6</sub> H <sub>7</sub> +CH <sub>3</sub> =A1+CH <sub>4</sub>	1.100E+13	0.00	0.0	[36]
CYC <sub>6</sub> H <sub>7</sub> =A1+H	7.900E+11	0.00	28420.0	[43]

Table XV: Kinetic data for Class 8: Decascading reactions of benzene (A1) formation and other cyclo-alkenyl decomposition reactions

### Reaction type 9: Olefin decomposition

Here ring specific rates are followed here from Tsang [51] as shown in Table XVI.

Reactions	A ( $\frac{\text{cm}^3}{\text{mol}\cdot\text{s}}$ )	n	E <sub>a</sub> ( $\frac{\text{cal}}{\text{mol}}$ )	Ref.
CYC <sub>6</sub> H <sub>10</sub> =C <sub>4</sub> H <sub>6</sub> +C <sub>2</sub> H <sub>4</sub>	1.050E+15	0.00	66700.0	[51]

Table XVI: Kinetic data Class 29: Cyclohexene decomposition

### 3.4. Results and Analysis

#### 3.4.1. Shock Tube

Even though there have been several shock tube experiments, only the ones from Sirjean et al. [23], Hong et al. [24] and Daley et al. [25] are considered for validation as they present the Ignition delay time (IDT). All experimental conditions are shown in Table XVII.

Ref.	CYC <sub>6</sub> H <sub>12</sub> [%]	O <sub>2</sub> [%]	Ar [%]	N <sub>2</sub> [%]	Φ[-]	T[K]	P[atm]
Sirjean[23]	0.5	4.5	95	-	1.0	1285-1661	8.3
	0.5	2.25	97.25	-	2.0	1582-1731	8.3
	0.5	9	90.5	-	0.5	1232-1478	8.3
Hong[24]	0.44	4	95.56	-	1.0	1276-1441	1.5
	0.22	4	95.78	-	0.5	1233-1384	3.0
	0.44	4	95.56	-	1.0	1232-1384	1.5
Daley[25]	2.28	20.53	-	77.19	1.0	964-1166	13.59
	1.15	20.77	-	78.08	0.5	980-1262	12.48

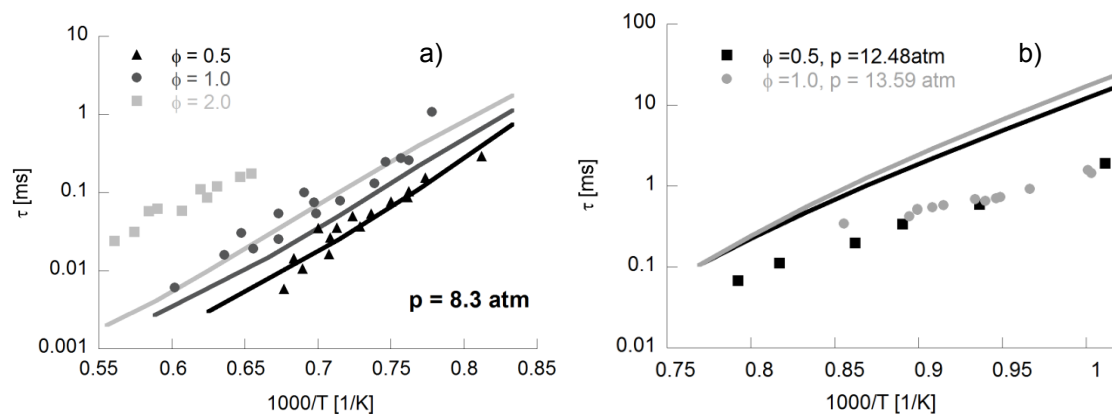
Table XVII: Shock tube Experimental data for cyclohexane [23-25]

Sirjean et al. [23] measures the ignition delay times of cyclohexane/O<sub>2</sub>/Ar mixtures for equivalence ratios ranging from 0.5 to 2.0 at pressures from 7.3 to 9.5 atm and temperatures from 1230 to 1840 K. The ignition delay was measured as the time interval between the reflected shock wave and 10 % of maximum concentration of excited OH radicals. Figure 16 a) visualizes these experiments vs the simulation. The simulations are carried out with a constant volume reactor model (i.e. shock tube) in LOGEsoft and IDT is calculated from 10 % of Max OH concentration calculated at specified temperature intervals and experimental conditions. The simulation fits very well to Φ = 0.5 and becomes slower for Φ = 1.0 and slowest for Φ = 2.0. The slope of the experiments though is well captured for all equivalence ratios.

Daley et al. [25] mixed cyclohexane with air and thus the oxygen concentration is higher (see Table XVII). Although the IDT for 13.59 atm is over-predicted; the trend is followed and also pressure dependence is captured. For Φ = 0.5 in Figure 16 b) the same behavior is confirmed. Figure 16 a) it is observed that the IDT was under-

predicted for  $p = 8.3$  atm and for higher pressures in Figure 16 b) it seems to be over-predicted. However, the trend is in accordance with the experimental data.

Daley et al. [25] validated the experiment with the mechanisms of Silke et al. [27] , Sirjean et al. [23] and Buda et al. [28] with the same results, an over-prediction. Whereas the fitting of the mechanism of Silke was fairly good, the mechanism of Buda et al. and Sirjean over-predicted the IDT with a factor of two and three, respectively. In summary the overall ignition trend is predicted well.



**Figure 16: Ignition delay times for a) Cyclohexane/ $O_2$ /Ar mixture at  $p=8.3$ atm and three equivalence ratios 0.5, 1.0 and 2.0 from Sirjean et al. [23] and b) Cyclohexane/air mixture at two  $\Phi=0.5, 1.0$  and two pressures 12.48 and 13.59 atm resp. from Daley et al. [25]. Experiments are symbols and simulations are lines.**

Figure 17 shows the comparison between the experiments from Hong et al. [24] and the simulated ignition delay times at  $p=1.5$  and 3 bar and two different equivalence ratios 0.5 and 1.0. On the right are the ignition delay times at  $p=1.5$  bar and on the left are the results of  $p=1.5$  and 3 bar for a stoichiometric mixture. The ignition delay times are in general slower for all conditions. The slope of the experiments though is well captured for all equivalence ratios. Also the model is able to capture the pressure dependence.

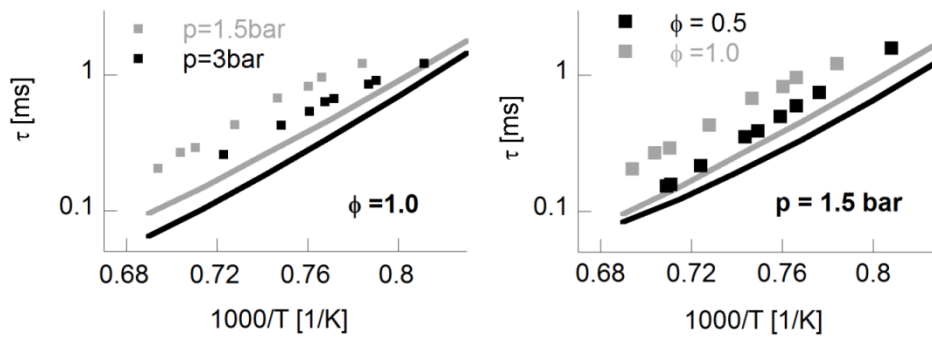


Figure 17: Ignition delay times for cyclohexane/O<sub>2</sub>/Ar mixture for a) stoichiometric mixture and two pressures p=1.5 and 3.0 bar b) p=1.5bar and two equivalence ratios 0.5 and 1.0 [24]. Experiments are symbols and simulations are lines.

### 3.4.2. Jet Stirred Reactor

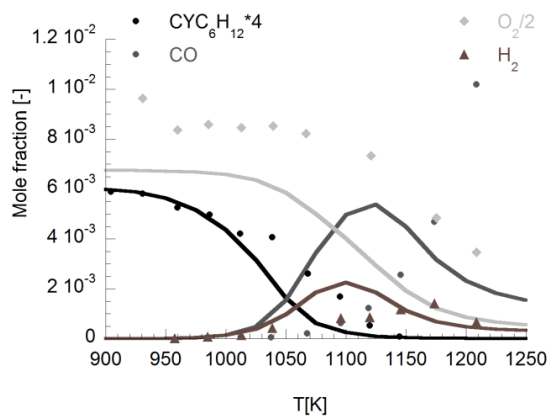
The JSR experiment gives species profiles at different temperatures. Here only stable products are measured. The validation of JSR results reveals different pathways and the mechanism's suitability in low and high temperature. The mechanism has been validated against experimental data [35]. From Figure 18 to Figure 19 illustrate the validation for a pressure of 1 atm in a temperature range from 900 K to 1250 K and  $\Phi = 1.0$ .

The experimental conditions can be found in Table XVIII. The simulations are carried out with the perfectly stirred reactor module in LOGEsoft for the given experimental conditions.

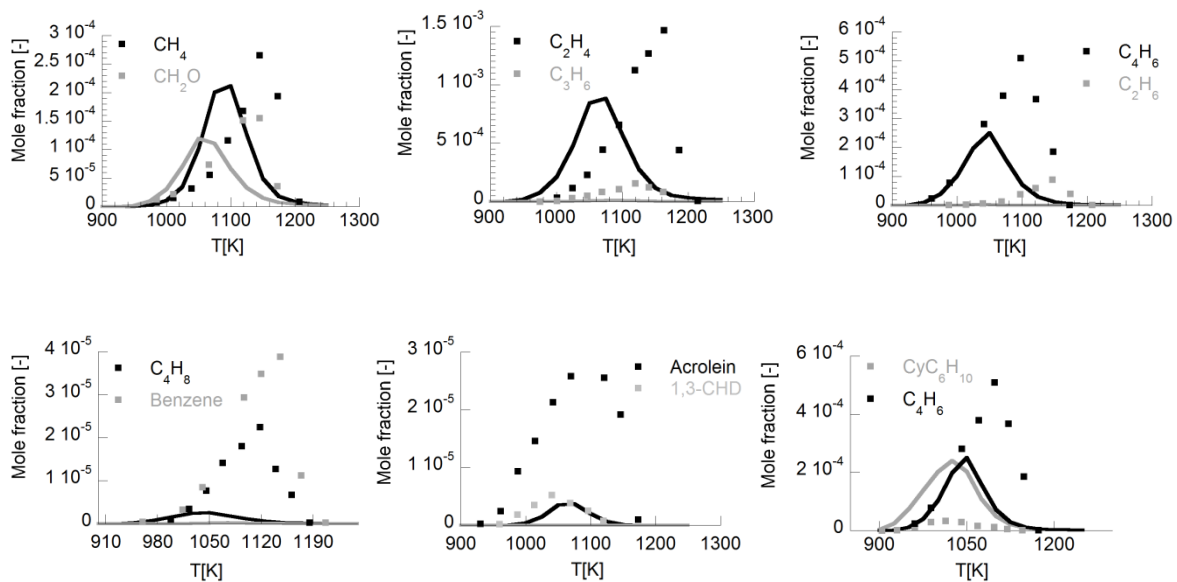
Ref.	Components			Experimental conditions			
	Cyclohexane [%]	O <sub>2</sub> [%]	N <sub>2</sub> [%]	$\Phi$ [-]	p [bar]	T [K]	Residence time [s]
<b>Bakali et al. 2000 [35]</b>	0.15	1.35	98.55	1.0	1.0	900-1250	0.07

Table XVIII: Experimental conditions for cyclohexane in a jet stirred reactor [35]

Figure 18 shows the main species in the decomposition of cyclohexane/O<sub>2</sub>/N<sub>2</sub> mixture in a jet stirred reactor at  $\Phi = 1.0$  and p=1bar. The simulated fuel decomposition follows the experimental points exactly until 1000K but further the decomposition becomes fast until 1150K, thus affecting the other specie profiles considerably e.g. high CO produced in this same temperature regime. The H<sub>2</sub> is quite well predicted, just a slight over-prediction in the region 1000-1100 K. The experimental points at 1150 K and 1200 K are well captured though.



**Figure 18: Main species profiles for cyclohexane/O<sub>2</sub>/N<sub>2</sub> decomposition in a JSR at  $\Phi= 1.0$  [35] at constant mean residence time 0.07s and  $p=1$ bar. Symbols: Experiments and Lines: Simulations.**



**Figure 19: Other species in the decomposition of cyclohexane/O<sub>2</sub>/N<sub>2</sub> mixture in a jet stirred reactor at  $\Phi= 1.0$  [35] at constant mean residence time 0.07s and  $p=1$ bar. Symbols: Experiments and Lines: Simulations.**

Looking at the other intermediates in Figure 19 it is clear a slight shift of profiles to the left. The fast fuel decomposition could be responsible for this effect. But the trend of the profiles in general looks good. Cyclohexene (CYC<sub>6</sub>H<sub>10</sub>) is also observed in flow analysis (Figure 21) to be dominant specie but in the Figure 19 above it is over-predicted by factor 4 though here the peak and trend is well captured. The ethene (C<sub>2</sub>H<sub>4</sub>) and 1,3-butadiene (C<sub>4</sub>H<sub>6</sub>) are the decomposition products of cyclohexene which are also well predicted confirming the flow analysis again. C<sub>2</sub>H<sub>4</sub> also arises from the ring opening of cyclohexane. The profiles of CH<sub>4</sub> and CH<sub>2</sub>O are quiet well



predicted. Although  $\text{CYC}_6\text{H}_{10}$  is over-predicted it doesn't help to influence the low 1, 3-cyclohexadiene ( $\text{CYC}_6\text{H}_8$ ) or benzene concentrations.

### 3.4.3. Flame speed

The mechanism has also been tested by modelling flame speed at 353 K. Ji et al. [32] in 2011 have determined laminar flame speeds for cyclohexane/air mixtures at  $p=1$  bar and  $T=353$  K for wide range of equivalence ratios. Further Wu et al. [30] in 2012 measured laminar flame speeds of cyclohexane from 1-10 atm. The experimental data along with the simulated data are shown in Figure 20. The model agrees very well to the experiments on the lean side and is slightly higher on the rich side from 1.0-1.3 and agrees well with the experiments  $\Phi$  from 1.4 to 1.7. This behavior is observed for the other cycloalkanes too in the following chapters (See Figure 44 and Figure 53).

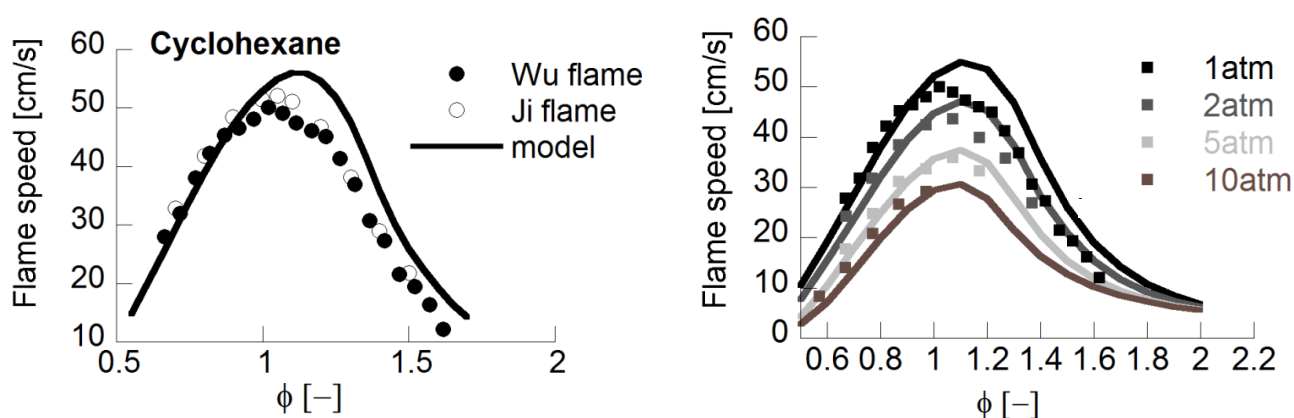


Figure 20: Laminar flame speed for cyclohexane/air flames (left) at 1 atm and 353 K [30, 32] and (right) 1-10atm [30, 32] . Lines: simulation, symbols: experiment.

### 3.4.4. Flow Analysis

The flow analysis of the cyclohexane is conducted for the  $\Phi=1.0$  and  $p=1$ bar jet stirred reactor from Bakali et al. [35] which is shown in Figure 21 below. The species profiles are discussed in following paragraphs.

#### Degradation of cyclohexane

Looking at the flow analysis in Figure 21, the common degradation pathway of cyclohexane is seen to proceed mainly *via* H-abstractions (Class 2) forming cyclohexyl ( $\text{CYC}_6\text{H}_{11}$ ) radical and secondly forming 1-hexene ( $\text{C}_6\text{H}_{12}\text{-D1}$ ) through the ring opening (Class 1). This cyclo-alkyl radical would further decompose either to the

corresponding cyclo-olefins (Class 3) or through ring opening isomerization (Class 5) to form 1-hexene ( $C_6H_{12}$ -D1). The former case constitutes most of the flux and is observed and  $CYC_6H_{10}$  formation is clear from the flow analysis in Figure 21.

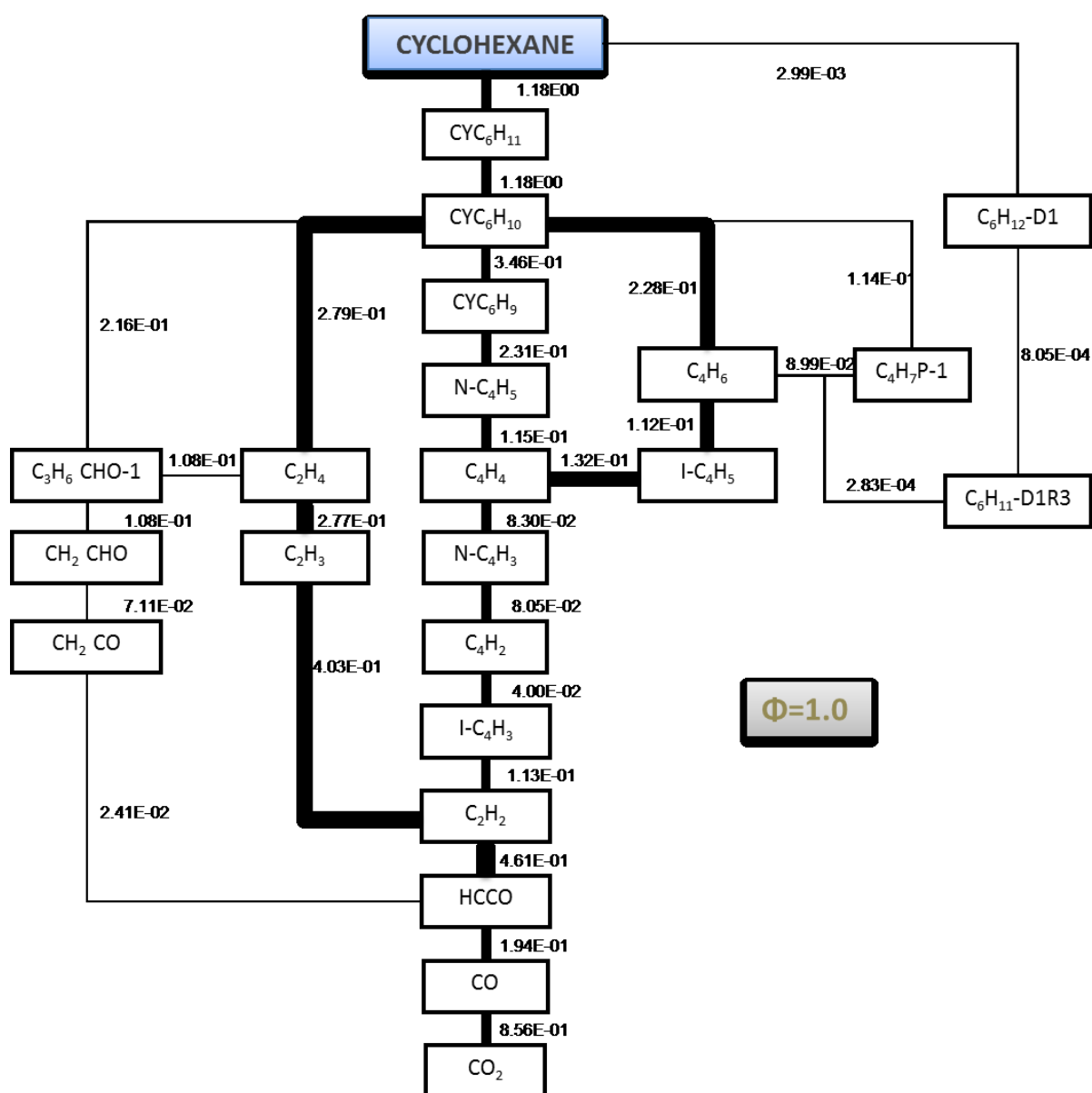


Figure 21: Flow analysis for cyclohexane/ $O_2$ / $N_2$  mixture in a jet stirred reactor at 1150 K,  $\Phi=1.0$  and atmospheric pressure from Bakali et al. [35].

The  $CYC_6H_{10}$  cyclo-olefin is further decomposed to its radical  $CYC_6H_9$  through H-abstractions (Class 6) which in turn forms  $N-C_4H_5$ . The  $N-C_4H_5$  radical reduces down to  $C_4H_4$  and further abstraction reactions dominate the flux forming  $N-C_4H_3$  and  $C_4H_2$  radical pool. The acetylene ( $C_2H_2$ ) is formed as a result. The main degradation pathway of  $C_2H_2$  is the formation of the ketyl radical (HCCO) in the reaction with O

atoms. Ketenyl mainly decomposes to CH and CO and the oxidation of CO leads finally to the main reaction product CO<sub>2</sub>. Cyclohexene (CYC<sub>6</sub>H<sub>10</sub>) is decomposed through other minor pathways through mostly radical addition on the double bond (Class 7) forming 1-butenyl (C<sub>4</sub>H<sub>7</sub>P-1), C<sub>3</sub>H<sub>6</sub>CHO-1 and C<sub>2</sub>H<sub>4</sub>. C<sub>2</sub>H<sub>4</sub> or ethylene formed further decomposes to form C<sub>2</sub>H<sub>3</sub> which contributes to forming C<sub>2</sub>H<sub>2</sub>. C<sub>3</sub>H<sub>6</sub>CHO-1 decomposes through CH<sub>2</sub>CHO and CH<sub>2</sub>CO to form HCCO. More C<sub>4</sub>H<sub>4</sub> is formed through C<sub>4</sub>H<sub>7</sub>P-1 and C<sub>4</sub>H<sub>6</sub> but contribute least to the flux.

Another pathway from cyclohexene is forming 1,3-butadiene (C<sub>4</sub>H<sub>6</sub>) which primarily is a product of Class 9 i.e. the olefin decomposition into products. C<sub>4</sub>H<sub>6</sub> goes down to I-C<sub>4</sub>H<sub>5</sub> and then joins the C<sub>4</sub> pool. The 1-hexene which is formed due to isomerisation of cyclohexane decomposes through allyl radical C<sub>6</sub>H<sub>11</sub>-D1R3 which further decomposes to 1, 3-butadiene. In the Figure 21 detailed mass flow analysis are presented for Φ=1.0 illustrating the high mass flows through C<sub>2</sub>H<sub>2</sub> and HCCO.

### 3.4.5. Sensitivity Analysis

Figure 22 and Figure 23 show the sensitivity analysis for cyclohexane/O<sub>2</sub>/N<sub>2</sub> mixture in a jet stirred reactor at p=1 atm, Φ=1.0 and T=1050 K and 1150 K respectively.

It is clear that the most sensitive reactions are from the base chemistry which forms C<sub>2</sub>H<sub>2</sub>, HCCO and finally CO and CO<sub>2</sub>. These are the most sensitive reactions here. Further, the reaction responsible for cyclohexyl (CyC<sub>6</sub>H<sub>11</sub>) formation is revealed here. The uni-molecular decomposition of cyclohexane (CyC<sub>6</sub>H<sub>12</sub>) to form cyclohexyl radical (CyC<sub>6</sub>H<sub>11</sub>) shows up in the sensitivity and has a negative value stressing the intensity on the backward reaction. The reaction forming cyclohexene has positive sensitivity and originates from the cyclo-alkyl radical decomposition reaction. The reactions forming CyC<sub>6</sub>H<sub>11</sub> and CyC<sub>6</sub>H<sub>10</sub> have higher sensitivities at 1050 K than that at 1150 K. Possibly these reactions could be responsible for the high reactivity in the 1000-1150 K temperature regime as observed in JSR simulations (Figure 18 and Figure 19). The OH addition on the cyclohexene forming C<sub>2</sub>H<sub>4</sub> and C<sub>3</sub>H<sub>6</sub>CHO is seen also in the flow analysis but of secondary importance to the decomposition of cyclohexene. The primary reaction decomposing cyclohexene is the H-abstraction forming cyclo-hexynyl (CYC<sub>6</sub>H<sub>9</sub>) radical which appears in the sensitivity and has a negative value making the backward reaction more sensitive.

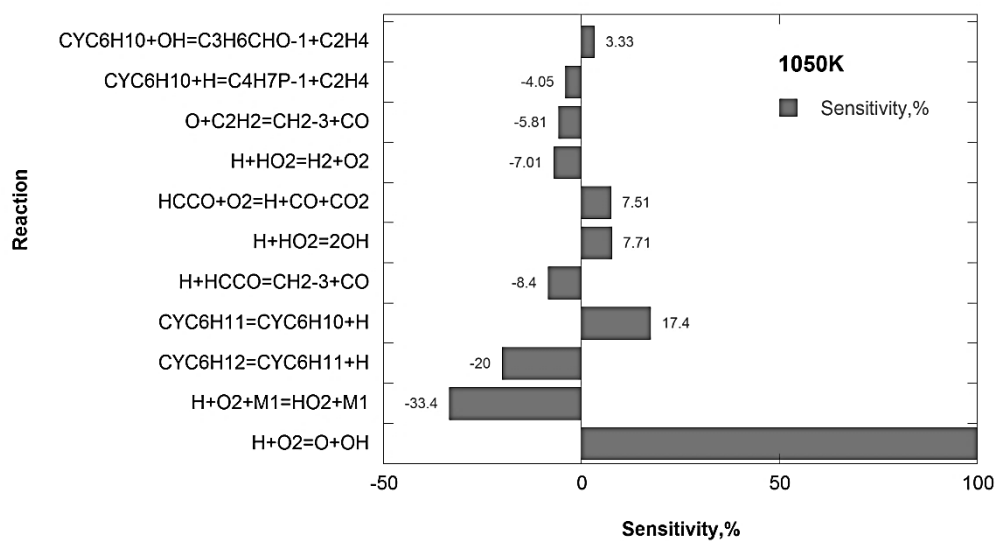


Figure 22: Sensitivity of cyclohexane/O<sub>2</sub>/N<sub>2</sub> in a JSR at T=1050 K, Φ=1.0 and p=1 bar. [35]

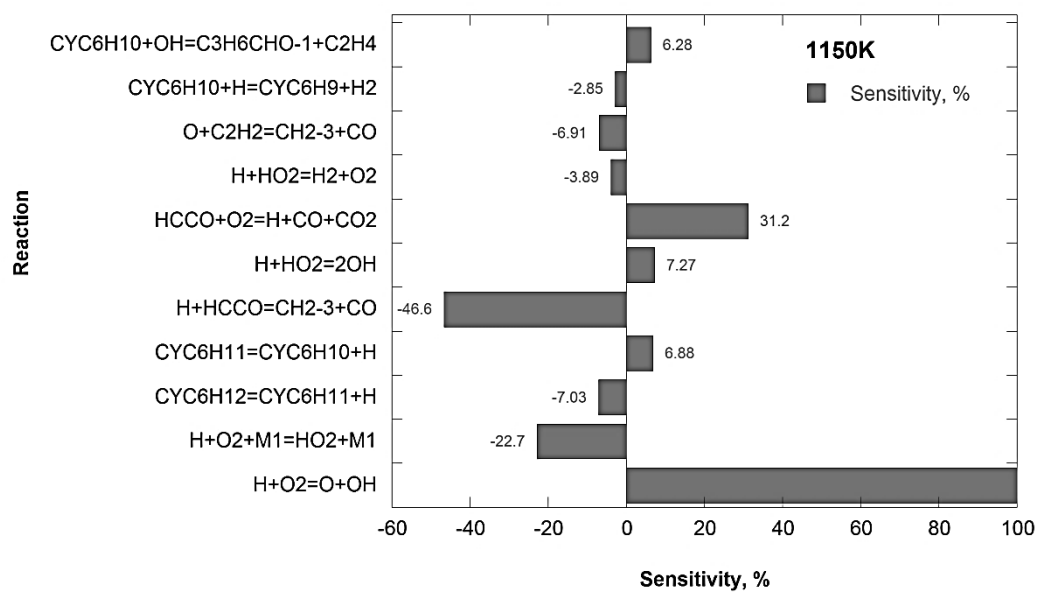


Figure 23: Sensitivity of cyclohexane/O<sub>2</sub>/N<sub>2</sub> in a JSR at T=1150 K, Φ=1.0 and p=1 bar. [35]

### 3.5. Conclusion on cyclohexane model

The cyclohexane mechanism developed in this work is a high temperature model with the sub-mechanism of 1-hexene mechanism added to account for its isomerization ring opening. With that it is possible to use cyclohexane as a reference component for heavy fuels like diesel, kerosene and jet fuel. Rate constants were compiled from literature and assigned to reaction classes for alkanes. The similarities and differences of linear and cyclic species were taken into account and attention was devoted to point out where specific rules are needed. The LOGEsoft software was used for all simulations. The kinetic model was found to be adequate to satisfactorily reproduce ignition delay, concentration profiles of major species in JSR and flame speed for a wide range of conditions. However, improvements have to be made in future work regarding high pressure range. Also, low temperature reactions should be added to make the model comprehensive. Here the olefin pathway is not well captured. The 1-hexene primarily breaks down to its allylic radical  $C_6H_{11}\text{-D1R3}$  and further to smaller products. This is extensively dealt with the next Chapter 4. In general, the overall kinetic was too slow for low pressure shock tube experiments while for higher pressures it is too fast. In the work of Alert 2013 [49], ring opening via  $\beta$ -scission yielding butadiene and ethene and dehydrogenation to form benzene were the major pathways in high temperature but with the allylic radicals ( $C_6H_{11}\text{-D1R3}$ ) preferred abstractions from fuel reactions (Class 2, see Chapter 4), this pathway changes. No more  $C_6H_{11}\text{-D1R6}$  is preferred from isomerization (Class 5) as before but rather Cyclohexene is formed (See flow analysis in Figure 21). For benzene, which is a major source of soot formation, the prediction was too low for 1 atm. Somehow the dehydrogenation pathway is not active and needs further investigation. But in whole these rules for cycloalkanes based on alkanes could be used for modelling the combustion process to include other cyclic species as seen in the following Chapters.

## 4. 1-HEXENE KINETIC MODEL

In this chapter, the development of 1-hexene chemical kinetic model has been discussed in detail. The various chemical interactions between the species during oxidation and their rate coefficients are discussed and tabulated.

The mechanism for the base species is the core C0-C4 chemistry which is the *Base mechanism*. The 1-hexene model in this thesis includes some updates from the publication which are viz.

- The presence of secondary allyl radical  $C_6H_{11}\text{-D1R3}$  has been taken into account (explained in detail in the Section 1-hexene kinetic model development4.3)
- Along with this, retro-ene reaction  $C_3H_6+C_3H_6=C_6H_{12}\text{-D1}$  has been added using the kinetic data provided by K.D. King [52].

### 4.1. Structure of 1-hexene

The chemical structure of 1-hexene is as shown in Figure 24 with double bond at the first position. Some important properties of 1-hexene are compiled in Table XIX.

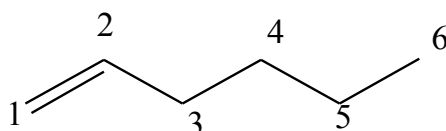


Figure 24: Structure of 1-hexene where the numbers indicate the H-abstraction site or position of the group. 1, 2- vinylic, 3-allylic, 4- 5-Secondary and 6-Primary sites

	1-HEXENE
Chemical formula	$C_6H_{12}\text{-D1}$
Density	0.673 g/cm <sup>3</sup> , liquid
Auto Ignition	253°C
Boiling Point	63 °C (at 336 K)
Melting point	-139.8 °C (at 133.3 K)
Vapor Pressure	18.7 kPa (at 20°C)
RON	76.5 (MON 63.4)
Cetane number	--

Table XIX: Some properties of 1-hexene

## 4.2. Research background

### Experimental studies

Contrary to alkanes, the oxidative behavior of olefins has been relatively little investigated. Regarding the work on hexenes, Yahyaoui et al. [1, 53] studied the oxidation of 0.1% 1-hexene in N<sub>2</sub> mixtures in a jet stirred reactor (JSR) between temperatures 750 and 1200 K at a pressure of 1 MPa. They also studied 0.1% 1-hexene diluted in Ar between temperatures 1270 and 1700 K, at pressures 0.2 and 1 MPa. In experimental studies, three equivalence ratios, 0.5, 1, and 1.5, were investigated.

Mehl et al. [54] performed yet another shock tube experiments to assess the behavior of the hexene linear isomers in the high temperature region at pressures between 8.5 to 12.1 atm at temperature range of 990 and 1460 K at an equivalence ratio of 1.0. They studied the effects of the position of the double bond into the alkyl chain. They also performed experiments on pentene isomer, over a pressure range of 0.93 and 1.16 atm along with another pressures ranging from 7.8 to 10.8 atm and over a temperature ranging from 993 and 1770 K at equivalence ratios of 0.5, 1.0 and 2.0.

The first systematic study on the effect of the position of the double bond in hexene linear isomers was provided by Bounaceur et al. [55], who determined the ignition behavior the three linear hexene isomers in a rapid compression machine (RCM) at different pressures.

Hansen et al. [56] studied fuel-rich ( $\Phi = 2.0$ ) 1-hexene premixed flame stabilized on a flat-flame burner under a reduced pressure of 40 mbar. They investigated the importance of fuel decomposition and benzene formation process in 1-hexene flame. They compared for this the mole fractions of species with a kinetic model basically from Law et al. with some modifications. The investigation was continued for laminar premixed stoichiometric ( $\Phi = 1.0$ ) and  $\Phi = 1.7$  1-hexene flames and validated against my model in Nawdiyal et al. [18].

Retro-ene reactions have been studied by King [52] in a VLPP study on the thermal decomposition of 1-hexene for the temperature range of 915 -1153 K. He found this

reaction losing its significance at higher temperatures. This reaction has been added in this work as an update to the published mechanism.

Burluka et al. [57] measured laminar and turbulent burning velocities for premixed 1-hexene flame at pressure 0.5 MPa and temperature 360 K in the Leeds MkII spherical bomb. The experiment incorporated Schlieren-based imaging to capture stages of flame development. The experiments have been conducted also for other C6 species *n*-hexane, 1-hexyne, 2,2 dimethyl-butane, 2-methylpentane, cyclohexane and cyclohexene to study the influence of structure on the turbulent flame velocities. Laminar burning velocities were used to interpret the data of turbulent velocities. The ranking was obtained for the different C6 structures for equivalence ratios 0.78 -1.67 as: 1-hexyne > cyclohexene > **1-hexene** > cyclohexane > *n*-hexane > 2-methylpentane > 2,2 dimethyl-butane.

### **Modelling studies**

Bounaceur et al. [55] have developed mechanism using automatic generator EXGAS program the model for the oxidation of 1-pentene and 1-hexene which was later extended to low-temperature kinetic mechanisms for the oxidation of these three linear isomers of 1-hexene and 1-heptene. The mechanism has been validated with two RCM studies between temperatures 600 and 900 K and with a JSR study at temperature above 780 K. The model gives a good prediction of IDT and specie profiles. Yahyaoui et al. [1, 53] assembled a detailed kinetic mechanism based on their preciously developed mechanism and validated against their own shock tube and JSR experiments. The results were in good agreement with the experimental data. Mehl et al. [58] developed a detailed kinetic mechanism to study isomers of hexene and gave a detailed approach to understand their reactivity over a wide range of operating conditions. Main reaction classes were broadly studied and simulations were compared with shock tube, JSR and RCM experiments. The model successfully predicted the reactivities 1-hexene isomers. The development of 1-hexene model in this thesis is broadly based on their study.



### 4.3. 1-hexene kinetic model development

The reaction mechanism for the olefin follows in general alkane behavior obviously possessing peculiarities of the double bond. They are explained in detail in the following parts in terms of important classes and respective reaction rates adopted.

The development of the sub-mechanism for 1-hexene oxidation follows the general concept introduced for the augmentation of the C1-C4 core chemistry for *n*-heptane degradation [59]. The current baseline mechanism builds on the model of Hoyermann et al. [60], which was developed with a special focus on tracing benzene formation pathways in acetylene, propene, and mixed propene flames. In analogy to cyclohexane, the sub-mechanism is divided into 9 reaction classes for high temperature following the approach of Curran et al. [4]. For the paraffinic part *n*-heptane mechanism rules proposed by Ahmed et al. [47] have been used and additional rules proposed by Mehl et al. [58] have been applied specifically to feature the double bond and dienes.

This published 1-hexene modelling study and the experimental studies of the Kohse-Höinghaus group [61-63] were the first works, in which the focus was directed on flame pairs and multi-fuel kinetic models in order to make the benzene formation pathway analysis more reliable (see e.g. the discussion in [64] on page 378). Important updates of the mechanism include toluene oxidation [47], and recently the flame chemistry of butane and butene isomers Osswald et al. [65] and Schenk et al. [66]. In the present study some modifications of the kinetic data were required in order to capture the oxidation of 1-hexene with regard to reactions of  $C_3H_4$  and  $C_6H_6$  species. Because fulvene was observed in the 1-hexene flames and was not initially present in the model, reactions involving this species have been added to the current mechanism using kinetic data provided by [67, 68] [69, 70].

All calculations have been performed with the current version of the LOGEsoft package [15]. The thermodynamic properties of several new species in the 1-hexene sub-mechanism were evaluated implementing Benson's group additivity method [17]. The Goos, Burcat, Rusic data base [16] was used for thermodynamic data of fulvene.

The complete model is composed of 281 species and 3092 reversible elementary reactions. The model development is discussed in detail below and is validated to predict flame structures along with laminar flame speed and shock tube experiments which are discussed in detail in Validation and Analysis part of this Chapter.

## High temperature oxidation

The high temperature oxidation starts typically with the homolytic cleavage of the molecules and proceeds through the interaction of smaller radicals with oxygen. Obviously the double bond influences the preferential breaking sites. Other relevant pathways and peculiar behaviors are described in the following paragraphs.

### Class 1: Unimolecular fuel decomposition (Initiation reactions)

The high temperature oxidation starts with the breaking of the fuel molecule into two radicals. Generally the favoured site is allylic thereby resulting in a resonantly stabilized radical ( $C_3H_5$ ) and *n*-propyl radical ( $N-C_3H_7$ ). For this and other reactions occurring close to the double bond Mehl et al. [58] coefficients have been applied (See Table XX). For the reactions happening on the paraffinic part *n*-heptane mechanism rules proposed by Ahmed et al. [47] have been used.

Other possible initiation reaction, including the cleavage of the relatively weak H-C allyl bond is also taken into account. Retro-ene reaction is also another way for dissociation of 1-hexene into propene. This has been studied by King [52] in a VLPP study of thermal decomposition of 1-hexene over a temperature range of 915-1153K. He found that this reaction becomes less important at high temperatures. This reaction has been newly added to the mechanism after the publication.

Reactions	A ( $\frac{cm^3}{mol \cdot s}$ )	n	E <sub>a</sub> ( $\frac{cal}{mol}$ )	Ref.
$C_6H_{12}-D1=C_3H_5+N-C_3H_7$	1.000E+16	0.00	71000	[58]
$C_6H_{12}-D1=C_2H_5+C_4H_7P-1$	1.000E+28	-3.80	90040	[47]
$C_6H_{12}-D1=CH_3+C_5H_9-D1R5$	1.000E+28	-3.80	91000	[47]
$C_6H_{12}-D1=C_2H_3+C_4H_9-1$	5.012E+16	0.00	82000	[58]
$C_6H_{12}-D1=H+C_6H_{11}-D1R3$ (allyl)	1.995E+15	0.00	84000	[58]
$C_6H_{12}-D1=H+C_6H_{11}-D1R4$	2.500E+27	-3.80	97020	[47]
$C_6H_{12}-D1=H+C_6H_{11}-D1R5$	2.500E+27	-3.80	97020	[47]
$C_6H_{12}-D1=C_3H_6+C_3H_6$	4.000E+12	0.00	58000	[52]

Table XX: Kinetic data for Class 1: Uni-molecular fuel decomposition of 1-hexene

Breakage of the double bond is practically negligible in most of the operating conditions, because of higher activation energy required for this breakage [58].

## Class 2: H-abstraction from the fuel molecule

Unlike in alkane oxidation where H-abstractions from olefins are considered only by H, O and OH radicals, here the H-atom abstraction reactions by small radicals such as H, O, OH, HO<sub>2</sub>, O<sub>2</sub> and CH<sub>3</sub> are considered.

The formation of allylic radical 1, 3-C<sub>6</sub>H<sub>11</sub> is preferred as compared to the primary while the secondary radicals are the slowest forming ones. For reactions yielding the allylic radical by H-atom abstraction with all radicals, the activation energy is 2000 cal/mol less than that for formation of primary radicals.

Activation energy of 1000 cal/mol less than that for the primary radicals is applied for H-abstraction with O<sub>2</sub>. Addition reactions on the double bonds are preferred to vinylic abstractions.

Reactions	$A \left( \frac{\text{cm}^3}{\text{mol}\cdot\text{s}} \right) \text{ per } H$	n	$E_a \left( \frac{\text{cal}}{\text{mol}} \right)$	Ref.
C <sub>6</sub> H <sub>12</sub> -D1+H=C <sub>6</sub> H <sub>11</sub> -D1R..+H <sub>2</sub>				
<b>Primary</b>	5.63E+07	2.0	7700	[47]
<b>Secondary</b>	2.45E+07	2.0	5000	[47]
<b>Allylic</b>	2.45E+07	2.0	3000	[47]*
C <sub>6</sub> H <sub>12</sub> -D1+OH=C <sub>6</sub> H <sub>11</sub> -D1R..+H <sub>2</sub> O				[47]
<b>Primary</b>	1.75E+09	0.97	1590	[47]
<b>Secondary</b>	2.34E+07	1.61	-35.8	[47]
<b>Allylic</b>	2.34E+07	1.61	-240	[47]*
C <sub>6</sub> H <sub>12</sub> -D1+O=C <sub>6</sub> H <sub>11</sub> -D1R..+OH				
<b>Primary</b>	3.66E+05	2.40	5500	[47]
<b>Secondary</b>	1.18E+05	2.50	2200	[47]
<b>Allylic</b>	1.18E+05	2.50	200	[47]*
C <sub>6</sub> H <sub>12</sub> -D1+CH <sub>3</sub> =C <sub>6</sub> H <sub>11</sub> -D1R..+CH <sub>4</sub>				
<b>Primary</b>	2.17E+11	0.0	11600	[47]
<b>Secondary</b>	2.00E+11	0.0	9500	[47]
<b>Allylic</b>	2.00E+11	0.0	7500	[47]*
C <sub>6</sub> H <sub>12</sub> -D1+HO <sub>2</sub> =C <sub>6</sub> H <sub>11</sub> -D1R..+H <sub>2</sub> O <sub>2</sub>				
<b>Primary</b>	2.68E+12	0.0	19400	[47]
<b>Secondary</b>	2.44E+12	0.0	17000	[47]
<b>Allylic</b>	2.44E+12	0.0	15000	[47]*
C <sub>6</sub> H <sub>12</sub> -D1+CH <sub>3</sub> O=C <sub>6</sub> H <sub>11</sub> -D1R..+CH <sub>3</sub> OH				
<b>Primary</b>	5.27E+10	0.0	7000	[47]
<b>Secondary</b>	5.48E+10	0.0	5000	[47]
<b>Allylic</b>	5.48E+10	0.0	3000	[47]*
C <sub>6</sub> H <sub>12</sub> -D1+O <sub>2</sub> =C <sub>6</sub> H <sub>11</sub> -D1R..+HO <sub>2</sub>				

<b>Primary</b>	4.17E+12	0.0	49000	[47]
<b>Secondary</b>	1.00E+13	0.0	47600	[47]
<b>Allylic</b>	1.00E+13	0.0	46600	[47]*
$C_6H_{12}-D1+C_2H_5=C_6H_{11}-D1R..+C_2H_6$				
<b>Primary</b>	1.67E+10	0.0	13400	[47]
<b>Secondary</b>	2.50E+10	0.0	10400	[47]
<b>Allylic</b>	2.50E+10	0.0	10200	[47]*
$C_6H_{12}-D1+C_2H_3=C_6H_{11}-D1R..+C_2H_4$				
<b>Primary</b>	1.67E+11	0.0	18000	[47]
<b>Secondary</b>	2.00E+11	0.0	16800	[47]
<b>Allylic</b>	2.00E+11	0.0	14800	[47]*
$C_6H_{12}-D1+CH_3O_2=C_6H_{11}-D1R..+CH_3O_2H$				
<b>Primary</b>	2.00E+12	0.0	20400	[47]
<b>Secondary</b>	2.00E+12	0.0	17700	[47]
<b>Allylic</b>	2.00E+12	0.0	15700	[47]*
[47]*-update				

Table XXI: Kinetic data for Class 2: H-abstractions on the fuel 1-hexene

### Class 3: Alkenyl radical decomposition

The radicals formed by abstraction can decompose depending on the type and position of the radical site. Decomposition of allyl radical is less favoured because of resonance stabilization.

Reactions	A ( $\frac{cm^3}{mol \cdot s}$ )	n	E <sub>a</sub> ( $\frac{cal}{mol}$ )	Ref.
<b>Primary</b>				
$C_6H_{11}-D1R6=C_2H_4+C_4H_7P-1$	1.000E+14	0.00	30000	[58]
$C_6H_{11}-D1R6=H+C_6H_{10}-D1D4$	2.000E+02	2.00	12200	[58]
<b>Secondary</b>				
$C_6H_{11}-D1R5=C_3H_5+C_3H_6$	3.162E+13	0.00	26000	[58]
$C_6H_{11}-D1R4=C_2H_3+C_4H_8-1$	1.000E+14	0.00	31000	[58]
$C_6H_{11}-D1R4=CH_3+C_5H_8-D1D4$	1.000E+14	0.00	33500	[58]
$C_6H_{11}-D1R4=H+C_6H_{10}-D1D4$	2.000E+02	2.00	12200	[58]
$C_6H_{11}-D1R4=H+C_6H_{10}-D1D3$	2.000E+02	2.00	12200	[58]
<b>Allyl</b>				
$C_6H_{11}-D1R3=C_2H_5+C_4H_6$	1.000E+13	0.00	35000	[58]
$C_6H_{11}-D1R3=H+C_6H_{10}-D1D3$	2.000E+02	2.00	19200	[58]

Table XXII: Kinetic data for Class 3: Hexenyl radical decomposition

Also, the decomposition near the double bond forming vinyl radical is almost negligible at low temperature conditions because high activation energy is required for vinyl radical formation. Decomposition with H radical results in the formation of dienes. The dienes are further decomposed shown in classes 6 and 8. The rate constants adopted here are from Mehl et al. [58] as shown in Table XXII.

#### Class 4: Alkyl radical + O<sub>2</sub> direct formation of olefin and HO<sub>2</sub>

According to Curran [4], this class of reaction depends on the number of carbon atoms in the molecule and their possible vibrations. With higher number of carbon atoms than four, the number of vibrations increase, delocalizing the excess energy of the C-O bond ( $\approx 34$  kcal/mol) which lowers the possibility of breaking of this bond and increases the possibility of forming ROO adduct which passes through the low temperature regime described in the following classes. This class of reaction is thus irrelevant for 1-hexene, and is therefore excluded.

#### Class 5: Alkenyl Radical isomerisation

This class of reaction is based on the type of radical site (primary, secondary, allylic) from which the transfer will occur and on the ring strain involved. The transition ring structure is the number of carbon atoms inside the ring with H atom included (smallest 3 ring and highest 5 ring). The rate constants are taken from Ahmed et al. [47].

Reactions	A ( $\frac{\text{cm}^3}{\text{mol}\cdot\text{s}}$ )	n	E <sub>a</sub> ( $\frac{\text{cal}}{\text{mol}}$ )	Ref.
<b>Primary to Secondary</b>				
3 ring: C <sub>6</sub> H <sub>11</sub> -D1R6=C <sub>6</sub> H <sub>11</sub> -D1R5	5.48E+08	1.62	38720	[47]
Reverse	1.74E+07	2.01	41230	[47]
4 ring C <sub>6</sub> H <sub>11</sub> -D1R6=C <sub>6</sub> H <sub>11</sub> -D1R4	1.39E+09	0.98	33720	[47]
Reverse	4.41E+07	1.38	36230	[47]
<b>Secondary to Secondary</b>				[47]
3 ring: C <sub>6</sub> H <sub>11</sub> -D1R5=C <sub>6</sub> H <sub>11</sub> -D1R4	9.59E+08	1.39	39650	[47]
Reverse	9.59E+08	1.39	39650	[47]
<b>Primary to Allylic(same as secondary)</b>				[47]
5 ring: C <sub>6</sub> H <sub>11</sub> -D1R6=C <sub>6</sub> H <sub>11</sub> -D1R3	2.54E+09	0.35	19740	[47]
Reverse	1.61E+08	0.74	22260	[47]
<b>Secondary to Allylic(same as secondary)</b>				[47]
3 ring: C <sub>6</sub> H <sub>11</sub> -D1R4=C <sub>6</sub> H <sub>11</sub> -D1R3	9.59E+08	1.39	39650	[47]
Reverse	9.59E+08	1.39	39650	[47]
4 ring: C <sub>6</sub> H <sub>11</sub> -D1R5=C <sub>6</sub> H <sub>11</sub> -D1R3	1.76E+08	0.76	34500	[47]
Reverse	3.50E+09	0.76	34500	[47]

Table XXIII: Kinetic data for Class 5: Isomerization of hexenyl radicals

#### Class 6: Diene abstractions

The dienes formed in Class 3 after decomposition of alkenyl radical with H atom are decomposed via H-abstractions in this class. C<sub>6</sub>H<sub>10</sub>, C<sub>6</sub>H<sub>10</sub>-D1D3, C<sub>6</sub>H<sub>10</sub>-D1D4, C<sub>5</sub>H<sub>10</sub>-D1D3 and C<sub>5</sub>H<sub>10</sub>-D1D4 are the five different dienes formed (See Figure 25).

The rate coefficients used are same as that in the abstraction of 1-hexene in Class 2 (See Table XXI).

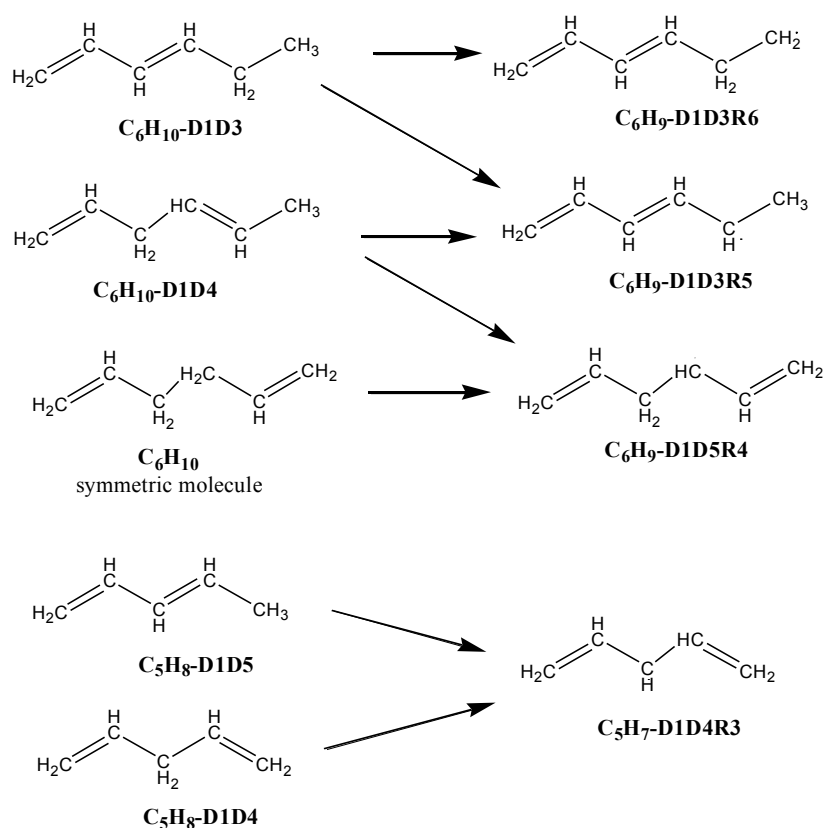


Figure 25: Radicals from dienes  $\text{C}_6\text{H}_{10}\text{-D1D3}$  and  $\text{C}_6\text{H}_{10}\text{-D1D4}$  and resonant species

### Class 7: Radical addition to the double bond

Addition of radicals to the double bond is an important feature of olefins. These reactions are specific only to olefins and do not occur in alkanes. The mechanism accounts for the addition reactions of H, OH and O radicals. Here, in contrast to Mehl's pathway of adducts formation, only formation of products is considered (See Figure 26). Addition of  $\text{HO}_2$  can directly forming epoxide has not been considered. The rate constant followed here are from Schenk et al. [66] with zero activation for H and OH additions, while for O radical an energy barrier of 200 cal/mol is applied.

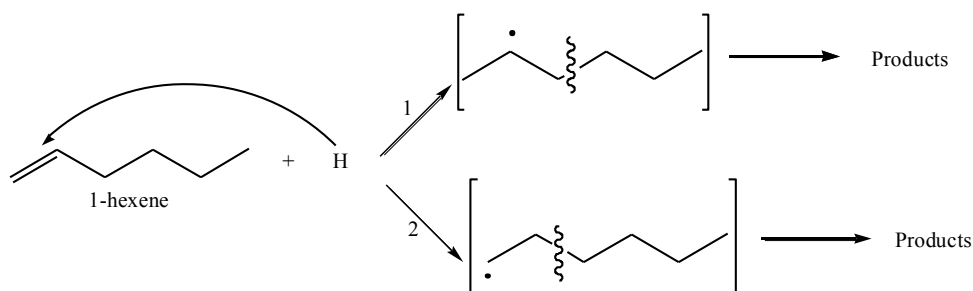


Figure 26: H addition at double bond and products

Reactions	A ( $\frac{\text{cm}^3}{\text{mol}\cdot\text{s}}$ )	n	E <sub>a</sub> ( $\frac{\text{cal}}{\text{mol}}$ )	Ref.
$\text{C}_6\text{H}_{12}\text{-D1}+\text{H}=\text{C}_2\text{H}_4+\text{C}_4\text{H}_9\text{-1}$	5.000E+12	0.00	0	[66]
$\text{C}_6\text{H}_{12}\text{-D1}+\text{H}=\text{C}_3\text{H}_6+\text{N-C}_3\text{H}_7$	5.000E+12	0.00	0	[66]
$\text{OH}+\text{C}_6\text{H}_{12}\text{-D1}=\text{CH}_3\text{CHO}+\text{C}_4\text{H}_9\text{-1}$	1.000E+13	0.00	0	[66]
$\text{OH}+\text{C}_6\text{H}_{12}\text{-D1}=\text{N-C}_3\text{H}_7+\text{C}_2\text{H}_5\text{CHO}$	1.000E+13	0.00	0	[66]
$\text{O}+\text{C}_6\text{H}_{12}\text{-D1}=\text{HCO}+\text{C}_5\text{H}_{11}\text{-R1}$	0.100E+08	1.60	200	[66]

Table XXIV: Kinetic data for Class 7: Addition on the double bond

### Class 8: Alkenyl radical decomposition (dienes)

The four different radicals formed from dienes are decomposed in the same way as the alkenyl radical with class 3 rates. For allyl radicals  $\text{C}_6\text{H}_9\text{-D1D5R3}$  and  $\text{C}_6\text{H}_9\text{-D1D3R5}$ , Mehl rates [58] are followed whereas for  $\text{C}_6\text{H}_9\text{-D1D3R6}$  and  $\text{C}_5\text{H}_7\text{-D1D4R3}$  Ahmed rates [47] are followed. Examples of some reactions with the rates adopted are showed in Table XXV.

Reactions	A ( $\frac{\text{cm}^3}{\text{mol}\cdot\text{s}}$ )	n	E <sub>a</sub> ( $\frac{\text{cal}}{\text{mol}}$ )	Ref.
$\text{C}_6\text{H}_9\text{-D1D5R3}=\text{H}+\text{C}_6\text{H}_8$	2.000E+08	0.00	19200	[58]
$\text{C}_6\text{H}_9\text{-D1D5R3}=\text{C}_2\text{H}_3+\text{C}_4\text{H}_6$	1.000E+13	0.00	35000	[58]
$\text{C}_6\text{H}_9\text{-D1D3R5}=\text{C}_4\text{H}_6+\text{C}_2\text{H}_3$	1.000E+13	0.00	35000	[58]
$\text{C}_6\text{H}_9\text{-D1D3R5}=\text{H}+\text{C}_6\text{H}_8$	3.000E+08	0.00	22500	[58]
$\text{C}_6\text{H}_9\text{-D1D3R6}=\text{N-C}_4\text{H}_5+\text{C}_2\text{H}_4$	1.000E+14	0.00	30000	[47]
$\text{C}_5\text{H}_7\text{-D1D4R3}=\text{C}_2\text{H}_3+\text{C}_3\text{H}_4$	1.000E+13	0.00	35000	[47]

Table XXV: Kinetic data for Class 8: Diene radical decomposition

### Class 9: Diene-decomposition

In this class the dienes are decomposed via  $\beta$ -scission as in class 1 of olefins (See Table XVI). Here, Ahmed rates are followed for decompositions and H-abstractions on straight chain and Mehl rates [58] are followed for reactions near the double bond.

Reactions	A ( $\frac{\text{cm}^3}{\text{mol}\cdot\text{s}}$ )	n	E <sub>a</sub> ( $\frac{\text{cal}}{\text{mol}}$ )	Ref.
C <sub>6</sub> H <sub>10</sub> =H+C <sub>6</sub> H <sub>9</sub> -D1D5R3	3.99E+15	0.00	84000	[58]
C <sub>6</sub> H <sub>10</sub> =C <sub>3</sub> H <sub>5</sub> +C <sub>3</sub> H <sub>5</sub>	1.00E+16	0.00	71040	[58]
C <sub>6</sub> H <sub>10</sub> -D1D4=H+C <sub>6</sub> H <sub>9</sub> -D1D3R5	1.99E+15	0.00	84000	[58]
C <sub>6</sub> H <sub>10</sub> -D1D4=C <sub>3</sub> H <sub>5</sub> +C <sub>3</sub> H <sub>5</sub>	1.00E+16	0.00	71040	[58]
C <sub>6</sub> H <sub>10</sub> -D1D3=H+C <sub>6</sub> H <sub>9</sub> -D1D3R6	2.50E+27	-3.80	97020	[47]
C <sub>6</sub> H <sub>10</sub> -D1D3=H+C <sub>6</sub> H <sub>9</sub> -D1D3R5	2.50E+27	-3.80	97020	[47]
C <sub>6</sub> H <sub>10</sub> -D1D3=C <sub>2</sub> H <sub>5</sub> +N-C <sub>4</sub> H <sub>5</sub>	1.00E+28	-3.80	90000	[47]

**Table XXVI: Kinetic data for Class 9: Diene decomposition**

#### 4.4. Results and Analysis

The model has been validated with shock tube [1, 53], flame structure [18] [71] [56] and flame speed [57] experiments and the results and analysis are in following paragraphs.

##### 4.4.1. Shock tube

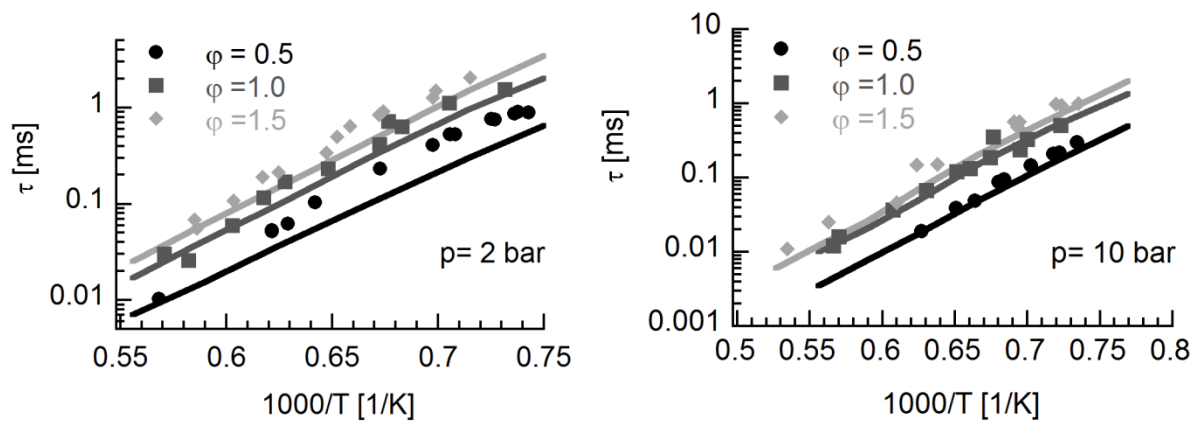
The detailed chemical kinetic mechanism for 1-hexene has been validated against experiments by Yahyaoui et al. in a shock tube [1, 53] at different conditions ranging from 1270 to 1700 K at p = 2 and 10 atm pressure and three equivalence ratios  $\Phi$  = 0.5, 1, and 1.5. Table XXVII shows the experimental conditions for shock tube experiments.

Reference	Components			Experimental conditions		
	1-hexene [%]	O <sub>2</sub> [%]	Ar [%]	$\phi$ [-]	Pressure [bar]	Temperature [K]
[53]*	0.1	1.8	98.1	0.5	2.0	1346-1760
	0.1	0.9	99.0	1.0	2.0	1418-1752
	0.1	0.6	99.3	1.5	2.0	1399-1711
	0.4	3.6	96.0	1.0	2.0	1345-1729
[1]	0.1	1.8	98.1	0.5	10.0	1310-1870K
	0.1	0.9	99.0	1.0	10.0	1310-1870K
	0.1	0.6	99.3	1.5	10.0	1310-1870K

\*The ignition delay is measured as the 50% of the maximum OH concentration

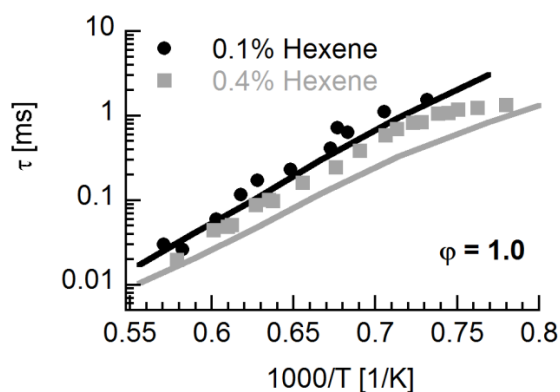
**Table XXVII: Shock Tube experimental literature for 1-hexene**





**Figure 27: Ignition delay times of 1-hexene at p=2bar (left) and p=10bar (right) at 0.1% fuel concentration in O<sub>2</sub>/Ar mixture [1, 53]. Symbols: Experiments and Lines: Simulations**

The comparison between the experiments and the simulated ignition delay times for 0.1% fuel concentration and three different equivalence ratios 0.5, 1.0 and 1.5 is seen in Figure 27. The operating conditions cover a temperature range of 1270 K to 1700 K at pressure 10 bar. For the same stoichiometric conditions, the p=10 bar results fit better to the experiments as compared to p=2 bar experiments. In general, a good agreement of the simulations with the experiments for different stoichiometric conditions is seen.



**Figure 28: Ignition delay of 1-hexene at p=2 bar at different fuel concentrations 0.1% and 0.4% [53]**

Figure 28 shows the comparison of experiments of 1-hexene with two different fuel concentrations at stoichiometric conditions. The simulations very well predict the influence of fuel concentration. For higher fuel concentration (0.4 %), there is a slight higher prediction of ignition delay times but in general the influence is well captured by the model and is within the average error of 12% [1, 53].

#### 4.4.2. Flame structure

The validation targets for the kinetic model are mole fraction profiles of premixed laminar low-pressure C<sub>6</sub>H<sub>12</sub>/O<sub>2</sub>/Ar flames for equivalence ratios of 1.0, 1.7 and 2.0. The flame conditions of the three flames are given in Table XXVIII.

Ref.	Nr.	Components			Experimental conditions		
		1-hexene [%]	O <sub>2</sub> [%]	Ar [%]	φ[-]	Pressure [Torr]	Cold gas velocity [cm/s]
[18]	Flame 1	4.0	36.0	60.0	1.0	15	128.1
[71]	Flame 2	11.1	58.9	30.0	1.7	30	49.2
[56]	Flame 3	12.7	57.3	30.0	2.0	30	49.2

Table XXVIII: Flame conditions of 1-hexene flame [18] [71] [56]

The flames were stabilized on a flat-flame McKenna-type burner and quantitative mole fraction profiles of more than 40 species from within each flame were measured using flame-sampling molecular-beam mass spectrometry with isomer-resolving capabilities. The details of the apparatus and procedures have been published elsewhere [65, 72] with only a few important aspects highlighted here, which are important for the purpose of validating the model. The accuracies of the mole fraction profiles are within 20 % for the major species, but somewhat larger for the intermediates [72-74]. Furthermore, it is expected that the experimental spatial location has an absolute accuracy of ±0.5 mm.

#### Major species and temperature profile

Figure 29 shows the mole fractions of the stable main products in 1-hexene/O<sub>2</sub>/Ar Φ=1.0, 1.7 and 2.0 flames. In general, the model shows for 1-hexene, O<sub>2</sub>, CO, CO<sub>2</sub>, O<sub>2</sub>, H<sub>2</sub>O, H<sub>2</sub> and Ar very good agreement with the experiments. The CO profile at Φ=1.0 is slightly under-predicted (although within error range); at other equivalence ratios it is very well predicted. For Φ=1.7, the experimental values of 1-hexene decomposition at the burner surface are lower than in the simulation, but this region is in general difficult to model [66]. Experimental temperature profiles are used for the simulation. They are given in Figure 29.

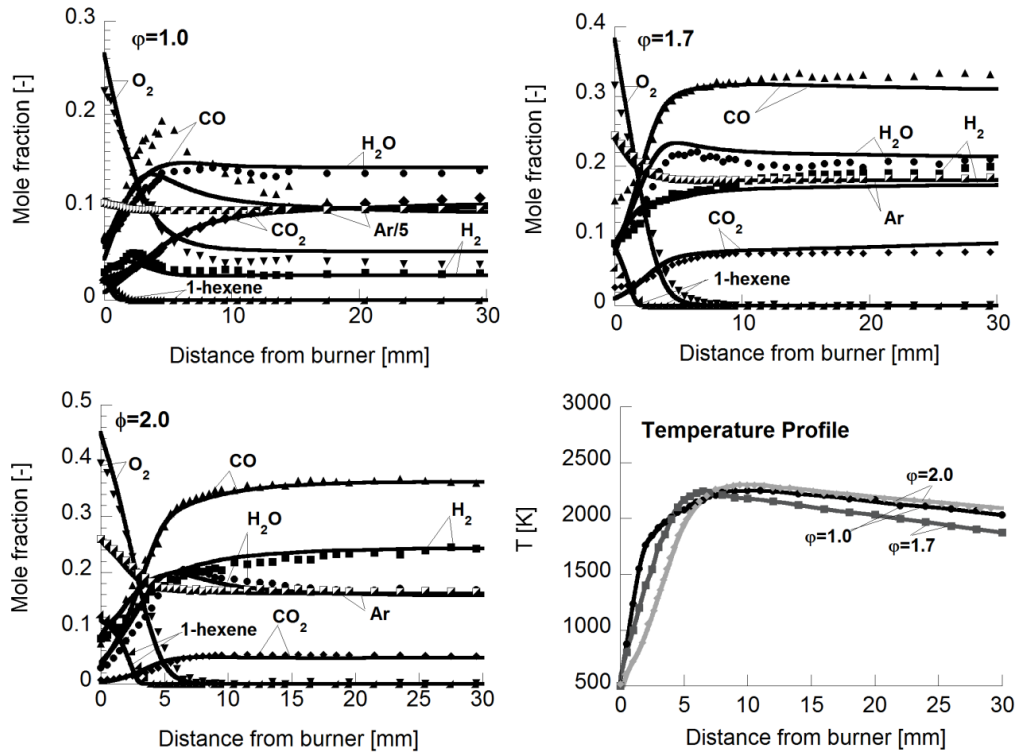


Figure 29: Measured major species (dots) and model prediction (lines) for 1-hexene/O<sub>2</sub>/Ar  $\Phi=1.0, 1.7$  and  $2.0$  flames and the measured temperature profile and model input [18].

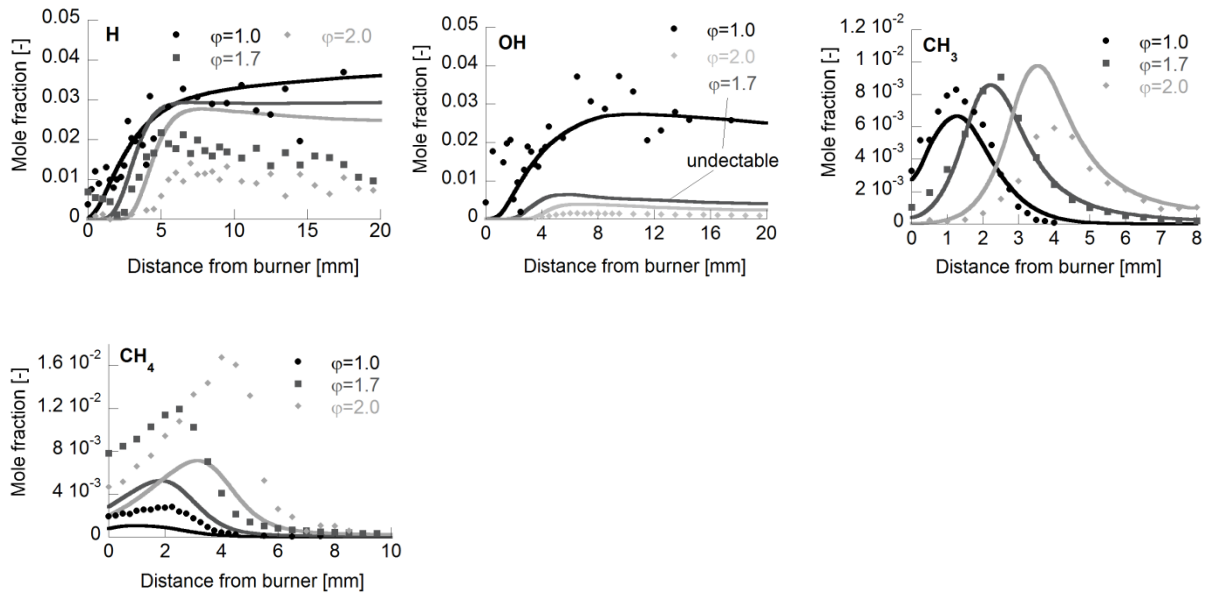
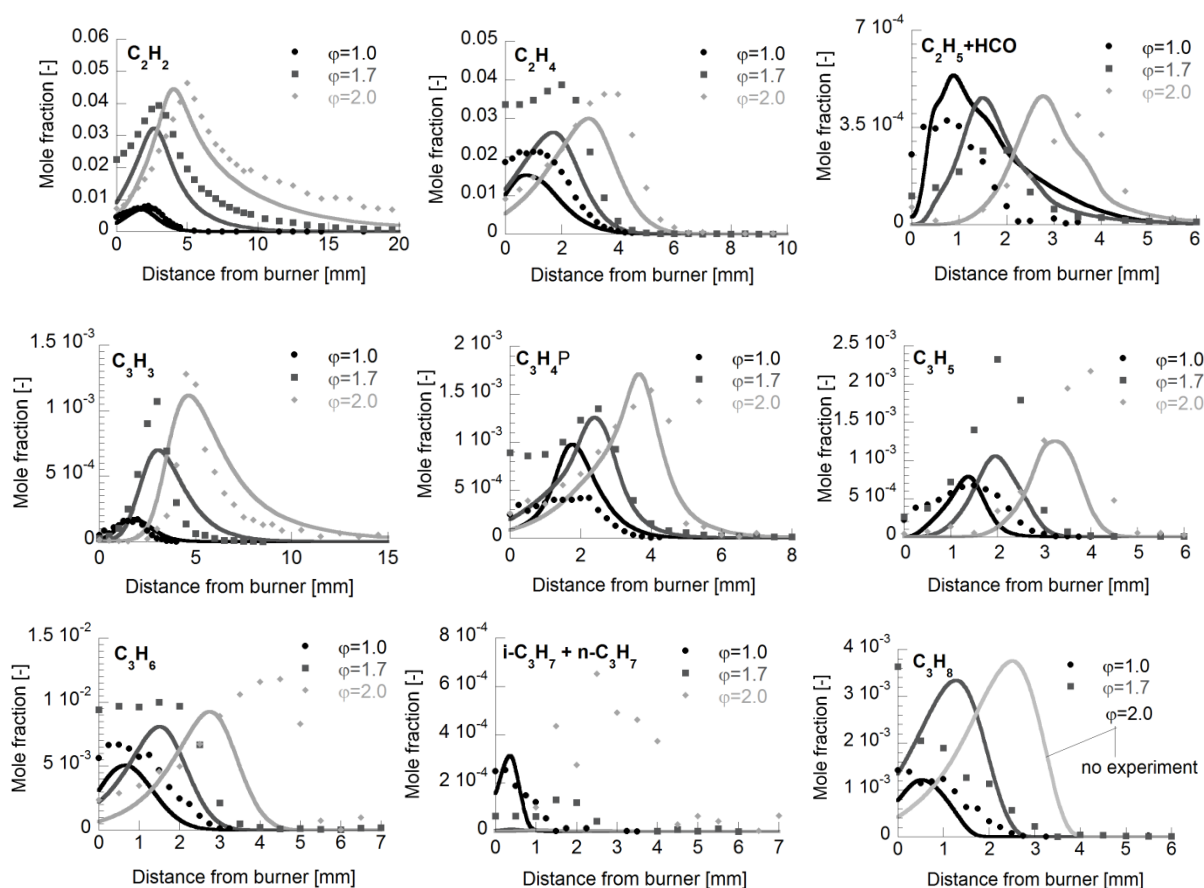


Figure 30: OH, H, CH<sub>3</sub> and CH<sub>4</sub> species profiles (dots) and model prediction (lines) for 1-hexene/O<sub>2</sub>/Ar  $\Phi=1.0, 1.7$  and  $2.0$  flames [18].

## C<sub>2</sub> and C<sub>3</sub> species relevant for benzene formation

As outlined above, the main degradation pathways lead to the accumulation of ethene (C<sub>2</sub>H<sub>4</sub>) and acetylene (C<sub>2</sub>H<sub>2</sub>) and these species can further react to C<sub>3</sub> species. Additionally, allyl radical (C<sub>3</sub>H<sub>5</sub>) is formed promptly via the decomposition of 1-hexene, especially under fuel rich conditions. This means that the propargyl radical (C<sub>3</sub>H<sub>3</sub>) is formed from two pathways, which operate on different chemical time scales, namely the build-up from acetylene and dehydrogenation of allyl [60].



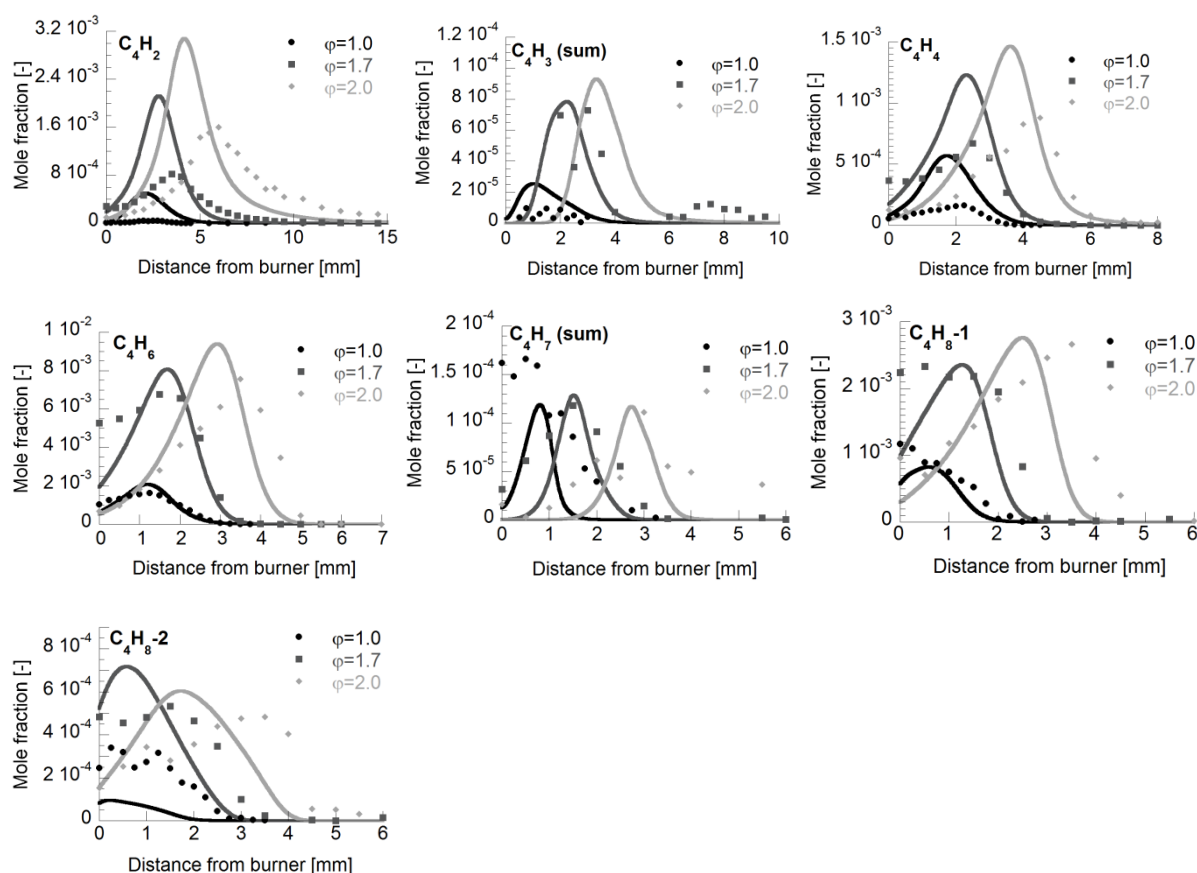
**Figure 31: C<sub>2</sub>H<sub>2</sub>, C<sub>2</sub>H<sub>4</sub>, C<sub>2</sub>H<sub>5</sub>, C<sub>3</sub>H<sub>3</sub>, C<sub>3</sub>H<sub>4</sub>, C<sub>3</sub>H<sub>4</sub>P, C<sub>3</sub>H<sub>5</sub>, and C<sub>3</sub>H<sub>6</sub> profiles (dots) and model prediction (lines) for 1-hexene/O<sub>2</sub>/Ar  $\Phi=1.0, 1.7$  and  $2.0$  flames [18].**

The early formation of allyl is specific for the 1-hexene flame. Since several assumed benzene pathways proceed via allyl, we find a fuel specific chemical environment for benzene formation. However, before we draw conclusions on this part of the 1-hexene flame chemistry it must be shown that the mole fraction profiles of abovementioned intermediates are captured by the model. This validation is shown in Figure 31. In general, a good agreement between experiment and model predictions is found for all equivalence ratios. The minor deviations are within the experimental

error. For some species like propene ( $C_3H_6$ ), the peak position is not exactly met by the simulation at higher equivalence ratios, which could be the retro-ene reaction which is for future scope of this study or might be the effect of the molecular beam sampling technique.

### Butenes and Butadienes

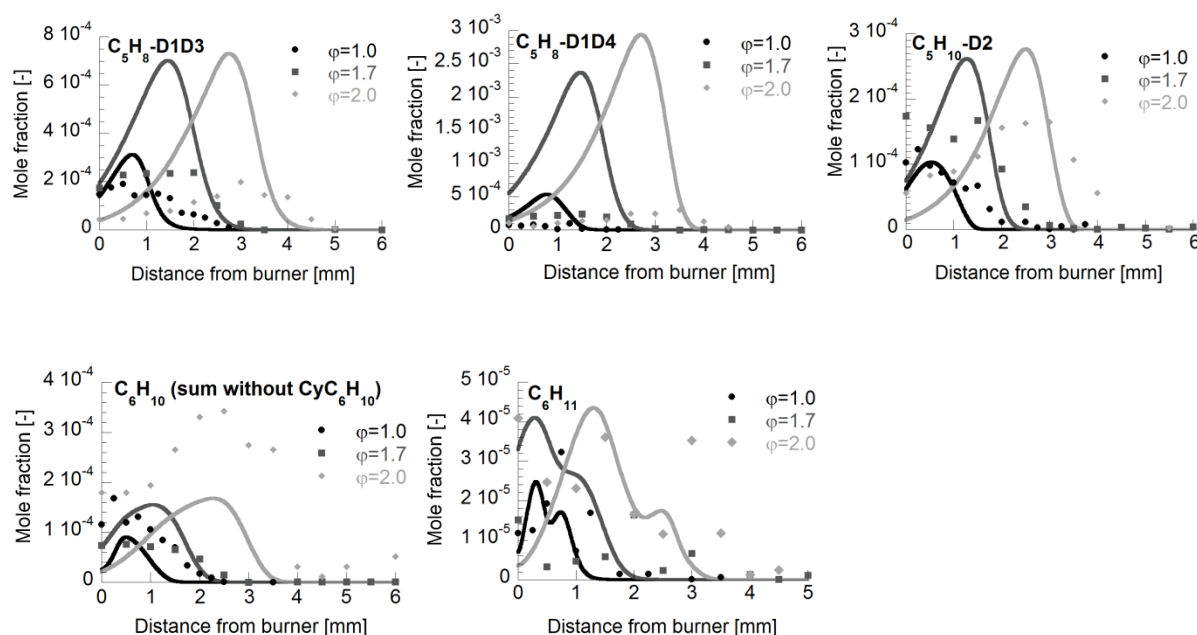
In Figure 32, it is seen that, 1,3-butadiene ( $C_4H_6$ ) is readily formed from the allyl radical  $C_6H_{11}$ -D1R3. One of two butene isomers; 1-butene ( $1-C_4H_8$ ) is also seen in the flow analysis as a product of decomposition of 1, 4-hexyl radical ( $C_6H_{11}$ -D1R4). So the complete flow of decomposition of these species goes down to the intermediates  $C_4H_4$ ,  $C_4H_3$  and  $C_4H_2$  which can also be seen in the main flux of 1-hexene for all three flames. The  $C_4H_6$ ,  $C_4H_7$  and  $C_4H_8$ -1 and  $C_4H_8$ -2 profiles are in very good agreement with the experiments. The lower intermediate species profiles for  $C_4H_4$  and  $C_4H_2$  are over-predicted but  $C_4H_3$  profile looks in very good agreement with the experiments.



**Figure 32: Butenes, Butadienes and other important C4 species formation profiles (dots) and model prediction (lines) for 1-hexene/ $O_2$ /Ar  $\Phi=1.0, 1.7$  and  $2.0$  flames [18].**

## Other olefins and Hexenyl radicals

It is evident from the Figure 33 below that the  $C_6H_{11}$ -D1R3 radical influences the profile of total  $C_6H_{11}$  radicals. The allylic site abstractions which were made faster in this study showed to be influential for the total profile. The simulation is in very good agreement with the experiments. The smaller olefin  $C_5H_{10}$ -D2 profile at stoichiometric conditions shows good agreement with the experiments while those at  $\Phi=1.7$  and 2.0 are slightly highly predicted but the profile shapes match the experimental profile shape.

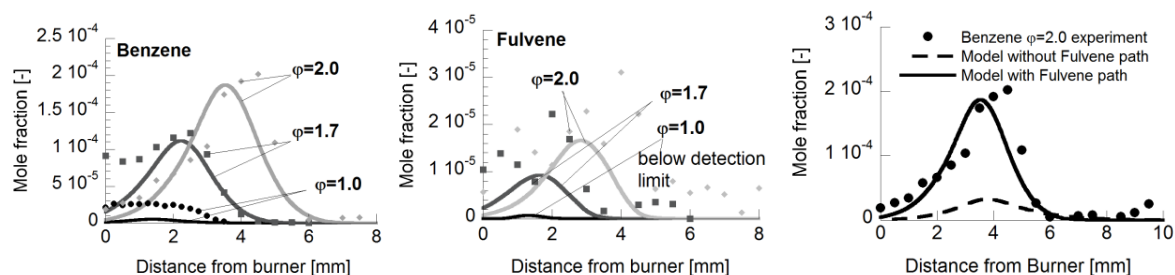


**Figure 33:**  $C_5H_{10}$ -D2,  $C_5H_8$ -D1D3,  $C_5H_8$ -D1D4 and  $C_6H_{10}$  and  $C_6H_{11}$  profiles (dots) and model prediction (lines) for 1-hexene/ $O_2$ /Ar  $\Phi=1.0, 1.7$  and 2.0 flames [18].

## Benzene formation pathways

In the previous work Nawdiyal et al. [18] which was focused to study the influence of fulvene pathway on the benzene concentration. In the section above it was shown that the chemical model captures benzene precursor mole fraction profiles providing a sound basis for analyzing benzene formation pathways. However, the sizeable concentrations of fulvene in the  $\Phi=2.0$  flame indicate that benzene formation via this intermediate plays an important role. Therefore benzene formation pathways via fulvene [67, 68, 75] were implemented in the model. With this change both fulvene and benzene mole fraction profiles could be successfully modelled (see Figure 34). The mass flow analysis shows that benzene formation is dominated by the fulvene

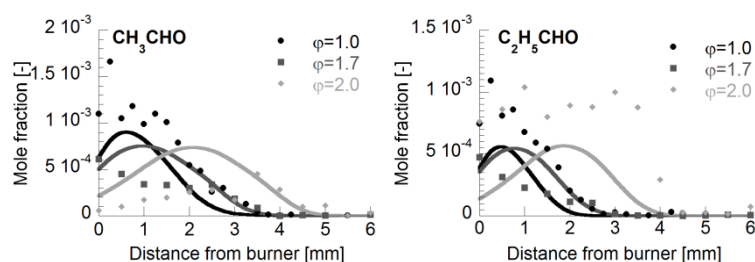
pathway (~62%), followed by propargyl recombination (~10%) and the minor pathways of  $H + A1CH_3$  (~8%), dehydrogenation of cyclohexane (~6%) and the  $n-C_4H_5 + C_2H_2$  (~3.3%) reaction. This analysis shows that the simultaneous measurement of fulvene and benzene concentrations was the key for deriving the contributions for the individual pathways. The findings indicate that benzene formation *via* fulvene may also be tested for other flames.



**Figure 34: Benzene, fulvene and influence of fulvene chemistry on the benzene formation profiles (dots) and model prediction (lines) for 1-hexene/O<sub>2</sub>/Ar  $\Phi=1.0, 1.7$  and  $2.0$  flames [18].**

### Aldehydes in the flow analysis

The important aldehydes formed in 1-hexene decomposition are  $CH_3CHO$  and  $C_2H_5CHO$ . These radicals are formed from the addition reactions with OH radical on 1-hexene. These are not so dominantly seen in the flux but are important reaction intermediates. The Figure 35 shows for  $CH_3CHO$  fairly good agreement of the model with all flames. In general, rich flames are slightly over-predicted and the stoichiometric flame is slightly under-predicted by the model. For  $C_2H_5CHO$  the  $\Phi=2.0$  flame is slightly under-predicted.



**Figure 35: Aldehydes  $CH_3CHO$  and  $C_2H_5CHO$  profiles (dots) and model prediction (lines) for 1-hexene/O<sub>2</sub>/Ar  $\Phi=1.0, 1.7$  and  $2.0$  flames [18].**

#### 4.4.3. Flame speed

Burluka et al. [57] measured laminar burning velocities for premixed 1-hexene flame at 0.5 MPa and 360K in the Leeds MkII spherical bomb.

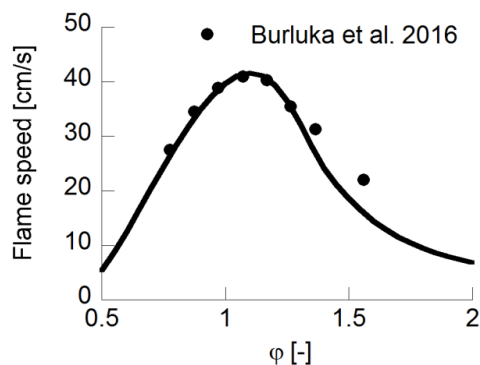


Figure 36: Hexene flame speed, 5 bar 360 K Burluka 2016 [57]

Figure 36 above shows the validation of the model against the flame speed experiment conducted by Burluka et al.[57] at 5 bar and 360K. The model predicts the flame speed very well and captures the peak of 42 cm/s at around  $\Phi=1.1$ .

#### 4.4.4. Flow Analysis

##### Degradation of 1-hexene

Common degradation pathways of 1-hexene, which operate for all equivalence ratios, proceed *via* the n-propyl ( $\text{N-C}_3\text{H}_7$ ) and the resonantly stabilized 1, 3-hexenyl ( $\text{C}_6\text{H}_{11}\text{-D1R3}$ ) radicals. These radicals are formed mainly through a unimolecular C-C-scission of 1-hexene and H-abstraction from 1-hexene respectively. This particular radical shows up because the formation of allyl radical is more favored as compared to the other five radicals. For the stoichiometric flame seen in Figure 37, the main products formed are  $\text{N-C}_3\text{H}_7$  and  $\text{C}_4\text{H}_9\text{-1}$  which are formed from unimolecular C-C-scission (Class 1) and addition through bimolecular reactions of H and OH with the fuel molecule (Class 7) respectively. It is followed by the H-abstraction from the fuel forming  $\text{C}_6\text{H}_{11}\text{-D1R3}$  (Class 2). For the rich flames Figure 38 and Figure 39, the H-abstractions from the fuel (Class 2) take over. Thus, the dominant specie there is the allyl radical  $\text{C}_6\text{H}_{11}\text{-D1R3}$  followed by  $\text{C}_6\text{H}_{11}\text{-D1R6}$  which is the primary radical. The n-propyl is also formed through unimolecular C-C-scission but is less important as compared to the H-abstractions. The addition through bimolecular reactions of H and



OH with the fuel molecule (Class 7) is also important which form the  $C_4H_9-1$  and  $C_2H_4$  species. Another flux seen here is the ring opening of cyclohexane ( $CYC_6H_{12}$ ) to 1-hexene which proceeds forming cyclohexyl radical ( $CYC_6H_{11}$ ) further going down the decomposition forming cyclohexene into  $C_4H_6$ .

The primary radical  $C_6H_{11}$ -D1R6 also forms  $CYC_6H_{11}$  adding to the flow. The  $C_6H_{11}$ -D1R3 radical is further decomposed to  $C_4H_6$ . The latter species involved in the decomposition are  $i-C_4H_5$ ,  $C_4H_4$  and  $i-C_4H_3$  forming  $C_2H_2$ . The  $C_3$  species further react to  $C_2$  species; especially to ethylene ( $C_2H_4$ ) which forms via the vinyl radical by dehydrogenation acetylene ( $C_2H_2$ ). The latter species is important for benzene formation, either directly through the reactions with  $n-C_4H_5$  [76] and  $i-C_4H_5$  [73, 77] or *via* the build-up of the propargyl radical [60]. The main degradation pathway of  $C_2H_2$  is the formation of the ketylenyl radical (HCCO) in the reaction with O atoms. Ketylenyl mainly decomposes to CH and CO and the oxidation of CO leads finally to the main reaction product  $CO_2$ . In the Figure 37, Figure 38 and Figure 39 below detailed mass flow analysis are presented for  $\Phi=1.0$ ,  $\Phi=1.7$  and  $\Phi=2.0$  illustrating the high mass flows through  $C_2H_4$ ,  $C_2H_3$  and  $C_2H_2$  and HCCO. The compilation (based on kinetic data from extensive studies by Miller, Temp, Wagner, and co-workers [see e.g. [68, 73, 78]) and the validation of the sub-mechanism involving these  $C_2$  species and their chemical coupling to  $C_3$  species via reactions of acetylene with CH,  $^3CH_2$  and  $^1CH_2$  is the chemical core of the model and also of paramount importance for the prediction flame speeds as extensively discussed in [59, 60]. The kinetic data of this sub-mechanism remained largely unchanged. Due to the complexity of a  $C_6$  fuel there exist many minor fuel degradation pathways via  $C_4$  and  $C_5$  species. These pathways are illustrated in the detailed flow analysis. However, one minor pathway of 1-hexene degradation has to be mentioned. In the kinetic model the formation of cyclohexane and its dehydrogenation to benzene is implemented [21, 29, 47] [43].

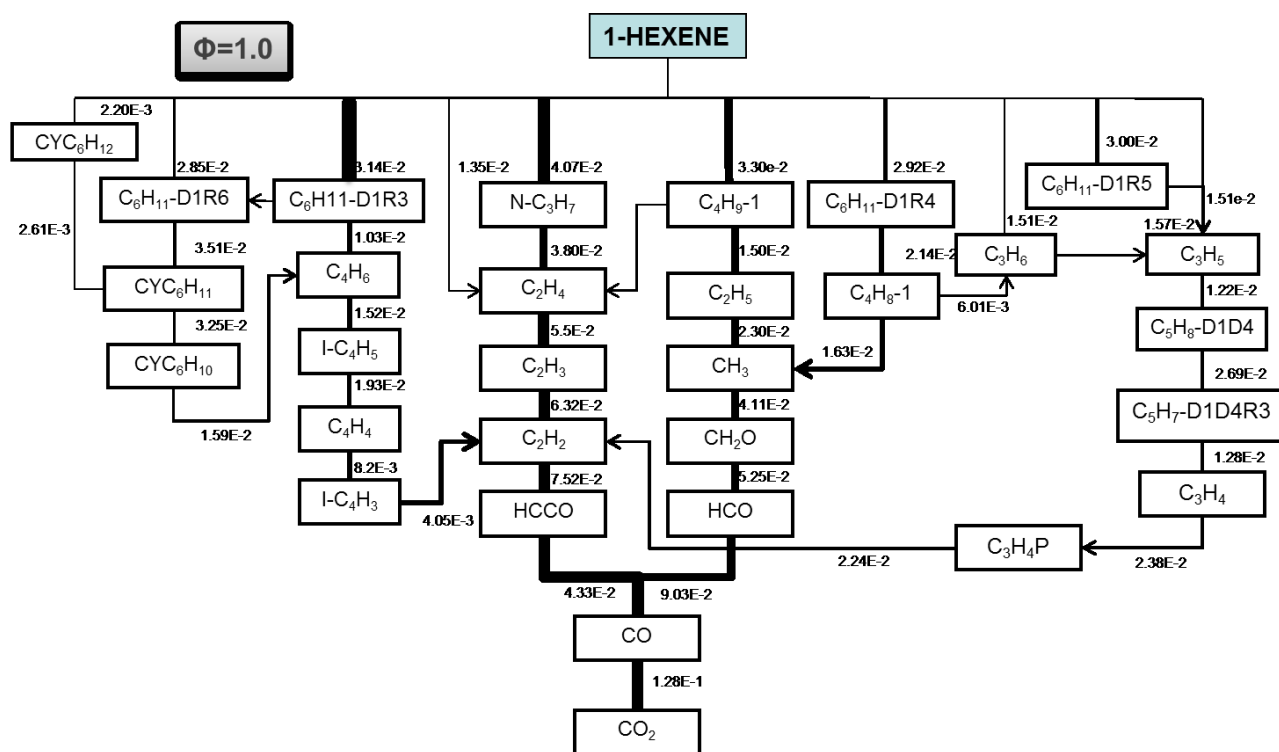


Figure 37: Flow analysis of 1-hexene/O<sub>2</sub>/Ar flame at  $\Phi=1.0$ , p=15 Torr [18]

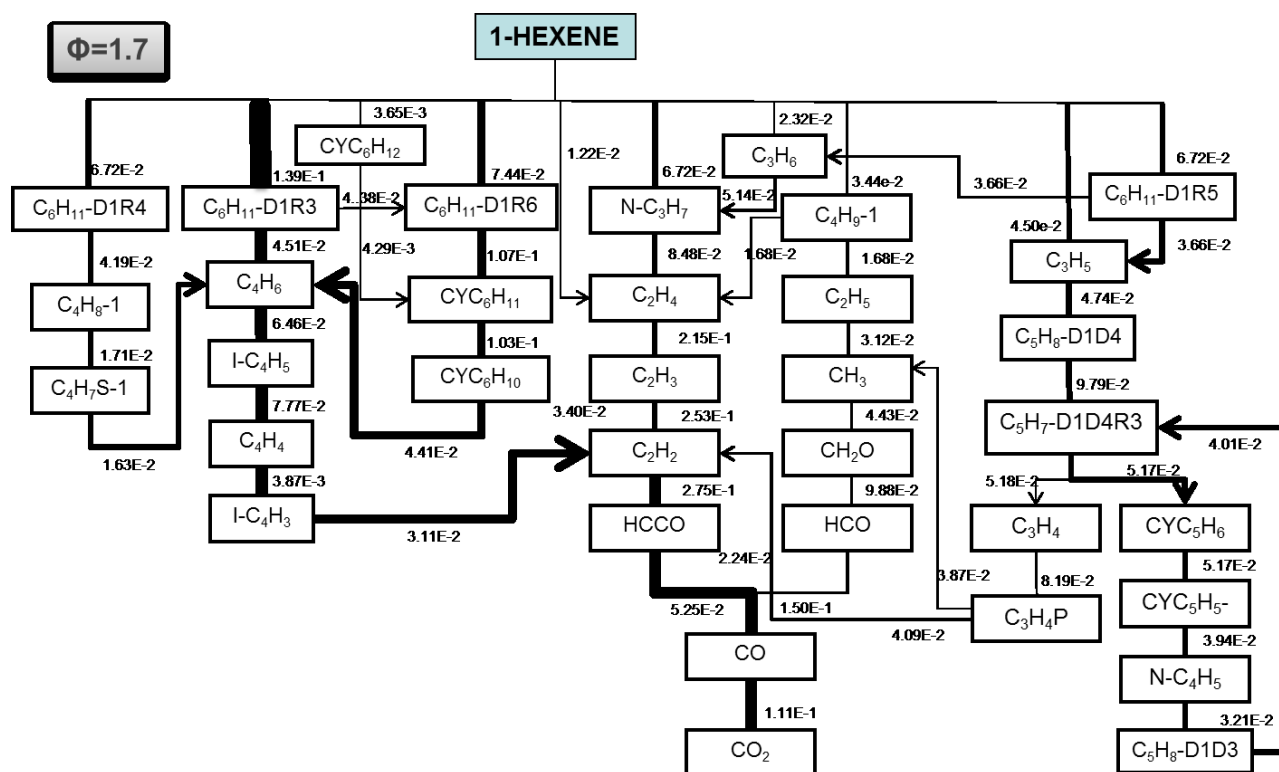


Figure 38: Flow analysis of 1-hexene/O<sub>2</sub>/Ar flame at  $\Phi=1.7$ , p=30 Torr [18]

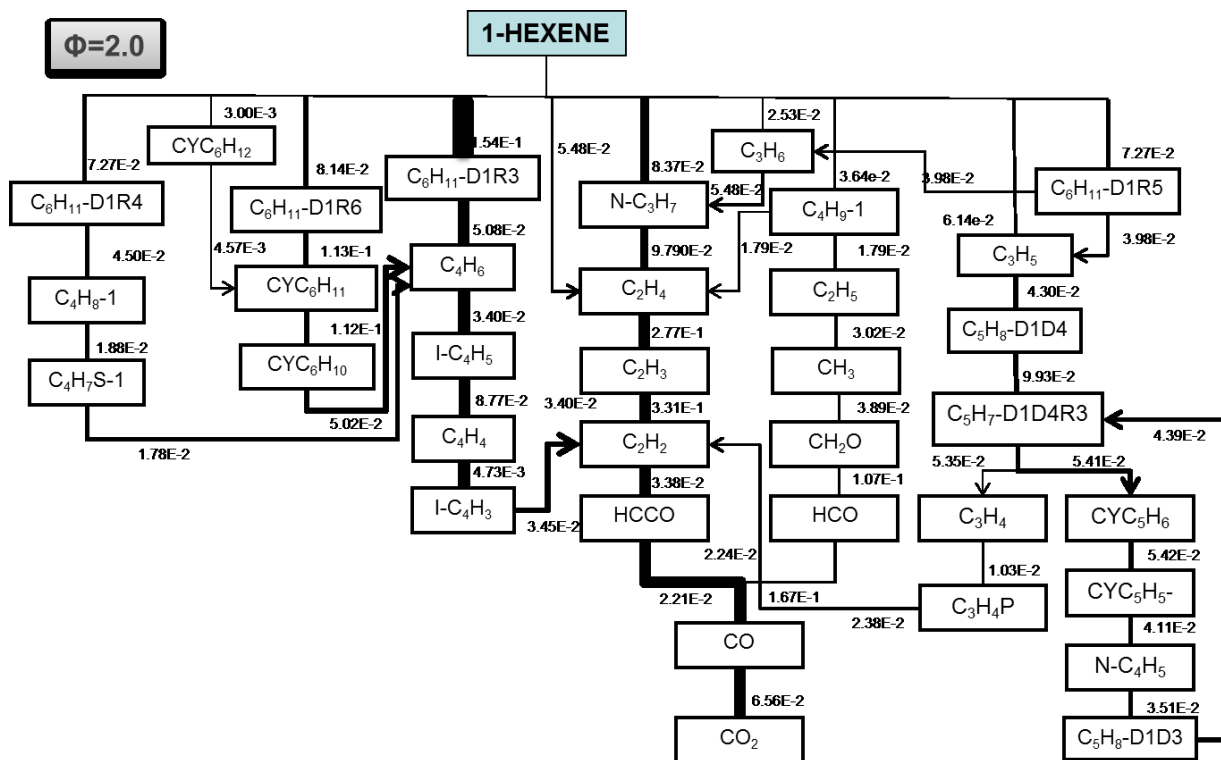


Figure 39: Flow analysis of 1-hexene/O<sub>2</sub>/Ar flame at  $\Phi=2.0$ ,  $p=30$  Torr [18]

#### 4.4.5. Sensitivity Analysis

Figure 40 and Figure 41 show the sensitivity analysis at  $T=1350\text{K}$  and  $T=1550\text{K}$  respectively for 1-hexene/O<sub>2</sub>/Ar mixture in a shock tube reactor at  $p=2$  bar,  $\Phi=1.0$ .

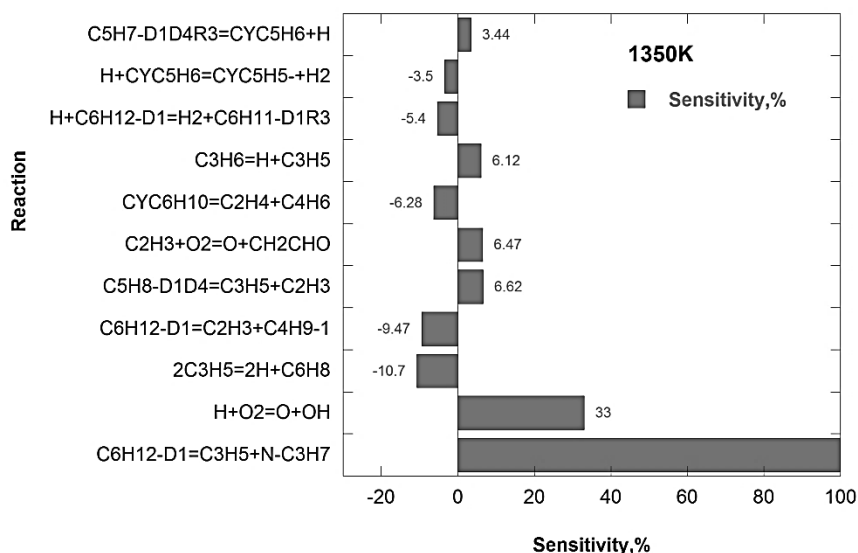
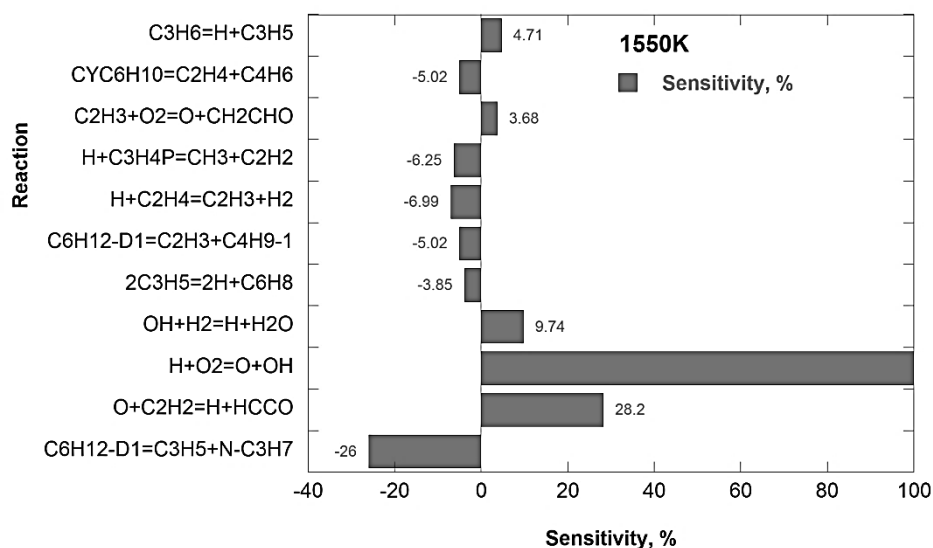


Figure 40: Sensitivity analysis for 1-hexene/O<sub>2</sub>/Ar mixture in a shock tube at  $p=2$  bar,  $\Phi=1.0$  and  $T=1350\text{K}$  [53]



**Figure 41: Sensitivity analysis for 1-hexene/O<sub>2</sub>/Ar mixture in a shock tube at p= 2bar, Φ= 1.0 and T=1550K [53]**

The uni-molecular decomposition of 1-hexene (C<sub>6</sub>H<sub>12</sub>-D1) to form n-propyl and allyl radical shows up in the sensitivity and has a negative value stressing the intensity on the backward reaction. It is 100 % sensitive for 1350 K while at 1550 K it is 25 % sensitive. Another class 1 reaction which shows up is the one forming C<sub>4</sub>H<sub>9</sub>-1 and C<sub>2</sub>H<sub>3</sub>. The intensities of these reactions are emphasized at 1350 K than those at 1550K. This completely is in agreement with the flow analysis at Φ=1.0 (Figure 37).

The H-abstraction of 1-hexene forming allyl C<sub>6</sub>H<sub>11</sub>-D1R3 radical (Class 2) is also observed at 1350 K with a negative 5.4 % sensitivity. The reaction becomes either very less sensitive or not at all sensitive at 1550 K since it is not observed. The diene C<sub>5</sub>H<sub>8</sub>-D1D4 and its decomposition (Class 8) into allyl radical and C<sub>2</sub>H<sub>3</sub> are observed to be 6.6 % sensitive. The dehydrogenation of this diene into C<sub>5</sub>H<sub>7</sub>-D1D4R3 and then isomerisation to form cyclopentadiene (CYC<sub>5</sub>H<sub>6</sub>) which further decomposes to cyclopentadienyl radical (CYC<sub>5</sub>H<sub>5</sub><sup>-</sup>) is also strongly observed at 1350 K. It is clear that the other most sensitive reactions are from the base chemistry which forms C<sub>2</sub>H<sub>2</sub>, HCCO and finally CO and CO<sub>2</sub>. These are the most sensitive reactions at 1550 K.

#### 4.5. Conclusion on 1-hexene model

This model is an update of the previously published model in Nawdiyal et al. [18]. The olefin oxidation is generally significant for the allyl radical formation, in this case  $C_6H_{11}$ -D1R3 radical which in the publication was not considered for the H-abstraction from the fuel. In this study, the effect is included which is evident in the  $C_6H_{11}$  profile. Though the argument was, if this radical is less important than the  $C_6H_{11}$ -D1R6 primary radical, it would result in increase in cyclohexyl ( $CYC_6H_{11}$ ) formation. This is not clearly seen in the model prediction. On contrary, cyclohexene ( $CYC_6H_{10}$ ) is seen to be extremely high. Possibly, there are other important pathways leading to this conclusion. Apart from this, the benzene and fulvene profiles are very good along with the other important species. The main degradation of 1-hexene proceeds through its  $\beta$ -scission forming *n*-propyl ( $N-C_3H_7$ ) and allyl ( $C_3H_5$ ) along with the H-abstraction forming the allyl radical  $C_6H_{11}$ -D1R3 which further decomposes to butadiene. The 1-hexene model predicts ignition delays very well and the flame structures are also very well captured. The flame speed is also perfectly predicted. Thus, it can be concluded that the 1-hexene chemical kinetic model developed in this study is a comprehensive model. It is able to simulate the ignition delay times, flame speed and specie profiles of most species accurately.

## 5. METHYLCYCLOHEXANE KINETIC MODEL

### 5.1. Structure of methylcyclohexane

The chemical structure of methylcyclohexane is as shown in Figure 42 with methyl group on cyclohexane ring. Some important properties of methylcyclohexane are compiled in Table XXIX.

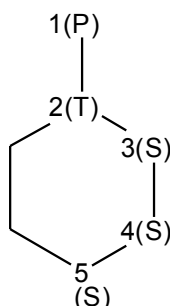


Figure 42: Structure of Methylcyclohexane where P, S and T are primary, secondary and tertiary H-sites while 1-5 are the C-atoms numbered.

	Methylcyclohexane (MCH)
Chemical formula	CYC <sub>7</sub> H <sub>14</sub>
Density	0.77 g/cm <sup>3</sup>
Auto Ignition	545 °F
Boiling Point	101 °C (374 K)
Melting point	-126.3 °C (-146.8 K)
Vapor Pressure	37 mmHg (20°C)
RON	74.8(MON 71)
Cetane number	20

Table XXIX: Table of chemical properties of methylcyclohexane

### 5.2. Research background

#### Experimental studies

Among the different groups of hydrocarbon components present in the various fuels like diesel and jet fuels, *n*-alkanes and aromatics are the most studied hydrocarbons. Cyclic hydrocarbons are not so extensively studied.

Early in 1989, Brown and King [33], carried out a VLPP experiment to study the decomposition of methylcyclohexane at temperatures 861-1218 K. They suggested a rate constant for the ring opening of methylcyclohexane. In 1997, Zeppieri group [79] conducted a high temperature (1050 – 1200 K) pyrolysis study of pure methylcyclohexane and oxidation studies of pure methylcyclohexane and its blend

with toluene in their Princeton turbulent flow reactor at atmospheric pressure. They highly investigated the effect of initial fuel concentration on the fuel decomposition and the main pathways involved. They found that the rates of oxidation depend greatly on the initial concentration and the main pathway of decomposition being the homolysis of the fuel producing cyclohexyl radical breaking down to more stable intermediates like ethene and 1,3-cyclopentadiene.

Vasu et al. [80] have measured ignition delay times for methylcyclohexane/air and methylcyclohexane/O<sub>2</sub>/Ar mixtures in a shock tube at pressures 1-50 atm. Low pressure ignition delay times were measured for methylcyclohexane/O<sub>2</sub>/Ar mixtures over a range of conditions: 0.25-1.0 % fuel mole fraction, 1.3-2.9 atm, 1225-1560 K for  $\phi=0.5$  to 2.0. The low pressure data was collected from 67 experiments which were scaled to a pressure of 1.5 atm using a correlation expression. High pressure data was measured for 1.96 % methylcyclohexane in air mixture of pressures from 17.2 to 49.2 atm, temperatures from 795 to 1098 K for  $\phi=1.0$ . Another group, Orme et al. [50] have investigated methylcyclohexane/O<sub>2</sub> mixtures in a high temperature shock tube at pressures 1, 2 and 4 atm for different equivalence ratios 0.5, 1.0 and 2.0. They have also developed a high temperature kinetic model for the oxidation of methylcyclohexane which they validated for their ignition delay experiments as well as flow reactor experiments [79].

Pitz [81] developed an oxidation mechanism of methylcyclohexane and validated against their own RCM experiment. They measured ignition delay times for methylcyclohexane/O<sub>2</sub>/diluent three different mixtures of N<sub>2</sub> and Ar (100 % N<sub>2</sub>, 100 % Ar, 50 % N<sub>2</sub> and 50 % Ar) at compressed pressures of 10, 15 and 20 atm and  $\Phi=1.0$ . The experiments were conducted with compression time 16.6 ms and compression ratio 10.5:1 at temperatures from 680 to 980 K. Ignition delays in RCM were also measured by Mittal and Sung [82]. They conducted experiments for methylcyclohexane/O<sub>2</sub>/Ar/N<sub>2</sub> mixtures at 15.1 and 25.5 bar compressed pressures and  $\Phi$  from 0.5 to 1.5 over 680-905K compressed temperature range from 680 to 905K. Later in 2013, they conducted yet another set of experiments in RCM for methylcyclohexane/O<sub>2</sub>/Ar/N<sub>2</sub> mixtures at 50 atm and  $\Phi$  from 0.5 to 1.5 over compressed temperature range from 690 to 910 K [83].

McEnally and Pfefferle report [84] on non-premixed methane/air flames doped with methylcyclohexane suggested different pathways for aromatic formation rather than the dehydrogenation of the ring. Also, they found out that the cycloalkanes mainly decompose through unimolecular decomposition or H-abstraction. Skeen et al. [85] have studied methylcyclohexane/O<sub>2</sub>/Ar flames at three different equivalence ratios 1.0, 1.75 and 1.9. The flames were stabilized on a flat-flame McKenna burner at pressures of 15, 20 and 30 Torr, respectively. The focus of the study was to investigate the formation of aromatic species and the competing pathways involved in it. Recently in 2014, Wang et al. [86] measured a premixed flame of methylcyclohexane with  $\Phi=1.75$  at 30 Torr along with methylcyclohexane pyrolysis at three different pressures of 30, 150 and 760 Torr.

Ji et al. [32] have determined laminar flame speeds for methylcyclohexane/air mixtures at  $p=1\text{bar}$  and  $T=353\text{K}$  for wide range of equivalence ratios. Later, Wu et al. 2012 [30] also measured laminar flame speeds of methylcyclohexane ranging from atmospheric pressure up to 20 atm at 353 K initial temperature.

### **Modelling studies**

Granata et al. [39] has developed a semi-detailed model for the oxidation and pyrolysis of cycloalkanes. The model has been validated for the pyrolysis experiment of Zeppieri et al. [79]. Orme et al. [50] later in 2006 developed a detailed high temperature kinetic model to simulate shock tube experiments conducted by the same group and also the Zeppieri flow reactor experiment. Pitz et al. [81] in 2007 developed a chemical model for methylcyclohexane oxidation. They added a newly developed low temperature mechanism for the oxidation of methylcyclohexane to their previously developed mechanism [42] and high temperature methylcyclohexane oxidation mechanism from Orme et al. [50] and validated the model against ignition delay times measured by them in a rapid compression machine.

Weber et al. [83] updated a previously developed LLNL model [81] which they validated for their RCM experiments. Wang et al. [86] proposed a model for the oxidation of methylcyclohexane which they validated for their pyrolysis and premixed flame experiments. Their Jetsurf v2.0 mechanism is an ongoing development of high temperature mechanisms of n-alkanes, cycloalkanes and alkylated cycloalkanes



including methylcyclohexane. The performance of this model has been tested for ignition delays, flame speed and premixed flames [87]. Narayanswamy et al. [88] developed a short mechanism for the previously developed methylcyclohexane mechanism by Pitz et al. [81] and validated for various experiments like shock tubes, flame speed and plug flow reactor.

### **5.3. Methylcyclohexane kinetic model development**

The sub-mechanism of Methylcyclohexane is formulated partly in analogy with the cyclohexane mechanism previously developed in 1-hexene model from Nawdiyal et al. [18]. The high temperature mechanism initiates with the ring opening in two channels viz. 1. forming Heptene and 2. forming Ethene and Propene. It also includes unimolecular initiation via C–H scission to produce five different methylcyclohexyl radicals and removal of methyl group forming cyclohexyl radical. The isomerization of cycloalkanes into olefins is another important pathway forming heptenyl radical. H-atom abstraction reactions by small radicals such as H, O, OH, HO<sub>2</sub>, CH<sub>3</sub> etc. are also included. Rules from Ahmed et al. [47] are followed in general while for the abstraction of tertiary hydrogen (between the ring and methyl group) Curran [42] and Orme [50] rates are applied. The methylcyclohexyl radicals break down mainly to form cyclo-olefins and to smaller olefins which are further decomposed following rules from Nawdiyal et al. [18].

The core model consists of C1-C4 base chemistry validated by Hoyermann et al. [60], Schenk et al. [66] and Nawdiyal et al. [18]. The base mechanism consists of 223 species and 1276 reversible reactions. The sub-mechanism from methylcyclohexane consists of 80 species and 2117 reversible reactions. The assembled mechanism thus consists of 303 species and 3393 reversible elementary reactions.

All calculations have been performed with the current version of the LOGEsoft package [15]. The thermodynamic properties of species were taken from Goos, Burcat, Rusic database [16]. For other several new species in the methylcyclohexane sub-mechanism were evaluated implementing Benson's group additivity method [17]. The mechanism development for the high temperature range is as follows.

## Class 1: Unimolecular fuel decomposition (Initiation reactions)

The three different types of decomposition pathways for methylcyclohexane are;

- 1. Ring opening:** The ring opening of the fuel molecule can occur at three different sites C2-C3, C3-C4 and C4-C5 (See Figure 42). The opening of the ring results in the formation of olefins. The ring opening at C2-C3 position yields the corresponding C<sub>7</sub>H<sub>14</sub>-D1 olefin. The rate coefficient for this pathway is taken from Tsang [21] in analogy to cyclohexane. For the positions C3-C4 and C4-C5, complex iso-olefins are formed and instead global reactions are written to form propene and ethylene. The rate coefficient for this pathway is taken in analogy to cyclohexane from Steil et al. [22]. Brown et al. [33] suggests different rates for channel 1 which is ring opening at C2-C3, channel 2 which is the sum of ring opening at C3-C4 and C4-C5, and channel 3 which is the fission to methyl and cycloalkyl radicals. Here, Brown rates are followed for channel 3 as shown in Table XXX.
- 2. Decomposition via H-abstraction:** Homolysis of the bonds can also occur at four different sites on the ring and one site on the methyl group. Thus, five different radicals are formed (CYC<sub>7</sub>H<sub>13</sub>-R1 to CYC<sub>7</sub>H<sub>13</sub>-R5). The rate coefficients for the reactions depend on the type of H atom involved and the site. For the primary site on the methyl group Ahmed *n*-heptane coefficients [47] are used while for the H atoms on the ring, analogy with cyclohexane has been used.
- 3. Removal of methyl radical** on the ring forming cyclohexyl radical (CYC<sub>6</sub>H<sub>11</sub>). Brown coefficients [33] are used for this particular decomposition reaction.

Reactions	A ( $\frac{\text{cm}^3}{\text{mol}\cdot\text{s}}$ )	n	E <sub>a</sub> ( $\frac{\text{cal}}{\text{mol}}$ )	Ref.
<b>1. Ring Opening</b>				
a. CYC <sub>7</sub> H <sub>14</sub> => C <sub>7</sub> H <sub>14</sub> -D1	5.010E+16	0.00	88220	[21]
b. CYC <sub>7</sub> H <sub>14</sub> => 2C <sub>2</sub> H <sub>4</sub> + C <sub>3</sub> H <sub>6</sub>	1.600E+16	0.00	90000	[22]
<b>2. H-abstraction</b>				
CYC <sub>7</sub> H <sub>14</sub> = H + CYC <sub>9</sub> H <sub>17</sub> -R1 to CYC <sub>9</sub> H <sub>17</sub> -R5	2.500E+27	-3.80	97020	[47]
<b>3. Removal of CH<sub>3</sub> group</b>				
CYC <sub>7</sub> H <sub>14</sub> = CH <sub>3</sub> + CYC <sub>6</sub> H <sub>11</sub>	1.259E+16	0.00	87950	[33]

Table XXX: Kinetic data for Class 1: Unimolecular decomposition of methylcyclohexane

The reactions taking place on the ring are treated in analogy to cyclohexane and where required typical methylcyclohexane rates are used. Ahmed rules [47] are used for decomposition via H-abstraction on the primary position only and the rest are treated in analogy to cyclohexane rates [18].

## Class 2: H-abstraction from the fuel molecule

Reactions	$A \left( \frac{\text{cm}^3}{\text{mol}\cdot\text{s}} \right) \text{ per } H$	n	$E_a \left( \frac{\text{cal}}{\text{mol}} \right)$	Ref.
$\text{CYC}_7\text{H}_{14} + \text{H} = \text{CYC}_7\text{H}_{13}\text{-R..} + \text{H}_2$				
<b>Primary</b>	5.63E+07	2.0	7700	[47]
<b>Secondary</b>	2.45E+07	2.0	5000	[47]
<b>Tertiary</b>	6.02E+05	2.4	2583	[42]
$\text{CYC}_7\text{H}_{14} + \text{OH} = \text{CYC}_7\text{H}_{13}\text{-R..} + \text{H}_2\text{O}$				
<b>Primary</b>	1.75E+09	0.97	1590	[47]
<b>Secondary</b>	2.34E+07	1.61	-35.8	[47]
<b>Tertiary</b>	1.70E+06	1.90	-1451	[42]
$\text{CYC}_7\text{H}_{14} + \text{O} = \text{CYC}_7\text{H}_{13}\text{-R..} + \text{OH}$				
<b>Primary</b>	3.66E+05	2.40	5500	[47]
<b>Secondary</b>	1.18E+05	2.50	2200	[47]
<b>Tertiary</b>	6.01E-10	6.36	893	[42]
$\text{CYC}_7\text{H}_{14} + \text{CH}_3 = \text{CYC}_7\text{H}_{13}\text{-R..} + \text{CH}_4$				
<b>Primary</b>	2.17E+11	0.0	11600	[47]
<b>Secondary</b>	2.00E+11	0.0	9500	[47]
<b>Tertiary</b>	8.96E+03	2.33	6147	[42]
$\text{CYC}_7\text{H}_{14} + \text{HO}_2 = \text{CYC}_7\text{H}_{13}\text{-R..} + \text{H}_2\text{O}_2$				
<b>Primary</b>	2.68E+12	0.0	19400	[47]
<b>Secondary</b>	2.44E+12	0.0	17000	[47]
<b>Tertiary</b>	2.80E+12	0.0	16013	[42]
$\text{CYC}_7\text{H}_{14} + \text{CH}_3\text{O} = \text{CYC}_7\text{H}_{13}\text{-R..} + \text{CH}_3\text{OH}$				
<b>Primary</b>	5.27E+10	0.0	7000	[47]
<b>Secondary</b>	5.48E+10	0.0	5000	[47]
<b>Tertiary</b>	1.90E+10	0.00	2800	[42]
$\text{CYC}_7\text{H}_{14} + \text{O}_2 = \text{CYC}_7\text{H}_{13}\text{-R..} + \text{HO}_2$				
<b>Primary</b>	4.17E+12	0.0	49000	[47]
<b>Secondary</b>	1.00E+13	0.0	47600	[47]
<b>Tertiary</b>	7.00E+12	0.0	46060	[42]
$\text{CYC}_7\text{H}_{14} + \text{C}_2\text{H}_5 = \text{CYC}_7\text{H}_{13}\text{-R..} + \text{C}_2\text{H}_6$				
<b>Primary</b>	1.67E+10	0.0	13400	[47]
<b>Secondary</b>	2.50E+10	0.0	10400	[47]
<b>Tertiary</b>	1.00E+11	0.0	7900	[42]
$\text{CYC}_7\text{H}_{14} + \text{C}_2\text{H}_3 = \text{CYC}_7\text{H}_{13}\text{-R..} + \text{C}_2\text{H}_4$				
<b>Primary</b>	1.67E+11	0.0	18000	[47]
<b>Secondary</b>	2.00E+11	0.0	16800	[47]
<b>Tertiary</b>	2.00E+11	0.0	14300	[42]
$\text{CYC}_7\text{H}_{14} + \text{CH}_3\text{O}_2 = \text{CYC}_7\text{H}_{13}\text{-R..} + \text{CH}_3\text{O}_2\text{H}$				
<b>Primary</b>	2.00E+12	0.0	20400	[47]
<b>Secondary</b>	2.00E+12	0.0	17700	[47]
<b>Tertiary</b>	--	--	--	[42]

Table XXXI: Kinetic data for Class 2: H-abstraction from methylcyclohexane as fuel

The H-abstraction from the cycloalkane takes place at five different sites viz. the primary (on the methyl group);  $CyC_7H_{13}-R1$ , secondary (on the ring);  $CyC_7H_{13}-R3$ ,  $CyC_7H_{13}-R4$ ,  $CyC_7H_{13}-R5$  and tertiary  $CyC_7H_{13}-R2$ .

The rates for the primary H abstractions are taken from Ahmed et al. [47], for secondary H abstractions from cyclohexane [18] and for the tertiary H abstractions from Curran et al. [42].

### Class 3: Alkyl radical decomposition

The cyclo-alkyl radicals undergo both C-H and C-C scissions to form cyclo-alkenes and other small products. The different cyclo-alkenes formed in this class are  $CYC_7H_{12}-D1$ ,  $CYC_7H_{12}-D2$ ,  $CYC_7H_{12}-D3$ ,  $CYC_7H_{12}-D4$  as seen in Table XXXII. Orme et al. [50] does not consider the formation of cyclo-olefins instead, they decompose the isomerized straight chain products formed from the cyclo-alkyl radicals. Also, the reactions occur in the reverse direction i.e. addition of alkyl radical (here  $C_5H_9-D1R5$ ) to the olefin (here  $C_2H_4$ ).

In the current mechanism, Ahmed coefficients [47] are used.

Reactions	A ( $\frac{cm^3}{mol \cdot s}$ )	n	E <sub>a</sub> ( $\frac{cal}{mol}$ )	Ref.
<b>Primary</b>				
$C_2H_4 + C_5H_9-D1R5 = CYC_7H_{13}-R1$	8.50E+10	0.00	77900	[47]
$H + CYC_7H_{12}-D1 = CYC_7H_{13}-R1$	1.00E+13	0.00	29000	[47]
<b>Tertiary</b>				
$C_2H_4 + C_5H_9-M2D1R4 = CYC_7H_{13}-R2$	8.50E+10	0.00	77900	[47]
$H + CYC_7H_{12}-D1 = CYC_7H_{13}-R2$	1.00E+13	0.00	29000	[47]
$H + CYC_7H_{12}-D2 = CYC_7H_{13}-R2$	1.00E+13	0.00	29000	[47]
<b>Secondary</b>				
$C_2H_4 + C_5H_9-D1R5 = CYC_7H_{13}-R3$	8.50E+10	0.00	77900	[47]
$H + CYC_7H_{12}-D2 = CYC_7H_{13}-R3$	1.00E+13	0.00	29000	[47]
$H + CYC_7H_{12}-D3 = CYC_7H_{13}-R3$	1.00E+13	0.00	29000	[47]
$C_2H_4 + C_5H_9-D1R5 = CYC_7H_{13}-R4$	8.50E+10	0.00	77900	[47]
$H + CYC_7H_{12}-D3 = CYC_7H_{13}-R4$	1.00E+13	0.00	29000	[47]
$H + CYC_7H_{12}-D4 = CYC_7H_{13}-R4$	1.00E+13	0.00	29000	[47]

Table XXXII: Kinetic data for Class 3: Alkyl radical decomposition for methylcyclohexane

### Class 4: Alkyl radical + O<sub>2</sub> direct formation of olefin and HO<sub>2</sub>

According to Curran [4], this class of reaction depends on the number of carbon atoms in the molecule and their possible vibrations. With higher number of carbon atoms than 4, the number of vibrations increase, delocalizing the excess energy of

the C-O bond ( $\approx 34$  kcal/mol) which lowers the possibility of breaking of this bond and increases the possibility of forming ROO adduct which passes through the low temperature regime. This class of reaction is thus irrelevant for cycloalkanes and is therefore excluded.

### Class 5: Alkyl Radical isomerisation

This class of reaction is based on the type of radical site (endo- or exo-ring) at which the ring opening will occur. Different straight alkenyl and iso-alkenyl radicals are formed in this class as seen in Table XXXIII. They will further decompose in Class 8. The rate constants are taken from Orme et al. [50]. The reverse reactions (in the ring closing direction) are exclusively written and follow Orme constants [50].

Reactions	A ( $\frac{\text{cm}^3}{\text{mol}\cdot\text{s}}$ )	n	E <sub>a</sub> ( $\frac{\text{cal}}{\text{mol}}$ )	Ref.
C <sub>7</sub> H <sub>13</sub> -D1R7 = CyC <sub>7</sub> H <sub>13</sub> -R1	1.00E+08	0.90	5900	[50]
C <sub>7</sub> H <sub>13</sub> -M2D1R6 = CyC <sub>7</sub> H <sub>13</sub> -R2	1.00E+08	0.90	5900	[50]
C <sub>7</sub> H <sub>13</sub> -D2R6 = CyC <sub>7</sub> H <sub>13</sub> -R3	1.00E+08	0.90	8700	[50]
C <sub>7</sub> H <sub>13</sub> -M2D1R6 = CyC <sub>7</sub> H <sub>13</sub> -R3	1.00E+08	0.90	8700	[50]
C <sub>7</sub> H <sub>13</sub> -D1R6 = CyC <sub>7</sub> H <sub>13</sub> -R4	1.00E+08	0.90	8500	[50]
C <sub>7</sub> H <sub>13</sub> -M4D1R6 = CyC <sub>7</sub> H <sub>13</sub> -R4	1.00E+08	0.90	5900	[50]
C <sub>7</sub> H <sub>13</sub> -M5D1R6 = CyC <sub>7</sub> H <sub>13</sub> -R5	1.00E+08	0.90	5900	[50]

Table XXXIII: Kinetic data for Class 5: Methylcycloalkyl radical isomerisation

### Class 6: Abstraction reactions from olefins

The olefins formed in classes 1 and 3 (C<sub>7</sub>H<sub>14</sub>-D1, CYC<sub>7</sub>H<sub>12</sub>-D1, CYC<sub>7</sub>H<sub>12</sub>-D2, CYC<sub>7</sub>H<sub>12</sub>-D3, CYC<sub>7</sub>H<sub>12</sub>-D4) undergo further abstraction through radical attackers H, OH, O, CH<sub>3</sub>, HO<sub>2</sub>, CH<sub>3</sub>O and O<sub>2</sub>. For simplicity, global reactions are written to from products. Here, coefficients from Nawdiyal et al. [18] are followed except for tertiary position where Curran iso-octane rates [42] are followed in analogy to fuel abstraction.

### Class 7: Addition of radical species

The mechanism accounts for the addition reactions of H, OH and O radicals on the olefins in analogy to 1-hexene model. The addition of H radical takes place at either C sites on the double bond and follows breaking of the ring. C<sub>2</sub>H<sub>4</sub> is a favourable product formed along with the side product remaining. In the addition of OH radical, the H from the OH group moves to the closest site and finally breaks to form a ketone or aldehyde along with C<sub>2</sub>H<sub>4</sub>. Complicated epoxy's being formed by the addition of O

radical; these types of reactions are not considered. The rate constants followed here are from Nawdiyal et al. [18] with zero activation for H and OH additions.

Reactions	$A \left( \frac{\text{cm}^3}{\text{mol}\cdot\text{s}} \right) \text{per } H$	n	$E_a \left( \frac{\text{cal}}{\text{mol}} \right)$	Ref.
CYC <sub>7</sub> H <sub>1</sub> -D.. + H = Products + H <sub>2</sub>				
<b>Primary</b>	5.63E+07	2.0	7700	[18]
<b>Secondary</b>	2.45E+07	2.0	5000	[18]
<b>Tertiary</b>	6.02E+05	2.4	2583	[42]
CYC <sub>7</sub> H <sub>1</sub> -D.. + OH = Products + H <sub>2</sub> O				
<b>Primary</b>	1.75E+09	0.97	1590	[18]
<b>Secondary</b>	2.34E+07	1.61	-35.8	[18]
<b>Tertiary</b>	1.70E+06	1.90	-1451	[42]
CYC <sub>7</sub> H <sub>1</sub> -D.. + O = Products + OH				
<b>Primary</b>	3.66E+05	2.40	5500	[18]
<b>Secondary</b>	1.18E+05	2.50	2200	[18]
<b>Tertiary</b>	6.01E-10	6.36	893	[42]
CYC <sub>7</sub> H <sub>1</sub> -D.. + CH <sub>3</sub> = Products + CH <sub>4</sub>				
<b>Primary</b>	2.17E+11	0.0	11600	[18]
<b>Secondary</b>	2.00E+11	0.0	9500	[18]
<b>Tertiary</b>	8.96E+03	2.33	6147	[42]
CYC <sub>7</sub> H <sub>1</sub> -D.. + HO <sub>2</sub> = Products + H <sub>2</sub> O <sub>2</sub>				
<b>Primary</b>	2.68E+12	0.0	19400	[18]
<b>Secondary</b>	2.44E+12	0.0	17000	[18]
<b>Tertiary</b>	2.80E+12	0.0	16013	[42]
CYC <sub>7</sub> H <sub>1</sub> -D.. + CH <sub>3</sub> O = Products + CH <sub>3</sub> OH				
<b>Primary</b>	5.27E+10	0.0	7000	[18]
<b>Secondary</b>	5.48E+10	0.0	5000	[18]
<b>Tertiary</b>	1.90E+10	0.00	2800	[42]
CYC <sub>7</sub> H <sub>1</sub> -D.. + O <sub>2</sub> = Products + HO <sub>2</sub>				
<b>Primary</b>	4.17E+12	0.0	49000	[18]
<b>Secondary</b>	1.00E+13	0.0	47600	[18]
<b>Tertiary</b>	7.00E+12	0.0	46060	[42]

Table XXXIV: Kinetic data for Class 6: Abstraction reactions from olefins in methylcyclohexane oxidation

Reactions	$A \left( \frac{\text{cm}^3}{\text{mol}\cdot\text{s}} \right)$	n	$E_a \left( \frac{\text{cal}}{\text{mol}} \right)$	Ref.
H+CYC <sub>7</sub> H <sub>12</sub> -D1=C <sub>2</sub> H <sub>4</sub> +C <sub>5</sub> H <sub>9</sub> -D1R5	5.000E+12	0.00	0	[18]
H+CYC <sub>7</sub> H <sub>12</sub> -D1=C <sub>2</sub> H <sub>4</sub> +C <sub>5</sub> H <sub>9</sub> -M2D1R4	5.000E+12	0.00	0	[18]
OH+CYC <sub>7</sub> H <sub>12</sub> -D1=CH <sub>2</sub> O+CYC <sub>6</sub> H <sub>11</sub>	1.000E+13	0.00	0	[18]
O+CYC <sub>7</sub> H <sub>12</sub> -D1=HCO+CYC <sub>6</sub> H <sub>11</sub>	1.000E+13	0.00	200	[18]

Table XXXV: Kinetic data for Class 7: Addition on the double bond

### Class 8: Alkenyl radical decomposition

Since in Class 6, the olefins are considered to decompose globally to products, no reactions pertaining to those species exist. This class includes only CYC<sub>6</sub>H<sub>9</sub> reactions which is the cyclohexane specie. Benzene formation through

dehydrogenation of  $\text{CYC}_6\text{H}_9$  and  $\text{CYC}_6\text{H}_7$  is considered in this class (See Chapter 3, Table XV).

### Class 9: Olefin decomposition

Since these are cyclo-olefins, ring specific rates are followed here in analogy to cyclohexane rates [51]. In this class the straight olefins ( $\text{C}_7\text{H}_{14}\text{-D1}$ ) are decomposed via  $\beta$ -scission following Nawdiyal et al. [18] as shown in Table XXXVI.

Reactions	$A \left( \frac{\text{cm}^3}{\text{mol}\cdot\text{s}} \right)$	n	$E_a \left( \frac{\text{cal}}{\text{mol}} \right)$	Ref.
$\text{CYC}_7\text{H}_{12}\text{-D1}=\text{C}_4\text{H}_8\text{-1}+\text{C}_3\text{H}_4$	1.350E+15	0.00	66600	[51]
$\text{CYC}_7\text{H}_{12}\text{-D2}=\text{C}_4\text{H}_6\text{12}+\text{C}_3\text{H}_6$	1.350E+15	0.00	66600	[51]
$\text{CYC}_7\text{H}_{12}\text{-D3}=\text{C}_4\text{H}_8\text{-1}+\text{C}_3\text{H}_4$	1.350E+15	0.00	66600	[51]
$\text{CYC}_7\text{H}_{12}\text{-D4}=\text{C}_4\text{H}_6+\text{C}_3\text{H}_6$	1.350E+15	0.00	66600	[51]
$\text{C}_7\text{H}_{14}\text{-D1}=\text{C}_3\text{H}_5+\text{C}_4\text{H}_9\text{-1}$	1.000E+16	0.00	71040	[18]

Table XXXVI: Olefin decomposition

## 5.4. Results and Analysis

The model has been validated for various experiments and the results and analysis are in following paragraphs.

### 5.4.1. Shock tube

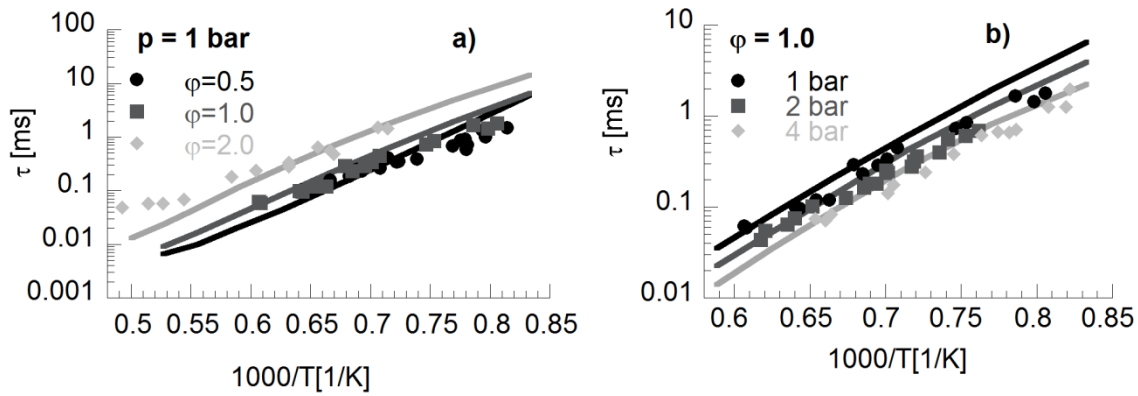
Orme et al. [50] have investigated methylcyclohexane/O<sub>2</sub>/Ar mixtures in a high pressure shock tube at pressures 1, 2 and 4atm for different equivalence ratios 0.5, 1.0 and 2.0. The experimental data is as given in the Table XXXVII below.

Reference	Components			Experimental conditions		
	Methyl-cyclohexane [%]	O <sub>2</sub> [%]	Ar [%]	$\Phi$ [-]	Pressure [atm]	Temperature [K]
Orme et al. 2006 [50]	0.5	10.5	89.00	0.500	1.0	1200-2100
	1.0	10.5	88.50	1.000	1.0, 2.0, 4.0	1200-2100
	1.0	5.25	93.75	2.000	1.0	1200-2100
	0.1	9.90	90.00	0.105	1.0	1200-2100

**Table XXXVII: Experimental conditions of methylcyclohexane from Orme et al. [50]**

The comparison between the experiments and the simulated ignition delay times at p=1 bar and three different equivalence ratios 0.5, 1.0 and 2.0 is seen in Figure 43 a) below. The ignition delay times were measured in a temperature range of 1200 K to 2100 K. The ignition delay at  $\Phi=0.5$  is slower in the range below 1200K but fit well for the higher temperatures. This trend is followed for  $\Phi=1.0$  but is less intensified while for  $\Phi=2.0$  it disappears. In Figure 43 b) for the stoichiometric condition, three different measurements were done at reflected pressures of p=1, 2 and 4bar. Results fit better to the experiments as compared to p=1bar experiments. In general, a good agreement of the simulations with the experiments is seen and the model is able to capture the pressure dependence too.

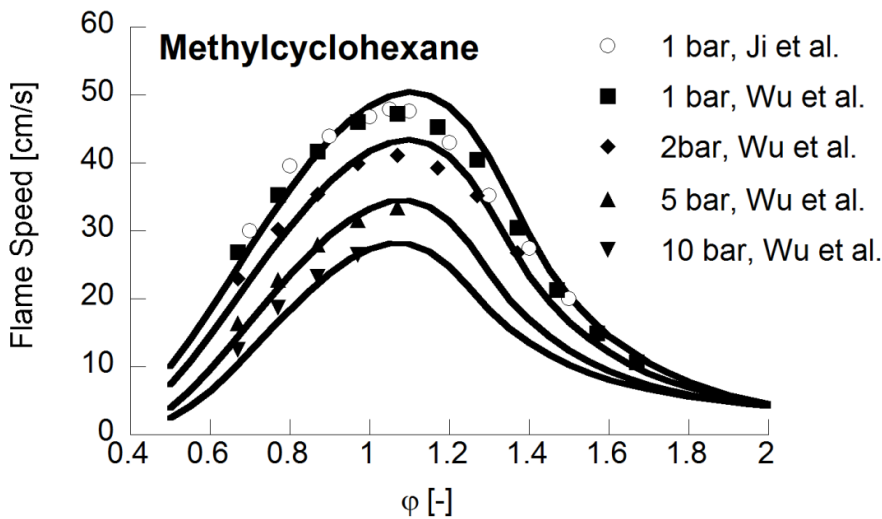




**Figure 43: Ignition delay times for methylcyclohexane/O<sub>2</sub>/Ar mixture for a) p=1 bar and  $\Phi=0.5$ , 1.0 and 2.0 b) stoichiometric mixture and three different pressures p=1, 2 and 4 bar [3]. Symbols: Experiments and Lines: Simulations**

#### 5.4.2. Flame speed

Ji et al. [32] have determined laminar flame speeds for methylcyclohexane/air mixtures at p=1 bar and T=353 K for wide range of equivalence ratios. Further Wu et al. [30] measured laminar flame speeds of methylcyclohexane from 1-10 atm.



**Figure 44: Comparison of laminar speeds of methylcyclohexane/air mixtures at different pressures of 1 atm [32] and 1-10 atm [30] at 353 K. Symbols: Experiments and Lines: Simulations**

The experimental data along with the simulated data is shown in Figure 44. The model agrees very well to the experiments on the lean side and is slightly higher on the rich side from  $\Phi=1.0-1.3$  and thereafter agrees perfectly with the experiments.

### 5.4.3. Flame structure

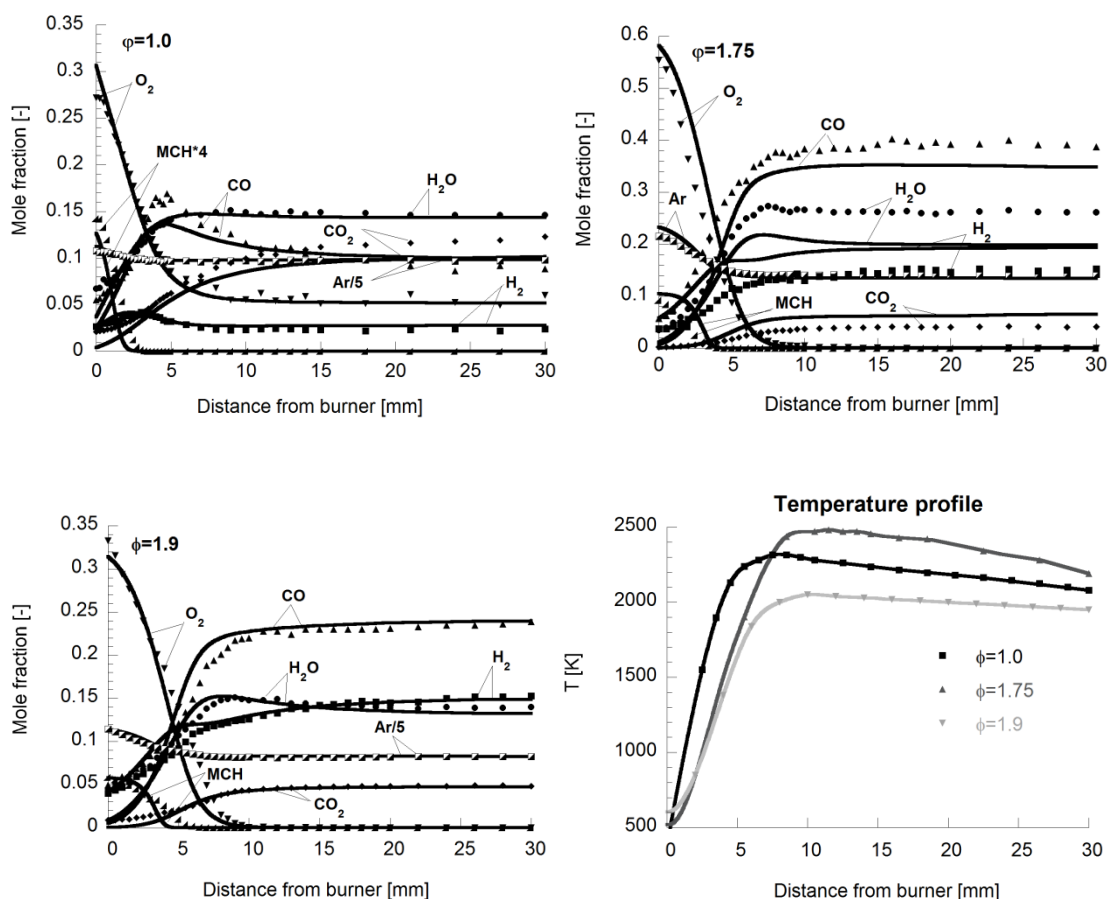
Skeen et al. [85] have studied methylcyclohexane/O<sub>2</sub>/Ar flames at three different equivalence ratios 1.0, 1.75 and 1.9. The flames were stabilized on a flat-flame McKenna burner at pressures between 15, 20 and 30 Torr, respectively. The focus of the study was to investigate the formation of aromatic species and the competing pathways involved in it. The flame conditions of the three flames are given in Table XXXVIII below.

Nr.	Components			Experimental conditions		
	MCH [%]	O <sub>2</sub> [%]	Ar [%]	$\phi$ [-]	Pressure [Torr]	Cold gas velocity [cm/s]
Flame 1	3.5	36.5	60.0	<b>1.0</b>	15	128
Flame 2	11.0	64.0	25.0	<b>1.75</b>	20	96
Flame 3	6.0	34.0	60.0	<b>1.9</b>	30	64

Table XXXVIII: Flame conditions [85]

#### Major species and temperature profile

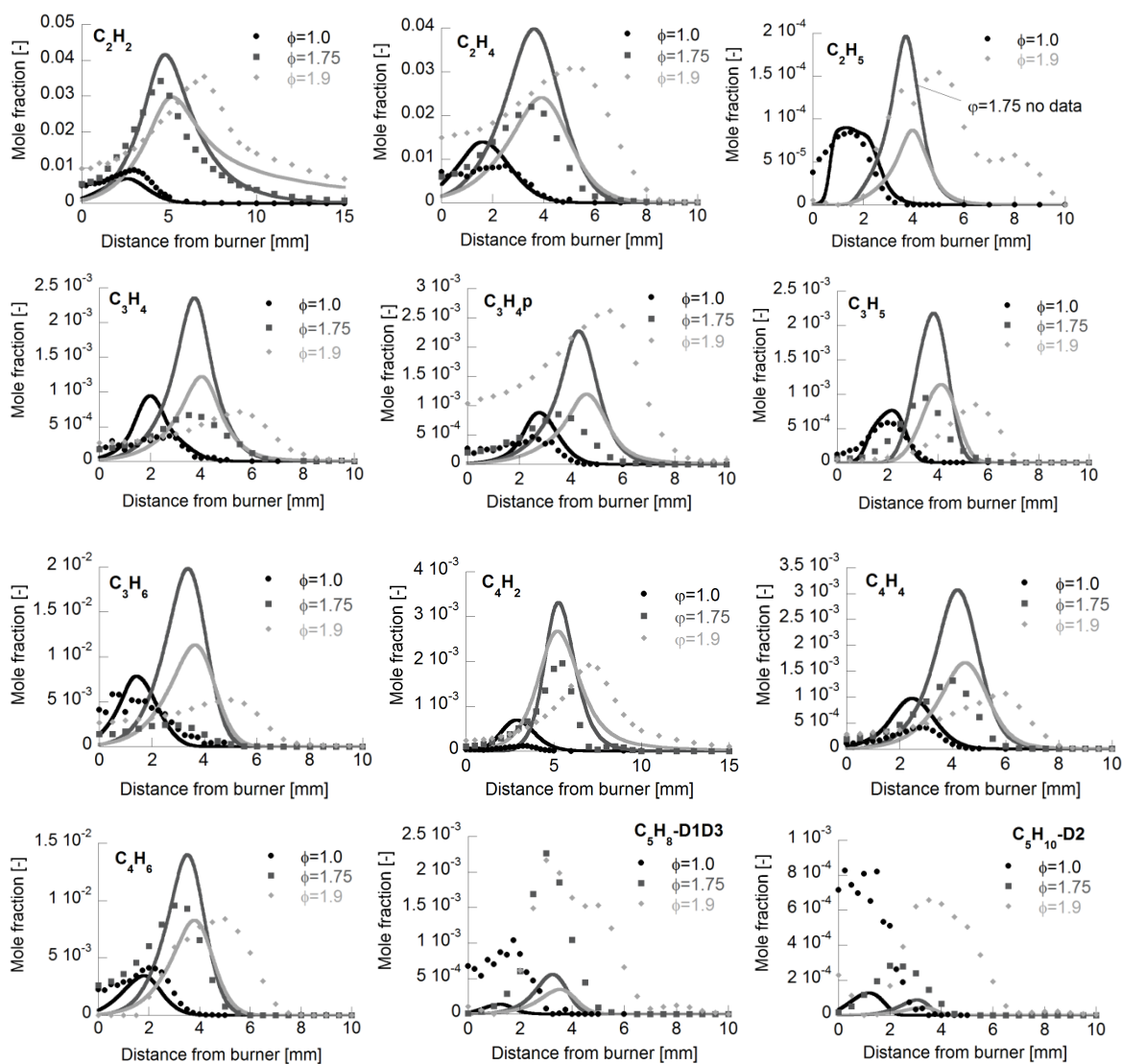
Figure 45 shows the mole fractions of the stable main products in methylcyclohexane/O<sub>2</sub>/Ar  $\Phi=1.0$ , 1.75 and 1.9 flames. For  $\Phi=1.0$  and 1.9, the model shows for methylcyclohexane, O<sub>2</sub>, CO, CO<sub>2</sub>, O<sub>2</sub>, H<sub>2</sub>O, H<sub>2</sub> and Ar very good agreement with the experiments. For  $\Phi=1.75$ , the experimental values of methylcyclohexane decomposition at the burner surface are lower than in the simulation, similar behavior is observed for CO and H<sub>2</sub>O profiles. While the profiles of CO<sub>2</sub> and H<sub>2</sub> are slightly over-predicted (although within error range); at other equivalence ratios it is very well predicted. Experimental temperature profiles are used for the simulation. They are given in Figure 45.



**Figure 45: Major species mole fraction and temperature profiles as a function of distance from the burner for methylcyclohexane/ $O_2$ /Ar flames at  $\Phi=1.0$ , 1.75 and 1.9 [85]. Symbols: Experiments and Lines: Simulations.**

### C2-C5 profiles in methylcyclohexane oxidation

As seen in Figure 46, various profiles ranging from C2 to C5 species have been shown. The most dominant  $C_2H_2$  and  $C_2H_4$  specie profiles are in good agreement with the experimental values. Propene is other important specie which shows up in the flow analysis (Figure 48) which is the product from the most formed  $CYC_7H_{13}-R_4$  and  $CYC_7H_{13}-R_5$  radicals.  $C_3H_6$  profile for  $\Phi=1.0$  looks in better agreement with the experiments than that at  $\Phi=1.9$  where it's slightly over-predicted. For  $\Phi=1.75$ , it's too high. Butadiene ( $C_4H_6$ ) profiles fit very well with the experimental data for all phi, except for  $\Phi=1.75$  where the profile is shifted more to the right but maintains the shape of the profile.



**Figure 46: C2-C5 profiles for methylcyclohexane/O<sub>2</sub>/Ar flames at  $\Phi=1.0$ , 1.75 and 1.9 [85]. Symbols: Experiments and Lines: Simulations.**

The reason for low CyC<sub>6</sub>H<sub>10</sub> could be owing to the only 22% contribution of uni-molecular decomposition of methylcyclohexane into CyC<sub>6</sub>H<sub>11</sub> and CH<sub>3</sub> which would further dehydrogenate to CyC<sub>6</sub>H<sub>10</sub>. The same reasoning could be given for low Benzene concentrations which would otherwise result from the dehydrogenation from CyC<sub>6</sub>H<sub>10</sub>.

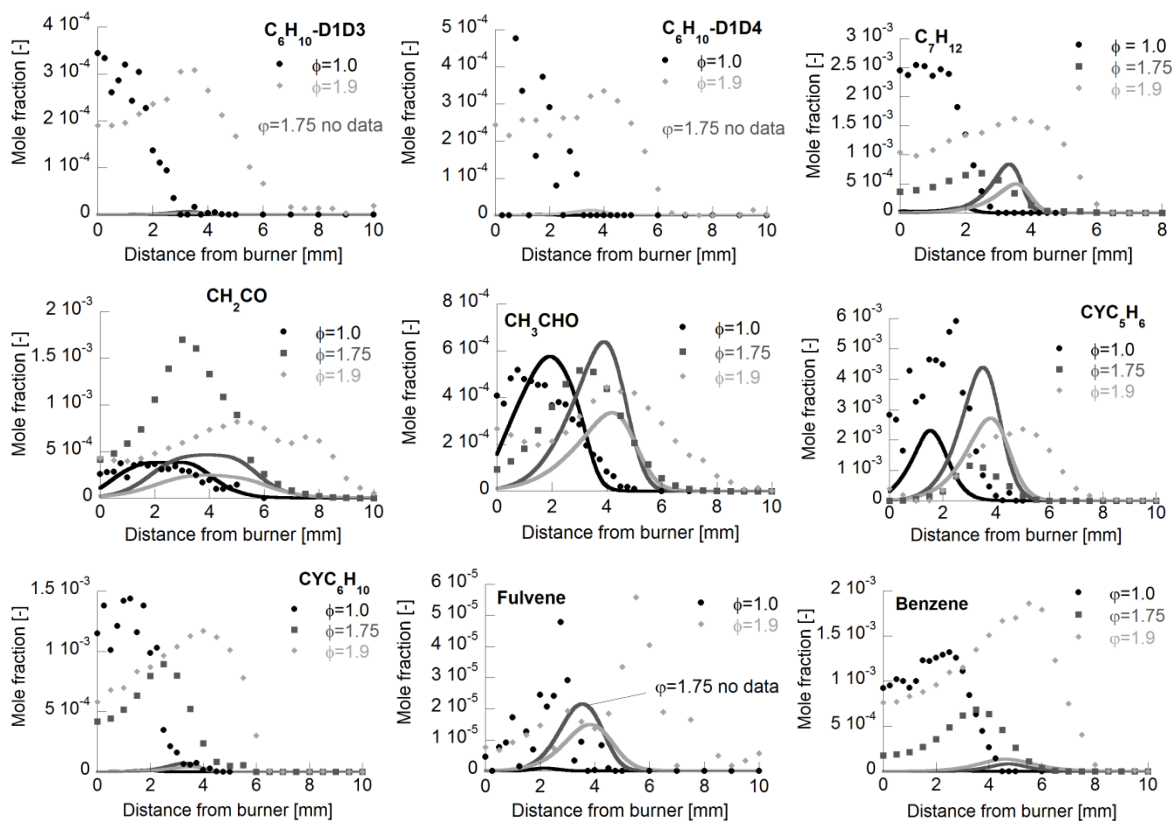
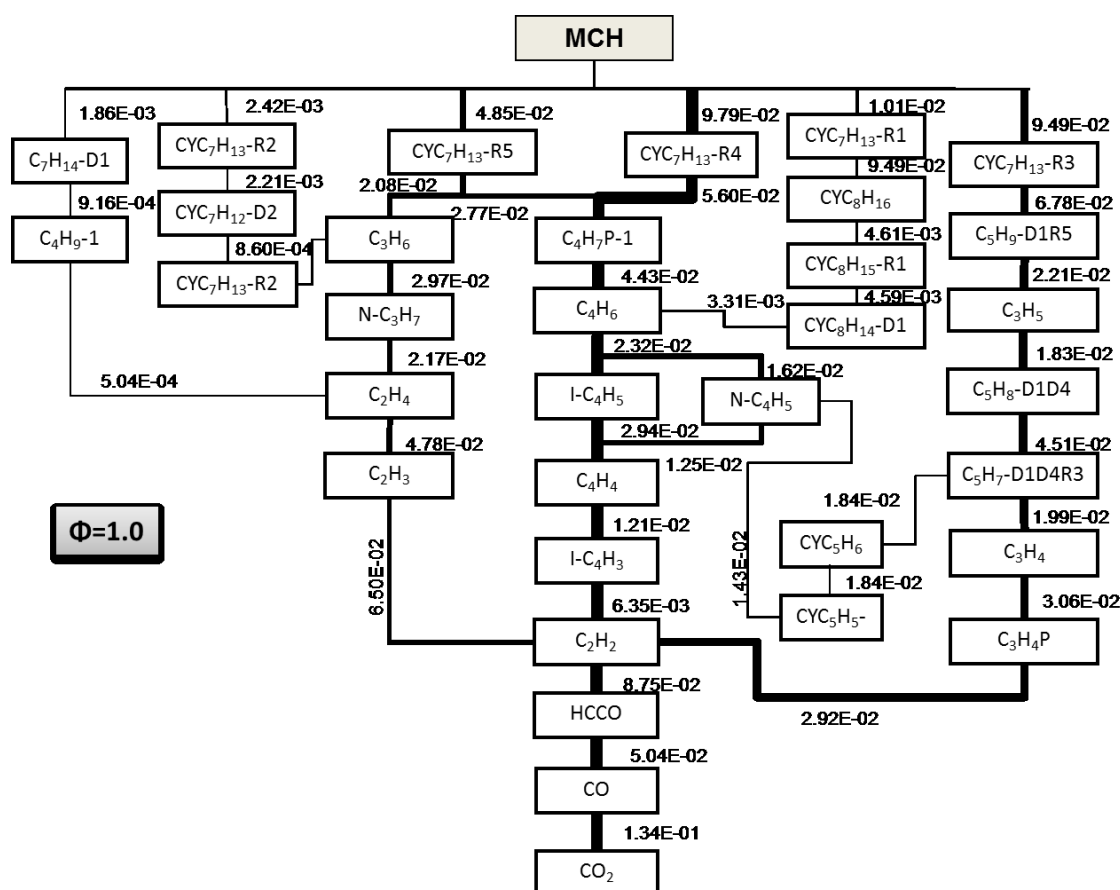


Figure 47: Cyclopentadiene, C6 and aldehydes profiles for methylcyclohexane/O<sub>2</sub>/Ar flames at  $\Phi=1.0, 1.75$  and  $1.9$  [85]. Symbols: Experiments and Lines: Simulations.

#### 5.4.4. Flow Analysis

##### Degradation of methylcyclohexane

Common degradation pathways of methylcyclohexane, which operate for all equivalence ratios, proceed *via* the secondary radicals CYC<sub>7</sub>H<sub>13</sub>-R4 followed by CYC<sub>7</sub>H<sub>13</sub>-R3 and CYC<sub>7</sub>H<sub>13</sub>-R5 radicals. These radicals are formed mainly through H-abstraction from the methylcyclohexane on the ring. These cyclo-alkyl radicals would further decompose either to the corresponding cyclo-olefins or through ring opening to form corresponding radical species. The latter case is observed and is clear from the flow analysis in Figure 48. For the stoichiometric flame seen in Figure 48, the main products formed are C<sub>3</sub>H<sub>6</sub>, C<sub>4</sub>H<sub>7</sub>P-1 and C<sub>5</sub>H<sub>9</sub>-D1R5 which are formed from alkyl radical decomposition (Class 3) from the three radicals mentioned above. The most of the flow is going through C<sub>4</sub>H<sub>7</sub>P-1 and the rest through C<sub>5</sub>H<sub>9</sub>-D1R5.



**Figure 48: Flow analysis for methylcyclohexane (MCH) decomposition of  $\Phi=1.0$  flame showing the major pathways [85]**

The  $C_4H_7P-1$  radical is further decomposed to  $C_4H_6$ . The latter species involved in the decomposition are  $I-C_4H_5$ ,  $C_4H_4$  and  $I-C_4H_3$  forming  $C_2H_2$ . The  $C_3$  species further react to  $C_2$  species; especially to ethylene ( $C_2H_4$ ) which forms via the vinyl radical by dehydrogenation acetylene ( $C_2H_2$ ). The  $C_5H_9-D1R5$  radical further decomposed to form allyl  $C_3H_5$  radical and some part to  $C_5H_8-D1D4$  (Class 8) through the alkenyl radical decomposition. The 1,4-heptadiene further decomposes to its corresponding radical specie  $C_5H_7-D1D4R3$ . The latter species is important for benzene formation, either directly through the reactions with  $n-C_4H_5$  [76] and  $i-C_4H_5$  [73, 77] or *via* the build-up of the propargyl radical [60]. The main degradation pathway of  $C_2H_2$  is the formation of the ketylenyl radical (HCCO) in the reaction with O atoms. Ketylenyl mainly decomposes to CH and CO and the oxidation of CO leads finally to the main reaction product  $CO_2$ . In the figure below detailed mass flow analysis are presented for  $\Phi=1.0$  illustrating the high mass flows through  $C_2H_4$ ,  $C_2H_3$  and  $C_2H_2$  and HCCO.

In a turbulent flow reactor study from Zeppeiri et al. [79] on methylcyclohexane, they found that in a certain temperature range under study (1058K, 1108K, 1154K and 1192K), the same intermediates viz. ethene ( $C_2H_4$ ), propene ( $C_3H_6$ ), acetylene ( $C_2H_2$ ), 1,3-butadiene ( $C_4H_6$ ) and isoprene ( $C_5H_8$ -M2D1D3) were formed in the similar quantities, from which they concluded that these are governed by one common mechanism. And this common mechanism is the C-C scission reactions. The decomposition of the cyclo-alkyl radicals involving both C-H and C-C scission occur at same rate unlike in aliphatic fuels where the C-H scissions occur at much higher frequencies than C-C scissions. These intermediates are observed for all three equivalence ratios. Here only stoichiometric case is presented.

#### **5.4.5. Sensitivity Analysis**

Figure 49 and Figure 50 show are the sensitivity analysis at  $T=1250$  K and  $1350$  K respectively of methylcyclohexane in 10.5 % oxygen at  $p=1$  bar and  $\Phi=1.0$ .

It is clear that the other most sensitive reactions are from the base chemistry for both temperatures. At  $1350$ K, the fuel is decomposed via H-abstraction to mainly form primary radical;  $CYC_7H_{13}$ -R1 (10.61%) and two secondary radicals  $CYC_7H_{13}$ -R3 (9.18 %) and  $CYC_7H_{13}$ -R4 (7.75 %).  $CYC_7H_{13}$ -R4 has a positive sensitivity while the other two are negatively sensitive. The same species are observed to be sensitive at  $1250$ K but  $CYC_7H_{13}$ -R3 (17.75%) is the most sensitive among the others which are  $CYC_7H_{13}$ -R4 (10.84%) and  $CYC_7H_{13}$ -R1 (16.95%).

The diene radicals  $C_6H_9$ -D1D5R3 and  $C_5H_7$ -D1D4R3 (also seen in the flow analysis) and diene  $C_5H_8$ -D1D4 show up at both temperatures and their decomposition (Class 8) products then isomerise to form  $CYC_6H_8$  and cyclopentadiene ( $CYC_5H_6$ ) respectively. These species contribute to the formation of benzene.

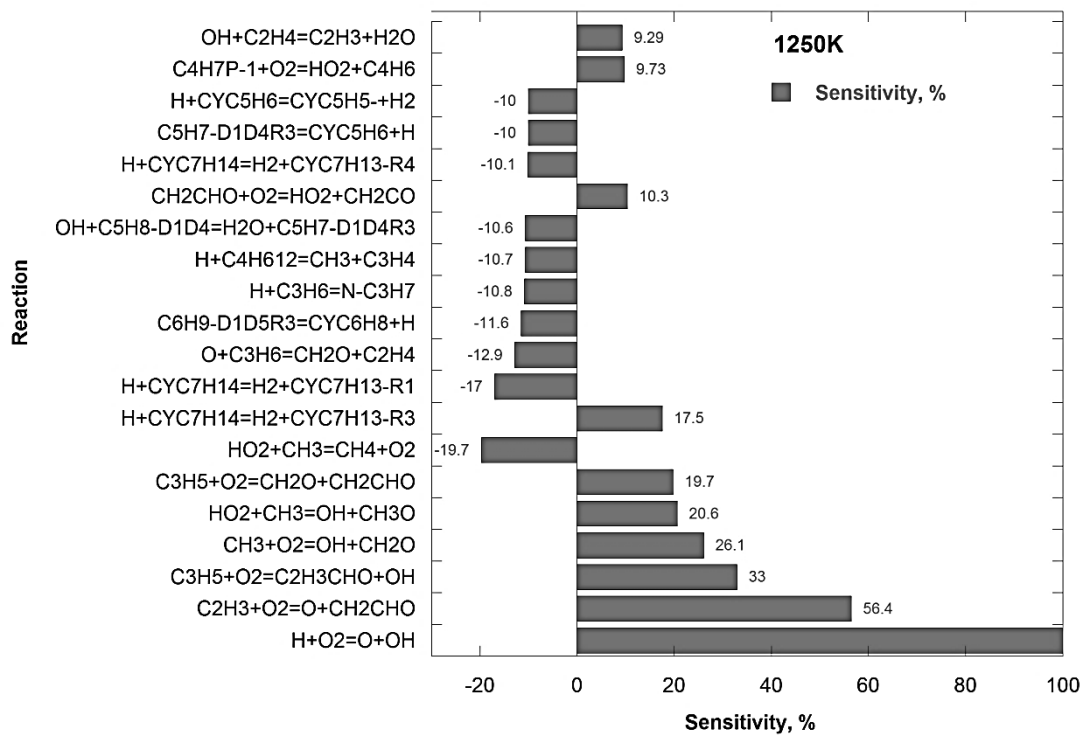


Figure 49: Sensitivity Analysis of MCH/O<sub>2</sub>/Ar mixture in a shock tube at p=1atm, Φ=1.0 at T=1250K [50]

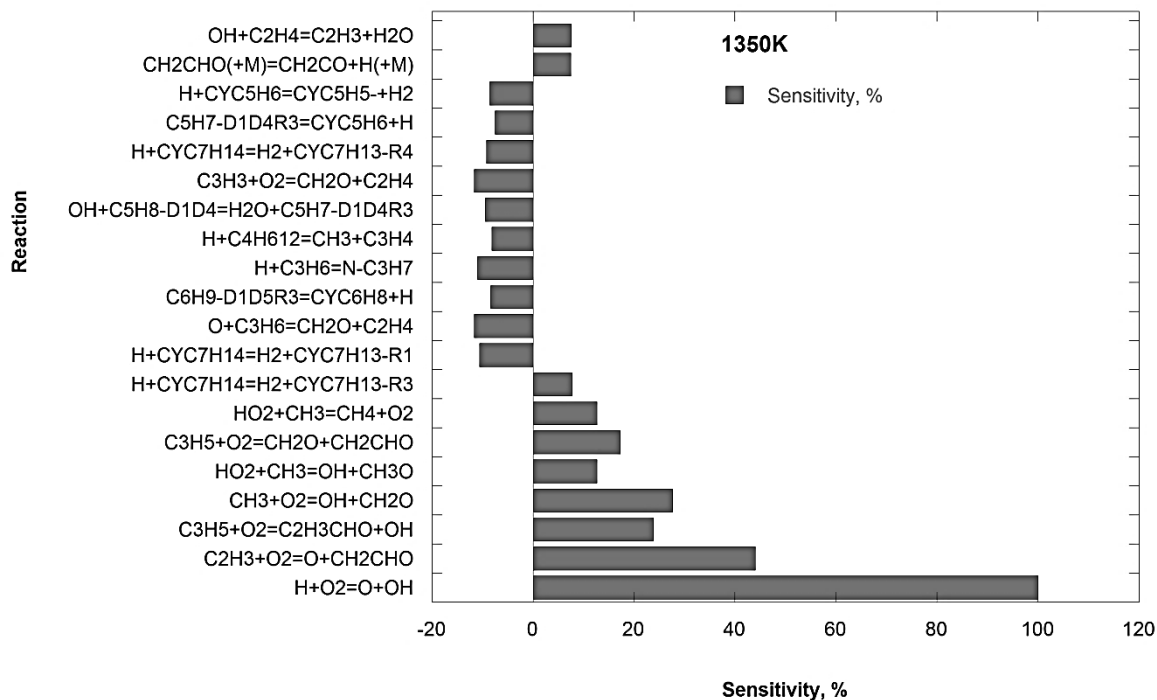


Figure 50: Sensitivity Analysis of MCH/O<sub>2</sub>/Ar mixture in a shock tube at p=1atm, Φ=1.0 at T=1350K [50]



## 5.5. Conclusion on methylcyclohexane model

The sub-mechanism of methylcyclohexane is formulated partly in analogy with the cyclohexane mechanism previously developed in 1-hexene model from Nawdiyal et al. [18]. A high temperature mechanism for the oxidation of methylcyclohexane has been developed and tested for ignition delays, flame speeds and premixed flame experiments. The similarities and differences of linear and cyclic species were taken into account and attention was devoted to point out where specific rules are needed. Most peculiar reactions being ring opening and ring closing reactions forming olefins are considered here. Like n-alkanes, decomposition of methylcyclohexane is also ruled with H-abstraction reactions from the fuel. The formation of dienes is another important pathway opening benzene formation routes.

The mechanism was tested for low pressure shock tube experiments from Orme et al. [50] along with flame structure profiles at three different equivalence ratios 1.0, 1.75 and 1.9 from Skeen et al. [85] and flame speed experiments from Wu et al. [30] and Ji et al. [32] for pressures between 1 and 10 atm. Although some profiles like benzene, fulvene are not well represented in Skeen premixed flame, the flame speeds are very well predicted. Also, the ignition delays for pressures 1 to 4 bar are quite precise. In general, a good agreement of the simulations with the experiments is seen and the model is able to capture the pressure dependence too. The model can be used further to develop higher cycloalkanes.

## 6. N-PROPYLCYCLOHEXANE KINETIC MODEL

### 6.1. Structure of N-propylcyclohexane

The chemical structure of n-propylcyclohexane is as shown in Figure 51 with propyl group on cyclohexane ring. Seven different radical positions are possible. Some important properties of n-propylcyclohexane are compiled in Table XXXIX.

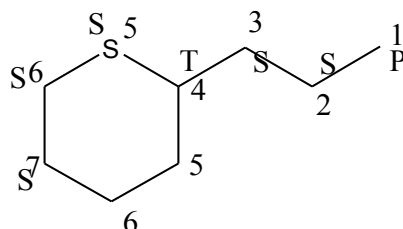


Figure 51: Structure of n-propylcyclohexane (*n*-PCH). P-primary, S-secondary, T-tertiary sites of H-abstraction. The carbon atoms are numbered from 1-7 and also indicate the radical position.

	<i>n</i> -PCH
Chemical formula	CYC <sub>9</sub> H <sub>18</sub>
Density	0.793 g/mL at 25°C(lit.)
Auto Ignition	478 °F
Boiling Point	155 °C
Melting point	-95° C
Vapor Pressure	8.7 mmHg ( 37.7 °C)
RON	-
Cetane number	-

Table XXXIX: Table of chemical properties of n-propylcyclohexane

### 6.2. Research background

#### Experimental studies

*n*-Propylcyclohexane is a component of the surrogate bio-kerosene model fuel. It has been used in the kinetic studies of kerosene Jet A-1 oxidation. It has also been used to assay kerosene/rapeseed oil methyl ester (RME) mixture (80/20, mol/mol; bio-kerosene).

Ristori et al. [89] were the first who studied the oxidation of *n*-propylcyclohexane in a jet stirred reactor. Experiments were conducted at 1 atm within a temperature range of 950-1250 K for equivalence ratios 0.5, 1.0 and 1.5. They also proposed a detailed kinetic mechanism for the oxidation of *n*-propylcyclohexane and validated against their experiments for *n*-propylcyclohexane and cyclohexane. Pousse et al. [90]

investigated laminar premixed methane flame doped with *n*-propylcyclohexane at 333 K and  $\Phi=0.68$ . Around 38 species were measured. They proposed a mechanism for the oxidation of *n*-propylcyclohexane and validated against their experiments and other jet stirred reactor experiments.

Dubois et al. [91] studied the oxidation of *n*-propylcyclohexane in a shock tube and spherical bomb. Ignition delay times were measured for *n*-propylcyclohexane/O<sub>2</sub>/Ar mixtures for temperatures 1250-1800 K and pressures 10-20 atm for varied equivalence ratios 0.2-1.5. The ignition delay times were measured in terms of 50 % maximum OH or CH radical emissions. For the flame speeds measurements, they used a heated stainless steel spherical bomb consisting of two concentric spheres at initial temperature 403 K, initial pressure 1 bar for equivalence ratios ranging from 0.6 to 1.75. The experiments were validated against two models from literature viz. Ristori et al. [89] and Zhao et al. [92] with some updates necessary according to the authors.

Crochet et al. [93] studied *n*-propylcyclohexane autoignition in a rapid compression machine at high pressures ranging from 0.45-1.34 MPa in the low temperature regime 620-930 K for lean *n*-propylcyclohexane /air mixtures with  $\Phi=0.3$ , 0.4 and 0.5. The experiments were initially conducted at 33.3-66.7 kPa pressures to end compressed gas (EOC) pressures of 0.45-1.34 MPa in 60 ms compression time. The ignition delay was measured as the time elapsed between the end of compression (EOC) and the onset of ignition (pressure peak). The data was found in synchronization with the corresponding lower alkylated cycloalkanes and cyclohexane ignition data along with the observation of NTC behavior. They also found bicyclic ethers and conjugated olefins formed in the low temperature oxidation. Tian et al. [94] measured ignition delay times for cyclohexane, ethylcyclohexane and *n*-propylcyclohexane in a shock tube for three equivalence ratios  $\Phi=0.5$ , 1.0 and 2.0 at 1.1 atm and temperature ranging from 1100 to 1650 K. The aim of the study was to understand if the branching chains influence the cycloalkane decomposition. They used three different mechanism for validation viz. Silke et al. [27], Sirjean et al. [23] and Jetsurf from Wang et al. [87]. Only Jetsurf was used simulate ethylcyclohexane and *n*-propylcyclohexane while the others are used for cyclohexane. Satisfactory results were observed and the models were able to represent the experimental data.

There is an order found in the ignition delay times which is  $n$ -propylcyclohexane < ethylcyclohexane < cyclohexane at high temperatures.

Ji et al. [32] have determined laminar flame speeds for cyclohexane/air, methylcyclohexane/air, ethylcyclohexane/air and  $n$ -propylcyclohexane/air mixtures at  $p=1$  bar and  $T=353$  K for wide range of equivalence ratios.

### **Modelling studies**

Ristori et al. [89] developed a high temperature mechanism for cyclohexane and added  $n$ -propylcyclohexane to it. He validated the mechanism against  $n$ -propylcyclohexane species concentration profiles measured in a JSR at temperatures of 950–1250 K,  $\Phi = 0.5$ –2.0, and pressure of 1.0 atm. Pousse et al. [90] proposed a mechanism for the oxidation of  $n$ -propylcyclohexane and validated against their experiments and other jet stirred reactor experiments. Jetsurf from Wang et al. [87] is another extensive model for the oxidation of  $n$ -propylcyclohexane tested for wide range of experiments. It has a high temperature and low temperature mechanism validated for various experimental studies.

### **6.3. N-propyl-cyclohexane kinetic model development**

The methylcyclohexane sub-mechanism is extended to the higher  $n$ -propylcyclohexane (CYC<sub>9</sub>H<sub>18</sub>). Based on the oxidation of methylcyclohexane mechanism, the high temperature mechanism for  $n$ -propylcyclohexane has been developed. It initiates with the ring opening in two channels viz. 1. forming straight chain olefin 1-nonene and 2. forming Ethene and 1-pentene. It also includes unimolecular initiation via C–H scission to produce seven different propylcyclohexyl radicals and removal of propyl group forming cycloethylhexyl, cyclomethylhexyl and cyclohexyl radical. The isomerization of cycloalkanes into olefins is another important pathway forming cyclo-alkyl radical. H-atom abstraction reactions by small radicals such as H, O, OH, HO<sub>2</sub>, CH<sub>3</sub> etc. are also included. Rules from Ahmed et al. [47] are followed in general while for the abstraction of tertiary hydrogen (between the ring and propyl group) Curran rates [42] are applied. The propylcyclohexyl radicals break down mainly to form cyclo-olefins and to smaller olefins.

The core model consists of C1-C4 base chemistry validated by Hoyermann et al. [60], Schenk et al. [66] and Nawdiyal et al. [18]. The base mechanism consists of 223

species and 1276 reversible reactions. The sub-mechanism from *n*-propylcyclohexane consists of 106 species and 2511 reversible reactions. The assembled mechanism thus consists of 329 species and 3787 reversible elementary reactions.

All calculations have been performed with the current version of the LOGEsoft package [15]. The thermodynamic properties of species were taken from The Goos, Burcat, Rusic data base [16]. For other several new species in the *n*-propylcyclohexane sub-mechanism were evaluated implementing Benson's group additivity method [17].

The mechanism development for the high temperature range is as follows. Since it is similar to the kinetic model for methylcyclohexane only specific reactions or species are mentioned here to avoid repetition.

### Class 1: Unimolecular fuel decomposition (Initiation reactions)

Reactions	$A \left( \frac{\text{cm}^3}{\text{mol}\cdot\text{s}} \right)$	n	$E_a \left( \frac{\text{cal}}{\text{mol}} \right)$	Ref.
<b>1. Ring Opening</b>				
a. $\text{CYC}_9\text{H}_{18} \Rightarrow \text{C}_9\text{H}_{18}\text{-D1}$	5.010E+16	0.00	88220	[21]
b. $\text{CYC}_9\text{H}_{18} \Rightarrow 2\text{C}_2\text{H}_4 + \text{C}_5\text{H}_{10}\text{-D1}$	1.600E+16	0.00	90000	[22]
<b>2. H-abstraction</b>				
$\text{CYC}_9\text{H}_{18} = \text{H} + \text{CYC}_9\text{H}_{17}\text{-R1 to } \text{CYC}_9\text{H}_{17}\text{-R5}$	2.500E+27	-3.80	97020	[47]
<b>3. Removal of CH<sub>3</sub> group</b>				
$\text{CYC}_9\text{H}_{18} = \text{N-C}_3\text{H}_7 + \text{CYC}_6\text{H}_{11}$	1.259E+16	0.00	87950	[33]
$\text{CYC}_9\text{H}_{18} = \text{C}_2\text{H}_5 + \text{CYC}_7\text{H}_{13}\text{-R1}$	6.500E+16	0.00	85000	[89]
$\text{CYC}_9\text{H}_{18} = \text{CH}_3 + \text{CYC}_8\text{H}_{15}\text{-R1}$	6.500E+16	0.00	85000	[89]

Table XL: Kinetic data for Class 1: Uni-molecular decomposition of *n*-propylcyclohexane

There are three different types of reactions taking place which are;

- Ring opening** and the formation of an olefin 1-nonene ( $\text{C}_9\text{H}_{18}\text{-D1}$ ): The rate coefficient for this pathway is taken from Tsang [21] in analogy to cyclohexane.
- Decomposition via H-abstraction** to form seven different radicals ( $\text{CYC}_9\text{H}_{17}\text{-R1}$  to  $\text{CYC}_9\text{H}_{17}\text{-R7}$ ): The reactions happening on the propyl chain are treated as straight chain type reactions thereby applying Ahmed rules [47].
- Breaking of the C-C bonds on the N-propyl chain** forming three different radicals: For breakage at the ring forming cyclohexyl radical ( $\text{CYC}_6\text{H}_{11}$ ), Brown coefficients [23] are used in analogy to cyclohexane while for the formation of

cycloethylhexyl radical (CYC<sub>8</sub>H<sub>15</sub>-R1) and cyclomethylhexyl radical (CYC<sub>7</sub>H<sub>13</sub>-R1)  
Ristori et al. [91] coefficients are used.

### Class 2: H-abstraction from the fuel molecule

Reactions	A ( $\frac{\text{cm}^3}{\text{mol}\cdot\text{s}}$ ) per H	n	E <sub>a</sub> ( $\frac{\text{cal}}{\text{mol}}$ )	Ref.
CYC <sub>9</sub> H <sub>18</sub> + H = CYC <sub>9</sub> H <sub>17</sub> -R.. + H <sub>2</sub>				
<b>Primary</b>	5.63E+07	2.0	7700	[47]
<b>Secondary</b>	2.45E+07	2.0	5000	[47]
<b>Tertiary</b>	6.02E+05	2.4	2583	[42]
CYC <sub>9</sub> H <sub>18</sub> + OH = CYC <sub>9</sub> H <sub>17</sub> -R.. + H <sub>2</sub> O				
<b>Primary</b>	1.75E+09	0.97	1590	[47]
<b>Secondary</b>	2.34E+07	1.61	-35.8	[47]
<b>Tertiary</b>	1.70E+06	1.90	-1451	[42]
CYC <sub>9</sub> H <sub>18</sub> + O = CYC <sub>9</sub> H <sub>17</sub> -R.. + OH				
<b>Primary</b>	3.66E+05	2.40	5500	[47]
<b>Secondary</b>	1.18E+05	2.50	2200	[47]
<b>Tertiary</b>	6.01E-10	6.36	893	[42]
CYC <sub>9</sub> H <sub>18</sub> + CH <sub>3</sub> = CYC <sub>9</sub> H <sub>17</sub> -R.. + CH <sub>4</sub>				
<b>Primary</b>	2.17E+11	0.0	11600	[47]
<b>Secondary</b>	2.00E+11	0.0	9500	[47]
<b>Tertiary</b>	8.96E+03	2.33	6147	[42]
CYC <sub>9</sub> H <sub>18</sub> + HO <sub>2</sub> = CYC <sub>9</sub> H <sub>17</sub> -R.. + H <sub>2</sub> O <sub>2</sub>				
<b>Primary</b>	2.68E+12	0.0	19400	[47]
<b>Secondary</b>	2.44E+12	0.0	17000	[47]
<b>Tertiary</b>	2.80E+12	0.0	16013	[42]
CYC <sub>9</sub> H <sub>18</sub> + CH <sub>3</sub> O = CYC <sub>9</sub> H <sub>17</sub> -R.. + CH <sub>3</sub> OH				
<b>Primary</b>	5.27E+10	0.0	7000	[47]
<b>Secondary</b>	5.48E+10	0.0	5000	[47]
<b>Tertiary</b>	1.90E+10	0.00	2800	[42]
CYC <sub>9</sub> H <sub>18</sub> + O <sub>2</sub> = CYC <sub>9</sub> H <sub>17</sub> -R.. + HO <sub>2</sub>				
<b>Primary</b>	4.17E+12	0.0	49000	[47]
<b>Secondary</b>	1.00E+13	0.0	47600	[47]
<b>Tertiary</b>	7.00E+12	0.0	46060	[42]
CYC <sub>9</sub> H <sub>18</sub> + C <sub>2</sub> H <sub>5</sub> = CYC <sub>9</sub> H <sub>17</sub> -R.. + C <sub>2</sub> H <sub>6</sub>				
<b>Primary</b>	1.67E+10	0.0	13400	[47]
<b>Secondary</b>	2.50E+10	0.0	10400	[47]
<b>Tertiary</b>	1.00E+11	0.0	7900	[42]
CYC <sub>9</sub> H <sub>18</sub> + C <sub>2</sub> H <sub>3</sub> = CYC <sub>9</sub> H <sub>17</sub> -R.. + C <sub>2</sub> H <sub>4</sub>				
<b>Primary</b>	1.67E+11	0.0	18000	[47]
<b>Secondary</b>	2.00E+11	0.0	16800	[47]
<b>Tertiary</b>	2.00E+11	0.0	14300	[42]
CYC <sub>9</sub> H <sub>18</sub> + CH <sub>3</sub> O <sub>2</sub> = CYC <sub>9</sub> H <sub>17</sub> -R.. + CH <sub>3</sub> O <sub>2</sub> H				
<b>Primary</b>	2.00E+12	0.0	20400	[47]
<b>Secondary</b>	2.00E+12	0.0	17700	[47]
<b>Tertiary</b>	--	--	--	[42]

Table XLI: Kinetic data for Class 2: H-abstraction from *n*-propylcyclohexane

The H-abstraction from the cycloalkane takes place at seven different sites viz. the primary  $CyC_9H_{17}-R1$  and two secondary sites  $CYC_9H_{17}-R2$  and  $CYC_9H_{17}-R3$  on the propyl chain; tertiary  $CYC_9H_{17}-R4$ ; and secondary sites on the ring viz.  $CYC_9H_{17}-R5$ ,  $CyC_9H_{17}-R6$ ,  $CyC_9H_{17}-R7$ . The rates for the primary and secondary sites on propyl chain are taken from Ahmed et al. [47], for secondary sites on the ring from cyclohexane [18] and for tertiary from Curran et al. [42] in analogy with methylcyclohexane.

### Class 3: Alkyl radical decomposition:

The cyclo-alkyl radicals undergo both C-H and C-C scissions to form cyclo-alkenes and other small products. The different cyclo-alkenes formed in this class are  $CYC_9H_{16}-D1$ ,  $CYC_7H_{16}-D2$ ,  $CYC_9H_{16}-D3$ ,  $CYC_9H_{16}-D4$ ,  $CYC_9H_{16}-D5$  and  $CYC_9H_{16}-D6$ . In the current mechanism, Ahmed coefficients [47] are used in analogy with methylcyclohexane.

Reactions	A ( $\frac{cm^3}{mol \cdot s}$ )	n	E <sub>a</sub> ( $\frac{cal}{mol}$ )	Ref.
<b>Primary</b>				
$C_2H_4 + C_5H_9-D1R5 = CYC_9H_{17}-R1$	8.50E+10	0.00	77900	[47]
$H + CYC_9H_{16}-D1 = CYC_9H_{17}-R1$	1.00E+13	0.00	29000	[47]
<b>Secondary</b>				
$C_3H_6 + CYC_6H_{11} = CYC_9H_{17}-R2$	8.50E+10	0.00	77900	[47]
$H + CYC_9H_{16}-D1 = CYC_9H_{17}-R2$	1.00E+13	0.00	29000	[47]
$H + CYC_9H_{16}-D2 = CYC_9H_{17}-R2$	1.00E+13	0.00	29000	[47]
$CH_3 + CYC_8H_{14}-D1 = CYC_9H_{17}-R3$	8.50E+10	0.00	77900	[47]
$H + CYC_9H_{16}-D2 = CYC_9H_{17}-R3$	1.00E+13	0.00	29000	[47]
$C_2H_5 + CYC_7H_{12}-D1 = CYC_9H_{17}-R4$	8.50E+10	0.00	77900	[47]
$H + CYC_9H_{16}-D3 = CYC_9H_{17}-R4$	1.00E+13	0.00	29000	[47]
$H + CYC_9H_{16}-D4 = CYC_9H_{17}-R4$	1.00E+13	0.00	29000	[47]
$N-C_3H_7 + CYC_6H_{10} = CYC_9H_{17}-R5$	8.50E+10	0.00	77900	[47]
$H + CYC_9H_{16}-D4 = CYC_9H_{17}-R5$	1.00E+13	0.00	29000	[47]
$H + CYC_9H_{16}-D5 = CYC_9H_{17}-R5$	1.00E+13	0.00	29000	[47]
$C_4H_7P-1 + C_5H_{10}-D1 = CYC_9H_{17}-R6$	8.50E+10	0.00	77900	[47]
$H + CYC_9H_{16}-D4 = CYC_9H_{17}-R6$	1.00E+13	0.00	29000	[47]
$H + CYC_9H_{16}-D5 = CYC_9H_{17}-R6$	1.00E+13	0.00	29000	[47]
$C_4H_7P-1 + C_5H_{10}-D1 = CYC_9H_{17}-R7$	8.50E+10	0.00	77900	[47]
$H + CYC_9H_{16}-D5 = CYC_9H_{17}-R7$	1.00E+13	0.00	29000	[47]
$H + CYC_9H_{16}-D6 = CYC_9H_{17}-R7$	1.00E+13	0.00	29000	[47]

Table XLII: Kinetic data for Class 3: Alkyl radical decomposition reactions for *n*-propylcyclohexane

### Class 5: Alkyl radical isomerization

This class of reaction is based on the type of radical site (endo- or exo-ring) at which the ring opening will occur. Different straight alkenyl and iso-alkenyl radicals are

formed in this class. They will further decompose in Class 8. The rate constants are taken from Orme et al. [50] The reverse reactions (in the ring closing direction) are exclusively written and follow Orme constants as shown in Table XLIII.

Reactions	A ( $\frac{\text{cm}^3}{\text{mol}\cdot\text{s}}$ )	n	E <sub>a</sub> ( $\frac{\text{cal}}{\text{mol}}$ )	Ref.
C <sub>2</sub> H <sub>4</sub> + C <sub>7</sub> H <sub>13</sub> -D1R7 => CYC <sub>9</sub> H <sub>17</sub> -R1	1.00E+08	0.90	5900	[50]
C <sub>3</sub> H <sub>6</sub> + CYC <sub>6</sub> H <sub>11</sub> => CYC <sub>9</sub> H <sub>17</sub> -R2	1.00E+08	0.90	5900	[50]
C <sub>9</sub> H <sub>17</sub> -D3R9 => CYC <sub>9</sub> H <sub>17</sub> -R3	1.00E+08	0.90	8700	[50]
CYC <sub>8</sub> H <sub>14</sub> + CH <sub>3</sub> => CYC <sub>7</sub> H <sub>13</sub> -R3	1.00E+08	0.90	8700	[50]
C <sub>2</sub> H <sub>5</sub> + CYC <sub>7</sub> H <sub>12</sub> -D1 => CYC <sub>9</sub> H <sub>17</sub> -R4	1.00E+08	0.90	8500	[50]
N-C <sub>3</sub> H <sub>7</sub> + CYC <sub>6</sub> H <sub>10</sub> => CYC <sub>9</sub> H <sub>17</sub> -R5	1.00E+08	0.90	5900	[50]
C <sub>9</sub> H <sub>17</sub> -D1R6 => CYC <sub>9</sub> H <sub>17</sub> -R6	1.00E+08	0.90	5900	[50]
N-C <sub>3</sub> H <sub>7</sub> + C <sub>6</sub> H <sub>10</sub> => CYC <sub>9</sub> H <sub>17</sub> -R7	1.00E+08	0.90	5900	[50]

Table XLIII: Kinetic data for Class 5: Alkyl radical isomerization for *n*-propylcyclohexane

### Class 6: Abstraction reactions from olefins

The olefins formed in classes 1 and 3 (CYC<sub>9</sub>H<sub>16</sub>-D1, CYC<sub>9</sub>H<sub>16</sub>-D2, CYC<sub>9</sub>H<sub>16</sub>-D3, CYC<sub>9</sub>H<sub>16</sub>-D4, CYC<sub>9</sub>H<sub>16</sub>-D5 and CYC<sub>9</sub>H<sub>16</sub>-D6) undergo further abstraction through radical attackers H, OH, O, CH<sub>3</sub>, HO<sub>2</sub>, CH<sub>3</sub>O and O<sub>2</sub>. For simplicity, global reactions are written to form products. Here, Ahmed coefficients [42] same as for H-abstraction from the fuel (Class 2) are followed for tertiary position otherwise Nawdiyal et al. [18] rates are used.

Reactions	A ( $\frac{\text{cm}^3}{\text{mol}\cdot\text{s}}$ ) per H	n	E <sub>a</sub> ( $\frac{\text{cal}}{\text{mol}}$ )	Ref.
CYC <sub>9</sub> H <sub>16</sub> -D.. + H = Products + H <sub>2</sub>				
<b>Primary</b>	5.63E+07	2.0	7700	[18]
<b>Secondary</b>	2.45E+07	2.0	5000	[18]
<b>Tertiary</b>	6.02E+05	2.4	2583	[42]
CYC <sub>9</sub> H <sub>16</sub> -D.. + OH = Products + H <sub>2</sub> O				
<b>Primary</b>	1.75E+09	0.97	1590	[18]
<b>Secondary</b>	2.34E+07	1.61	-35.8	[18]
<b>Tertiary</b>	1.70E+06	1.90	-1451	[42]
CYC <sub>9</sub> H <sub>16</sub> -D.. + O = Products + OH				
<b>Primary</b>	3.66E+05	2.40	5500	[18]
<b>Secondary</b>	1.18E+05	2.50	2200	[18]
<b>Tertiary</b>	6.01E-10	6.36	893	[42]
CYC <sub>9</sub> H <sub>16</sub> -D.. + CH <sub>3</sub> = Products + CH <sub>4</sub>				
<b>Primary</b>	2.17E+11	0.0	11600	[18]
<b>Secondary</b>	2.00E+11	0.0	9500	[18]
<b>Tertiary</b>	8.96E+03	2.33	6147	[42]

Table XLIV: Kinetic data for Class 6: Abstraction reactions from olefins



### Class 7: Addition of radical species

The mechanism accounts for the addition reactions of H, OH and O radicals on the olefins in analogy to 1-hexene. The addition of H radical takes place at either C sites on the double bond and follows breaking of the ring.  $CYC_7H_{13}-R1$  is a favourable product formed from most of the cyclo-olefins. In the addition of OH radical, the H from the OH group moves to the closest site and finally breaks to form an aldehyde along with  $CYC_6H_{11}$ . Complicated epoxy's being formed by the addition of O radical; these types of reactions are not considered. The rate constants followed here are from Nawdiyal et al. [18] with zero activation for H and OH additions. Below in Table XLV is an example of  $CYC_9H_{16}-D1$  olefin.

Reactions	A ( $\frac{cm^3}{mol \cdot s}$ )	n	E <sub>a</sub> ( $\frac{cal}{mol}$ )	Ref.
$H+CYC_9H_{16}-D1=CYC_6H_{11}+C_3H_6$	5.000E+12	0.00	0	[18]
$H+CYC_9H_{16}-D1=C_2H_4+CYC_7H_{13}-R1$	5.000E+12	0.00	0	[18]
$OH+CYC_9H_{16}-D1=C_2H_5CHO+CYC_6H_{11}$	1.000E+13	0.00	0	[18]
$OH+CYC_9H_{16}-D1=CH_3CHO+CYC_7H_{13}-R1$	1.000E+13	0.00	0	[18]

Table XLV: Kinetic data for Class 7: Addition on the double bond

### Class 8: Alkenyl radical decomposition

Since in Class 6, the olefins are considered to decompose globally to products, no reactions pertaining to those species exist. This class includes only  $CYC_6H_9$  reactions which is the cyclohexane specie. Benzene formation through dehydrogenation of  $CYC_6H_9$  and  $CYC_6H_7$  is considered in this class (See Chapter 3, Table XV).

### Class 9: Olefin decomposition

Since these are cyclo-olefins, ring specific rates are followed here in analogy to cyclohexane rates [51]. In this class the straight olefins ( $C_9H_{16}-D1$ ) are decomposed via  $\beta$ -scission following Nawdiyal et al. [18] as shown in Table XLVI.

Reactions	A ( $\frac{cm^3}{mol \cdot s}$ )	n	E <sub>a</sub> ( $\frac{cal}{mol}$ )	Ref.
$C_9H_{16}-D1=C_3H_5+C_6H_{13}-R1$	1.000E+16	0.00	71040	[18]

Table XLVI: Olefin decomposition

## 6.4. Results and Analysis

### 6.4.1. Shock tube

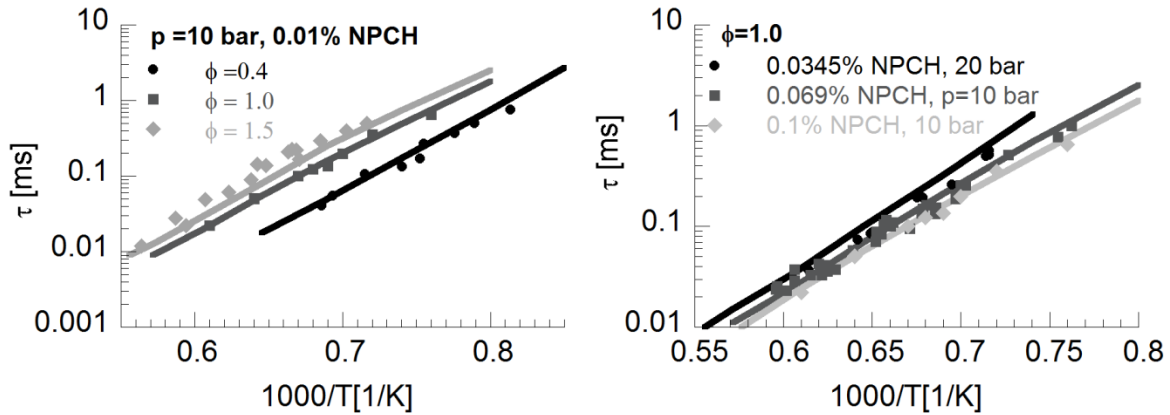
Dubois et al. [91] measured ignition delay times for *n*-propylcyclohexane/O<sub>2</sub>/Ar mixtures for temperatures 1250-1800 K and pressures 10-20 atm for varied equivalence ratios 0.2-1.5. The ignition delay times are measured in terms of 50% maximum OH or CH radical emissions.

Reference	Components			Experimental conditions		
	n-propyl-cyclohexane [ppmv]	O <sub>2</sub> [%]	Ar [%]	φ [-]	Pressure [bar]	Temperature [K]
Dubois et al. 2009 [91]	75-1000	0.45-6.8	93.1-99.5	0.2-1.5	10-20	1250-1800
	500	0.45	99.5	1.5	10	1250-1800
	1000	0.90	99.0	1.5	10	1250-1800
	500	0.45	99.5	1.5	20	1250-1800
	345	0.47	99.5	1.0	20	1250-1800
	690	0.93	99.0	1.00	10	1250-1800
	1000	1.35	98.6	1.00	10	1250-1800
	960	2.55	97.4	0.51	10	1250-1800
	360	0.97	99.0	0.50	10	1250-1800
	178	0.48	99.5	0.5	20	1250-1800
	290	0.97	99.0	0.4	10	1250-1800
	145	0.49	99.5	0.4	20	1250-1800
	290	0.97	99.0	0.40	10	1250-1800
	1000	3.36	96.5	0.4	10	1250-1800
	110	0.49	99.5	0.3	20	1250-1800
	1000	4.49	95.4	0.3	10	1250-1800
	215	0.98	99.0	0.3	10	1250-1800
	150	0.99	99.0	0.2	10-	1250-1800
	75	0.50	99.5	0.20	20	1250-1800
	1000	6.76	93.1	0.20	10	1250-1800

**Table XLVII: Experimental data for *n*-propylcyclohexane (*n*-PCH) ignition delay times [91]**

Some selected experiments are validated here (See Table XLVII) to express the essence of the experiments showing the effect of pressure on ignition delay times. Also, the effect of fuel and O<sub>2</sub> concentrations on ignition delay times is expressed here. In Figure 52, on the left are experiments for 0.01% constant fuel concentration and p=10bar for φ= 0.4, 1.0 and 1.5 compared to the simulations. It is seen that the ignition delay times decrease with decreasing equivalence ratios and the simulations agree to the same behaviour. For the simulations, ignition delay times are calculated in terms of 50% maximum of OH concentration and they fit very well with the experiments for all φ range. On the right of Figure 52, is a case of three different fuel

concentrations for  $\Phi=1.0$  at pressures 10 and 20 bar. There seems to be no large difference between the ignition delay times falling in this range. With the increasing  $O_2$  concentrations, the ignition delay times decrease but the pressure effect is not significant. Same behaviour is captured by the simulations.



**Figure 52: Ignition delay times for *n*-propylcyclohexane/ $O_2$ /Ar mixture for constant fuel concentration 0.01% and  $p=10$  bar and  $\Phi=0.4, 1.0$  and  $2.0$  [91]. Symbols: Experiments and Lines: Simulations**

#### 6.4.2. Flame speed

Along with ignition delay times, Dubois et al. [91] conducted flame speed measurements for *n*-propylcyclohexane/air mixtures. They used a heated stainless steel spherical bomb consisting of two concentric spheres at initial temperature 403 K, initial pressure 1 bar for equivalence ratios ranging from 0.6 to 1.75. Ji et al. [32] have also determined laminar flame speeds for *n*-propylcyclohexane/air mixtures at  $p=1$  bar and  $T=353$  K for wide range of equivalence ratios. Both measurements along with the simulations are shown in the Figure 53. The model is able to capture the lean side flame speeds for both experiments very well. The maximum flame speed ( $1.05 < \Phi < 1.10$ ) is slightly over-predicted but the model also shows the maximum around the same equivalence ratio. The flame speeds on the rich side ( $1.1 < \Phi < 1.4$ ) of the flame are slightly over-predicted but thereafter fit the experimental data very well.

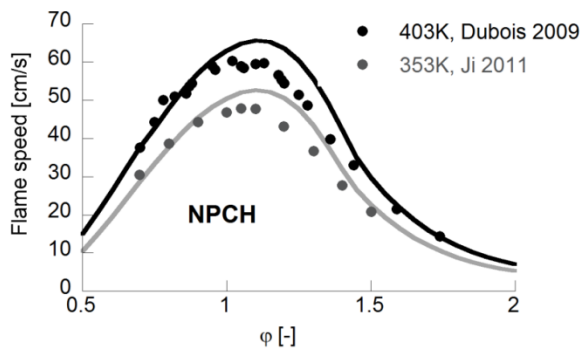


Figure 53: Flame speed of *n*-propylcyclohexane/air mixtures at  $p=1$  bar and  $T=353$  K [91]

### 6.4.3. Flame structure

Pousse et al. [90] investigated laminar premixed methane flame doped with *n*-propylcyclohexane at 333 K and  $\Phi=0.68$ . A McKenna burner housed in a vacuum chamber and equipped with a quartz microprobe with 50  $\mu\text{m}$  diameter hole and type B thermocouple of 200  $\mu\text{m}$  diameter was used. Temperature profiles (Figure 54) and around 38 species were measured. Here two different temperature profiles were measured; one without the probe and the other in presence of probe (accounting for thermal perturbation) which means the measured temperature profile is lower than the other. To account for this, the distance between the junction of the thermocouple and the end of the probe was taken to be twice the diameter of the sampling tube. For simulations, they used an average temperature profile shifted 0.5 mm away from the burner surface to compensate for this difference in measurements. In this study, temperature profile calculated from LOGEsoft and freely propagating flame setup is used for validation against experiments with no shift in the temperature profile (Figure 54).

The experimental conditions are mentioned in the Table XLVIII below with some important profiles as compared with simulations shown in Figure 54, Figure 55 and Figure 56.

Reference	Components				Experimental conditions		
	Methane [%]	NPCH [%]	O <sub>2</sub> [%]	Ar [%]	Φ [-]	Pressure [Torr]	Cold gas velocity [cm/s]
Pousse et al. 2010 [90]	7.1	0.81	36.8	55.29	0.68	50 (6.7kPa)	49.2

Table XLVIII: Experimental conditions for *n*-propylcyclohexane/CH<sub>4</sub> laminar premixed flame at T=333 K, and gas flow rate=5.44 l/min [90]

### Major species and temperature profile

Figure 54 shows the profiles of fuel *n*-propylcyclohexane along with O<sub>2</sub>, CO, CO<sub>2</sub>, O<sub>2</sub>, H<sub>2</sub>O and H<sub>2</sub> profiles in oxidation of *n*-propylcyclohexane/CH<sub>4</sub> flame at Φ=0.68 at initial temperature of T=333 K. The figure also shows the calculated temperature profile from LOGEsoft in contrast to the experimental temperature profiles. The fuel is seen to decompose readily and around 0.5 mm height it is completely consumed in contrast to the experimental height of 1.0 mm. If 0.5 mm shift would be accounted for in the temperature profile, the result height would match to the experiment. But otherwise, in general, the profile of fuel decomposition agrees well with the experiment. Similar conclusions can be drawn for other profiles e.g. CO, H<sub>2</sub>, O<sub>2</sub> and H<sub>2</sub>O. While the profile of CO is in good agreement up to 4 mm height but thereafter it is slightly over-predicted although within error range of ±10 %.

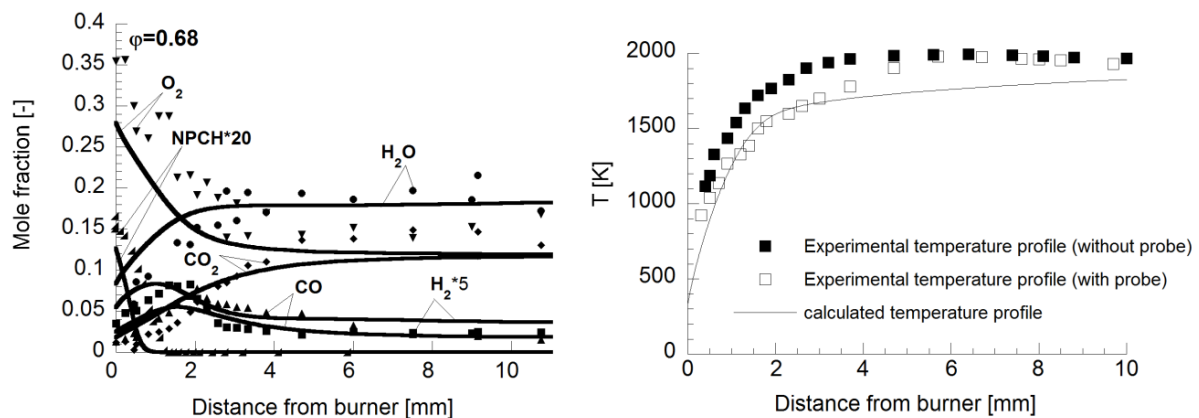
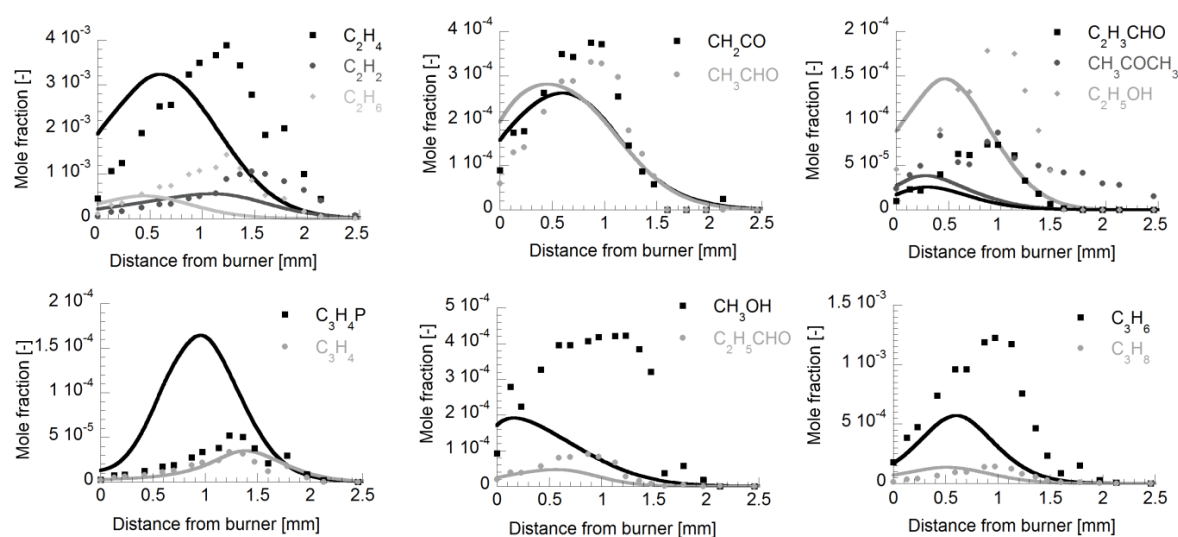


Figure 54: Fuel decomposition of *n*-propylcyclohexane/CH<sub>4</sub> laminar premixed flame (left) and temperature profile (right) at initial temperature of T=333 K, and gas flow rate=5.44 l/min [95]

Figure 55 above shows profiles of different species C0 to C3 in the Φ=0.68 flame. Ethylene (C<sub>2</sub>H<sub>4</sub>) is the most dominant C2 specie and also produced first. The model is able to simulate matching amounts of C<sub>2</sub>H<sub>4</sub> but the peak is slightly shifted to the left.

Another main specie is acetylene ( $C_2H_2$ ) shows good prediction up to height 1 mm but shows low values at the peak (at 1.5 mm) but is within the error range. Propene ( $C_3H_6$ ) and Propane ( $C_3H_8$ ) are other important species observed. The propene peak is low by a factor of 2.5 but the profile shape is well captured. Propane profiles agree very well with the experiments. The  $C_3H_4$  profile is very well predicted but the  $C_3H_4P$  is over-predicted. The oxygenated species like ethanol ( $C_2H_5CHO$ ),  $CH_2CO$  and acetaldehyde ( $CH_3CHO$ ) profiles are well predicted with the same shift in peak observed as for other species. The same reasoning of 0.5mm shift (as mentioned above) can be applied for all species.

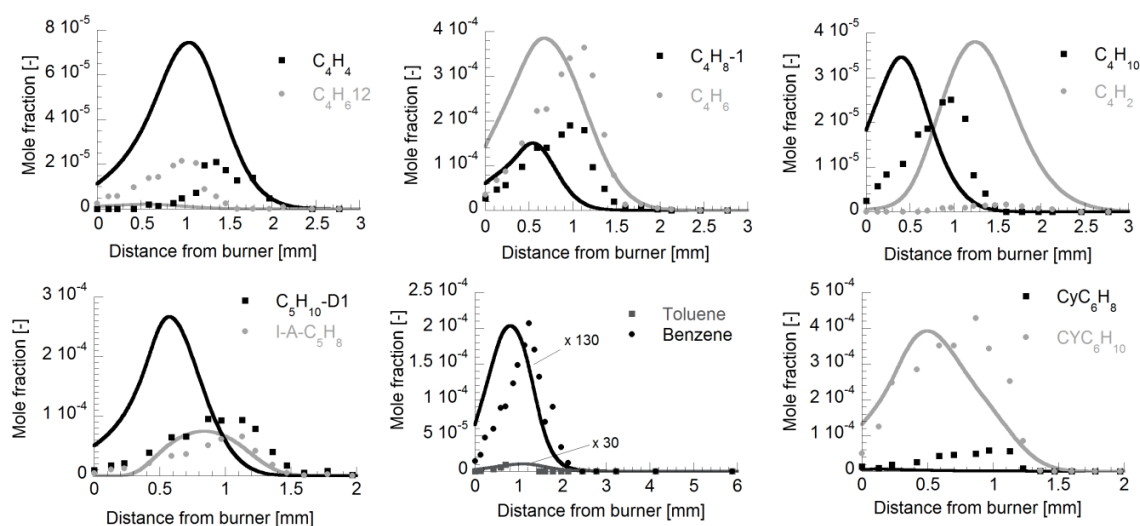


**Figure 55: C0-C3 profile in *n*-propylcyclohexane/ $CH_4$  laminar premixed flame at  $T=333$  K, and gas flow rate= $5.44$  l/min [90]**

Figure 56 shows profiles of species C4, C5 and C6. Although 1, 2-butadiene ( $C_4H_6-12$ ) is under-predicted by a factor 10, the most dominant species 1, 3-butadiene ( $C_4H_6$ ), 1-butene (1- $C_4H_8$ ) and *iso*-pentene (I-A- $C_5H_8$ ) are very well predicted. The profiles of  $C_4H_2$  and  $C_4H_4$  are also over-predicted. Also contrary to methylcyclohexane flame (Chapter 5), where cyclohexene ( $CYC_6H_{10}$ ) profiles were very low, for this flame the  $CYC_6H_{10}$  profiles agree very well with the experimental data. Although, the product from dehydrogenation of  $CYC_6H_{10}$  i.e.  $CYC_6H_8$  is under-predicted. This could be the reason for the reasonably low concentration of benzene. In the Figure 56, it is expressed as a factor of 130. Toluene profile is also low and expressed as a factor of 30. The mechanism has global reactions for cyclo-olefins

into products. In short, the direct pathway from cyclo-olefin;  $CYC_7H_{12}$  to toluene is missing which could be the reason for the low level of toluene.

The model was also validated against experiment from Ristori et al. [89] who studied the oxidation of *n*-propylcyclohexane in a jet stirred reactor at 1 atm within a temperature range of 950-1250K for equivalence ratios 0.5, 1.0 and 1.5 and constant residence time 0.07s. The results are showed in Other Results.



**Figure 56: C4, C5 and C6 profiles in *n*-propylcyclohexane/CH<sub>4</sub> laminar premixed flame at T=333 K, and gas flow rate=5.44 l/min [90]**

#### 6.4.4. Flow Analysis

The flow analysis of the *n*-propylcyclohexane is conducted for the  $\Phi=0.68$  flame from Pousse et al. [90] which is shown in Figure 57 below. It is an integrated flow analysis with the numbers indicating the carbon flow expressed in mole/m<sup>3</sup>. The species profiles are discussed in following paragraphs.

#### Degradation of propylcyclohexane

In analogy to methylcyclohexane, the common degradation pathways of *n*-propylcyclohexane also proceed mainly *via* the secondary radicals on the ring i.e.  $CYC_9H_{17}-R5$  and  $CYC_9H_{17}-R6$  radicals. They are followed by the secondary radical on the *n*-propyl chain  $CYC_9H_{17}-R2$ . These radicals are formed mainly through H-abstraction from the propylcyclohexane on the ring and on the chain respectively. These cyclo-alkyl radicals would further decompose either to the corresponding cyclo-olefins or through ring opening to form corresponding radical species. The latter





latter species involved in the decomposition are I-C<sub>4</sub>H<sub>5</sub>, C<sub>4</sub>H<sub>4</sub> and I-C<sub>4</sub>H<sub>3</sub> forming C<sub>2</sub>H<sub>2</sub>. The main degradation pathway of C<sub>2</sub>H<sub>2</sub> is the formation of the ketyl radical (HCCO) in the reaction with O atoms. Ketyl mainly decomposes to CH and CO and the oxidation of CO leads finally to the main reaction product CO<sub>2</sub>. In the Figure 57 below detailed mass flow analysis are presented for  $\Phi=0.68$  illustrating the high mass flows through C<sub>3</sub>H<sub>3</sub> and C<sub>2</sub>H<sub>2</sub> and HCCO.

### 6.4.5. Sensitivity Analysis

show the sensitivity analyses at T=1350 K and 1550K respectively of *n*-propylcyclohexane in a shock tube (See Table XLVII) at  $p=10$  bar and  $\Phi=1.0$ .

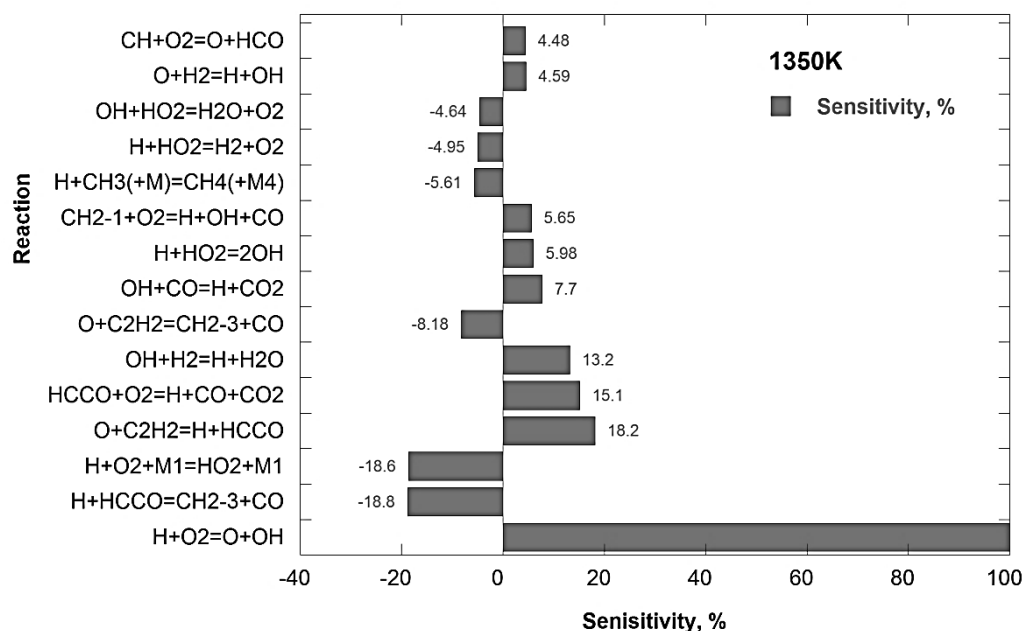
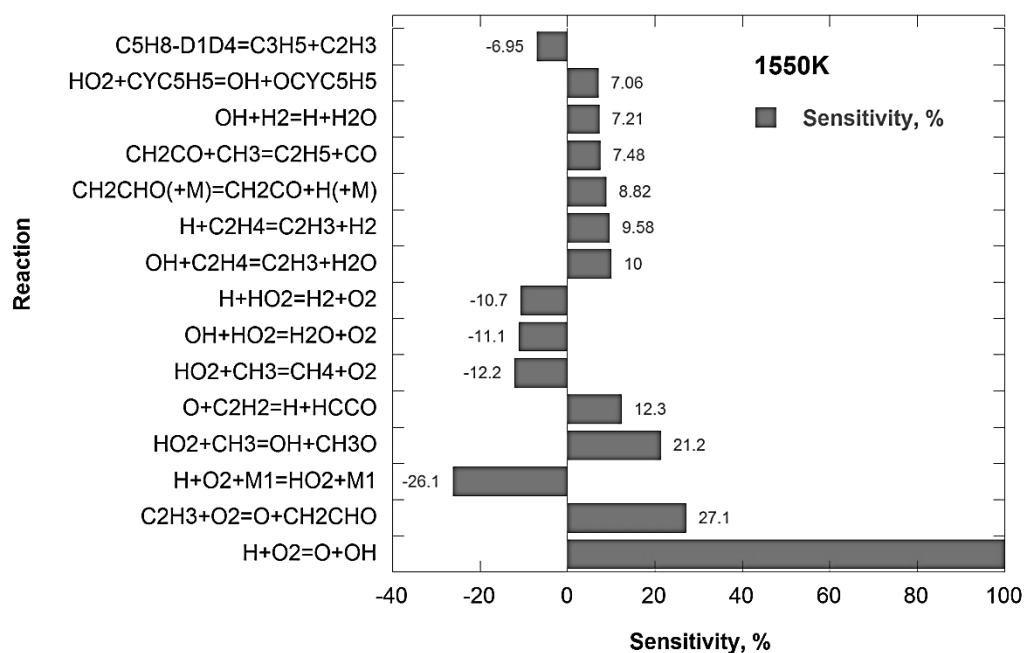


Figure 58: Sensitivity analysis of *n*-propylcyclohexane/O<sub>2</sub>/Ar mixture in a shock tube at 1350K at  $p=10$ bar and  $\Phi=1.0$  [91]



**Figure 59: Sensitivity analysis of *n*-propylcyclohexane/O<sub>2</sub>/Ar mixture in a shock tube at 1550K at p=10bar and Φ=1.0 [91]**

It is clear that the other most sensitive reactions are from the base chemistry for both temperature ranges. At 1350 K, the dienes C<sub>5</sub>H<sub>8</sub>-D1D4 shows up and its decomposition (Class 8) products. These species isomerize to cyclopentadiene (CYC<sub>5</sub>H<sub>6</sub>) which further decomposes to CYC<sub>5</sub>H<sub>5</sub>- is also strongly observed at 1350 K. At 1550 K, these reactions are not observed as sensitive and the base chemistry dominates.

## 6.5. Conclusion on *n*-propylcyclohexane

The methylcyclohexane sub-mechanism is extended to the higher *n*-propylcyclohexane  $\text{CYC}_9\text{H}_{18}$ , based on the oxidation of methylcyclohexane mechanism. Similar to methylcyclohexane, the high temperature mechanism for *n*-propylcyclohexane has been developed. Apart from the H-abstractions, the peculiar feature of *n*-propylcyclohexane is the opening of the ring and forming straight corresponding olefin. The formation is obvious in the flow analysis though H-abstractions are seen to dominate. The ring abstractions are of much importance which further forms cyclohexene and  $\text{C}_5\text{H}_8\text{-D1D4}$  diene thus opening the benzene formation routes through its dehydrogenation.

The mechanism has been developed and tested for ignition delays, flame speeds and premixed flame experiments. Some profiles from Pousse et al. [90] premixed flame like benzene and toluene are not well represented which could be mean there are other pathways to benzene formation than the dehydrogenation of cyclohexene or  $\text{C}_5\text{H}_8\text{-D1D4}$ . Dubois et al. [91] and Ji et al. [32] made flame speed measurements for *n*-propylcyclohexane/air mixtures which on the rich side ( $1.1 < \Phi < 1.4$ ) of the flame are slightly over-predicted but otherwise predict the experimental data very well.

Also, the ignition delays for pressures 10-20 bar are quite precise. With the increasing  $\text{O}_2$  concentrations, the ignition delay times decrease but the pressure effect is not significant. Same behaviour is captured by the simulations.

## 7. CONCLUSIONS AND FUTURE SCOPE

### 7.1. Summary of conclusions

Real fuels are composed of many hydrocarbons which are difficult to model, therefore surrogate fuel modelling becomes important. A surrogate fuel model is the representative of the real fuel. Considering, naphtha as the future fuel, the naphtha surrogate fuel model would be constituted of cycloalkanes like methylcyclohexane or the heavier *n*-propylcyclohexane. Thus, emphasizing the importance of studying their oxidation chemistry. *n*-Propylcyclohexane is often used in surrogate kerosene model fuel and methylcyclohexane which is a mono-alkylated cycloalkane is also widely used to represent the cycloalkane part of jet fuel surrogates. In spite of the importance of these cycloalkanes their chemistry is relatively less investigated. Cyclohexane on the other hand is the only cycloalkane which is extensively studied. Along the cycloalkane decomposition path, olefins are also formed through their ring opening. 1-hexene is the first product formed from cyclohexane combustion.

This thesis is a combined work of understanding the high temperature chemistry of cycloalkanes viz. methylcyclohexane based on previously developed cyclohexane (Nawdiyal et al.) and extending it to generate the larger *n*-propylcyclohexane mechanism. The detailed kinetic reaction mechanism model for the oxidation of 1-hexene (C<sub>6</sub>H<sub>12</sub>-D1) previously developed (Nawdiyal et al. 2015) has been added. The complete model is composed of 329 species and 2065 reactions with 3796 reversible elementary reactions. Further, these models have been validated against different experiments such as shock tubes, jet stirred reactors and laminar flames to cover full range of temperatures, pressures and equivalence ratios making the models comprehensive. The LOGEsoft software was used for all simulations. The thermodynamic properties of several new species in the mechanism were evaluated implementing Benson's group additivity method [17]. The Goos, Burcat, Rusic data base was used for thermodynamic data of fulvene [16] and for some other species.

Initially, the cyclohexane mechanism was developed taking into account the similarities and differences of linear and cyclic species and specific rules were applied from various sources. The sub-mechanism of 1-hexene mechanism added to account for its isomerization ring opening. Further, the model was built up adding the

sub-mechanism of methylcyclohexane which was formulated partly in analogy with the cyclohexane mechanism along with other literature sources. Finally, the high temperature mechanism for the oxidation of *n*-propylcyclohexane was added and the final model was complete.

The individual models were tested for ignition delays, flame speeds and premixed flame experiments. The flow analysis and sensitivity analysis were conducted in order to understand the degradation of the fuels.

The kinetic model was found to be adequate to satisfactorily reproduce ignition delay, concentration profiles of major species in JSR and flame speed for a wide range of conditions. The allylic radicals ( $C_6H_{11}$ -D1R3) preferred abstractions from fuel influences the  $C_6H_{11}$  profiles in the 1-hexene model. But it also influences the otherwise isomerization path of  $C_6H_{11}$ -D1R6 to cyclohexyl radical ( $CYC_6H_{11}$ ) which would further form cyclohexene ( $CYC_6H_{10}$ ). It is observed that  $CYC_6H_{10}$  profiles in 1-hexene flames and cyclohexane speciation are over-predicted.

The major decomposition pathway of the cycloalkanes is through H-abstractions on the ring. The path which leads towards ring opening to form olefin is observed for cyclohexane and methylcyclohexane but is very low. The fulvene pathway influence on benzene profiles of 1-hexene is obvious but do not seem to affect the cycloalkanes. This infers there are other benzene formation pathways in cycloalkanes. Some possible pathways would be the dehydrogenation of dienes and dehydrogenation of cyclo-olefins.

## 7.2. Future Scope

The *n*-propylcyclohexane was developed only for the high temperature regime. Only the 1-hexene model has both high and low temperature regimes developed. So it is necessary in the future to account the low temperature chemistry of the cycloalkanes. Also, the various benzene formation routes need to be investigated. In the past, fulvene pathway had considerably influenced the 1-hexene benzene profiles. Similarly, possibly diene dehydrogenation through cyclopentadiene formation can be investigated along with the ring opening to direct formation of cyclohexyl radical and the dehydrogenation of cycloolefins to benzene and toluene.

## REFERENCES

1. Yahyaoui, M., N. Djebaili-Chaumeix, P. Dagaut, C.-E. Paillard, and S. Gail, *Kinetics of 1-hexene oxidation in a JSR and a shock tube: Experimental and modeling study*. Combustion and flame, 2006. **147**(1): p. 67-78.
2. Ramirez, H.P.L., K. Hadj-Ali, P. Diévar, G. Moréac, and P. Dagaut, *Kinetics of Oxidation of Commercial and Surrogate Diesel Fuels in a Jet-Stirred Reactor: Experimental and Modeling Studies*. Energy & Fuels, 2010. **24**(3): p. 1668–1676.
3. Dagaut, P., *On the kinetics of hydrocarbons oxidation from natural gas to kerosene and diesel fuel*. Physical Chemistry Chemical Physics, 2002. **4**(11): p. 2079–2094.
4. Curran, H.J., P. Gaffuri, W.J. Pitz, and C.K. Westbrook, Combustion and Flame, 1998. **114**(1): p. 149–177.
5. Andrae, J.C.G., P. Björnbom, R.F. Cracknell, and G.T. Kalghatgi, *Autoignition of toluene reference fuels at high pressures modeled with detailed chemical kinetics*. Combustion and Flame, 2007. **149**(1): p. 2–24.
6. <https://www.worldenergy.org/>.
7. Chang, J., G. Kalghatgi, A. Amer, and Y. Viollet, *Enabling High Efficiency Direct Injection Engine with Naphtha Fuel through Partially Premixed Charge Compression Ignition Combustion*. 2012, SAE International.
8. Turns, S.R., *An Introduction to Combustion Concepts and Applications*. Third ed. 2012, New York: McGraw-Hill.
9. T. Edwards, L.M., *Surrogate Mixtures to represent complex Aviation and Rocket fuels*. AIAA Paper, 1999(99-2217): p. 1-11.
10. Jechura, J. 2016; Available from: [http://crudemarketing.chevron.com/crude/north\\_american/hibernia.aspx](http://crudemarketing.chevron.com/crude/north_american/hibernia.aspx).
11. <http://crudemarketing.chevron.com>.
12. Griffiths, J.F., *Spontaneous Ignition of Hydrocarbon Fuels at Temperatures in the Range 750-1500K*. 1998, University of Leeds: UK.
13. Warnatz, J., U. Maas, and R.W. Dibble, *Combustion: Physical and Chemical Fundamentals, Modeling and Simulation, Experiments, Pollutant Formation*. Fourth ed. 2006, Berlin/Heidelberg: Springer.
14. I. Glassman and R.A. Yetter, *Combustion*. Fourth ed. 2008, UK: Academic press.

15. LOGEsoft, in [http://loge.se/Products/LOGE\\_Products.html](http://loge.se/Products/LOGE_Products.html).
16. Goos, E., A. Burcat, and B. Ruscic. *Extended third millennium ideal gas and condensed phase thermochemical database for combustion with updates from active thermochemical tables*. 2010; Available from: <ftp://ftp.technion.ac.il/pub/supported/aetdd/thermodynamics>.
17. Benson, S.W., *Thermochemical Kinetics*. 1976, New York: John Wiley and Sons Inc.
18. Nawdiyal, A., N. Hansen, T. Zeuch, L. Seidel, and F. Mauss, *Experimental and modelling study of speciation and benzene formation pathways in premixed 1-hexene flames*. Proceedings of the Combustion Institute, 2015. **35**(1): p. 325-332.
19. Battin-Leclerc, F., J.M. Simmie, and E. Blurock, *Cleaner Combustion: Developing Detailed Chemical Kinetic Models*. 2013, London: Springer.
20. El-Mahallawy, F. and S.E.-D. Habik, *Fundamentals and Technology of Combustion*. 2002, UK: Elsevier Science Ltd.
21. Tsang, W., *Thermal stability of cyclohexane and 1-hexene*. International Journal of Chemical Kinetics, 1978. **10**(11): p. 1119-1138.
22. Steil, U., M. Braun-Unkhoff, C. Naumann, and P. Frank. *Experimental Study of the pyrolysis of cyclohexane at shock tube relevant conditions*. in *Proceedings of the European Combustion Meeting*. 2005.
23. Sirjean, B., F. Buda, H. Hakka, P.A. Glaude, R. Fournet, V. Warth, F. Battin-Leclerc, and M. Ruiz-Lopez, *The autoignition of cyclopentane and cyclohexane in a shock tube*. . Proceedings of the Combustion Institute, 2007. **31**(1): p. 277–284.
24. Hong, Z., K.-Y. Lam, D.F. Davidson, and R.K. Hanson, *A comparative study of the oxidation characteristics of cyclohexane, methylcyclohexane, and n-butylcyclohexane at high temperatures*. Combustion and Flame, 2011. **158**(8): p. 1456-1468.
25. Daley, S.M., A.M. Berkowitz, and M.A. Oehlschlaeger, *A shock tube study of cyclopentane and cyclohexane ignition at elevated pressures*. International Journal of Chemical Kinetics, 2008. **40**(10): p. 624–634.
26. Peukert, S., C. Naumann, M. B.-Unkhoff, and U. Riedel, *Formation of H-atoms in the pyrolysis of cyclohexane and 1-hexene: A shock tube and modeling study*. International Journal of Chemical Kinetics, 2011. **43**(3): p. 107–119.
27. Silke, E.J., W.J. Pitz, C.K. Westbrook, and M. Ribaucour, *Detailed chemical kinetic modeling of cyclohexane oxidation*. The Journal of Physical Chemistry A, 2007. **111**(19): p. 3761-3775.

28. Buda, F., B. Heyberger, R. Fournet, P.-A. Glaude, V. Warth, and F. Battin-Leclerc, *Modeling of the gas-phase oxidation of cyclohexane*. Energy & fuels, 2006. **20**(4): p. 1450-1459.
29. Voisin, D., A. Marchal, M. Reuillon, J.-C. Boettner, and M. Cathonnet, *Experimental and Kinetic Modeling Study of Cyclohexane Oxidation in a JSR at High Pressure*. Combustion science and technology, 1998. **138**(1-6): p. 137-158.
30. Wu, F., A.P. Kelley, and C.K. Law, *Laminar flame speeds of cyclohexane and mono-alkylated cyclohexanes at elevated pressures*. Combustion and Flame, 2012. **159**(4): p. 1417-1425.
31. Davis, S.G. and C.K. Law, *Determination of and Fuel Structure Effects on Laminar Flame Speeds of C1 to C8 Hydrocarbons*. Combustion Science and Technology, 1998. **140**(1-6): p. 427-449.
32. Ji, C., E. Dames, B. Sirjean, H. Wang, and F.N. Egolfopoulos, *An experimental and modeling study of the propagation of cyclohexane and mono-alkylated cyclohexane flames*. Proceedings of the Combustion Institute, 2011. **33**(1): p. 971-978.
33. Brown, T.C. and K.D. King, *Very low-pressure pyrolysis (VLPP) of methyl- and ethynyl-cyclopentanes and cyclohexanes*. International journal of chemical kinetics, 1989. **21**(4): p. 251-266.
34. Gulati, S.K. and R.W. Walker, *Addition of cyclohexane to slowly reacting H<sub>2</sub>-O<sub>2</sub> mixtures at 480° C*. Journal of the Chemical Society Faraday Transactions 2, 1989. **85**(11): p. 1799.
35. El Bakali, A., M. Braun-Unkhoff, P. Dagaut, P. Frank, and M. Cathonnet, *Detailed kinetic reaction mechanism for cyclohexane oxidation at pressure up to ten atmospheres*. Proceedings of the Combustion Institute, 2000. **28**(2): p. 1631-1638.
36. Wang, Z., Z. Cheng, W. Yuan, J. Cai, L. Zhang, F. Zhang, F. Qi, and J. Wang, *An experimental and kinetic modeling study of cyclohexane pyrolysis at low pressure*. Combustion and Flame, 2012. **159**(7): p. 2243-2253.
37. Lemaire, O., M. Ribaucour, M. Carlier, and R. Minetti, *The production of benzene in the low-temperature oxidation of cyclohexane, cyclohexene, and cyclohexane-1,3-diene*. Combustion and Flame, 2001. **127**(1-2): p. 1971-1980.
38. Tanaka, S., *Two-stage ignition in HCCI combustion and HCCI control by fuels and additives*. Combustion and Flame, 2003. **132**(1-2): p. 219-239.
39. Granata, S., T. Faravelli, and E. Ranzi, *A wide range kinetic modeling study of the pyrolysis and combustion of naphthenes*. Combustion and Flame, 2003. **132**(3): p. 533-544.



40. Cavallotti, C., R. Rota, T. Faravelli, and E. Ranzi, *Ab initio evaluation of primary cyclo-hexane oxidation reaction rates*. Proceedings of the Combustion Institute, 2007. **31**(1): p. 201-209.
41. Ranzi, E., M. Dente, A. Goldaniga, G. Bozzano, and T. Faravelli, *Lumping procedures in detailed kinetic modeling of gasification, pyrolysis, partial oxidation and combustion of hydrocarbon mixtures*. Progress in Energy and Combustion Science, 2001. **27**(1): p. 99–139.
42. Curran, H.J., P. Gaffuri, W.J. Pitz, and C.K. Westbrook, *A Comprehensive Modeling Study of iso-Octane Oxidation*. Combustion and Flame, 2002. **129**: p. 253-280.
43. Zhang, H.R., L.K. Huynh, N. Kungwan, Z. Yang, and S. Zhang, *Combustion Modeling and Kinetic Rate Calculations for a Stoichiometric Cyclohexane Flame. 1. Major Reaction Pathways*. The Journal of Physical Chemistry A, 2007. **111**(19): p. 4102–4115.
44. Law, M.E., P.R. Westmoreland, T.A. Cool, J. Wang, N. Hansen, C.A. Taatjes, and T. Kasper, *Benzene precursors and formation routes in a stoichiometric cyclohexane flame*. Proceedings of the Combustion Institute, 2007. **31**(1): p. 565–573.
45. Gong, C.-M., Z.-R. Li, and X.-Y. Li, *Theoretical kinetic study of thermal decomposition of cyclohexane*. Energy & Fuels, 2012. **26**(5): p. 2811-2820.
46. Sirjean, B., P.-A. Glaude, M. Ruiz-Lopez, and R. Fournet, *Detailed kinetic study of the ring opening of cycloalkanes by CBS-QB3 calculations*. The Journal of Physical Chemistry A, 2006. **110**(46): p. 12693-12704.
47. Ahmed, S.S., F. Mauß, and T. Zeuch, *The Generation of a Compact n-Heptane / Toluene Reaction Mechanism Using the Chemistry Guided Reduction (CGR) Technique*. Zeitschrift für Physikalische Chemie, 2009. **223**(4-5): p. 551–563.
48. Kiefer, J.H., K.S. Gupte, L.B. Harding, and S.J. Klippenstein, *Shock tube and theory investigation of cyclohexane and 1-hexene decomposition*. The Journal of Physical Chemistry A, 2009. **113**(48): p. 13570-13583.
49. Alert, C., *Development and Validation of a Detailed Chemical Kinetic Model for Cyclohexane*. 2013, BTU Cottbus-Senftenberg: Cottbus, Germany.
50. Orme, J.P., H.J. Curran, and J.M. Simmie, *Experimental and modeling study of methyl cyclohexane pyrolysis and oxidation*. The Journal of Physical Chemistry A, 2006. **110**(1): p. 114-131.
51. Tsang, W., *Decyclization of Cyclohexene, 4-Methylcyclohexene, and 4-Vinylcyclohexene in a Single-Pulse Shock Tube*. The Journal of Chemical Physics, 1965. **42**(5): p. 1805-1809.

52. King, K.D., *Very low-pressure pyrolysis (VLPP) of hex-1-ene. Kinetics of the retro-ene decomposition of a mono-olefin*. International Journal of Chemical Kinetics, 1979. **11**(10): p. 1071-1080.
53. Yahyaoui, M., N. Djebaïli-Chaumeix, C.-E. Paillard, S. Touchard, R. Fournet, P.-A. Glaude, and F. Battin-Leclerc, *Experimental and modeling study of 1-hexene oxidation behind reflected shock waves*. Proceedings of the Combustion Institute, 2005. **30**(1): p. 1137-1145.
54. Mehl, M., W.J. Pitz, C.K. Westbrook, K. Yasunaga, C. Conroy, and H.J. Curran, *Autoignition behavior of unsaturated hydrocarbons in the low and high temperature regions*. Proceedings of the Combustion Institute, 2011. **33**(1): p. 201–208.
55. Bounaceur, R., V. Warth, B. Sirjean, P.A. Glaude, R. Fournet, and F. Battin-Leclerc, *Influence of the position of the double bond on the autoignition of linear alkenes at low temperature*. Proceedings of the Combustion Institute, 2009. **32**(1): p. 387-394.
56. Hansen, N., W. Li, M.E. Law, T. Kasper, P.R. Westmoreland, B. Yang, T.A. Cool, and A. Lucassen, *The importance of fuel dissociation and propargyl+allyl association for the formation of benzene in a fuel-rich 1-hexene flame*. Physical Chemistry Chemical Physics, 2010. **12**(38): p. 12112-12122.
57. Burluka, A.A., R.G. Gaughan, J.F. Griffiths, C. Mandilas, C.G.W. Sheppard, and R. Woolley, *Turbulent burning rates of gasoline components, Part 1 – Effect of fuel structure of C6 hydrocarbons*. Fuel, 2016. **167**: p. 347–356.
58. Mehl, M., G. Vanhove, W.J. Pitz, and E. Ranzi, *Oxidation and combustion of the n-hexene isomers: A wide range kinetic modeling study*. Combustion and Flame, 2008. **155**(4): p. 756-772.
59. Ahmed, S.S., F. Mauß, G. Moréac, and T. Zeuch, *A comprehensive and compact n-heptane oxidation model derived using chemical lumping*. Physical Chemistry Chemical Physics, 2007. **9**(9): p. 1107-1126.
60. Hoyermann, K., F. Mauß, and T. Zeuch, *A detailed chemical reaction mechanism for the oxidation of hydrocarbons and its application to the analysis of benzene formation in fuel-rich premixed laminar acetylene and propene flames*. Physical Chemistry Chemical Physics, 2004. **6**(14): p. 3824-3835.
61. Atakan, B., A.T. Hartlieb, J. Brand, and K. Kohse-Höinghaus, *Experimental investigation of premixed fuel-rich low-pressure propene/oxygen/argon flames by laser spectroscopy and molecular-beam mass spectrometry*. Proceedings of the Combustion Institute, 1998. **27**: p. 435-444.
62. Lamprecht, A., B. Atakan, and K. Kohse-Höinghaus, *Fuel-rich Propene and Acetylene Flames: A Comparison of Their Flame Chemistries*. Combustion and Flame, 2000. **122**: p. 483–491.

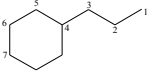
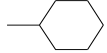
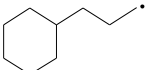
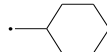
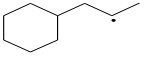
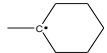
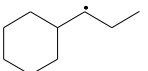
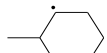
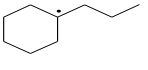
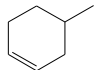
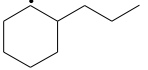

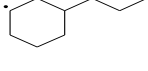
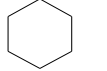
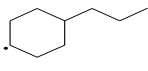
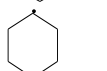
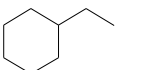
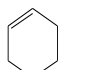
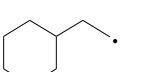
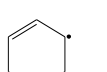
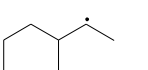
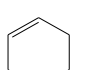
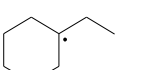
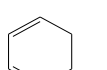
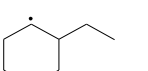
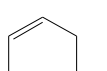
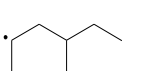
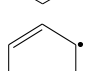
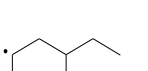
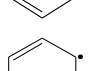
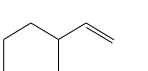
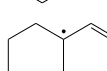
63. B. Atakan, A.L., K. Kohse-Höinghaus, *An experimental study of fuel-rich 1,3-pentadiene and acetylene/propene flame*. Combustion and Flame, 2003. **133**: p. 431–440.
64. Zhang, H.R., E.G. Eddings, A.F. Sarofim, and C.K. Westbrook, *Fuel dependence of benzene pathways*. Proceedings of the Combustion Institute, 2009. **32**: p. 377–385.
65. P. Osswald, U. Struckmeier, T. Kasper, K. Kohse-Höinghaus, J. Wang, T.A. Cool, N. Hansen, and P.R. Westmoreland, *Isomer-specific fuel destruction pathways in rich flames of methyl acetate and ethyl formate and consequences for the combustion chemistry of esters*. The Journal of Physical Chemistry A, 2007. **111**(19): p. 4093-4101.
66. Schenk, M., L. Leon, K. Moshhammer, P. Osswald, T. Zeuch, L. Seidel, F. Mauss, and K. Kohse-Höinghaus, *Detailed mass spectrometric and modeling study of isomeric butene flames*. Combustion and Flame 2013. **160**(3): p. 487–503.
67. Miller, J.A. and C.F. Melius, *Kinetic and thermodynamic issues in the formation of aromatic compounds in flames of aliphatic fuels*. Combustion and Flame, 1992. **91**(1): p. 21-39.
68. Pope, C.J. and J.A. Miller, *Exploring old and new benzene formation pathways in low-pressure premixed flames of aliphatic fuels*. Proceedings of the Combustion Institute, 2000. **28**(2): p. 1519–1527.
69. Miller, J.A. and S.J. Klippenstein, *The Recombination of Propargyl Radicals and Other Reactions on a C<sub>6</sub>H<sub>6</sub> Potential*. Journal of Physical Chemistry A, 2003. **107**(39): p. 7783–7799.
70. Marinov, N.M., W.J. Pitz, C.K. Westbrook, A.M. Vincitore, M.J. Castaldi, S.M. Senkan, and C.F. Melius, *Aromatic and polycyclic aromatic hydrocarbon formation in a laminar premixed n-butane flame*. Combustion and Flame, 1998. **114**(1): p. 192-213.
71. Hansen, N., T. Kasper, B. Yang, T.A. Cool, W. Li, P.R. Westmoreland, P. Osswald, and K. Kohse-Höinghaus, *Fuel-structure dependence of benzene formation processes in premixed flames fueled by C<sub>6</sub>H<sub>12</sub> isomers*. Proceedings of the Combustion Institute, 2011. **33**(1): p. 585-592.
72. Hansen, N., T.A. Cool, P.R. Westmoreland, and K. Kohse-Höinghaus, *Recent contributions of flame-sampling molecular-beam mass spectrometry to a fundamental understanding of combustion chemistry*. Progress in Energy and Combustion Science, 2009. **35**(2): p. 168–191.
73. Hansen, N., J.A. Miller, T. Kasper, K. Kohse-Höinghaus, P.R. Westmoreland, J. Wang, and T.A. Cool, *Benzene formation in premixed fuel-rich 1,3-butadiene flames*. Proceedings of the Combustion Institute, 2009. **32**(1): p. 623–630.



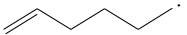

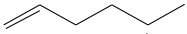
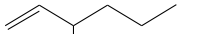
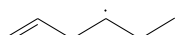
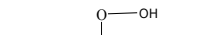

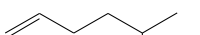
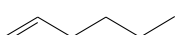


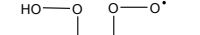
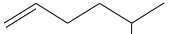



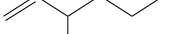

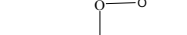
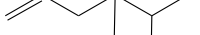
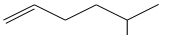
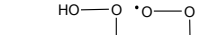




74. Hansen, N., T. Kasper, and B. Yang, Proceedings of the Combustion Institute 2011. **33**(1): p. 585–592.
75. Marinov, N.M., M.J. Castaldi, C.F. Melius, and W.Tsang, *Aromatic and polycyclic aromatic hydrocarbon formation in a premixed propane flame*. Combustion science and technology, 1997. **128**(1-6): p. 295–342.
76. Wang, H. and M. Frenklach, *A Detailed Kinetic Modeling Study of Aromatics Formation in Laminar Premixed Acetylene and Ethylene Flames*. Combustion and Flame, 1997. **110**: p. 173–221.
77. Hansen, N., S.J. Klippenstein, C.A. Taatjes, J.A. Miller, J. Wang, T.A. Cool, B. Yang, R. Yang, L. Wei, and C. Huang, *Identification and Chemistry of C<sub>4</sub>H<sub>3</sub> and C<sub>4</sub>H<sub>5</sub> Isomers in Fuel-Rich Flames*. The Journal of Physical Chemistry A, 2006. **110**(10): p. 3670–3678.
78. Böhlend, T., K. He'berger, F. Temps, and H.G. Wagner, *The reaction of CH<sub>2</sub>(X<sub>3</sub>B<sub>1</sub>) with C<sub>6</sub>H<sub>6</sub>*. Berichte der Bunsengesellschaft für physikalische Chemie 1989. **93**(1): p. 80–87.
79. Zeppieri, S., K. Brezinsky, and I. Glassman, *Pyrolysis studies of methylcyclohexane and oxidation studies of methylcyclohexane and methylcyclohexane/toluene blends*. Combustion and flame, 1997. **108**(3): p. 266-286.
80. Vasu, S.S., D.F. Davidson, Z. Hong, and R.K. Hanson, *Shock tube study of methylcyclohexane ignition over a wide range of pressure and temperature*. Energy & Fuels, 2008. **23**(1): p. 175-185.
81. Pitz, W.J., C.V. Naik, T.N. Mhaoldúin, C.K. Westbrook, H.J. Curran, J.P. Orme, and J.M. Simmie, *Modeling and experimental investigation of methylcyclohexane ignition in a rapid compression machine*. Proceedings of the combustion institute, 2007. **31**(1): p. 267-275.
82. Mittal, G. and C.-J. Sung, *Autoignition of methylcyclohexane at elevated pressures*. Combustion and Flame, 2009. **156**(9): p. 1852-1855.
83. Weber, B.W., W.J. Pitz, M. Mehl, E.J. Silke, A.C. Davis, and C.-J. Sung, *Experiments and modeling of the autoignition of methylcyclohexane at high pressure*. Combustion and Flame, 2014. **161**(8): p. 1972-1983.
84. McEnally, C.S. and L.D. Pfefferle, *Fuel decomposition and hydrocarbon growth processes for substituted cyclohexanes and for alkenes in nonpremixed flames*. Proceedings of the Combustion Institute, 2005. **30**(1): p. 1425-1432.
85. Skeen, S.A., B. Yang, A.W. Jasper, W.J. Pitz, and N. Hansen, *The Chemical Structure of Low-Pressure Premixed Methylcyclohexane Flames as Benchmarks for the Development of a Predictive Combustion Chemistry Model*. Energy & Fuels, 2011. **25**(12): p. 5611–5625.

86. Wang, Z., L. Ye, W. Yuan, L. Zhang, Y. Wang, Z. Cheng, F. Zhang, and F. Qi, *Experimental and kinetic modeling study on methylcyclohexane pyrolysis and combustion*. Combustion and Flame, 2014. **161**(1): p. 84-100.
87. Wang, H., E. Dames, B. Sirjean, D.A. Sheen, R. Tango, A. Violi, J.Y.W. Lai, F.N. Egolfopoulos, D.F. Davidson, R.K. Hanson, C.T. Bowman, C.K. Law, W. Tsang, N.P. Cernansky, D.L. Miller, and R.P. Lindstedt, *A high-temperature chemical kinetic model of n-alkane (up to n-dodecane), cyclohexane, and methyl-, ethyl-, n-propyl and n-butyl-cyclohexane oxidation at high temperatures*. September 19, 2010(JetSurF version 2.0).
88. Narayanaswamy, K., H. Pitsch, and P. Pepiot, *A chemical mechanism for low to high temperature oxidation of methylcyclohexane as a component of transportation fuel surrogates*. Combustion and Flame, 2015. **162**(4): p. 1193-1213.
89. Ristori, A., P. Dagaut, A.E. Bakali, and M. Cathonnet, *The Oxidation of N-Propylcyclohexane: Experimental Results and Kinetic Modeling*. Combust. Sci. Technol., 2001. **165**(1): p. 197–228.
90. Pousse, E., R. Porter, V. Warth, P.A. Glaude, R. Fournet, and F. Battin-Leclerc, *Lean methane premixed laminar flames doped by components of diesel fuel II: n-Propylcyclohexane*. Combustion and Flame 2010. **157**: p. 75–90.
91. Dubois, T., N. Chaumeix, and C.-E. Paillard, *Experimental and modeling study of n-propylcyclohexane oxidation under engine-relevant conditions*. Energy & Fuels, 2009. **23**(5): p. 2453-2466.
92. Zhao, Z., J. Li, A. Kazakov, and F.L. Dryer, *Combustion science and technology*, 2005. **177**: p. 89–106.
93. Crochet, M., G. Vanhove, M. Ribaucour, and R. Minetti. *n-Propylcyclohexane lean oxidation and autoignition at low temperatures and elevated pressures*. in *Proceedings of the European Combustion Meeting*. 2010.
94. Tian, Z., Y. Zhang, F. Yang, L. Pan, X. Jiang, and Z. Huang, *Comparative Study of Experimental and Modeling Autoignition of Cyclohexane, Ethylcyclohexane, and n-Propylcyclohexane*. Energy & Fuels, 2014. **28**(11): p. 7159-7167.
95. Battin-Leclerc, F., *Detailed chemical kinetic models for the low-temperature combustion of hydrocarbons with application to gasoline and diesel fuel surrogates*. Progress in Energy and Combustion Science, 2008. **34**(4): p. 440-498.

# APPENDIX

## I. Specie Structures

SPECIE STRUCTURE	SPECIE NAME	SPECIE STRUCTURE	SPECIE NAME
	n-Propylcyclohexane (NPCH); $CYC_9H_{18}$		Methylcyclohexane (MCH); $CYC_7H_{14}$
	$CYC_9H_{17}$ -R1		$CYC_7H_{13}$ -R1
	$CYC_9H_{17}$ -R2		$CYC_7H_{13}$ -R2
	$CYC_9H_{17}$ -R3		$CYC_7H_{13}$ -R3
	$CYC_9H_{17}$ -R4		$CYC_7H_{12}$ -D5
	$CYC_9H_{17}$ -R5		$C_7H_{12}$ -D1D6
	$CYC_9H_{17}$ -R6		Cyclohexane; $CYC_6H_{12}$
	$CYC_9H_{17}$ -R7		$CYC_6H_{11}$
	Ethylcyclohexane (ECH); $CYC_8H_{16}$		$CYC_6H_{10}$
	$CYC_8H_{15}$ -R1		$CyC_6H_9$ -R3
	$CYC_8H_{15}$ -R2		$CyC_6H_9$ -R4
	$CYC_8H_{15}$ -R3		$CyC_6H_8$ -D1D2
	$CYC_8H_{15}$ -R4		$CyC_6H_8$ -D1D3
	$CYC_8H_{15}$ -R5		$CyC_6H_7$ -D1D4R3
	$CYC_8H_{15}$ -R6		$CyC_6H_7$ -D1D3R2
	$CYC_8H_{14}$ -D1		$CYC_8H_{13}$ -D1R3

Specie Structure	Specie name	Specie Structure	Specie name
	1-hexene C <sub>6</sub> H <sub>12</sub> -D1		C <sub>6</sub> H <sub>11</sub> O <sub>2</sub> -D1HP6R4
	C <sub>6</sub> H <sub>11</sub> -D1R6		C <sub>6</sub> H <sub>11</sub> O <sub>2</sub> -D1HP6R5
	C <sub>6</sub> H <sub>11</sub> -D1R5		C <sub>6</sub> H <sub>11</sub> O <sub>2</sub> H-D1HP3
	C <sub>6</sub> H <sub>11</sub> -D1R4		C <sub>6</sub> H <sub>11</sub> O <sub>2</sub> H-D1HP4
	C <sub>6</sub> H <sub>11</sub> -D1R3		C <sub>6</sub> H <sub>11</sub> O <sub>2</sub> H-D1HP5
	C <sub>6</sub> H <sub>11</sub> O-D1O3		C <sub>6</sub> H <sub>11</sub> O <sub>2</sub> H-D1HP6
	C <sub>6</sub> H <sub>11</sub> O-D1O4		C <sub>6</sub> H <sub>11</sub> O <sub>4</sub> -D1HP3P4
	C <sub>6</sub> H <sub>11</sub> O-D1O5		C <sub>6</sub> H <sub>11</sub> O <sub>4</sub> -D1HP3P5
	C <sub>6</sub> H <sub>11</sub> O-D1O6		C <sub>6</sub> H <sub>11</sub> O <sub>4</sub> -D1HP3P6
	C <sub>6</sub> H <sub>11</sub> O <sub>2</sub> -D1P3		C <sub>6</sub> H <sub>11</sub> O <sub>4</sub> -D1HP4P3
	C <sub>6</sub> H <sub>11</sub> O <sub>2</sub> -D1P4		C <sub>6</sub> H <sub>11</sub> O <sub>4</sub> -D1HP4P5
	C <sub>6</sub> H <sub>11</sub> O <sub>2</sub> -D1P5		C <sub>6</sub> H <sub>11</sub> O <sub>4</sub> -D1HP4P6
	C <sub>6</sub> H <sub>11</sub> O <sub>2</sub> -D1P6		C <sub>6</sub> H <sub>11</sub> O <sub>4</sub> -D1HP3P5
	C <sub>6</sub> H <sub>11</sub> O <sub>2</sub> -D1HP3R4		C <sub>6</sub> H <sub>11</sub> O <sub>4</sub> -D1HP4P5

Specie Structure	Specie name	Specie Structure	Specie name
	C <sub>6</sub> H <sub>11</sub> O <sub>2</sub> -D1HP3R5		C <sub>6</sub> H <sub>11</sub> O <sub>4</sub> -D1HP5P6
	C <sub>6</sub> H <sub>11</sub> O <sub>2</sub> -D1HP4R3		C <sub>6</sub> H <sub>11</sub> O <sub>4</sub> -D1HP6P3
	C <sub>6</sub> H <sub>11</sub> O <sub>2</sub> -D1HP4R5		C <sub>6</sub> H <sub>11</sub> O <sub>4</sub> -D1HP6P4
	C <sub>6</sub> H <sub>11</sub> O <sub>2</sub> -D1HP4R6		C <sub>6</sub> H <sub>11</sub> O <sub>4</sub> -D1HP6P5
	C <sub>6</sub> H <sub>11</sub> O <sub>2</sub> -D1HP5R3		C <sub>6</sub> H <sub>10</sub> -D1D3
	C <sub>6</sub> H <sub>11</sub> O <sub>2</sub> -D1HP5R4		C <sub>5</sub> H <sub>11</sub> -R2
	C <sub>6</sub> H <sub>11</sub> O <sub>2</sub> -D1HP5R6		C <sub>5</sub> H <sub>11</sub> -R3
	C <sub>6</sub> H <sub>11</sub> O <sub>2</sub> -D1HP6R3		C <sub>5</sub> H <sub>10</sub> -D1
	C <sub>6</sub> H <sub>10</sub> -D1D4		C <sub>5</sub> H <sub>10</sub> -D2
	C <sub>6</sub> H <sub>10</sub>		C <sub>5</sub> H <sub>9</sub> -D1R3
	C <sub>6</sub> H <sub>10</sub> O-D1E34		C <sub>5</sub> H <sub>9</sub> -D2R1(resonant specie)
	C <sub>6</sub> H <sub>10</sub> O-D1E35		C <sub>5</sub> H <sub>9</sub> -D1R4
	C <sub>6</sub> H <sub>10</sub> O-D1E36		C <sub>5</sub> H <sub>9</sub> -D1R5
	C <sub>6</sub> H <sub>10</sub> O-D1E45		C <sub>5</sub> H <sub>9</sub> -D2R4
			C <sub>5</sub> H <sub>9</sub> -D2R5



Specie Structure	Specie name	Specie Structure	Specie name
	C <sub>6</sub> H <sub>10</sub> O-D1E46		C <sub>5</sub> H <sub>8</sub> O-D1K5
	C <sub>6</sub> H <sub>10</sub> O-D1E56		C <sub>5</sub> H <sub>8</sub> -D1D3
	C <sub>6</sub> H <sub>10</sub> O <sub>3</sub> -D1K3HP4		C <sub>5</sub> H <sub>8</sub> -D1D4
	C <sub>6</sub> H <sub>10</sub> O <sub>3</sub> -D1K3HP5		C <sub>5</sub> H <sub>8</sub> -D1D3R5
	C <sub>6</sub> H <sub>10</sub> O <sub>3</sub> -D1K3HP6		(C <sub>5</sub> H <sub>8</sub> -D1D4R3, resonant specie)
	C <sub>6</sub> H <sub>10</sub> O <sub>3</sub> -D1K3HP6		C <sub>5</sub> H <sub>9</sub> O-D1K5R5
	C <sub>6</sub> H <sub>9</sub> -D1D3R6		C <sub>5</sub> H <sub>9</sub> O-D1K3R5
	C <sub>6</sub> H <sub>9</sub> -D1D4R3		C <sub>5</sub> H <sub>9</sub> O-D1K4R5
	C <sub>6</sub> H <sub>9</sub> -D1D5R3		C <sub>4</sub> H <sub>6</sub> O-D1K3
	C <sub>5</sub> H <sub>11</sub> -R1		C <sub>4</sub> H <sub>6</sub> O-D1K4
	C <sub>4</sub> H <sub>5</sub> O-D1K3R4		
	C <sub>4</sub> H <sub>5</sub> O-D1K4R3		

R() –radical(), D()-double bond, HP()-hydroperoxy group, O()-oxy group, P()-peroxy group, E()-epoxy group, K()-ketone. The number inside parenthesis denotes the H abstraction site or the group position.

## II. Other Results

### 1. 1-Hexene in Jet Stirred Reactor

The JSR data [1] covers a range of 750 K to 1050 K. Simulations were performed assuming isothermal, constant pressure at a residence time of 0.5 s. Figure 60 and Figure 61 show the oxidation of 1-hexene at  $\Phi = 0.5$  and 1.0 respectively. Both the conditions show good agreement with the experiments.

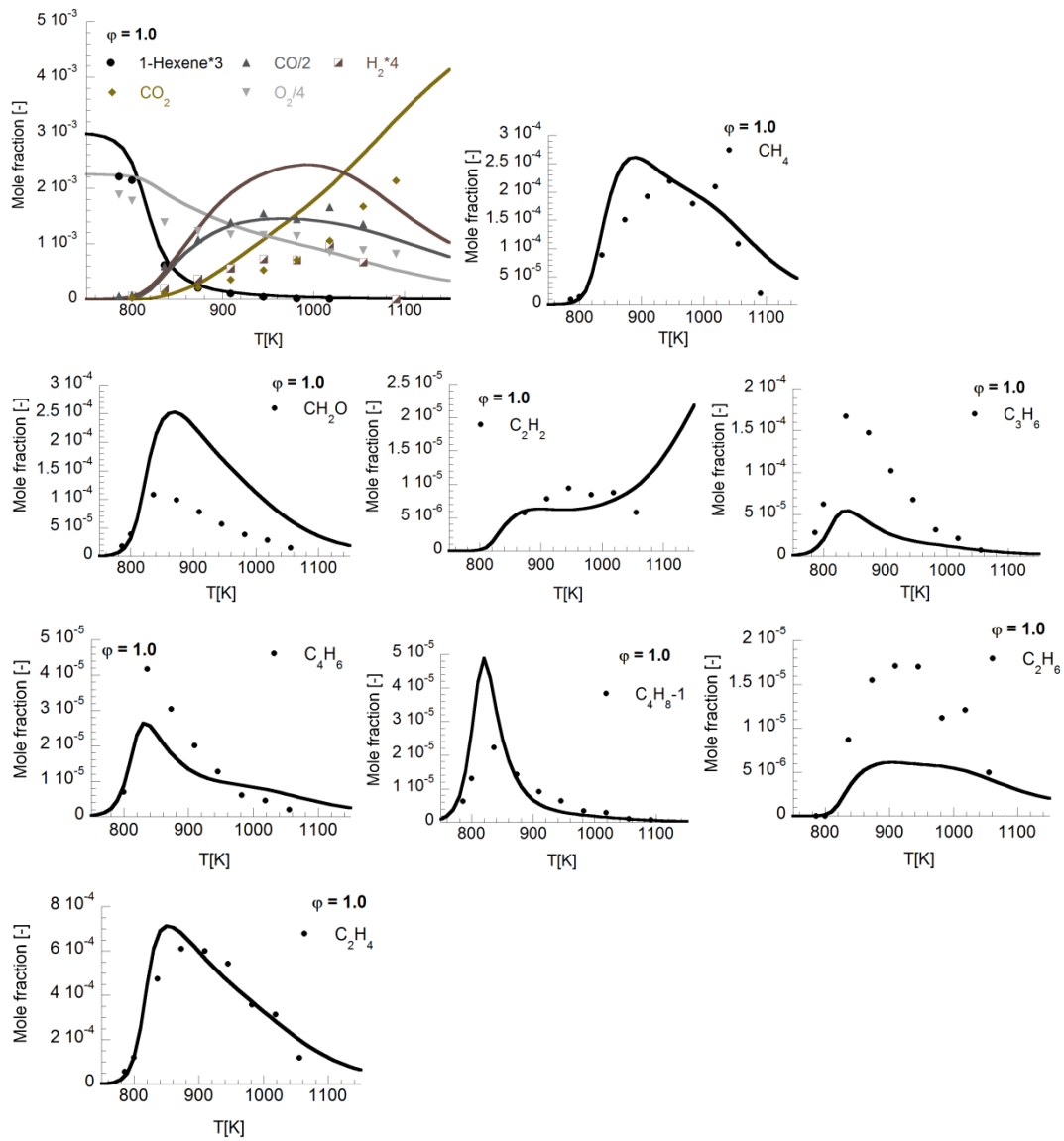


Figure 60: 1-hexene decomposition in a jet stirred reactor at  $\Phi=1.0$  and  $p=10$  atm from Dagaut et al. [1]

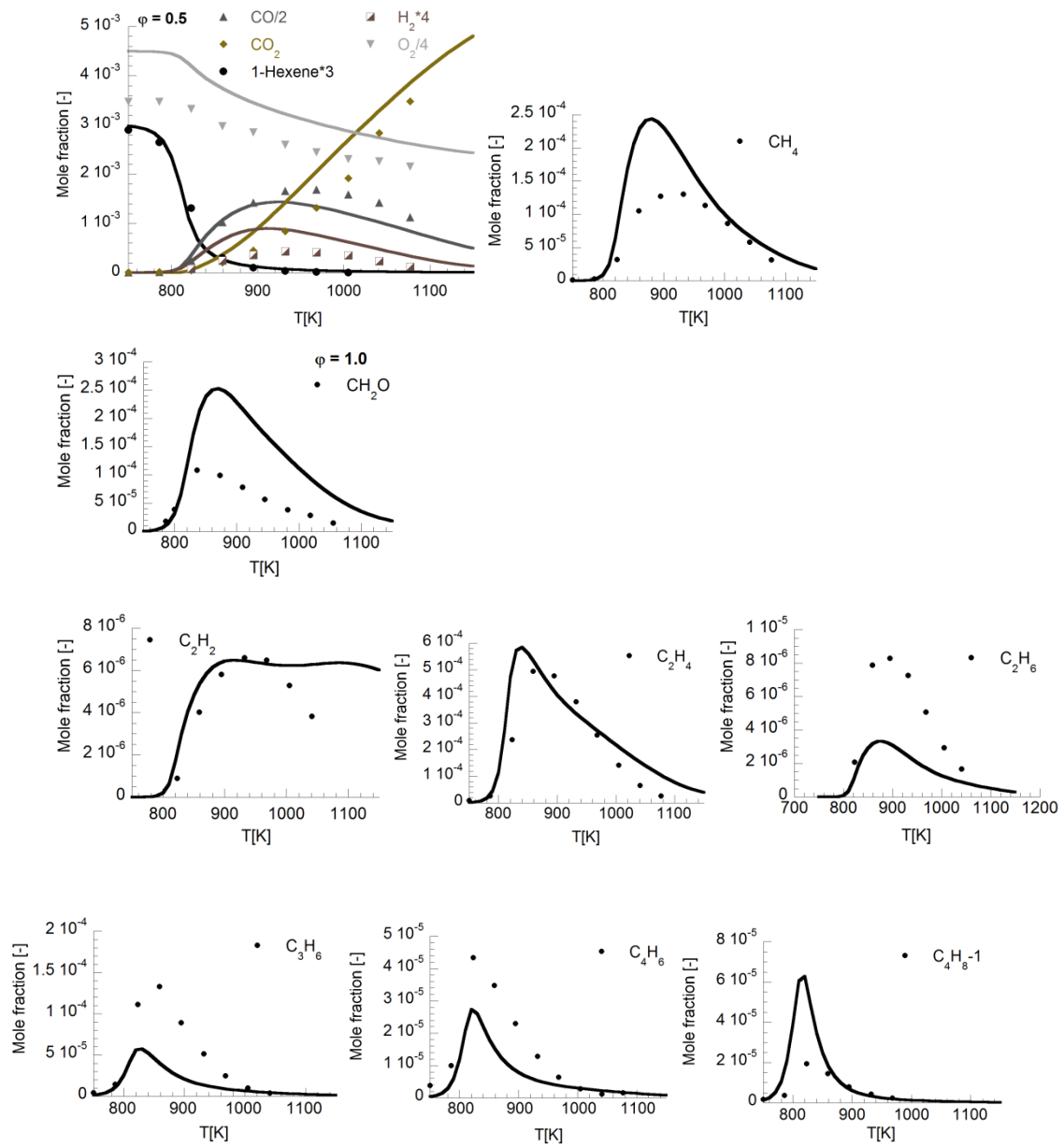


Figure 61: 1-hexene decomposition in a jet stirred reactor at  $\Phi=0.5$  and  $p=10$  atm from Dagaut et al. [1]

## 2. Flame structure of methylcyclohexane

The model has been validated against experiments from Wang et al. [86] who measured a premixed flame of methylcyclohexane with  $\Phi=1.75$  at 30 Torr along with methylcyclohexane pyrolysis at three different pressures of 30, 150 and 760 Torr.

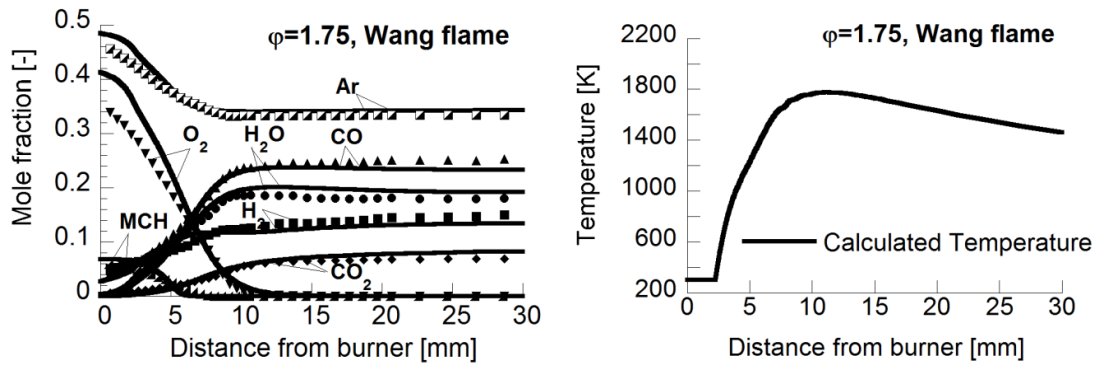


Figure 62: Methylcyclohexane fuel decomposition in Wang flame [86] at  $\Phi = 1.75$

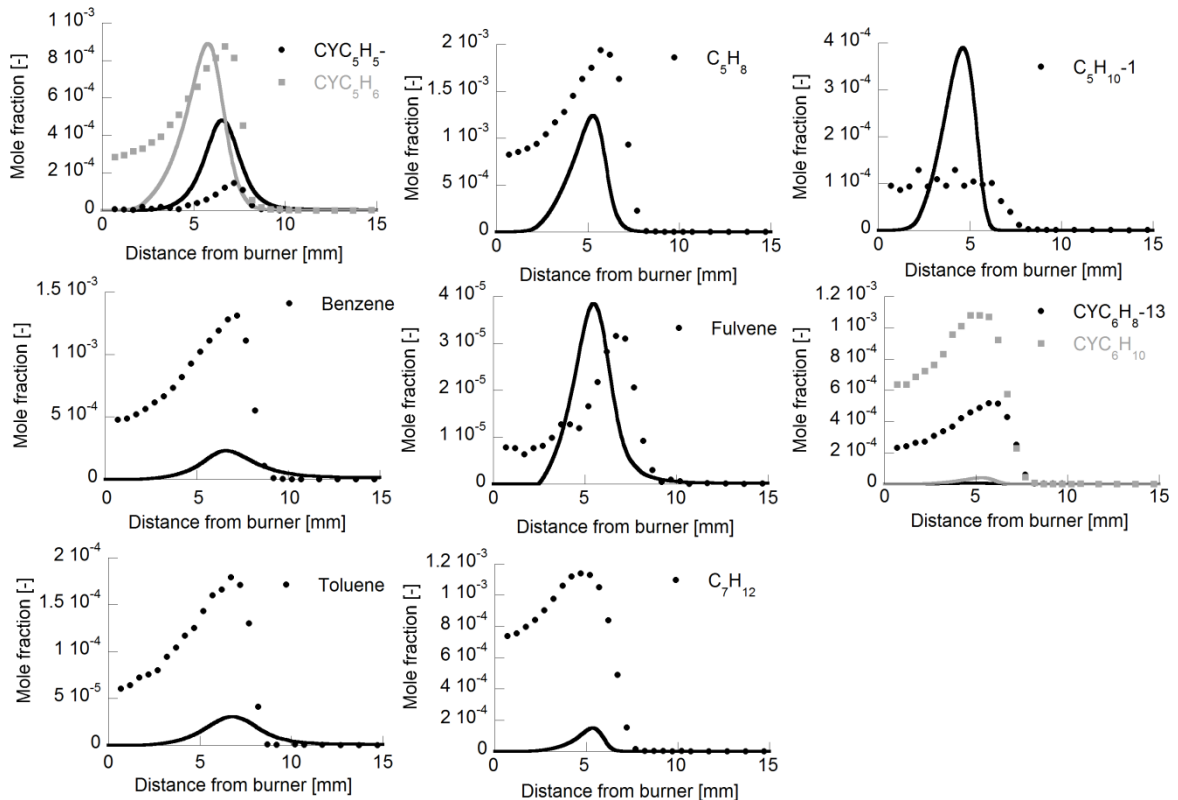
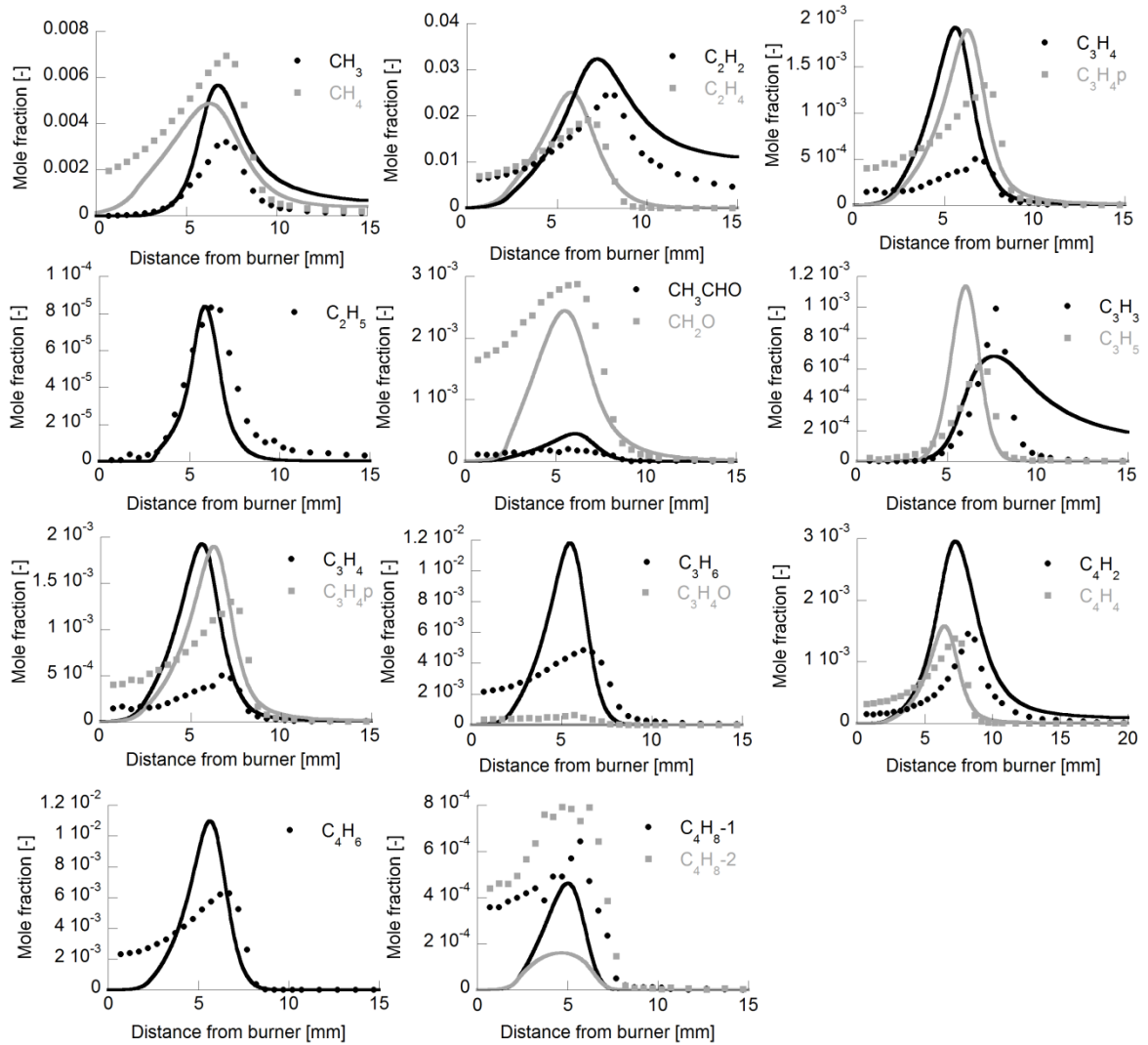


Figure 63: Intermediate species in methylcyclohexane fuel decomposition in Wang flame [86] at  $\Phi = 1.75$



**Figure 64: Intermediate species in methylcyclohexane fuel decomposition in Wang flame [86] at  $\Phi=1.75$**

Figure 62 gives the main species profiles while Figure 63 and Figure 64 show the intermediate species concentrations. These profiles can be compared with methylcyclohexane/ $O_2$ /Ar flame profiles at  $\Phi= 1.75$  from Skeen et al. [85] which is described in Chapter 5 in the validation section.

### 3. Jet Stirred Reactor (*n*-PCH)

Ristori et al. 2001 [89] studied the oxidation of *n*-propylcyclohexane in a jet stirred reactor at 1 atm within a temperature range of 950-1250K for equivalence ratios 0.5, 1.0 and 1.5 and constant residence time 0.07 s. Details about the experimental conditions are given in Table XLIX.

Reference	Components			Experimental conditions			
	NPCH [%]	O <sub>2</sub> [%]	N <sub>2</sub> [%]	$\phi$ [-]	Pressure [bar]	Temperature [K]	Residence time [s]
Ristori et al. 2001 [89]	0.1	2.70	97.20	0.5	1.0	950-1250	0.07
	0.1	1.35	98.55	1.0	1.0	950-1250	0.07
	0.1	0.90	99.00	1.5	1.0	950-1250	0.07

Table XLIX: Experimental conditions for NPCH

#### Major species

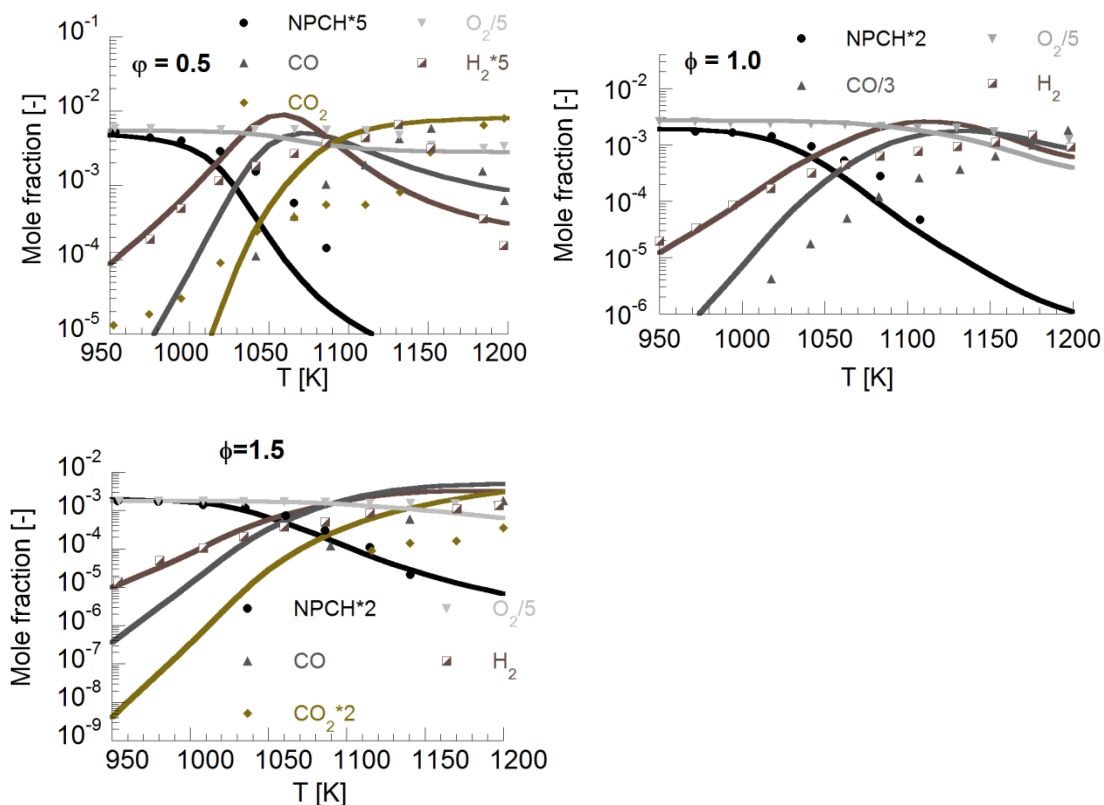
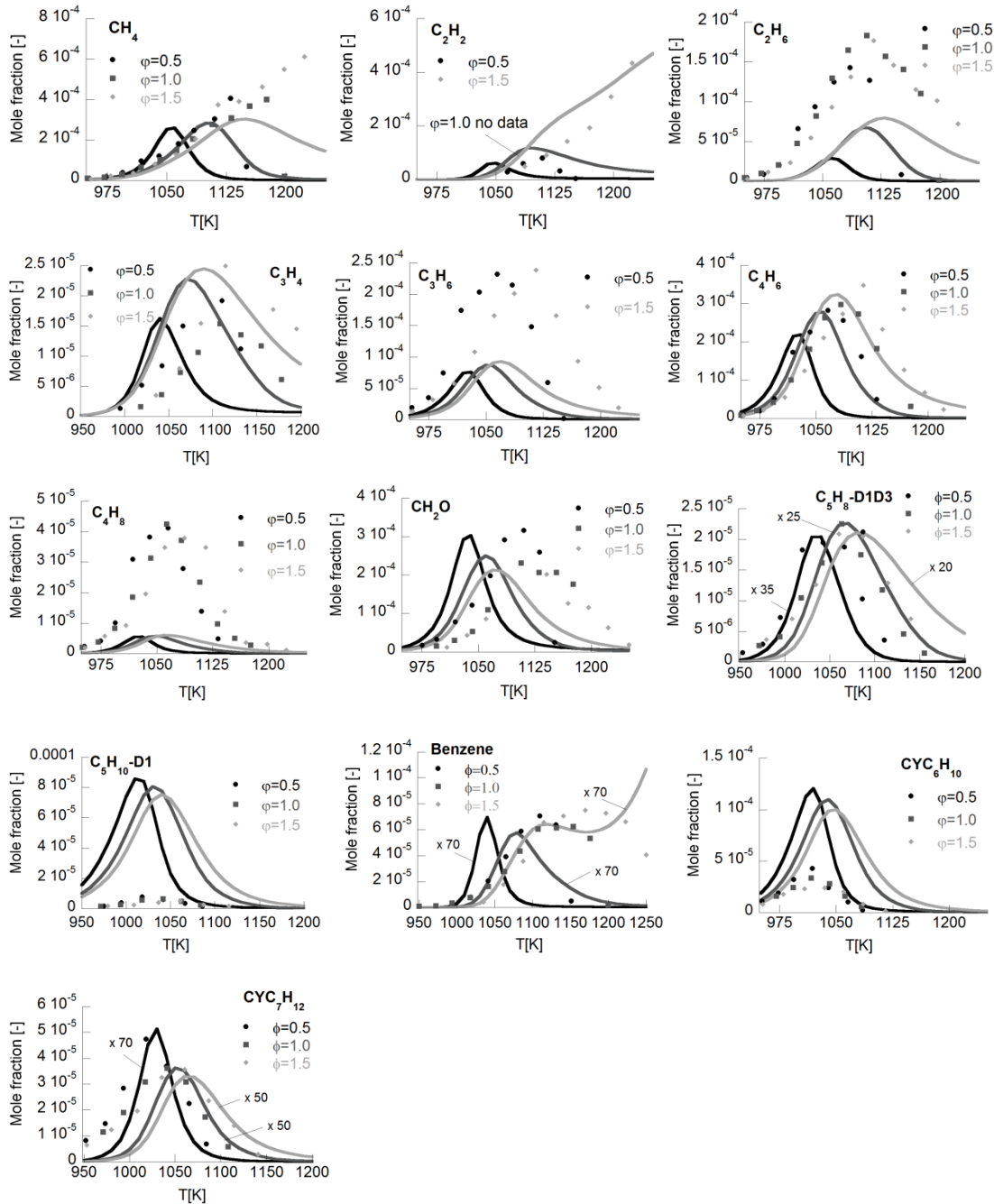


Figure 65: Main species profiles for *n*-propylcyclohexane/O<sub>2</sub>/N<sub>2</sub> decomposition in a JSR at  $\Phi=0.5$ , 1.0 and 1.5 [89] at constant mean residence time 0.07s and p=1bar. Symbols: Experiments and Lines: Simulations.

The fuel decomposition for  $\Phi=1.0$  is slightly fast between 1050 and 1100 K but it is seen to agree with the experiments for other two phi. The profiles of CO, CO<sub>2</sub> and H<sub>2</sub> are slightly over-predicted than the experiments but the profile shapes are well represented for all three cases (See Figure 65 and Figure 66)



**Figure 66: Other profiles for *n*-propylcyclohexane/O<sub>2</sub>/N<sub>2</sub> decomposition in a JSR at  $\Phi=0.5, 1.0$  and  $1.5$  [89] at constant mean residence time 0.07s and p=1bar. Symbols: Experiments and Lines: Simulations.**

### III. Low temperature oxidation of 1-hexene

The oxidation reactions lower than approximately 900 K defines the low temperature regime. Olefin low temperature oxidation in general is similar to that of alkanes. It is constituted of Classes 10 to 25 which are discussed in the following paragraphs. The low temperature sub-mechanism includes O<sub>2</sub> additions forming peroxides which later produce hydro-peroxides and ketohydro-peroxides and finally decompose into smaller aldehydes and ketones. The aldehydes and ketones are further decomposed by H-abstraction reactions following *n*-heptane rules [47].

#### Class 10: Oxygen additions

The low temperature oxidation of 1-hexene begins with the addition of alkenyl radicals to oxygen forming RO<sub>2</sub> adduct (alkenyl peroxy radical). For primary and secondary alkenyl radicals *n*-heptane rates [47] are followed with zero activation energy, but in case of the allylic site, 1000 cal/mol energy barrier has been applied because loss of resonance in the ROO adduct following Mehl et al. [58]. Smaller Arrhenius coefficient of 1.0E+9.5 for alkyl radical is considered by Mehl et al. [58].

Reactions	A ( $\frac{\text{cm}^3}{\text{mol}\cdot\text{s}}$ )	n	E <sub>a</sub> ( $\frac{\text{cal}}{\text{mol}}$ )	Ref.
C <sub>6</sub> H <sub>11</sub> -D1R6 + O <sub>2</sub> → C <sub>6</sub> H <sub>11</sub> O <sub>2</sub> -D1P6	2.000E+12	0.00	0.00	[47]
C <sub>6</sub> H <sub>11</sub> -D1R3 + O <sub>2</sub> → C <sub>6</sub> H <sub>11</sub> O <sub>2</sub> -D1P3	1.995E+09	0.00	1000	[58]

Table L: Kinetic data for Class 10: Oxygen addition to alkenyl radicals

In current mechanism, the backward reactions are calculated with thermochemistry. Mehl et al. [58] applies 20,000-25,000 cal/mol for alkenyl peroxy radical with O<sub>2</sub> group on allyl position whereas 30,000 cal/mol for alkylperoxy radicals.

#### Class 11: R + R'O<sub>2</sub> = RO + R'O

In this class, the adduct from class 10 reacts with the alkenyl radicals to form two alkoxy i.e. RO radicals. *n*-Heptane rate of 7.0E+12 exp(1000/RT) cm<sup>3</sup>/mol·s by Ahmed et al. [47] are followed for all types of reactions. An example for primary alkenyl radical is given in below.



Reactions	A ( $\frac{\text{cm}^3}{\text{mol}\cdot\text{s}}$ )	n	E <sub>a</sub> ( $\frac{\text{cal}}{\text{mol}}$ )	Ref.
C <sub>6</sub> H <sub>11</sub> -D1R6 + C <sub>6</sub> H <sub>11</sub> O <sub>2</sub> -D1P6 → 2C <sub>6</sub> H <sub>11</sub> O-D1O6	7.00E+12	0.0	-1000	[47]

Table LI: Kinetic data for Class 11: R+R'O<sub>2</sub>=RO+RO

### Class 12: RO<sub>2</sub> (Alkyl peroxy radical) isomerization

This class includes the reaction in which the internal H-atom abstraction of RO<sub>2</sub> radical forms QOOH. Isomerization for all possible ring sizes 5, 6 and 7 are taken into account and n-heptane rates [47] are followed (See Figure 67). Transitions over the double bond are not considered owing to the restraint resulting from the double bond. Primary H-atom is easily abstracted in comparison to secondary H-atoms.

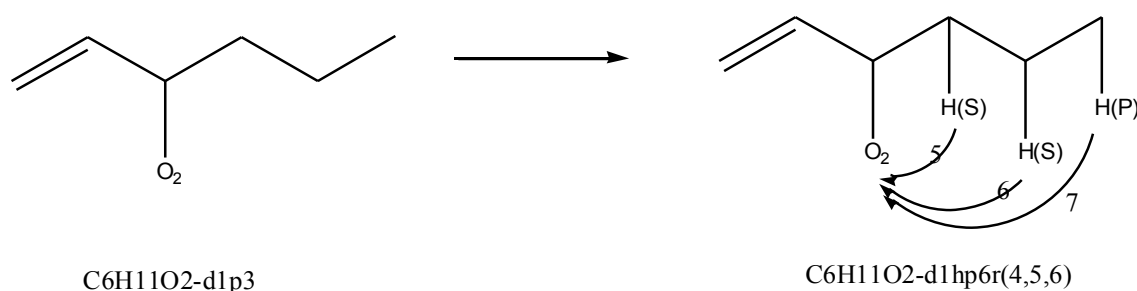


Figure 67: Internal isomerization of alkenyl-peroxy radical example allyl-peroxy radical C<sub>6</sub>H<sub>11</sub>O<sub>2</sub>-D1P3 showing 5, 6 and 7 ring transfers.

Reactions	A ( $\frac{\text{cm}^3}{\text{mol}\cdot\text{s}}$ ) per H	n	E <sub>a</sub> ( $\frac{\text{cal}}{\text{mol}}$ )	Ref.
5 ring-Primary	2.98x10 <sup>12</sup>	0.0	29650	[47]
	6.31x10 <sup>11</sup>	0.0	29100	[58]
5 ring-Secondary	2.98x10 <sup>12</sup>	0.0	27850	[47]
	6.31x10 <sup>11</sup>	0.0	26400	[58]
5 ring-Allyl	2.98x10 <sup>12</sup>	0.0	27850	[47]
	6.31x10 <sup>11</sup>	0.0	22100	[58]
6 ring-Primary	2.47x10 <sup>11</sup>	0.0	23860	[47]
	1.00x10 <sup>11</sup>	0.0	23000	[58]
6 ring-Secondary	2.48x10 <sup>11</sup>	0.0	22150	[47]
	1.00x10 <sup>11</sup>	0.0	20300	[58]
6-ring-Allyl	2.48x10 <sup>11</sup>	0.0	22150	[47]
	1.00x10 <sup>11</sup>	0.0	16000	[58]
7 ring-Primary	2.06x10 <sup>10</sup>	0.0	21100	[47]
	3.98x10 <sup>10</sup>	0.0	23000	[58]
7 ring-Secondary	2.06x10 <sup>10</sup>	0.0	19349	[47]
	3.98x10 <sup>10</sup>	0.0	20300	[58]
7 ring-Allyl	2.06x10 <sup>10</sup>	0.0	19349	[47]
	3.98x10 <sup>10</sup>	0.0	20300	[58]

Table LII: Kinetic data for Class 12: Internal isomerization of hexynyl-peroxy radical

Rate constants for abstraction of primary H-atom for all possible ring transfer is given in Table LII. Here, rates for allyl H-atom abstraction is considered same as secondary H-atom abstraction which is about 1800 cal/mol less than that needed for primary one. According to Mehl et al. [58] activation energy needed to abstract secondary H-atom is 2700 cal/mol less than needed for primary H-atom abstraction. Allyl H-atom abstraction according to Mehl et al. [58] is the fastest with activation energy 7000 cal/mol less than primary H-atom

### Class 13: $\text{RO}_2 + \text{HO}_2 = \text{RO}_2\text{H} + \text{O}_2$

In this class, alkenyl peroxy radical  $\text{RO}_2$  reacts with another radical  $\text{HO}_2$  making this reaction bimolecular. The H radical from  $\text{HO}_2$  is transferred to the peroxy radical forming hydroperoxide  $\text{RO}_2\text{H}$  and  $\text{O}_2$ . The *n*-heptane rate constants [47] are followed here as seen below for example of  $\text{C}_6\text{H}_{11}\text{O}_2$ -D1P6 in .

Reactions	$A \left( \frac{\text{cm}^3}{\text{mol}\cdot\text{s}} \right)$	n	$E_a \left( \frac{\text{cal}}{\text{mol}} \right)$	Ref.
$\text{C}_6\text{H}_{11}\text{O}_2\text{-D1P6} + \text{HO}_2 = \text{C}_6\text{H}_{11}\text{O}_2\text{H-D1HP6} + \text{O}_2$	1.75E+10	0.00	-3269	[47]

Table LIII: Kinetic data for Class 13:  $\text{RO}_2 + \text{HO}_2 = \text{RO}_2\text{H} + \text{O}_2$

### Class 14: $\text{RO}_2 + \text{H}_2\text{O}_2 = \text{RO}_2\text{H} + \text{HO}_2$

This reaction class also forms hydroperoxide  $\text{RO}_2\text{H}$  as in the previous class. The rate constants for this reaction class are from Ahmed et al. [47].

Reactions	$A \left( \frac{\text{cm}^3}{\text{mol}\cdot\text{s}} \right)$	n	$E_a \left( \frac{\text{cal}}{\text{mol}} \right)$	Ref.
$\text{C}_6\text{H}_{11}\text{O}_2\text{-D1P6} + \text{H}_2\text{O}_2 = \text{C}_6\text{H}_{11}\text{O}_2\text{H-D1HP6} + \text{HO}_2$	2.40E+14	0.00	10000	[47]

Table LIV: Kinetic data for Class 14:  $\text{RO}_2 + \text{H}_2\text{O}_2 = \text{RO}_2\text{H} + \text{HO}_2$

### Class 15: $\text{RO}_2 + \text{CH}_3\text{O}_2 = \text{RO} + \text{CH}_3\text{O} + \text{O}_2$

In this reaction class  $\text{RO}$ ,  $\text{CH}_3\text{O}$  and  $\text{O}_2$  are formed through interaction of two peroxy radicals;  $\text{RO}_2$  and  $\text{CH}_3\text{O}_2$ . Since, three products are formed this reaction works in only forward direction and reverse reaction is not possible. *n*-Heptane reaction rates are followed here [47].

Reactions	$A \left( \frac{\text{cm}^3}{\text{mol}\cdot\text{s}} \right)$	n	$E_a \left( \frac{\text{cal}}{\text{mol}} \right)$	Ref.
$\text{C}_6\text{H}_{11}\text{O}_2\text{-D1P6} + \text{CH}_3\text{O}_2 = \text{C}_6\text{H}_{11}\text{O-D1O6} + \text{CH}_3\text{O}$	1.40E+16	-1.61	1855	[47]

Table LV: Kinetic Class 15:  $\text{RO}_2 + \text{CH}_3\text{O}_2 = \text{RO} + \text{CH}_3\text{O} + \text{O}_2$

**Class 16: RO<sub>2</sub> + R'O<sub>2</sub> = RO + RO + O<sub>2</sub>**

In this reaction class, two peroxy radicals react to form two RO radicals and O<sub>2</sub>. This reaction also proceeds in forward direction and reverse reaction is not possible. The rate constants for this reaction class are same as that used for class 15 and are taken from *n*-heptane rates [47].

Reactions	A ( $\frac{\text{cm}^3}{\text{mol}\cdot\text{s}}$ )	n	E <sub>a</sub> ( $\frac{\text{cal}}{\text{mol}}$ )	Ref.
C <sub>6</sub> H <sub>11</sub> O <sub>2</sub> -D1P6 + C <sub>6</sub> H <sub>11</sub> O <sub>2</sub> -D1P6 = C <sub>6</sub> H <sub>11</sub> O-D1O6 + C <sub>6</sub> H <sub>11</sub> O-D1O6 + O <sub>2</sub>	1.40E+16	-1.61	1855	[47]

Table LVI: Kinetic data for Class 16: RO<sub>2</sub> + R'O<sub>2</sub> = RO + RO + O<sub>2</sub>

**Class 17: RO<sub>2</sub>H = RO + OH**

In this reaction class, the alkenyl hydroperoxide, RO<sub>2</sub>H decomposes into two radicals, alkoxy radical RO and OH radical making it a chain branching step. *n*-Heptane reaction rates are followed here [47].

Reactions	A ( $\frac{\text{cm}^3}{\text{mol}\cdot\text{s}}$ )	n	E <sub>a</sub> ( $\frac{\text{cal}}{\text{mol}}$ )	Ref.
C <sub>6</sub> H <sub>11</sub> O <sub>2</sub> H-D1HP6 = C <sub>6</sub> H <sub>11</sub> O-D1O6 + OH	1.26E+16	-1.61	42430	[47]

Table LVII: Kinetic data for Class 17: RO<sub>2</sub>H = RO + OH

**Class 18: RO decomposition**

In this reaction class, the alkoxy radical RO decomposes into aldehydes or ketones and other small alkenyl radicals. The reaction can occur in both directions with forward rates taken from *n*-heptane [47]. The reverse rates are calculated through thermochemistry.

Reactions	A ( $\frac{\text{cm}^3}{\text{mol}\cdot\text{s}}$ )	n	E <sub>a</sub> ( $\frac{\text{cal}}{\text{mol}}$ )	Ref.
C <sub>6</sub> H <sub>11</sub> O-D1O6=C <sub>5</sub> H <sub>9</sub> -D1R5+CH <sub>2</sub> O	1.00E+11	0.00	11880	[47]
C <sub>6</sub> H <sub>11</sub> O-D1O5=C <sub>4</sub> H <sub>7</sub> P-1+CH <sub>3</sub> CHO	1.00E+11	0.00	11880	[47]
C <sub>6</sub> H <sub>11</sub> O-D1O5=CH <sub>3</sub> +C <sub>5</sub> H <sub>8</sub> O-D1K5	1.00E+11	0.00	11880	[47]
C <sub>6</sub> H <sub>11</sub> O-D1O4=C <sub>3</sub> H <sub>5</sub> +C <sub>2</sub> H <sub>5</sub> CHO	1.00E+11	0.00	11880	[47]
C <sub>6</sub> H <sub>11</sub> O-D1O4=C <sub>2</sub> H <sub>5</sub> +C <sub>4</sub> H <sub>6</sub> O-D1K4	1.00E+11	0.00	11880	[47]
C <sub>6</sub> H <sub>11</sub> O-D1O3=N-C <sub>3</sub> H <sub>7</sub> +C <sub>2</sub> H <sub>3</sub> CHO	1.00E+11	0.00	11880	[47]
C <sub>6</sub> H <sub>11</sub> O-D1O3=C <sub>2</sub> H <sub>3</sub> +N-C <sub>3</sub> H <sub>7</sub> CHO	1.00E+11	0.00	11880	[47]

Table LVIII: Kinetic data for Class 18: RO decomposition

**Class 19: QOOH = QO + OH (Heterocycle formation)**

In this reaction class, hydroperoxy alkenyl radical QOOH decomposes to form cyclic ether QO (or epoxide) and OH radical. Epoxides are highly reactive species owing

to the bond strain. Thus, this reaction class is generally very sensitive to the low temperature oxidation for ignition delay. The current model takes into account 3-ring, 4-ring and 5-ring cyclic ether formations. Mehl et al. [58] also considers 3-ring oxiran, 4-ring oxetan and 5-ring furan formations. For the current mechanism, rate constants are according to *n*-heptane [47].

Reactions	A ( $\frac{\text{cm}^3}{\text{mol}\cdot\text{s}}$ )	n	E <sub>a</sub> ( $\frac{\text{cal}}{\text{mol}}$ )	Ref.
3 ring	$1.00 \times 10^{12}$	0.0	18000	[58]
	$3.00 \times 10^{11}$	0.0	22000	[47]
4 ring	$1.58 \times 10^{11}$	0.0	17000	[58]
	$2.50 \times 10^{10}$	0.0	15251	[47]
5 ring	$2.50 \times 10^{10}$	0.0	8500	[58]
	$2.08 \times 10^9$	0.0	22000	[47]

**Table LIX: Kinetic data for Class 19: Cyclic ether formation**

### **Class 20: QOOH = diene + HO<sub>2</sub> (HO<sub>2</sub> β-decomposition)**

Here, hydroperoxy alkenyl radical (QOOH) formed in class 12 is decomposed to form diolefin or diene and HO<sub>2</sub> through β-scission. C-O bond is weaker than C-C, thus the formation of HO<sub>2</sub> is preferred than breakage of carbon chain especially at low temperature. The QOOH species involved in this class are the ones which have OOH group attached the carbon besides the one having radical site. Mehl et al. [58] employs a rate constant of  $1 \times 10^{14} \exp(-23000/RT) \text{ cm}^3/\text{mol}\cdot\text{s}$  where primary QOOH radical is concerned. When OOH group is on allylic site then rate constant of  $1 \times 10^{14} \exp(-20000/RT) \text{ cm}^3/\text{mol}\cdot\text{s}$  and when it is adjacent to allylic site then rate constant of  $1 \times 10^{14} \exp(-27000/RT) \text{ cm}^3/\text{mol}\cdot\text{s}$  are employed. According to *n*-heptane rates, primary reaction is penalized with 7600 cal/mol activation energy while secondary reaction with 11000 cal/mol. Frequency factor is same for both with  $1 \times 10^{11} \text{ s}^{-1}$ . So clearly Mehl et al. [58] uses higher rates than *n*-heptane rates. Here, Mehl et al. [58] rates are followed at the double bond and *n*-heptane rates [47] are followed for primary and secondary QOOH radicals.

Reactions	A ( $\frac{\text{cm}^3}{\text{mol}\cdot\text{s}}$ )	n	E <sub>a</sub> ( $\frac{\text{cal}}{\text{mol}}$ )	Ref.
HO <sub>2</sub> +C <sub>6</sub> H <sub>10</sub> =C <sub>6</sub> H <sub>11</sub> O <sub>2</sub> -D1HP6R5	1.00E+11	0.00	7600	[47]
HO <sub>2</sub> +C <sub>6</sub> H <sub>10</sub> =C <sub>6</sub> H <sub>11</sub> O <sub>2</sub> -D1HP5R6	1.00E+11	0.00	11000	[47]
HO <sub>2</sub> +C <sub>6</sub> H <sub>10</sub> -D1D4=C <sub>6</sub> H <sub>11</sub> O <sub>2</sub> -D1HP4R5	1.00E+11	0.00	11000	[47]
HO <sub>2</sub> +C <sub>6</sub> H <sub>10</sub> -D1D4=C <sub>6</sub> H <sub>11</sub> O <sub>2</sub> -D1HP5R4	1.00E+14	0.00	23000	[58]
HO <sub>2</sub> +C <sub>6</sub> H <sub>10</sub> -D1D3=C <sub>6</sub> H <sub>11</sub> O <sub>2</sub> -D1HP3R4	1.00E+14	0.00	20000	[58]
HO <sub>2</sub> +C <sub>6</sub> H <sub>10</sub> -D1D3=C <sub>6</sub> H <sub>11</sub> O <sub>2</sub> -D1HP4R3	1.00E+14	0.00	27000	[58]

**Table LX: Kinetic data for Class 20: QOOH = diene + HO<sub>2</sub> (HO<sub>2</sub> β-decomposition)**

Mehl et al. [58] also considers this class along with direct elimination of HO<sub>2</sub> from ROO radical. They use rate constant of  $3 \times 10^{12} \exp(29500/RT)$  cm<sup>3</sup>/mol·s for secondary hydrogen whereas where allyl H is involved the activation energy is reduced to 26000 cal/mol. Direct eliminations are not considered in the current model.

### **Class 21: QOOH = diene + carbonyl + OH**

In this class, QOOH radical undergoes decomposition to form dienes, carbonyl (aldehyde or ketone) and OH radical. This reaction being tri-molecular, the reverse reaction is considered negligible. *n*-Heptane rates [47] are followed for this class which are  $5.0 \times 10^{13} \exp(-25460/RT)$  cm<sup>3</sup>/mol·s .

Reactions	A ( $\frac{\text{cm}^3}{\text{mol}\cdot\text{s}}$ )	n	E <sub>a</sub> ( $\frac{\text{cal}}{\text{mol}}$ )	Ref.
C <sub>6</sub> H <sub>11</sub> O <sub>2</sub> -D1HP6R4=>OH+CH <sub>2</sub> O+C <sub>5</sub> H <sub>8</sub> -D1D4	5.00E+13	0.00	25460	[47]
C <sub>6</sub> H <sub>11</sub> O <sub>2</sub> -D1HP5R3=>OH+CH <sub>3</sub> CHO+C <sub>4</sub> H <sub>6</sub>	5.00E+13	0.00	25460	[47]
C <sub>6</sub> H <sub>11</sub> O <sub>2</sub> -D1HP4R6=>OH+C <sub>4</sub> H <sub>6</sub> O-D1K4+C <sub>2</sub> H <sub>4</sub>	5.00E+13	0.00	25460	[47]
C <sub>6</sub> H <sub>11</sub> O <sub>2</sub> -D1HP3R5=>OH+C <sub>2</sub> H <sub>3</sub> CHO+C <sub>3</sub> H <sub>6</sub>	5.00E+13	0.00	25460	[47]

**Table LXI: Kinetic data for Class 21: QOOH= Diene + Carbonyl + OH**

### **Class 22: Addition of O<sub>2</sub> to QOOH**

At low temperatures, hydroxyl-alkyl radicals (e.g. C<sub>6</sub>H<sub>11</sub>O<sub>2</sub>-D1HP6R5) adducts undergo O<sub>2</sub> addition due to their relative stability thus forming hydroxyl-alkyl-peroxyl radicals (e.g. C<sub>6</sub>H<sub>11</sub>O<sub>4</sub>-D1HP6P5). For this class, the rate constants for forward reactions are taken from Ahmed rules [47] (same as class 10) and that for reverse from thermodynamic data calculation using LOGEsoft [15].

Reactions	A ( $\frac{\text{cm}^3}{\text{mol}\cdot\text{s}}$ )	n	E <sub>a</sub> ( $\frac{\text{cal}}{\text{mol}}$ )	Ref.
C <sub>6</sub> H <sub>11</sub> O <sub>2</sub> -D1HP6R4+O <sub>2</sub> => C <sub>6</sub> H <sub>11</sub> O <sub>4</sub> -D1HP6P4	2.000E+12	0.00	0.00	[47]

Table LXII: Kinetic data for Class 22: Addition of O<sub>2</sub> to QOOH

### Class 23: Isomerisation of O<sub>2</sub>QOOH and formation of ketohydroperoxide and OH

In this reaction class, ketohydroperoxides are formed through internal isomerization of O<sub>2</sub>QOOH species. The OH radical is removed from the OOH group and H-atom from the same carbon-atom transfers to the peroxy group to form hydroperoxy. 5-ring, 6-ring and 7-ring formations are considered with the type of radical involved either primary or secondary (allyl radical is considered as secondary). The rate coefficients followed here are from *n*-heptane [47]. This reaction class is also sensitive for calculations of ignition delay times.

Reactions	A ( $\frac{\text{cm}^3}{\text{mol}\cdot\text{s}}$ ), per H	n	E <sub>a</sub> ( $\frac{\text{cal}}{\text{mol}}$ )	Ref.
<b>5 ring</b> - Primary	1.490E+12	0.0	26700	[47]
- Secondary	1.490E+12	0.0	24900	[47]
- Allyl (same as secondary)	1.490E+12	0.0	24900	[47]
<b>6 ring</b> – Primary	1.240E+12	0.0	20900	[47]
- Secondary	1.240E+12	0.0	19150	[47]
- Allyl (same as secondary)	1.240E+12	0.0	19150	[47]
<b>7 ring</b> – Primary	1.240E+12	0.0	18100	[47]
- Secondary	1.240E+12	0.0	16349	[47]
- Allyl (same as secondary)	1.240E+12	0.0	16349	[47]

Table LXIII: Kinetic data for Class 23: Isomerisation of O<sub>2</sub>QOOH to form ketohydroperoxide

### Class 24: Decomposition of ketohydroperoxide to form oxygenated radical species and OH

In this class, the ketohydroperoxide decomposes to form oxygenated radical and OH. The rate constants are according to *n*-heptane rates [47] which are  $1.0 \times 10^{16} \exp(-42000/RT) \text{ cm}^3/\text{mol}\cdot\text{s}$ . Since, it is a tri-molecular reaction, the reaction proceeds only in forward direction. C<sub>4</sub>H<sub>6</sub>O-D1K4 is found in this class too and is an important ketone formed. Since the products include two radicals, this class is highly unstable making it reactive and thus accelerating the ignition delay time.

## Class 25: Cyclic ether reactions with OH and HO<sub>2</sub>

In this class, the cyclic ethers react with OH and HO<sub>2</sub> to form aldehydes/ketones along with one radical and H<sub>2</sub>O. The reaction starts with H-abstraction with breakage of weak C-O bond of epoxide and thereafter scission of C<sub>6</sub> chain to form products. The H-abstraction occurs either on H-C-O (H-atom bound to a C-atom which is bound to the O-atom in the ring structure) or on H-C-C (H-atom bound to a C-atom which is bound to another C-atom outside the ring structure) depending which H-atom is abstracted. H-atom on H-C-O ring is more likely to be abstracted and secondary site H abstraction is more important as it is closer to O-atom and more likely to occur. *n*-Heptane rates [47] are applied for this class.

Reactions	A ( $\frac{\text{cm}^3}{\text{mol}\cdot\text{s}}$ )	n	E <sub>a</sub> ( $\frac{\text{cal}}{\text{mol}}$ )	Ref.
<b>Reactions with OH</b>				
H-C-C (P)	3.83x10 <sup>7</sup>	1.53	774	[47]
H-C-C (S)	2.34x10 <sup>7</sup>	1.61	-358	[47]
H-C-O (P)	9.50x10 <sup>7</sup>	1.61	-358	[47]
H-C-O (S)	8.84x10 <sup>9</sup>	1.00	-148	[47]
<b>Reactions with HO<sub>2</sub></b>				
H-C-C (P)	3.33x10 <sup>7</sup>	2.55	15470	[47]
H-C-C (S)	7.40x10 <sup>7</sup>	2.60	13890	[47]
H-C-O (P)	3.00x10 <sup>4</sup>	2.60	13890	[47]
H-C-O (S)	1.08x10 <sup>4</sup>	2.55	1529	[47]

Table LXIV: Kinetic data for Class 25: Cyclic ether reactions with OH and HO<sub>2</sub>

## Nomenclature

Symbol	Unit	Description
A	m <sup>2</sup>	Area
A'	s <sup>-1</sup> (1 <sup>st</sup> order)	Pre-exponential factor
a <sub>1</sub> -a <sub>5</sub>	-	Polynomials for high temperature range
a <sub>6</sub> -a <sub>7</sub>	-	Polynomials for low temperature range
C <sub>p</sub> , C <sub>v</sub>	J/K	Heat capacities at constant pressure & volume resp.
c <sub>p</sub> , c <sub>v</sub>	J/(kg·K)	Specific heat capacity at constant pressure and volume resp.
$\bar{c}_p$ , $\bar{c}_v$	J/(mol·K)	Molar heat capacity at constant pressure and volume resp.
c <sub>i,j</sub>	mol	consumption of species
D	m <sup>2</sup> /s	Diffusion coefficient
E <sub>a</sub>	J/mol	Activation energy
E <sub>i,r</sub>	-	Sensitivity of species i in reactions r
$\dot{E}$	J/s	Energy flowrate
F <sub>cent</sub>	-	F-center of Fall-off pressure range
f <sub>i,j</sub>	mol	Formation of species
g	m/s <sup>2</sup>	Gravitational acceleration
H, h	J, J/kg	Enthalpy & Specific Enthalpy resp.
k	-	Rate of reaction
k <sub>B</sub>	J/K	Boltzmann constant
K <sub>c</sub>	-	Equilibrium constant of reaction
l <sub>coll</sub>	m (or nm)	Molecular Mean free path
l	m	Length
m	kg	Mass
$\dot{m}$	kg/s	Mass flowrate
$\dot{m}''$ , $\dot{m}_i''$	kg/(s·m <sup>2</sup> )	Total and individual Bulk mass fluxes of species i
$\dot{m}_{i,diff}''$	kg/(s·m <sup>2</sup> )	Diffusive mass flux of species i
$\dot{m}'''$	kg/(s·m <sup>3</sup> )	Mass production rate per unit volume
n	-	Number of atoms
p	N/(m <sup>2</sup> ) or Pa	Pressure
Pr	-	Prandtl number
$\dot{Q}''$	W/(m <sup>2</sup> )	Heat flux vector
r	m	Radius
R	J/(mol·K)	Universal gas constant (8.3144598 J/(mol·K))
S	J/K	Entropy
S <sub>L</sub>	m/s	Flame speed
t	s	Time
T	K	Absolute temperature
T <sub>b</sub>	K	Flame temperature



$T^*, T^{**}, T^{***}$	-	Reduced temperatures
$U, u$		Internal energy, specific internal energy
$u_x, u_y, u_z$	m/s	Bulk velocity components (Cartesian) in x, y and z directions
$u_r, u_\theta, u_\phi$	m/s	Bulk velocity components (Spherical)
$u_r, u_\theta, u_x$	m/s	Bulk velocity components (Cylindrical)
$u_{i,diff}$	m/s	Diffusion velocity of species i
$u_i$	m/s	Total velocity
$\bar{u}$	m/s	Mean velocity
$V$	$m^3$	Volume
$W$	kg/mol	Molar mass (molecular weight)
$\bar{x}_i$	-	Mole fraction
$[X]$	kmol/ $m^3$	Molar concentration of species X
$Y_i$	-	Mass fraction of i specie
$Z_{rot}$	-	Rotational collision number

### Greek symbols

---

$\lambda$	W/(m·K)	Thermal conductivity
$\eta$	kg/(m·s)	Viscosity
$\nu, \nu', \nu''$	-	Total, reactant and product stoichiometric coefficients
$\sigma$	m	Particle (molecular) diameter
$\rho$	kg/m <sup>3</sup>	Density
$\omega$	-	Reduced collision integral
$\Phi$	-	Equivalence ratio
$\varepsilon$	-	Mean molar parameter (diffusion)
$\tau$	s	Residence time or ignition delay time

### Subscripts

---

a, -a	Activation, deactivation
A, B	Species name
b	Burned
coll	Collisions
cv	Control volume
diff	Diffusion
exp	Exp
f	Forward
g	Generated
i	Species
M	Collision partner, third body specie
n	number
p	Constant pressure
P	Product

r	Reverse, reaction
rel	Relative
U,u	Uni-molecular, unburnt
v	Constant volume
x,y,z	Directions
0	Initial
$\infty$	Infinity

### **Abbreviations**

---

AKI	Antiknock index
CN	Cetane number
CV	Control volume
IDT	Ignition delay time
JSR	Jet stirred reactor
ON	Octane number
RCM	Rapid compression machine
RON, MON	Research & Motor Octane numbers respectively
ST	Shock tube
VOC	Volatile organic compounds
VLPP	Very low pressure pyrolysis